Carbon and sulfur isotope biosignatures in Mars-analogue hydrothermal environments

Arola Moreras Martí

A thesis submitted for the degree of PhD
at the
University of St Andrews

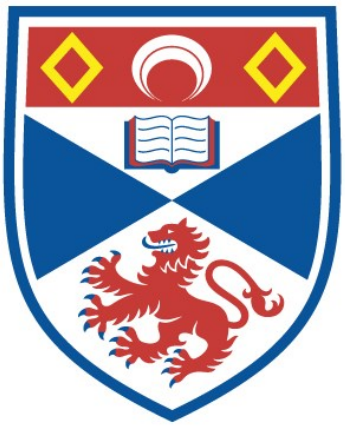

2021

Candidate's declaration

I, Arola Moreras Marti, do hereby certify that this thesis, submitted for the degree of PhD, which is approximately 45,000 words in length, has been written by me, and that it is the record of work carried out by me, or principally by myself in collaboration with others as acknowledged, and that it has not been submitted in any previous application for any degree.

I was admitted as a research student at the University of St Andrews in September 2016.

I received funding from an organisation or institution and have acknowledged the funder(s) in the full text of my thesis.

Date Signature of candidate

07-09-2020

Supervisor's declaration

I hereby certify that the candidate has fulfilled the conditions of the Resolution and Regulations appropriate for the degree of PhD in the University of St Andrews and that the candidate is qualified to submit this thesis in application for that degree.

Date Signature of supervisor

Permission for publication

In submitting this thesis to the University of St Andrews we understand that we are giving permission for it to be made available for use in accordance with the regulations of the University Library for the time being in force, subject to any copyright vested in the work not being affected thereby. We also understand, unless exempt by an award of an embargo as requested below, that the title and the abstract will be published, and that a copy of the work may be made and supplied to any bona fide library or research worker, that this thesis will be electronically accessible for personal or research use and that the library has the right to migrate this thesis into new electronic forms as required to ensure continued access to the thesis.

I, Arola Moreras Marti, confirm that my thesis does not contain any third-party material that requires copyright clearance.

The following is an agreed request by candidate and supervisor regarding the publication of this thesis:

Printed copy

No embargo on print copy.

Electronic copy

Embargo on all of electronic copy for a period of 1 year on the following ground(s):

- Publication would preclude future publication

Supporting statement for electronic embargo request

I have two papers I want to publish from my PhD work before the information is available to the public.

Title and Abstract

- I agree to the title and abstract being published.

Date	Signature of candidate
07-09-2020	

Date	Signature of supervisor

Underpinning Research Data or Digital Outputs

Candidate's declaration

I, Arola Moreras Marti, hereby certify that no requirements to deposit original research data or digital outputs apply to this thesis and that, where appropriate, secondary data used have been referenced in the full text of my thesis.

Date Signature of candidate

07-09-2020

Abstract

The study of terrestrial environments that bear similarity to Mars provides valuable information for interpreting data from missions, including how to find evidence of relict life on the red planet. Stable isotope signatures evidencing microbial metabolic activity are commonly used as a biosignature tool. Here, an interdisciplinary study investigating two volcanic hydrothermal systems in Iceland is presented, with additional contextualisation through a comparison with a non-volcanic hypersaline spring. This thesis combines mineralogy, geochemistry, microbial community DNA, and stable isotope systems (carbon and sulfur) to analyse: i) the preservation of isotopic biosignatures in hydrothermal and hypersaline springs, and ii) the relationships between the biosignatures and the geochemistry of these environments.

Firstly, a characterisation of two Mars analogue hydrothermal environments in Iceland (Kerlingarfjöll and Kverkfjöll), reveals deep volcanic processes controlling the geochemistry of the hydrothermal pools. The volcanic processes create two very distinct pH environments, with Kerlingarfjöll circum-neutral and Kverkfjöll acidic, with distinct water geochemistry and mineralogy. The water geochemistry is found to be a key parameter controlling the microbial communities, based on pH differences and the different electron donors and acceptors available. Secondly, carbon isotope fractionations preserved as sedimentary organic carbon, are controlled in Kerlingarfjöll and Kverkfjöll systems by temperature. Low temperature pools favour carbon CO_2 fixation pathways that produce larger or more variable carbon isotope fractionations. Lastly, sulfur isotope values ($\delta^{34}S$) recorded in the sediments are not conclusive as geochemical biosignatures in Kerlingarfjöll and Kverkfjöll sediments. This is due to abundant H_2S with abiotic $\delta^{34}S$ values overwhelming biological $\delta^{34}S$ values. Conversely,

when combining $\delta^{34}S$ with $\Delta^{33}S$ and $\Delta^{36}S$ as a Quadruple Sulfur Isotope system (QSI), two pools in Kerlingarfjöll show complex S-cycling combining biological and volcanic processes. Importantly, the non-volcanic hypersaline spring preserves larger fractionations in $\delta^{34}S$ and large $\Delta^{33}S$ values, typical of reduction and disproportionation of sulfur by microorganisms. The main environmental variables causing larger S isotope fractionations in the hypersaline spring are the salinity stress and the limitation of electron donors and acceptors in the environment.

Overall, this thesis improves the understanding of carbon and sulfur isotopes as biosignature tools for investigating hydrothermal and hypersaline environments in Mars, and opens the door for the use of QSI as a more robust biosignature for future missions.

Acknowledgements

Thank you, Gràcies.

To my supervisors Claire and Aubrey, for introducing me to the fascinating world of astrobiology and isotopes, and for your guidance, support and understanding throughout these years. I am very grateful to have had the opportunity to work and learn from such inspiring scientists. To Mark F.P. for being such a versatile figure: from your patience in the lab to your help by reading manuscripts, your support, and friendship. To Eva for being the best pastoral supervisor, making sure I was doing okay and the project was on its way. To Sami for your always encouraging chats, and for trusting me to be part of organising Goldschmidt. To Mel and Alex for being the beginning of the story, "once upon a time in a clean lab in Oxford…"

To Mark C., Toni, Tomasso, Batzi, Colin, Matthew, Lotta and Elyse for your generous help during these years. To colleagues from the School of Earth and Environmental Sciences and PhD students Simon, Nicky, James, Solène, Jess, Laura, and many others. To the St Andrews Ultimate Frisbee Club for making me run around keeping me fit physically and mentally. To the friends that came from there, Hannes and Janis.

To the friends that live away - Kim, Mari, Marta and Guillem - for the long phone calls and messages, helping me to put things into perspective and to stay grounded. To the friends that live here Hebe, Sarah and Anna for distracting me doing exciting plans. To Sarah R. for your mentoring and friendship, for always believing in me and helping me overcome difficult times. To Natalya, Bethan and Eloise, for sticking together through all these years, for your encouragement, office chats, cries and laughs together, stickers and adventure trips. One of the best things that this PhD has provided is your incredible friendship that I will forever treasure. To Nick and Dan for adding the perfect hilarious

touch to the group. To Lisa for putting up with me, for your support and care, even when I was the grumpiest. You are the sister that I never had, making St Andrews home and our sofa conversations my much-loved thing.

To família Moreras and família Martí, for being the air blowing from Barcelona that kept the ship going. To my parents Ignasi and Griselda and my brother Nil, for your huge unconditional support and love that kept me afloat during difficult times through this journey. We also now share an adoration for Crail - I know you are thinking of retiring there. And finally to David, for always being there, to listen and to comfort, for finding the right words when I was worn-out, and for your continuous love and support.

Again, gràcies to all of you. It is not an overstatement to say that without you, this could not have been possible.

This work was supported by the UK Space Agency, Science & Technology Facilities Council [111RESEES003].

Contents

List of Figures

List of Tables

1 Introduction

1.1 Motivation

This project was conceived with the aim to characterise Mars analogue hydrothermal systems, and to study their capability to preserve stable isotope biosignatures (carbon and sulfur). The use of stable isotopes to evidence relic life on Earth dates back decades; whereas their utility in the search for evidence of life on other planets has been revolutionised in recent years. This was caused by the arrival of the Sample Analysis at Mars (SAM) instrument, on board the Curiosity Rover on Mars in 2012. The SAM instrument has been measuring S isotope signatures *in situ* on the Martian surface. Furthermore, these measurements will be part of upcoming Mars sample return international ambitions.

Given the importance of isotopic signatures unravelling biological processes, understanding how they might preserve evidence of microbial life in Mars analogue environments is crucial. Similarly, it is also significant to distinguish biosignatures from abiotic production. This distinction is now and will be key for the interpretation of biological measurements of *in-situ* or returned Martian samples, with further implications for the search for life on exoplanets. Finally, volcanically-driven microbial habitats are common to both the early Earth and Mars and are therefore an ideal target environment to explore the utility of carbon and sulfur stable isotope systems for this endeavour.

1.2 Aims and objectives

The core objective of this thesis was to develop and understand the link between the microorganisms present in hydrothermal environments and the stable isotope biosignatures that they leave behind. This work takes an integrated multidisciplinary approach, by using both geochemical and microbiological methodologies to address the following research questions:

Q1. What are the geochemical and mineralogical characteristics of Mars hydrothermal analogues in contrasting lithological settings?

Q2. What microbial life is supported in these hydrothermal analogue environments?

Q3. Are carbon and sulfur stable isotope ratios robust biosignatures in these Mars analogue hydrothermal systems?

Q4. How does a hydrothermal system compare with other sulfur-rich environments for the preservation and detection of sulfur isotope biosignatures?

1.3 Thesis Overview

Chapter 2 of this thesis provides a comprehensive literature review and summary of Mars' geological history, Mars analogue work, and microbial biosignatures within relevant terrestrial environments. It also establishes the knowledge gap in the literature that led to the origin of this work.

Chapter 3 details the experimental, analytical, and fieldwork methods used for the acquisition of the majority of the data for this project.

Chapter 4 focuses on characterising hydrothermal environments within two analogue Icelandic volcanic settings, Kerlingarfjöll and Kverkfjöll. This chapter reports the aqueous geochemistry and mineralogy of these two sites, including analysis of major anions and cations, *in situ* measurements, and mineralogical analyses such as XRD, VNIR, and XRF. This chapter addresses Q1, above.

Chapter 5 details carbon and sulfur stable isotope biosignatures and microbial community DNA analyses in order to address Q2 and Q3 above. This work informs about the potential for sulfur and carbon isotope ratios to be preserved as biosignatures in hydrothermal environments.

Chapter 6 is a microbiology experimental study culturing Microbial Sulfate Reducers from Kerlingarfjöll and Kverkfjöll pools. The goal is to understand the main environmental variables that affect the growth of Microbial Sulfate Reduction (MSR) communities in these pools.

Chapter 7 aims to take the key concepts explored in all the previous chapters and compare them to a non-volcanic sulfur-rich Mars analogue environment: the Axel Heiberg Island hypersaline spring Lost Hammer (LH). Here LH samples are compared to those from the hydrothermal environments in Iceland. The potential for using QSI (Quadruple Sulfur Isotopes) as a geochemical biosignature is explored through measurements and explained two open-system steady-state S isotope box models. This chapter addresses Q3 and Q4.

The impact of this study, main findings and the outlook for future work are summarised in Chapter 8. This chapter provides a concluding discussion of the implications of this research by updating the knowledge gap.

A manuscript combining the characterisation of Kerlingarfjöll and Kverkfjöll (XRD, XRF, analysis and water chemistry data) from Chapter 1 with the 16s rRNA results from Chapter 2, is currently under review in the Geobiology journal.

A. Moreras-Marti, C.R. Cousins, M. Fox-Powell, A.L. Zerkle, F. Gazquez, H.E.A. Brand, (in review). Volcanic controls on the microbial habitability of Mars analogue hydrothermal environments, *Geobiology*.

A different manuscript with the QSI results from LH and Kerlingarfjöll and Kverkfjöll is in preparation to be submitted in Geochemistry Cosmo Acta (GCA) journal.

A. Moreras-Marti, C.R. Cousins, E. Stueeken, M. Fox-Powell, T. Di Rocco, A.L. Zerkle, (in prep). Quadruple Sulfur Isotope (QSI) biosignatures results from terrestrial Mars analogue systems, *GCA*.

2 Literature review

This thesis explores two Mars analogue hydrothermal systems, and examines their ability to preserve stable isotope biosignatures. The following review discusses the background literature relevant to this work. It begins by briefly explaining the geological and mineralogical history of Mars, moving to Mars' sulfur cycle, and then introducing the main hydrothermal systems on Mars. The MSL Curiosity Rover and future 2020 missions are also discussed. The second part focuses on reviewing hydrothermal Mars analogues' studies, with a section dedicated to the microbial communities inhabiting them. The last part introduces sulfur and carbon as isotopic microbial biosignatures and the microorganisms related with the sulfur cycle.

2.1 Mars

2.1.1 Brief geological history of Mars

The geological history of Mars is divided into three main epochs: the Noachian, the Hesperian and the Amazonian. The Pre-Noachian period extended from the accretion and differentiation of the planet (4.5 Ga ago) to the beginning of the Noachian (4.1 Ga ago) (Tanaka, 1986). During the Pre-Noachian the planet differentiated into crust, mantle and core (Borg et al., 2003; Lee & Halliday, 1997). This era was dominated by impacts that shaped the terrain with large craters (Carr & Head, 2010; Solomon & Head, 2007). Additionally, it is thought that the difference in elevation of around 1-3 km between the northern and southern hemispheres, was formed by then (McGill & Squyres, 1991). Towards the end, the Tharsis volcanic dome may have started to form and rise (Nimmo & Tanaka, 2005; Solomon et al., 2005).

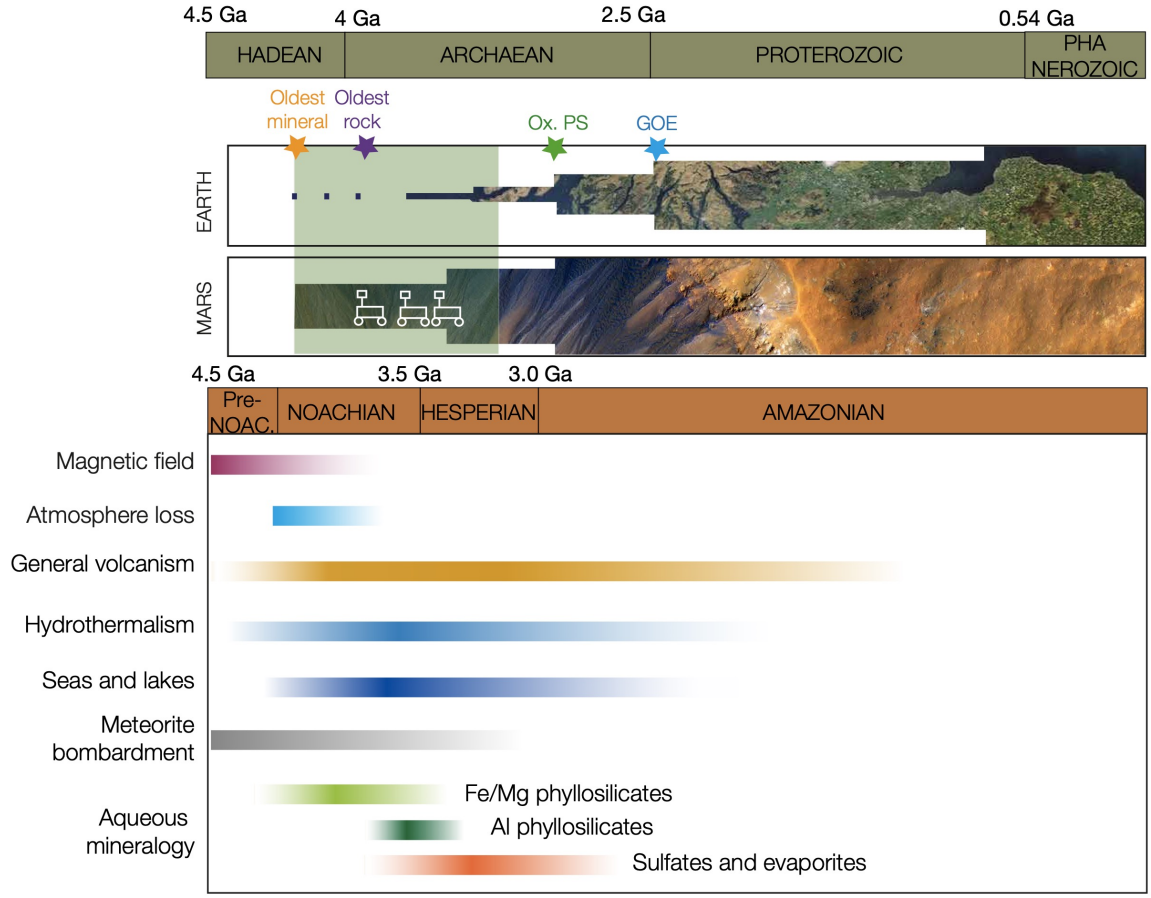

Figure 2-1. Time line of major events during Mars geological history adapted from Wordsworth (2016). Geological Martian eons compared with Earth geological eons. For Earth, the oldest mineral and rock, oxygenic photosynthesis (Ox. PS), and the Great Oxygenation Event (GOE) are indicated by stars. Area of Earth and Mars indicates the amount of crust preserved over different epochs (from Michalski et al, 2013 and references therein). The green shadowed area represents the period on Mars when it is thought that there were more opportunities for life to have arisen. The three rovers (from left to right) - future ExoMars, Mars2020 and active MSL - are represented on the timescale.

The Noachian period, named after Noachis Terra, lasted from 4.1 Ga ago to around 3.7 Ga ago (Tanaka, 1986). Most of the features that can be observed today on the Martian surface were shaped during the Noachian; it is the period with the highest intensity of geological events throughout Mars' history (Carr & Head, 2010). Firstly, a high rate of meteorite bombardment continued during the Noachian, creating impact craters on the surface (Segura et al., 2002). Secondly, volcanism was established in different regions of Mars (Phillips et al., 2001). This volcanic activity was significant for the evolution of the Martian surface, as it extended throughout most of its geological history: from the Noachian to the Amazonian (Figure 2-1) (Anguita et al., 2001). The Tharsis volcanic

dome is the largest volcanic complex in the Solar System as a result of the lack of global plate tectonics on Mars: the growth of the dome is related to a large static mantle plume on the inside of the planet (e.g. Anderson et al., 2001; Carr & Head, 2010). Through the study and observation of large tectonic features around Tharsis, it is known that the major volcanic episodes were from mid to late Noachian (Anderson et al., 2001; Phillips et al., 2001; Viviano-Beck et al., 2017). During that period of time, the Tharsis volcano complex released large quantities of volcanic gases that had a direct impact on the Noachian climate, and potentially to any life that could have emerged on the Martian surface (Ehlmann et al., 2016). Throughout the Noachian there is evidence of flowing surface water, with rivers that worked their way through by eroding the Martian surface (Malin & Edgett, 2003; Milton, 1973). These rivers also broke into crater basins, creating deltas with sedimentary structures (Fasset & Head, 2008; Howard et al., 2005; Moore et al., 2003).

The delta formation, sedimentary structures, and valley networks require precipitation of some sort in order to form. It is thought that precipitation or snow melt events happened during the Noachian, producing the large delta deposits (Figure 2-2) (Malin & Edget, 2003). A warm and wet climate would be required to allow sufficient rainfall to transport such large volumes of material and form geomorphological features (Craddock & Howard, 2002; Schon et al., 2012). Despite this evidence, climate models still struggle to predict what type of atmosphere could have sustained stable warm conditions on the Martian surface (e.g. Forget et al., 2013; Tian et al., 2010). A warm climate could have been stimulated by a mix of volcanic CO_2 and water, and potentially other volcanic gasses (e.g., CH_4, SO_2), providing a greenhouse effect (Colaprete & Toon 2003; Forget & Pierrehumbert, 1997; Mischna et al., 2000). Other theories suggest that Noachian Mars was icy and cold, but sporadic warm episodes were created through meteorite impacts, volcanic eruptions or methane "burps" (Kite et al., 2017; Wordsworth et al., 2017). Another plausible scenario is a warm but semi-arid climate, able to create sporadic precipitation episodes (Ramirez & Craddock, 2018).

The Noachian period was also characterised by the formation of clays, specifically phyllosilicates (Ehlmann et al., 2011, Newsom, 2005; Wray et al., 2009). The Phyllocian is the period for clay formation on the Martian surface and lasts from the Pre-Noachian

to Noachian (Bibring et al., 2006). Clay minerals are an alteration product that resulted from intense water/rock interaction which happened at the surface and subsurface (Ehlmann et al., 2011). The phyllosilicates found in Noachian terrains are largely Fe/Mg-smectites (Figure 2-1), which evidence waters of pH 5-6, as most smectites form around this specific pH range (Grotzinger et al., 2014). As these conditions are considered Earth-like, the ancient clays are highly relevant for reconstructing habitable Martian conditions centred around the Noachian, and are the focus of recent surface exploration (Grotzinger et al., 2014).

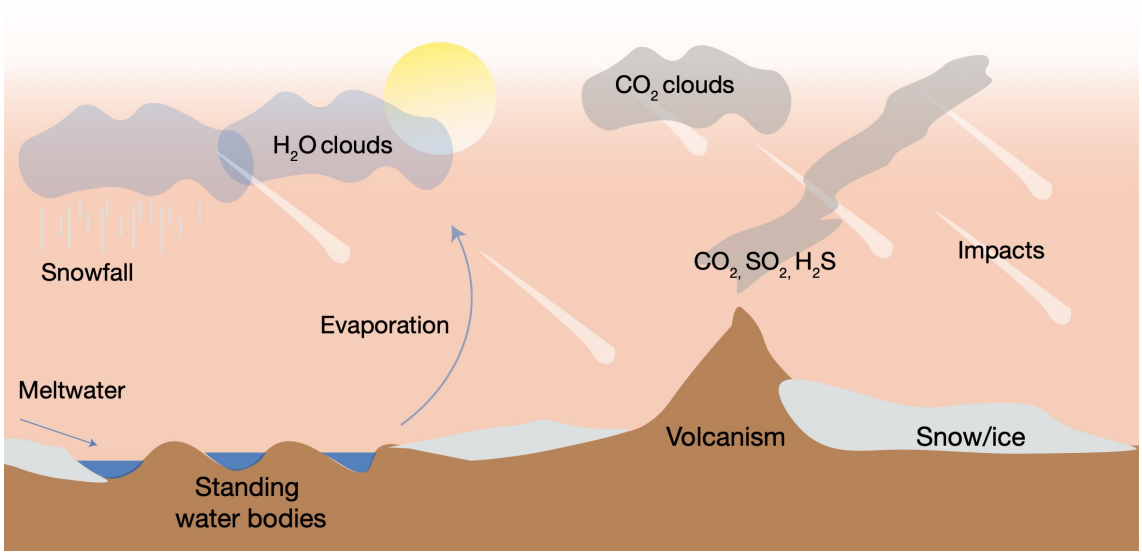

Figure 2-2. Diagram adapted from Wordsworth (2016) showing the main processes happening on Mars' surface during the Noachian and Early Hesperian periods.

The End of the Noachian and start of the Hesperian was marked by a global transition, when it is thought that Mars lost its internal magnetic dynamo, and with it, its atmosphere (Brain & Jakosky, 1998; Stevenson, 2001; Lillis et al., 2008). Volcanism continued on the Martian surface, with Tharsis activity at its highest intensity during the end of Noachian- early Hesperian (Figure 2-2) (Bouley et al., 2017). This period also coincides with the earliest record of life on Earth (Figure 2-1) (Michalski et al., 2013). The Hesperian is named after the Hesperia Planum, which are younger planes than the ones defining the Noachian. The Hesperian period extends from the end of the heavy bombardment at 3.7 Ga to 3 Ga, and coincides temporally with the Archaean Earth. The Hesperian was marked by the decline of meteorite impacts and hydrological processes, but the formation of canyons, large outflow channels, lakes and potential seas persisted

(Andrews-Hanna & Phillips, 2007a; Carr & Head, 2010). The formation of phyllosilicates also declined, but was followed by accumulation of large, thick and extended deposits of sulfates (Figure 2-1) (Bibring et al., 2006). The polar ice sheets were also formed during this period (Andrews-Hanna et al., 2007b). The pressure induced by the freezing of groundwater potentially created floods and outburst flows during this period (Wang et al., 2006b).

Finally, the Amazonian period extends from approximately 3 Ga to the present. A lower activity level was present on the Martian surface, with fluvial and volcanic rates still in decline (Figure 2-1). After the loss of atmosphere and subsequent exposure to erosion and solar wind, aeolian and glacial processes started to increasingly influence the Martian surface (Carr, 2007). The majority of ice formed on the Martian surface was created during the Amazonian (Fasset et al., 2010; Madeleine et al., 2009). Volcanic activity continued, but potentially diminished throughout this period (Carr & Head, 2010; Mangold et al., 2010). In other words, Mars' surface became effectively geologically dormant during the Amazonian.

2.1.2 Mars mineralogy

Evidence for the presence of liquid water and a distinct climate during the Noachian is based on geomorphological features, but also on mineralogical evidence (Banfield, 2002). The search for habitable conditions on early Mars is focused, in part, on the nature of the aqueous environments recorded within sediments, which capture some of the planet's first potentially habitable conditions (Bishop et al., 2013). The mineralogical composition of associated sediments has been key to reconstructing the different climatic events that happened during Mars' past (Banfield, 2002; Poulet et al., 2005; Mangold et al., 2007; Mustard et al., 2007). The two most influential orbital instruments that have helped to characterise Martian mineralogy are: i) the Compact Reconnaissance Imaging Spectrometer for Mars (CRISM), (Murchie et al., 2007) on board the Mars Reconnaissance Orbiter (MRO), and ii) Mars Express Observatoire pour la Mineralogue, l'Eau, les Glaces et l'Activite (OMEGA) (Bibring et al., 2004). Both have been instrumental in the remote detection of Martian surface minerals, using hyperspectral visible to near-infrared (VNIR) reflectance spectrometry. Surface landers and rovers have also helped study surface minerals at local scales. The landers Mars

Exploration Rovers (MER) Spirit and Opportunity explored Gusev crater and Meridiani Planum respectively; the Mars Science Laboratory (MSL) Curiosity rover is currently exploring Gale Crater.

The Martian crust is the precursor to most of the sediments present on the surface (Grotzinger & Milliken, 2012b). Most of the Martian surface is dominated by volcanic rocks, identified as basalts, although they have a distinct mineral composition from terrestrial basalts. Martian basalts have a lower % of SiO_2 (subalkaline) and they are typically more Fe-rich (Balta & McSween, 2013; McLennan, 2003; McSween et al., 2009). As Mars exploration advances, variations in the baseline composition of volcanic rocks are being detected, showing higher % of SiO_2 and K_2O (McSween et al., 2006). The primary mineralogy of Martian basalts is composed of plagioclase, pyroxene, olivine and Fe/Ti oxides (Ehlmann & Edward, 2014; Taylor & McLennan, 2009). The secondary mineralogy is typically composed of phyllosilicates (Fe/Mg smectites, also Al-phyllosilicates), sulfates, and Fe-oxides (Bibring et al., 2006; Ehlmann et al., 2011). This results in Ca, Mg, and Fe being the main cations released in solution from Martian basalts during water-rock interaction (McLennan, 2003; McLennan et al., 2018).

Fe/Mg smectites are found throughout the Noachian and early Hesperian stratigraphy, and are interpreted as resulting from circum-neutral pH and reduced aqueous conditions (e.g. Dehouck et al., 2016; Ehlmann et al., 2010; Ehlmann & Edwards, 2014 and references therein; Hurowitz et al., 2017; Vaniman et al., 2014; Viennet et al., 2017). Aqueous alteration also operated on local scales within the broader global context. For example, the formation of Fe/Mg trioctahedral clays were related to hydrothermal processes, and montmorillonite and dioctahedral Fe/Mg smectites were formed in subaerial environments during sporadic impact-generated conditions (Bishop et al., 2018). Fe^{2+} smectites that may have formed in reducing conditions were also detected in Gale crater, as forming precursors of the Fe^{3+} smectites detected by orbit from later periods in Mars' history were more oxidising conditions dominated (Chemtob et al., 2017). Overall, a picture of a wet early Mars with reducing conditions evolving to an environment increasingly dry with more oxidised surface conditions has emerged. This observation has been at both local and global scales, from the evidence provided by the phyllosilicates (Bishop et al., 2018; Luo et al., 2017, Ramirez & Craddock, 2018).

Younger, overlying sulfates (jarosite, gypsum, alunite and Mg-Ca-Fe sulfates) indicate increasingly acidic waters and saline SO_4^{2-} rich environments into the Hesperian period (Figure 2-1, Figure 2-3). For example, jarosites were discovered at Meridiani by MER (Klingelhöfer et al., 2004). The source of the sulfates is hotly contested, but there are four main potential pathways: i) deposition of atmospheric sulfurous aerosols, ii) magmatic hydrothermal waters, iii) basalt weathering, and iv) brine-fed acid lakes (Gendrin et al., 2005). The first is associated with the degassing of volcanic sulfur on Mars, mainly in the Tharsis region (Johnson et al., 2008). Reduced H_2S volcanic gas is oxidised to H_2SO_4 and subsequently precipitated on the surface (Levin & Summers, 2011; Settle, 1979). Sulfates could have also been formed by evaporation of waters derived from acid alteration of basalts. This last process of acidic alteration of basalts ("acidic fog"), is known to produce: Mg, Fe, Ca, and Al sulfates, together with Fe-oxides (Tosca et al., 2004). Sulfates that require low pH waters to form (alunite and jarosite), were found in the Columbus crater and the Cross crater with associated Al-phyllosilicates (Ehlmann et al., 2016; Wray et al., 2011). Overall, it seems formation of sulfate deposits is regulated by local rather than larger scale processes (Ehlmann et al., 2016).

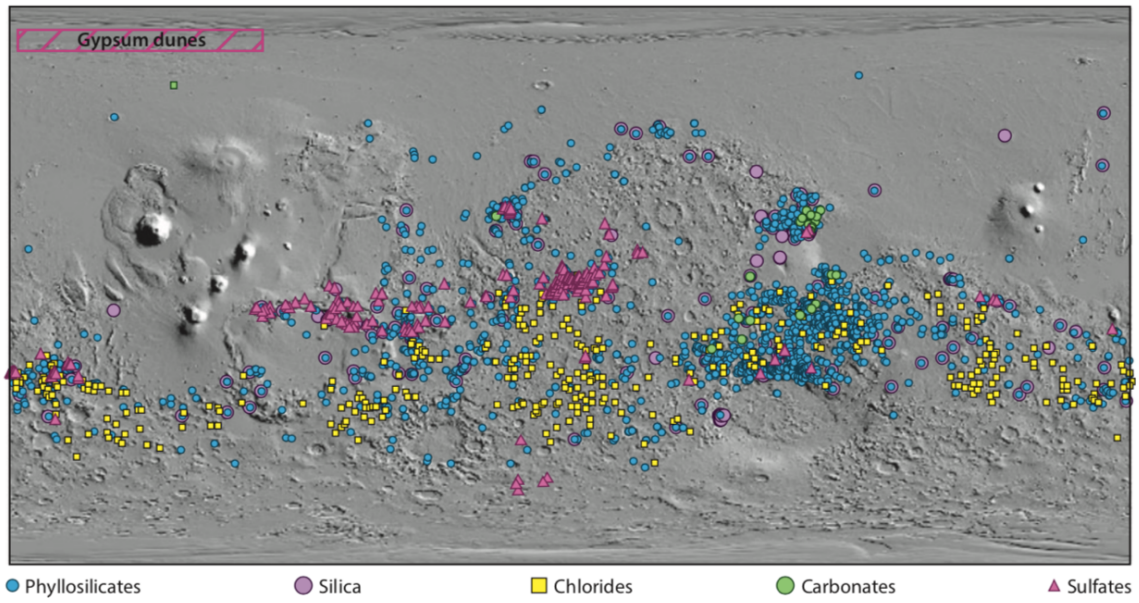

Figure 2-3. Distribution of detected mineral deposits on the Martian surface from Ehlmann et al. (2014).

The formation of Fe-oxides is also related to the acidic alteration of basalts (Tosca et al., 2004, 2008). Nevertheless, at Meridiani Planum distinct Fe-oxides are present as hematite concretions formed from groundwater (Klingelhöfer et al., 2004; Squyres et al., 2004). In the sedimentary record the spherules occur associated with jarosite (Klingelhöfer et al., 2004). This sedimentary association has been interpreted as a recharge of a chemically distinct groundwater (higher pH or more oxidised), that led to a rapid concretion of hematites forming from the breakdown of jarosite (e.g. McLennan et al., 2005). The association of hematites with jarosite at Meridiani Planum has directed other hypotheses for hematite formation. These are: i) aqueous diagenesis from movement of reducing fluids with a posterior oxidation (e.g. Chan et al., 2004), ii) precipitation in acid saline lakes (e.g. Bowen et al., 2008), and iii) hydrothermal alteration of jarosite (e.g. Golden et al., 2008). Spherules of Fe-oxides (hematite and goethite) were also found by Spirit at Home Plate. In this environment, their origin is related to hydrothermal processes (Ruff et al., 2007).

Finally, carbonates are the missing piece in the puzzle of Martian mineralogy. If the Noachian atmosphere was dominated by volcanic gases including CO_2, larger volumes of C-bearing minerals are expected to be found (Edwards & Ehlmann, 2015). Instead, carbonate mineral deposits on the Martian surface typically comprise only small volumes of Fe/Mg carbonates in relation with Noachian smectites (Ehlmann et al., 2008; Wray et al., 2016). On the other hand, carbonate deposits could be locked in subsurface deposits yet to be found (Michalski & Niles, 2010; Morris et al., 2010; Michalski et al., 2013).

2.1.3 The sulfur cycle on Mars

Sulfur (S) is one of the most abundant elements on the Martian surface (Baird et al., 1976; Franz et al., 2019a; King & McLennan, 2010). Our knowledge of S abundance on Mars is largely derived from remote sensing instruments on board spacecraft orbiters, in addition to landers and studies of Martian meteorites. Martian meteorites suggest the presence of high S concentrations in the Mars interior, with average concentrations of 6 % wt. SO_3 found in shergottites (Martian basaltic meteorites) (Meyer, 2012). The concentrations of S on Mars' surface are evident through observations and measurements of high SO_3 concentrations in the Martian soil (6 wt. %) (Taylor &

McLennan, 2009). The overall average concentration of Martian near surface sulfur (SO_3) is 4.40 wt. % (McLennan et al., 2010). The main S oxidation states found on Mars are: S^{2-} (pyrrhotite, FeS_{1-x}), S^{1-}(e.g. pyrite, FeS_2), S^{4+} (SO_2(g), SO_2^{2-} bisulfide, SO_3^{2-} bisulfite), S^{6+} (SO_3, SO_4^{2-} sulfate, SO_2^{2+} sulfone) and S^+, S^{2+}, (S_3) (Franz et al., 2019a).

Reduced S is found in primary igneous S from Martian meteorites, but also on the Martian surface (Franz et al., 2017). In meteorites, the reduced S is mainly in the form of sulfides, including some reduced Fe-S minerals (e.g. pyrite and pyrrhotite) (Meyer, 2012 and references therein). Reduced Fe-S minerals have been found typically at the grain boundaries, which makes them susceptible to alteration by weathering processes, readily forming oxidised secondary phases (King & McLennan, 2010). Sulfide minerals (Fe-S, Ca-S, Mg-S) have also been observed on the Martian surface by the Sample Analyser at Mars (SAM), they are hypothesised to be product of hydrothermalism and groundwater dissolution (Franz et al., 2017). Secondary S phases found in meteorites are sulfates, and sulfate-carbonates (e.g. Bridges et al., 2001). The main sulfate forms found on the Martian surface are gypsum ($CaSO_4{\cdot}2H_2O$), jarosite ($KFe^{3+}{}_3(OH)_6(SO_4)_2$) and magnesium sulfates ($MgSO_{4x}$) (Bibring et al., 2006; Gendrin et al., 2005). The high concentrations of S demonstrate that the S cycle was likely a key component of Mars geological and geochemical history (Figure 2-4).

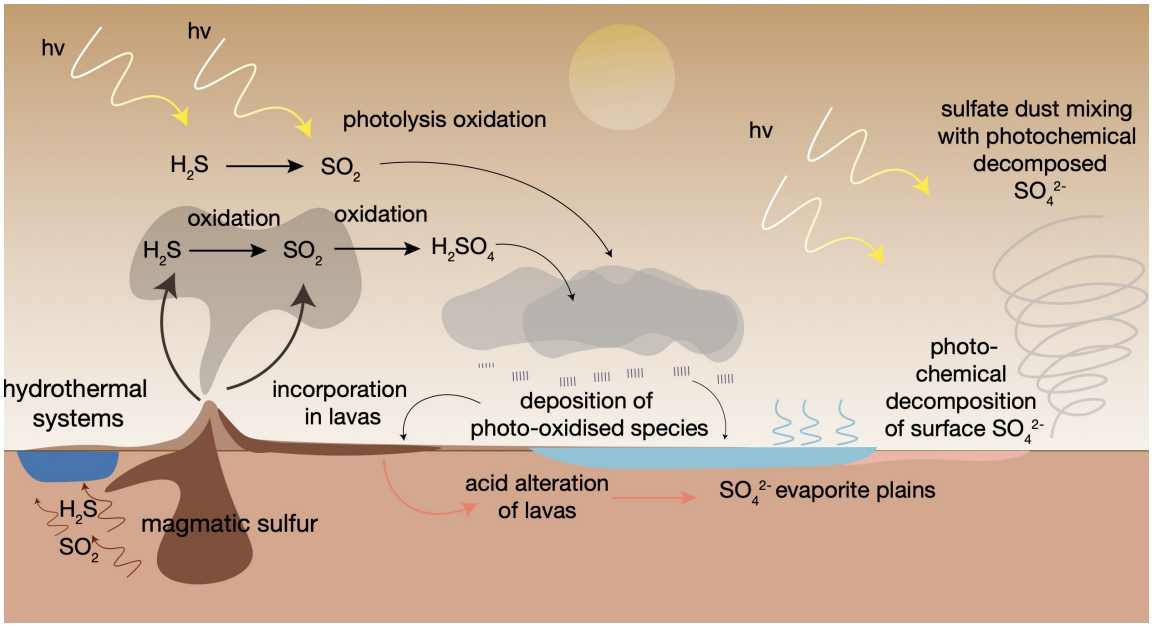

Figure 2-4. Schematic describing the S cycle on the Martian surface in the Noachian-Hesperian time period. Drawing modified from Farquhar (2000b), and Franz et al. (2017). Volcanic H_2S and SO_2 undergo photolysis alteration in the atmosphere. Then, it is deposited on the Martian surface and through different processes is incorporated into the basalt or sulfate deposits. H_2S and SO_2 could have also degassed to hydrothermal systems.

The origin of the abundant surface S species derives ultimately from a S-rich interior, from the mantle and crust. Reduced forms of S were transferred from the Mars interior (Figure 2-4) to the surface through magmatic or hydrothermal gas, sulfide fluids, and sulfide minerals in magma (King & McLennan, 2010). The prolific volcanism that extended from the Noachian to Hesperian led to significant amounts of reduced S outgassing to the surface (Figure 2-4) (King & McLennan, 2005; Righter et al., 2009). The outgassing involved a large injection of S gases (H_2S and SO_2) into the atmosphere (Settle, 1979; Tian et al., 2010). Mass-independent S-isotope (S-MIF) anomalies from SO_2 and H_2S measured in Martian meteorites suggests that atmospheric chemistry was a key influence on the Martian S cycle (Farquhar et al., 2000b; Franz et al., 2014). The results provide evidence for photochemical reactions fractionating H_2S and SO_2 in the Martian atmosphere. When in the atmosphere, H_2S would have photo-oxidised to SO_2, and SO_2 precipitated or further photo-dissociated. Both photo-altered SO_2 and H_2S were deposited on the Martian surface with a distinctive S-MIF signal (Franz et al., 2014). Hydrothermal circulation, and meteorite impacts into S-rich sediments, provided an active geochemical cycle which subsequently homogenised this S-MIF signal on the

Martian surface (Figure 2-4). The delivery of dust into the atmosphere also played a role in the homogenisation of the S-MIF signal, between the atmospheric S species and surface sulfates (Farquhar et al., 2000b).

All of these processes reflect the transport of H_2S and SO_2 from Mars' interior to the atmosphere, and to eventual surface deposition. Once on the surface, the majority of S species were oxidised to SO_3 and SO_4^{2-}. However the provenance of these sulfates is diverse. Two sources mentioned previously are i) air fall/ash deposition of volcanic sulfate (ash deposits, sulfate from volcanic outgassing), and ii) secondary deposition in aqueous settings, and atmospheric deposition (atmospheric aerosols trapping oxidised S as sulfate from volcanic outgassing, photochemical alteration of S gases). Sulfate can also be derived from the alteration of sulfide in mafic-ultramafic rocks on the Martian surface (Hurowitz et al., 2006; Tosca et al., 2004). This would results in low-pH fluids, and the observation of jarosite and other Fe^{3+} minerals that require very acidic water conditions to form on the Martian surface (Klingelhöfer et al., 2004). Groundwater, fluvial, aeolian and glacial processes recycled and transported these sulfates (Herkenhoff et al., 2008; McLennan et al., 2019). Furthermore, evaporation processes caused sulfates to form large layered deposit plains (Tosca et al., 2005).

2.1.4 Martian hydrothermal systems

Hydrothermal systems and their relevance to habitability

Localised hydrothermal systems are important with respect to the habitability of Mars. Analogue hydrothermal systems on Earth are known to provide the basic requirements to sustain chemotrophic organisms through surface and subsurface heat (Cockell & Lee, 2002; Osinski et al., 2013; Schulze-Makuch et al., 2007). These basic requirements are liquid water, geochemical energy sources, and reducing-oxidising conditions (Cockell et al., 2016). As mentioned above, the wider climatic conditions on early Mars are still under much debate (Wordsworth, 2016). Regardless, within either a 'warm' or 'cold' climatic scenario, subsurface and surface hydrothermalism would have provided liquid water conditions for life. Within a colder climatic scenario, surface volcanic systems erupting underneath glaciers could have provided stable conditions for life (Figure 2-5).

Through volcano-ice interaction, the presence of liquid water would be maintained, and the ice cover would provide protection from UV radiation (Cousins & Crawford, 2011).

Regarding geochemical energy sources, hydrothermal fluids are excellent dissolvers of elements from host rocks. This dissolution liberates anions and cations in the water (Fe^{2+}, Fe^{3+}, Cl^{-}, SO_4^{2-}, NO_2^{-}, NO_3^{-}, P^{+}, Na^{+}, K^{+}, etc) that can be used by microorganisms to produce energy for growth and to build biomass. Lastly, hydrothermal environments produce waters with redox gradients, for example created by deeper reducing conditions mixing with oxidising conditions towards the surface. The chemical reactions that happen between the reduced and oxidised species can be exploited by microorganisms via microbial lithotrophic metabolisms (Des Marais & Walter, 2019b; Pirajno & Kranedonk, 2017; Westall et al., 2018). Furthermore, hydrothermal systems present a range of acid to alkaline conditions, and temperatures. On Earth, the microbial communities that inhabit the very high or low pH and temperature hydrothermal systems are called extremophiles. The presence of microorganisms in such extreme environments on Earth shows that it is possible for life to flourish in conditions that resemble early Mars or the more acidic, sulfate-rich late Mars (Hays et al., 2017). Hydrothermal systems also present some barriers for habitability. These systems tend to be ephemeral, and present a potentially shorter geological life span compared with other more stable environments such as lakes or deltas. Furthermore, they tend to be geographically-localised which makes them difficult to detect and study from orbit (Pirajno & Kranedonk, 2017), and also may limit the microbial colonisation of new, emerging habitats due to a lack of connectivity between habitable environments (Cousins et al., 2013).

Exogenic or Endogenic-derived hydrothermal systems

As described previously, the Noachian was characterised by intense and widespread volcanism, and a high rate of impacts (Phillips et al., 2001; Segura et al., 2002) . During that period, large amounts of heat were released through endogenic volcanic activity but also exogenic activity, from space bodies bombarding the Martian surface (Schubert et al., 1990). Directly linked to this endogenic and exogenic activity is the formation of localised hydrothermal systems (Abramov & Kring, 2005; Gulick, 1998). There is evidence of the existence of such systems both on the surface (e.g. Farmer, 1996) and

within the subsurface of the planet (Ehlmann et al., 2011). The detection of such systems is based on geomorphological and stratigraphic features (evidence of liquid water, impact craters, volcanic edifices). Also mineral deposits attributed to hydrothermal activity (such as sulfates, sulfides, hydrated phyllosilicates, jarosite, hematite, and amorphous silica) (Schulze-Makuch et al., 2007).

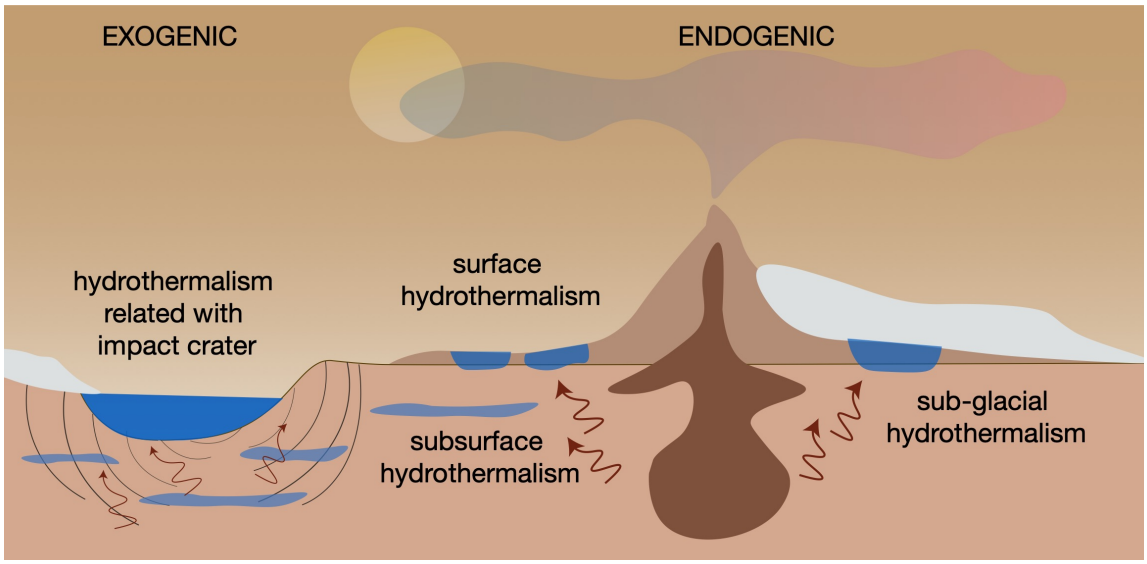

Figure 2-5. Schematic representation of the main hydrothermal systems (exogenic and endogenic) on the Martian surface during the Noachian and Hesperian periods.

Hydrothermal systems caused by exogenic impacts formed within the impact craters themselves (Abramov & Kring, 2005; Newsom, 1980; Rathbun &Squyres, 2002). The heat produced from the impact shock combined with the presence of significant ground ice created conditions conducive to hydrothermal activity (Figure 2-5). Conversely, endogenic hydrothermal systems related to volcanism were also active on the Martian surface (e.g. related to large volcanic complexes such as Tharsis and Elysium (Lanz & Saric, 2009; Schulze-Makuch et al., 2007). Specifically in Tharsis, intense volcanic activity is known to have triggered important hydrothermal events (Tanaka & Chapman, 1990). The Tharsis region was also associated with large deposits of ice (Cassanelli & Head, 2019), which could have created flowing water events, with hydrothermal water circulation (Tanaka et al., 2003). In the following section, different examples for Mars hydrothermal systems will be reviewed. These include systems from exogenic and endogenic origin, but also within endogenic, surface and subsurface systems, and subglacial volcanism (represented in schematic Figure 2-5).

Examples of hydrothermal systems on Mars

An example of an exogenic impact-crater generated hydrothermal system is the Toro Crater, located on the north edge of Syrtis Major. Spectroscopic observations detected hydrated silica, chlorites, and smectites between other typical hydrothermal mineralogy products (Marzo et al., 2010). The specific crater morphology also helped identify the exogenic origin of this hydrothermal system (Marzo et al., 2010).

A case of an endogenic hydrothermal system is Home Plate, in Gusev Crater. Home Plate hosts a relict surface hydrothermal system that was studied by the rover Spirit. Spirit observed opaline silica associated with volcanic material, evidencing hydrothermal activity (Ming et al., 2008; Ruff et al., 2007). High concentrations of amorphous SiO_2 (opal-A) were detected, which requires the presence of water for its formation (Ruff et al., 2011). An interesting observation from these locations was the high Ti concentrations present in the soil. Together, the high Si and Ti concentrations in this hydrothermal system evidenced intense basalt leaching, produced by contact with acidic waters (Squyres et al., 2008). The origin of the acidic water has been variously attributed to either fumarole acid leaching (Squyres et al., 2008), or hot spring geysers (Ruff & Farmer, 2016a).

The Syrtis Major volcanic complex is a larger example of endogenic volcanism with an associated surface hydrothermal system (Hiesinger & Head, 2004). Syrtis Major (Figure 2-6 A) is a Hesperian-aged volcanic system, with two related calderas: Meroe Patera and Nili Patera. The Nili Patera caldera presents a prominent volcanic cone topography (Figure 2-6 B). As with Home Plate, one of the main features that defines the hydrothermal system associated with Nili Patera caldera, are the hydrated silica deposits detected from orbital observations (Ehlmann et al., 2009; Skok et al., 2010).

Finally, a different case of Martian hydrothermal activity is the Eridania Basin hydrothermal seafloor (Michalski et al., 2017). The Eridania region is placed between Terra Cimmeria and Terra Sirenum, in the southern highlands of Mars. Remnant magnetism revealed that this area underwent ancient crustal spreading (Connerney et al., 2005). Mineralogy analysis reveals a clay-carbonate rich deposit at the bottom of the basin (saponite, mg-nontronite, serpentine and berthierine) (Michalski et al., 2017).

These mineralogy resembles typical hydrothermal alteration within volcanic ultramafic rocks, which were formed on ancient Mars (more than 2.3 Ga ago). The presence of Fe^{2+} clays reveals reducing conditions at the bottom of the basin, with chloride deposition at higher latitudes, toward the rim of the basin, interpreted to form from the evaporation of the basin sea water (Michalski et al., 2017).

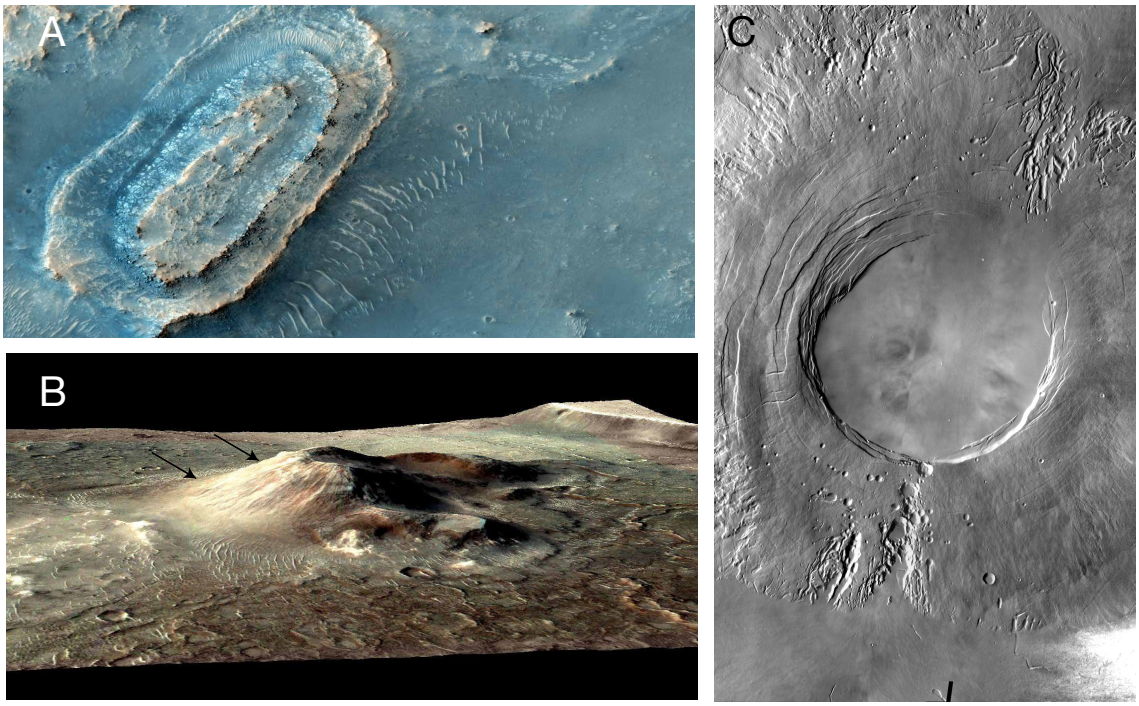

Figure 2-6. Images of Martian hydrothermal systems. a) NE Syrtis Major. In the image is a large shield volcano. Image taken by MRO, instrument HiRISE; the colours from the infrared colour composites (IRB). Credit to NASA/JPL-Caltech/University of Arizona. b) Nilli Patera volcanic cone. False colour derived from infrared wavebands from CRISM. Light tone patched areas are hydrothermal deposits (indicated with arrows). Credit to NASA/JPL-JHU-APL/Brown-Univ. c) Arsia Mons, image taken by with the Thermal Emission Imaging on Mars Odyssey. Credit to NASA/JPL-Caltech/University of Arizona.

Some of the Noachian clays have been suggested to be produced through subsurface hydrothermal activity under reduced and alkaline conditions (Ehlmann et al., 2011). Other minerals that accompany the Fe/Mg clays indicate temperatures >400 °C, only achievable at subsurface conditions (Ehlmann et al., 2011). Furthermore, impact craters have helped to expose the subsurface hydrothermal mineralogy of the Noachian and Hesperian periods. The materials exhumed in McLaughlin Crater reveal another subsurface hydrothermal system created by deep hydrothermal fluid-rich areas altering the crust (Michalski et al., 2013). These hydrothermal fluids were mixed with magmatic

fluids and Ca-Mg brines, with a surface representation of sulfates and layered clays with ice deposits (Michalski et al., 2013).

Lastly, endogenic Mars hydrothermalism has also been linked to glacial surface deposits, such as Arsia Mons (Scanlon et al., 2014). Arsia Mons erupted subglacially under high confining ice pressures in the late Hesperian (Figure 2-6 C). The eruption produced liquid meltwater creating fan-shaped deposits observed around the Tharsis Montes volcanic edifices (Scanlon et al., 2014). Another similar subglacial volcano is Sisyphi Montes. Sisyphi Montes is located in the Sisyphi Planum region on Mars, aged from late Noachian to late Hesperian (Tanaka & Scott, 1987). The mineral assemblages of gypsum, sulfates, smectites, zeolites and iron oxides characterise the subglacial intrusion (Ackiss et al., 2018), and are consistent with alteration minerals identified in glaciovolcanic hydrothermal sites in Iceland (Cousins et al., 2013).

2.1.5 NASA MSL Curiosity Rover and upcoming 2020 missions

The Sample Analyser at Mars (SAM) landed in 2012 on the Martian surface inside the Curiosity rover, with the main goal of detecting organic molecules (Grotzinger et al., 2012a). Since then, SAM has made a series of important measurements that have made several breakthroughs in our understanding of past Martian processes and habitability (ten Kate, 2018). In 2015, SAM detected the presence of organic molecules mixed with perchlorate salts in the Martian regolith (Freissinet et al., 2015). Four years later, it measured organics in Gale Crater lacustrine mudstones (Eigenbrode et al., 2018). The organics from lacustrine mudstone were released through pyrolysis, and the main organic products obtained were thiophenic, aromatic, and aliphatic compounds. Their conservation in the mudstone was linked to a sulfurisation process (Eigenbrode et al., 2018). Sulfurisation is the process of oxidation of sulfide around the organics acting as a coating. It protects the organics inside from further oxidation and promotes their preservation (Hebting et al., 2006).

Another significant discovery for SAM has been the measurement of methane variations in the Martian atmosphere; methane concentrations seem to be seasonal, as they peak in a rhythmic variation (Webster et al., 2015, 2018). It is thought that the source of methane is a large subsurface reservoir of unknown origin (Webster et al., 2018).

Methane could have been produced through serpentinisation of mafic minerals such as olivine and pyroxene (Oze, 2005), ultraviolet degradation of organics (Keppler et al., 2012), or geothermal processes (Etiope et al., 2011). This methane reservoir could also conceivably have been a product of biological processes such as methanogenesis (Atreya et al., 2007; Mumma et al., 2009). Last, SAM has also measured a large variability in the sulfur isotope composition measured in the sediments from Gale Crater (Franz et al., 2017). The large isotopic variations (Figure 2-7) are proposed to be equilibrium fractionation between sulfate and sulfide, due to an impact-driven hydrothermal system, with related atmospheric processing of sulfur gasses during warm periods (Franz et al., 2017)

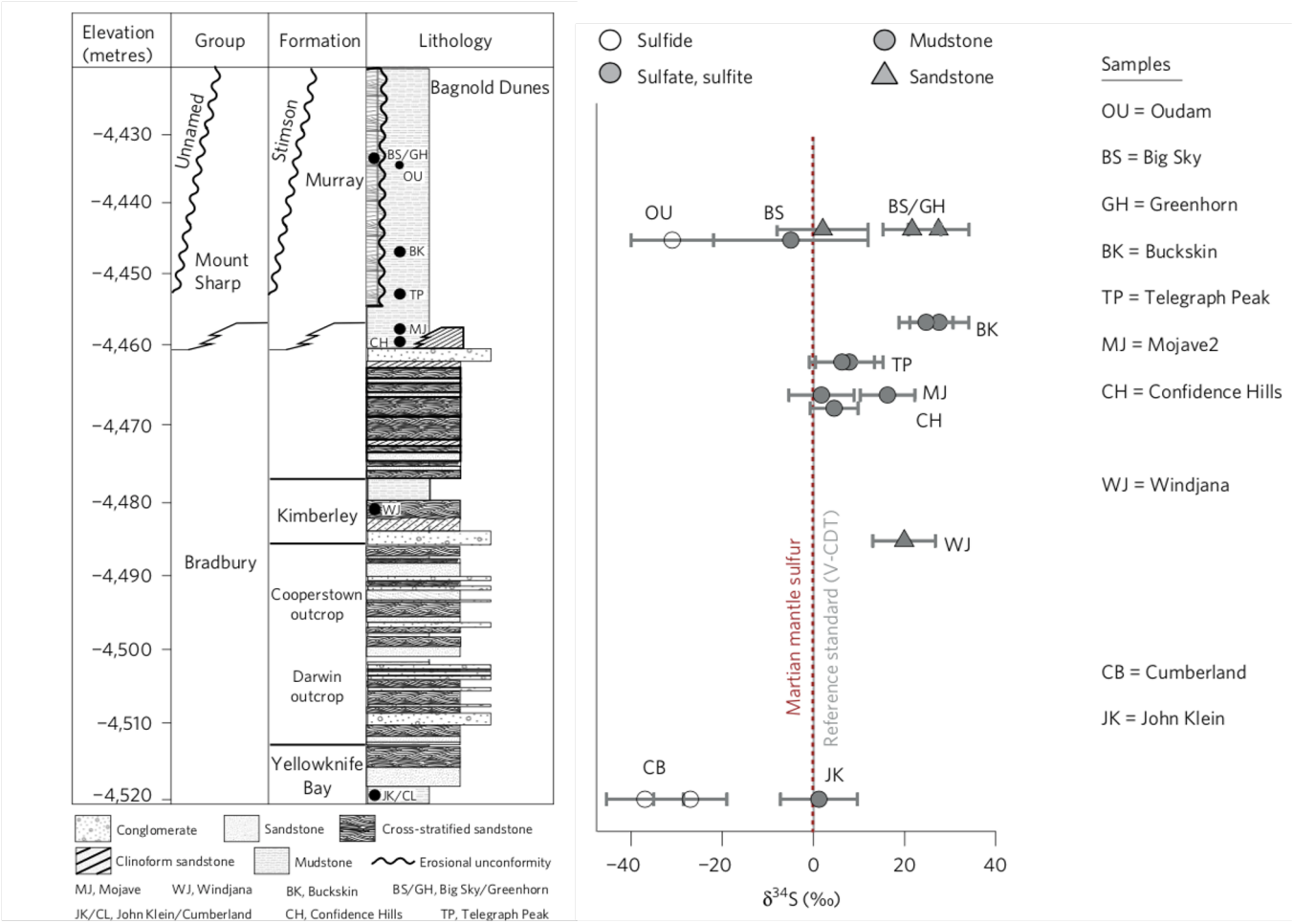

Figure 2-7. S isotope measurements performed in the Gale Crater mudstone (stratigraphy on the left for facies from Yellowknife Bay to Pahrumpp Hills) by the SAM instrument in the Curiosity Rover. Large S isotope fractionations can be seen between the sulfate and the sulfide. Image from Franz et al.(2017).

There are two upcoming rover missions to Mars, both launching in 2020: ESA's ExoMars 2020 mission (rover named Rosalind Franklin), and NASA's Mars 2020 mission. Both have a main goal to search for ancient environments where there is the potential for biosignature preservation, and for evidence of life that possibly once thrived on Mars. The two rovers will use different instruments and strategies to search for organic biosignatures.

The ExoMars 2020 mission will land at Oxia Planum (Figure 2-8 A), on Noachian age materials, targeted in order to maximise the potential for the preservation of organic biosignatures (Quantin et al., 2015). Oxia Planum is located in the Cogoon Valles system, between Ares Vallis and Marwth Vallis, very close to the global dichotomy. Oxia Planum is a clay-bearing deposit with evidence of Noachian phyllosilicates and later fluvio-deltaic deposits. Evidence of Fe/Mg saponite or smectite/mica phyllosilicates have been detected with OMEGA and CRISM. The Fe/Mg smectites cover more than 100 km^2 of terrain and are associated with rocks of early Noachian age, representing long-lived aqueous alteration processes (Mandon et al., 2019; Quantin et al., 2015). This unit is cut by hydrological geomorphological structures including valleys and inverted channels. The smectite unit is overlain by an 80 m thick deltaic unit of Hesperian age. The delta fan has a composition of hydrated silicates, and reveals the presence of a large standing water body covering the valley system. Overlying that is a lava layer considered to be Amazonian in age, eroded by aeolian processes (Quantin et al., 2015). The ExoMars Rosalind Franklin rover will be able to drill up to 2m (De Sanctis et al., 2017), which will be an advantage for the investigation of potential subsurface organic biosignatures.

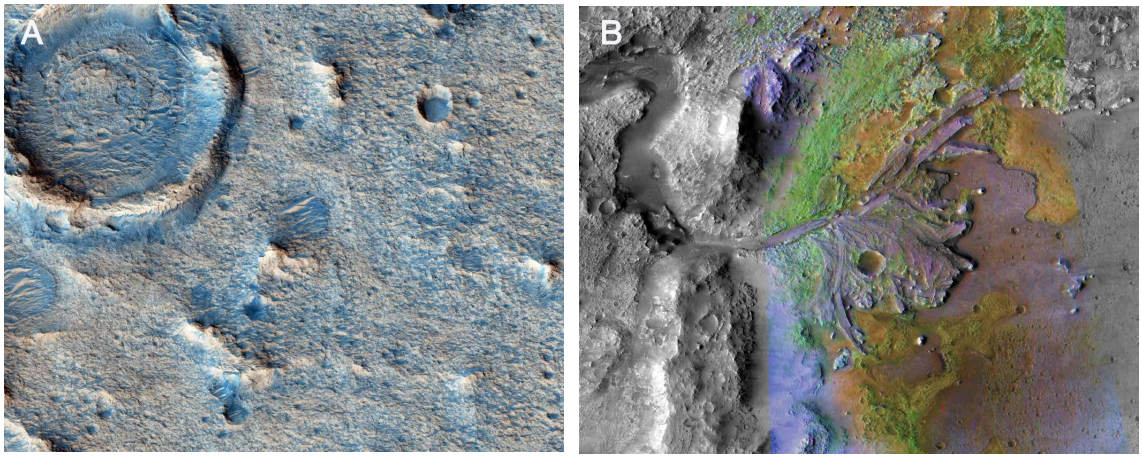

Figure 2-8. Images of landing sites for a) ExoMars 2020 mission: Oxia Planum. HiRISE image combined with CRISM. Credit to NASA/JPL-Caltech/University of Arizona. b) NASA 2020 mission: Jezero crater with the clear shape of deltaic deposits. Image taken by MRO's HiRISE and IRB colours from CRISM superimposed to show presence of minerals. Green colour is for carbonates, orange olivine sand eroding from carbonate-containing rocks.

The NASA 2020 mission will land at Jezero crater (Figure 2-8 B). Jezero crater is located north-east of the Syrtis Major volcanic province, described above in Section 2.1.4. The impact crater has a diameter of 45 km, and is an open lake basin acting as a catchment for two rivers that drained waters from the area of Nili Fossae (Fasset & Head, 2005). The rivers created fan deltas that delivered sedimentary materials (Figure 2-8 B) including hydrous minerals such as smectite clays, revealing episodes of water activity on Early Mars (Ehlmann et al., 2008a; Goudge et al., 2015, 2017). These deltaic deposits are thought to be ideal for the sequestration and preservation of organic material (Ehlmann et al., 2008a). Jezero crater fluvio/deltaic sediment deposition is aged between the late Noachian and early Hesperian, and thought to represent circum-neutral/low salinity waters (Fasset & Head, 2005; Goudge et al., 2017; Schon et al., 2012). Of the two fluvio/deltaic systems, the western one is dominated by Fe/Mg smectites, and the northern by Mg-Carbonates (Ehlmann et al., 2009; Goudge et al., 2015). A volcanic unit, comparable to the one identified at Oxia Planum, overlies most of the basin fill (Goudge et al., 2015; Schon et al., 2012). The NASA 2020 mission will target the deltaic bottom sediment sets, Fe-Mg smectites and lacustrine Mg-carbonates. It is thought that the lacustrine units have the highest potential to preserve organic matter (Ehlmann et al., 2008a; Gupta & Horgan, 2018). Notably, the NASA 2020 mission has a complex mechanism for collecting and storing rock samples inside sealed tubes, for a future

sample return mission. These returned samples open up potential to use a full suite of analytical capabilities on Earth. For Jezero's deltaic and lake samples collected for a return mission, there are plans to perform chemical and isotopic measurements to search for biosignatures (Gupta & Horgan, 2018). It is therefore fundamental to inform what kind of samples should be prioritised for storage during the mission.

2.2 Mars Analogues

Analogues - places on Earth that resemble environments on Mars (or other planetary bodies)- can be used as working models for past or present day processes on Mars, aiding the interpretation of data returned from missions. Analogues can be used to inform about the habitability of certain environments, and to understand how life can be preserved in the sediments or in the rock record. The astrobiological study of any analogue involves: i) understanding how the environment creates the conditions that makes the environment habitable, ii) identifying the life that inhabits those environments, and iii) recognising how life is preserved in the resulting geological record as a biosignature (Preston et al., 2014). They are also important for testing future mission instrumentation that will go to Mars by helping to find the best way to detect Mars-relevant minerals and biosignatures with mission instruments (Allender et al., 2020; Black ,2018). Overall, our interpretation of Martian geology and mineralogy is largely based on our understanding of terrestrial analogue deposits (Preston et al., 2014).

These Mars analogue locations, comparable in their environmental conditions, morphology, geochemistry and lithology to Mars have been studied for decades (Preston et al., 2014). Previous analogue studies have included evaporative lakes (e.g. Western Australia: Benison & Bowen, 2006; Conner & Benison, 2013), iron-sulfate acid watercourses (e.g. Rio Tinto: Amils et al., 2007; Fernandez-Remolar et al., 2005), impact craters (e.g. Devon Island: Cockell & Lee, 2002, Osinski et al., 2013), and hydrothermal environments (Black & Hynek, 2018b; Cousins et al., 2018; Ruff & Farmer, 2016a). Mineralogical and aqueous geochemical studies at analogue sites are of relevance to the habitability of early Mars, as the local geochemistry determines the availability of

different energy and carbon sources for life, and provides a modern-day natural laboratory within which to explore the relationship between aqueous geochemistry and the deposited minerals.

An example of an iron-rich terrestrial Mars analogue site is Rio Tinto, Spain. Rio Tinto has been studied as an analogue for the acidic sulfate and iron-rich waters that flowed during the Hesperian that produced sulfate deposits (Amils et al., 2007). Rio Tinto is located in the south of Spain, and originates from the waters that infiltrate into a gossan deposit (iron sulfides, pyrite). This causes the river to flow out of the gossan with high concentrations of sulfates, and form iron oxide deposits, like the ones detected in Meridiani Planum (Fernandez-Remolar et al., 2005). There have been many studies of the microbial communities in the river, as extremophiles thrive in the river in intense conditions of metal concentrations and low pH. These extremophiles generate morphological biosignatures that are preserved in the iron sulfate jarosite, iron oxyhydroxides, and iron oxide minerals formed (Sánchez-Andrea et al., 2011, 2013, 2014). All these minerals have been detected by the NASA Opportunity rover on the Meridiani Planum (Kaplan et al., 2015; Klingelhöfer et al., 2004).

2.2.1 Hydrothermal Mars analogue systems

Terrestrial subaerial hydrothermal systems are excellent analogues for Mars hydrothermal systems. They promote environments with a wide variety of pH and temperature, and mineralogy resembling those of Mars hydrothermal systems (Pirajno & Kranendonk, 2017). They are also rich in volcanic gases that expel sulfide and promote high concentrations of sulfate in the waters, that can be used by microorganisms (Des Marais & Walter, 2019b; Westall et al., 2018). The volcanic gases alter the basaltic rocks around generating mineral assemblages that resemble typical Mars alteration products (Black & Hynek, 2018b; Cousins & Crawford, 2011; Hynek et al., 2018). Some of the terrestrial hydrothermal activity products are Al-clays such as kaolinite, montmorillonite, Ca-Al-Fe-Mg sulfate, Fe oxides, and hydrated SiO_2 (e.g. Black & Hynek, 2018; Cousins & Crawford, 2011; Cousins et al., 2013; Ruff & Farmer, 2016a; Szynkiewicz et al., 2018, 2019a,b). One example of a Mars hydrothermal analogue is the El Tatio hydrothermal system, in Chile (Figure 2-9). El Tatio is an analogue of Home Plate, Gusev Crater, and was studied by Ruff & Farmer (2016). El Tatio

is located in a desert environment, presenting very low rainfall and very high UV exposure. Water pH from El Tatio resembles the pH interpreted for fluids operating at Home Plate, and presents structures made with opal A silica sinters, with nodular outcrops that are morphologically-similar to the ones found in Home Plate (Figure 2-9). Ruff & Farmer (2016) revealed the El Tatio nodular structures to be a mixture between abiotic and biotic processes. (Figure 2-9).

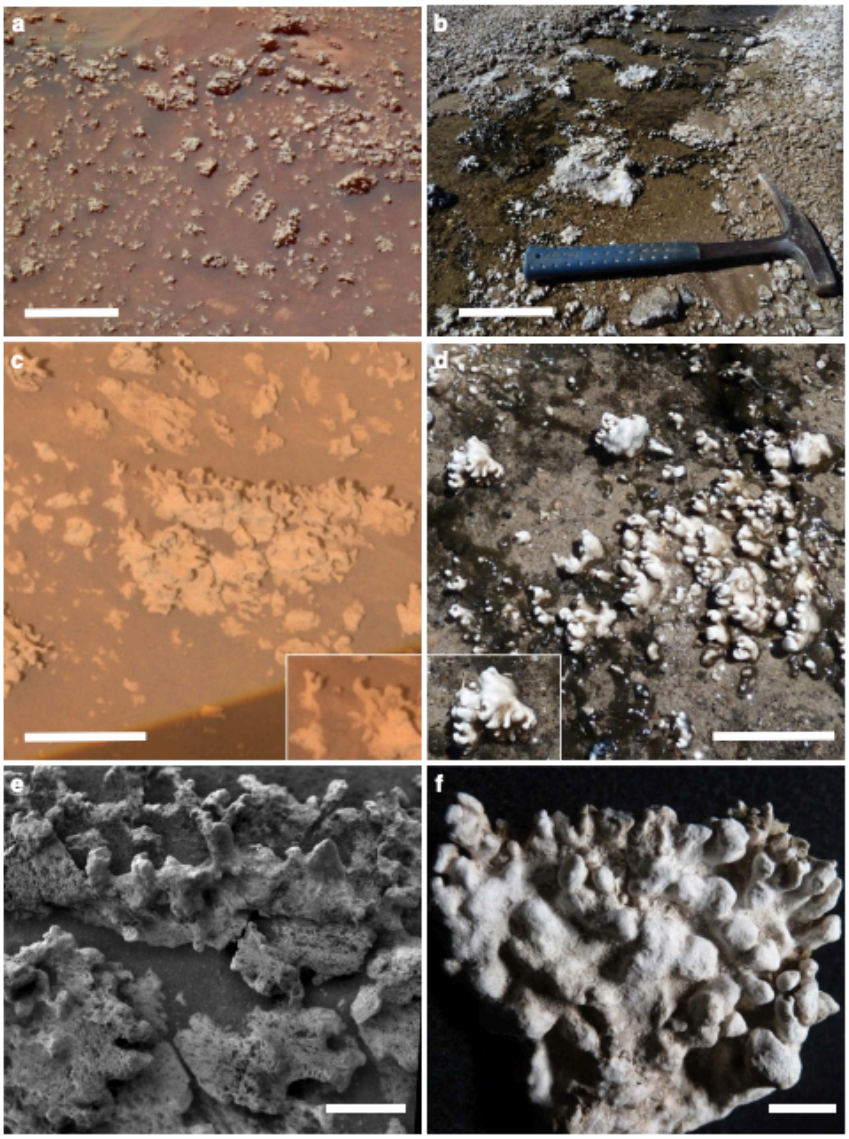

Figure 2-9. Images from El Tatio (Chile) hydrothermal analogue study from Ruff et al. (2016). a) is the opaline from Mars Home Plate, b) at the same scale for El Tatio. Scale bar a and b is 10cm. c) Home Plate high-resolution image with 5cm scale bar, d) El Tatio closer image, 5cm scale bar. e) closer scale at silica structures Mars, with f) closer look at silica structures at El Tatio (scale bar e,f, 1cm).

2.2.2 Microbiology of terrestrial hydrothermal systems

Hydrothermal systems are a candidate location for the origin of life on Earth, as thermodynamic modelling predicts spontaneous reactions can generate the basic blocks for life (Russell, 2003; Shock & Schulte, 1998). The universal tree of life also supports a hydrothermal origin of life, as thermophiles occupy the deepest phylogenetic branches (Barns et al., 1996). Usually, at temperatures above 60 °C, macroorganisms are absent in hydrothermal systems and the main productivity is driven by microorganisms (Rothschild & Mancinelli, 2001).

Yellowstone National Park (USA) is one of the most well studied terrestrial hydrothermal systems. A study by Meyer-Dombard et al. (2005) presents a variety of chemotrophic and phototrophic thermophilic communities dominating the Yellowstone hydrothermal system. *Crenarchaea,* affiliated with deep branching in the tree of life, exist in all the pools. The bacterial community at the locations studied is dominated by *Aquificales* and *Thermo-desulfobacteriales*. They represent anaerobic hydrogen oxidation as the central metabolism of these ecosystem (Meyer-Dombard et al., 2005). Other studies in Yellowstone by Colman et al. (2016, 2019) describe how deep geological processes of phase separation control the ecology of thermophilic communities through the availability of nutrients (minerals, gases, dissolved ions). Moreover, the main metabolism of the springs are mineral-based such as S^0 oxidation/reduction and Fe-oxidation/reduction predominating in the sediments (Colman et al., 2016, 2019). In Iceland, a study observed *Aquificales* phylum dominating the community across 12 different hot springs (temperatures from 70- 97 °C, pH from 2-7) (Reigstad et al., 2010). Another study of Archaea diversity in Icelandic hot springs shows that the community at high temperature (80-90 C) acidic (pH 2) solfataras is dominated by *Sulfolobales* and *Thermoproteales*(Kvist et al., 2007).

2.2.3 Mars-analogues used for this study

For this research, two sites in Iceland and one in the Canadian Arctic were explored as Mars analogues (Figure 2-10). These two localities were ideal to serve as analogues due to their exposed outcrops, lack of vegetation, little anthropogenic disturbance, year-

round or seasonal sub-zero temperatures, and low levels of precipitation (Cousins, 2015; Pollard et al., 2009).

One of the unique characteristics of Iceland is the similarity with Martian volcanism; they can be compared at many levels, from the geomorphology to the lithology to the type of volcanic events. Iceland is a volcanic island, that lies on top of a mantle plume and is part of the Mid Atlantic Ridge (Gudmundsson, 2000; Sigvaldason 1974). Iceland was formed as a result of a rifting episode leading to the opening of the North Atlantic (60 Ma) (Sigmundsson & Sæmundsson, 2008), and comprises predominantly of basalt. The majority of the basalts are of tholeiitic composition, transitioning to alkali (Jakobsson et al., 2008; Sigmarsson, & Steinthórsson 2007). Even though Icelandic basalts are younger, they are relevant to Mars as they are enriched in Fe relative to most terrestrial basalts, reassembling the composition of basaltic shergottites (Nicholson & Latin, 1992).

Iceland also exhibits geomorphological Mars analogue features such as rootless craters (formed by steam explosions when lava crosses a wet surface) (Fagents & Thordarson, 2007), and glaciovolcanism (Cousins & Crawford, 2011; Cousins et al., 2013; Cousins, 2015). Due to its high latitude, many of Iceland's volcanoes were once (and some are still) covered by glaciers, which leads to subglacial volcanism, resembling Martian volcanism in Tharsis, NE Syrtis, Arsia Mons, Sysphi Montes and other volcanic systems (Ackiss et al., 2018; Cassanelli & Head, 2019; Hiesinger & Head, 2004; Scanlon et al., 2014). Icelandic subglacial volcanism has important implications for habitability studies, as the sub-ice eruptions create subglacial lakes and hydrothermal activity (Björnsson, 2003; Jóhannesson et al., 2007; Óladóttir et al., 2011a). Furthermore, there have been microbiological studies in these volcanically-driven subglacial lakes, showing microbial communities similar to the surface hydrothermal systems. The communities were dominated by anaerobic and microaerobic chemolithotrophic Fe/reduction, sulfate reduction and sulfide oxidation, (Gaidos et al., 2009; Marteinsson et al., 2013). More recently, surface manifestations of volcano-ice hydrothermal activity have been studied at the subglacial-erupted volcano Kverkfjöll. Surface active hydrothermal pools, mudpots, hot springs and glacial melt water lakes were found resulting from volcano-ice interaction here (Cousins et al., 2013). The chemical conditions of these

hydrothermal surface systems are sulfate dominated, with temperatures between 0-99 °C and acidic to neutral pH (2- 7.5), and secondary mineral alteration was dominated by sulfates (gypsum, jarosite), iron oxides (goethite, hematite) and pyrite (Cousins et al., 2013). A microbial study by Cousins et al. (2018) at the Kverkfjöll hydrothermal spring (38- 60 °C, pH 3-5) revealed a community differentiated between the source and downstream sites. At the source (micro-oxic conditions) the microbial community was dominated by bacteria *Hydrogenobaculum* and archaea *Thermoproteales*. Conversely, downstream (oxic conditions), the environment was dominated by archaea *Sulfolobales* and other bacterial sulfide oxidisers (Cousins et al., 2018).

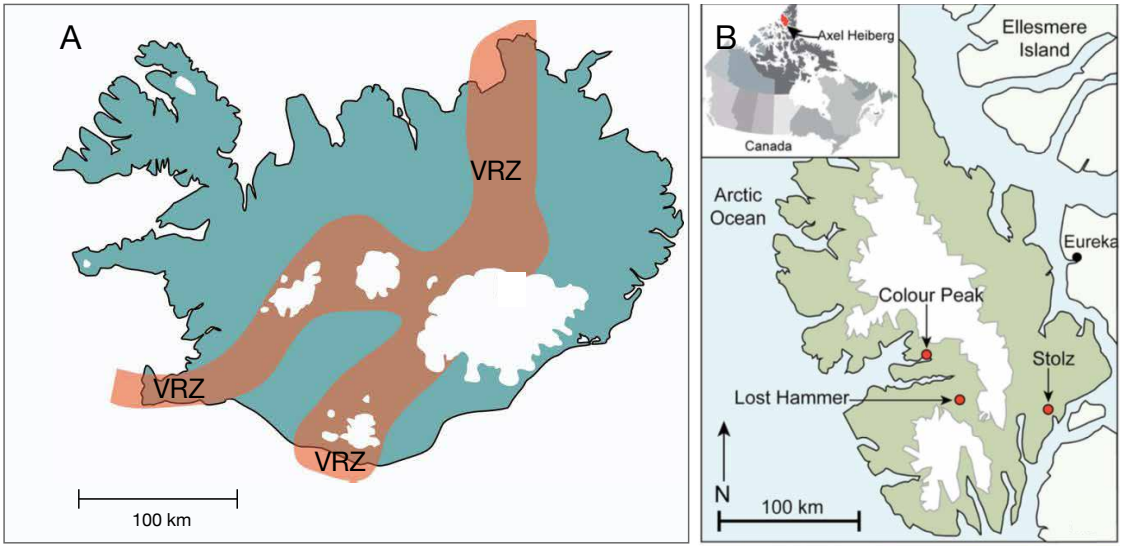

Figure 2-10. Maps from analogues relevant for this thesis, Iceland and AHI. a) Iceland map with Volcanic Rifting Zone in orange (VRZ). b) AHI map from Fox-Powell et al. (2019) with Lost Hammer site indicated, relevant for this study.

Arctic Axel Heiberg Island (AHI), Canada, is also an ideal Mars analogue (Battler et al., 2013; Pollard et al., 2009). AHI has multiple salt diapirs, low air temperatures, with permafrost underlying the surface (Battler et al., 2013; Fox-Powell et al., 2019; Pollard et al., 1999, 2009). Hypersaline springs surrounded by cold and dry conditions are directly analogous to the Martian late Noachian-Hesperian period (Pollard et al., 2009). The saline springs present in AHI maintain their liquid state despite the sub-zero air temperatures they experience (Pollard et al., 1999), and permafrost polygonal terrains have been found in the region, similar to those identified on Mars (Pollard et al., 2009). Microbial communities have also been found within the hypersaline springs (Colangelo

et al., 2019; Magnuson et al., 2020). Similar hypersaline springs may even be responsible for structures observed on Mars (Battler et al., 2013). This site provides a non-volcanic, but high-sulfur environmental contrast to the Icelandic hydrothermal sites.

2.3 Microbial Biosignatures

A biosignature is a physical or chemical change to an environment, which is a direct consequence of biological activity that creates an object, substance or pattern (Cockell et al., 2016; Hays et al., 2017; Schwieterman et al., 2018). The most characteristic type of biosignature used to reconstruct ancient macroscopic life on Earth are fossils. However, the formation of biosignatures is not restricted to a macroscopic scale, biosignatures can also be formed at microscopic scale, and also at a molecular or an atomic scale. For example, by preserving anomalies in isotopic masses, or in organic compounds specific to life.

Examples of biosignatures for the detection of life on other planets are organic biomarkers, spectral gases in atmospheres, microbial-sedimentary structures, and isotopic biosignatures, amongst others (Rugheimer et al., 2015; Simoneit & Summons, 1998; Westall, 2008) (summarised in Figure 2-11). The study of biosignatures in analogue environments is essential to learn how to detect and recognise them as evidence for life elsewhere. Equally important is to know how to detect and understand abiotic (non-biological) processes that can produce similar signatures (Des Marais et al., 2002). These will help to distinguish biological signatures from abiotic ones, and guide the process of analysing and detection (Hays et al., 2017). Biosignatures produced by microbial activity are particularly relevant for Mars exploration, as it is thought that if life ever emerged on Mars, it would have been microbial (Westall, 2008).

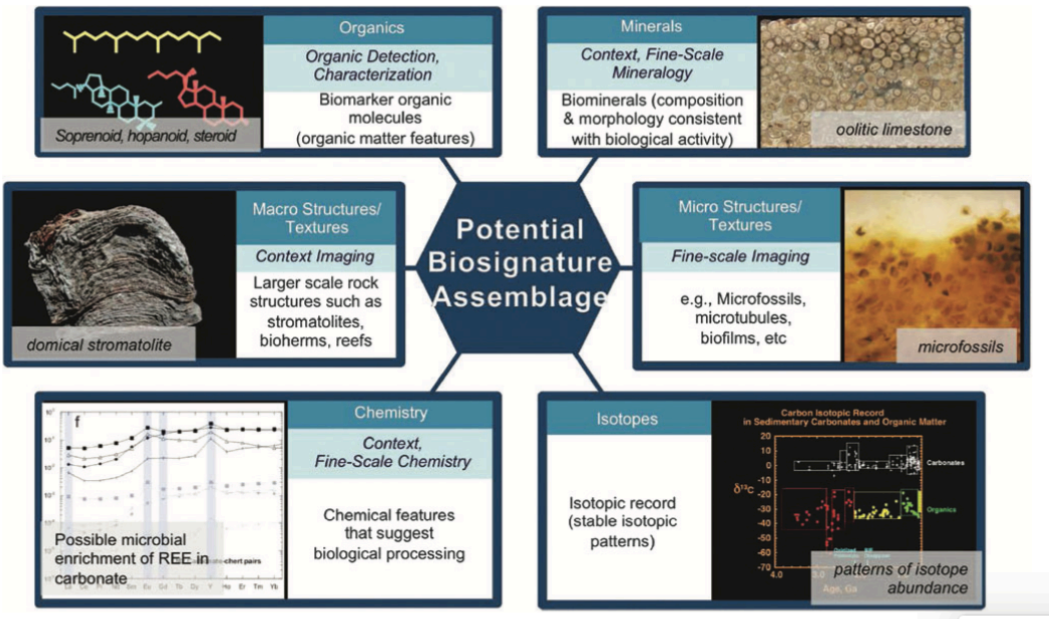

Figure 2-11. Diagram from Hays et al. (2017) presenting the different types of biosignature assemblages in which the astrobiology community is considering for exploration purposes.

Microorganisms can live in associations of microbial mats or biofilms, producing macroscopic biological fabrics that eventually get preserved in the rock record (Djokic et al., 2017). Other types of lithological microbial biosignature include tubular or granulated fabrics in basaltic volcanic glass in ocean (e.g. McLoughlin et al., 2009) and subglacial (Cousins et al., 2009) settings. Organic biomarkers exist as distinctive organic carbon molecules in a rock (Morowitz, 1993). These can be molecules such as fatty acids, porphyrins, amino acids and others that help sustain key biochemical functions in organisms and are part of the cellular structure (Summons et al., 2008).

Isotopic biosignatures provide evidence for the metabolic activity of microorganisms. This metabolic activity can be measured using the difference in the masses of isotopes from associated geochemical products captured in sediments, rocks or minerals (e.g. Des Marais & Jahnke, 2019a; Horita, 2005; Kaplan & Rittenberg, 1964b). Carbon and sulfur are commonly-used stable isotopes for these metabolic processes (Havig et al., 2017). Other traditional (e.g. N, O: Kobayashi et al., 2019) and non-traditional (e.g. Fe, Cu: Icopini et al., 2004; Navarrete et al., 2011) stable isotope systems have been used in a similar manner, including in hydrothermal settings.

On Earth, organic biomarkers have been shown to preserve under taphonomic windows – time and space ideal sedimentary and diagenetic conditions that facilitate preservation (Summons et al., 2011). Some of these ideal conditions are: burial on clay-rich-fine grained sediments, rapid cementation, reducing conditions in sediments and water, precipitation in silica sinters, etc. (Farmer & Des Marais, 1999; Hays et al., 2017; Westall & Cavalazzi, 2011). Instead, other processes can decrease the preservation of biosignatures or eliminate them. Some examples of these processes on Earth are weathering, diagenesis, high temperature and pressure, impact cratering, surface oxidants and radiation (Hays et al., 2017 and references therein). Post-burial diagenesis can also alter the preservation of biosignatures by compacting, cementing, dissolving and replacing biosignatures through time (Westall, 2008). All these processes are applicable to Mars' dynamics, a side from processes on Earth deriving from plate tectonics. Biosignatures are far from infallible tools and their preservation over time is complicated.

2.3.1 S and C stable isotope biosignatures

Carbon (C) and sulfur (S) isotopes are influenced by biological processes, and can be recorded in the rock record (e.g. Canfield et al., 2001; Fike et al., 2015; Havig et al., 2011, 2017). Enzymatic reactions performed by life can play major roles in the isotopic composition of biomolecules produced during assimilatory processes, and compounds cycled during dissimilatory processes. Enzymes perform kinetically controlled chemical reactions that happen at faster rates than if they were produced abiotically. The product of these enzymatic reactions are typically enriched in the lighter isotope relative to the reactant, with the magnitude of the differences in isotopic compositions between the reactant and the product the result of the isotopic discrimination that happens during that reaction (Brunner & Bernasconi 2005; Canfield & Thamdrup 1994; Canfield et al., 2001; Chambers et al. 1975; Fry et al. 1984). The magnitude of this discrimination, also called fractionation, can help to identify the specific enzymatic reaction mechanisms responsible (Canfield & Teske 1996, Johnston et al. 2005b, Leavitt et al. 2013, Philippot et al. 2007, Shen et al. 2001). The light isotope products and heavy isotope reactants can become biosignatures when preserved in the sediment or rock record (Fike et al., 2015 and references therein).

On Earth, deep time records for C isotopes ($\delta^{13}C$) have been documented mainly based on inorganic and organic carbon from stratigraphic studies of marine carbonate rocks. The carbon isotope record of geological time is to a large extent defined by changes in the partitioning of carbon between organic carbon and carbonate, linked directly to the biosphere and the global carbon cycle (Saltzman & Thomas, 2012). Deep time records of Earth's S isotopes ($\delta^{34}S$) are based on marine sulfate (gypsum, anhydrite, marine barites, Carbonate Associated Sulfate (CAS)) and pyrite (Canfield 2001a; Claypool et al., 1980; Richardson et al., 2019). Records from $\delta^{34}S$ evaporites helped reconstruct the nature of ancient ocean basins and past seawater sulfate (Raab & Spiro, 1991), and CAS $\delta^{34}S$ informes about carbonate abiotic and biological carbonate precipitation (Fike et al., 2015; Rose et al., 2019). The deep time $\delta^{34}S$ pyrite records are mainly from Microbial Sulfate Reduction (MSR), but are also connected to the overlying sea water column (Canfield 1991, Fike et al., 2015).

2.3.2 Carbon isotope biosignatures

Carbon (C) has two stable isotopes, ^{12}C and ^{13}C. In autotrophy, carbon is fixed into biomolecules from oxidised forms of carbon, such as CO_2. During the autotroph process, carbon isotope fractionations between the substrate (CO_2) and product (organic C) are produced, with the magnitude of fractionation depending on the enzymes involved for different carbon fixation pathways (Zerkle et al., 2005), (Figure 2-12).

The predominant carbon fixation pathways in microorganisms are: i) the reductive pentose phosphate cycle (Calvin- Benson- Bassham cycle), ii) reductive tricaborxylic acid cycle (TCA), iii) 3-hydroxypropionate cycle (3-HP), iv) reductive acetyl-CoA, and v) Ribulose Biphosphate Carboxylase-Oxygenase (RuBisCO). The TCA and 3-HP pathways produce carbon isotope fractionations no larger than 20 ‰, and the Acetyl-CoA pathway typically produces fractionations between 15 to 40 ‰ (House et al., 2003; Preuß et al., 1989; Zerkle et al., 2005). RuBisCO is mainly used by cyanobacteria, algae and plants, and produces fractionations of up to 30 ‰ (Hayes, 2001; House et al., 2003).

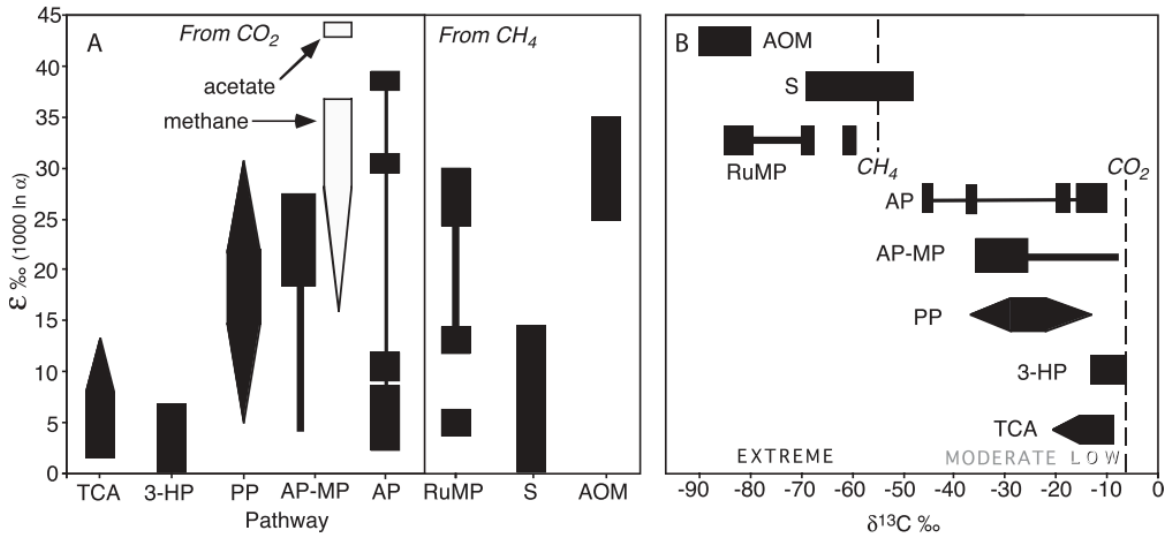

Figure 2-12. Main C isotope fractionations produced by different carbon fixation pathways from Zerkle et al. 2005).

Some of the oldest evidence of life on Earth is argued on the basis of C isotope values measured from organic carbon ($\delta^{13}C_{Org}$) (e.g. Des Marais 1997, Shidlowski, 2001). Through the carbon fixation pathways just described, the organic C (biomass) in the sediment is depleted in ^{13}C while the inorganic C (preserved as carbonate in sediments) is enriched in ^{13}C (Zeebe & Wofl-Gladrow, 2001). Measurements of $\delta^{13}C_{Org}$ in sediments deposited during the Archaean broaden the hypothesis of how early life evolved on Earth (Schidlowski, 2001). For example, the 3.23-3.5 Ga volcanic sequence in Pilbara and Kaapval (Australia and South Africa, respectively) cratons, present $\delta^{13}C_{org}$ from -41 to -25 ‰ (Des Marais, 1997; Strauss, 1992). The $\delta^{13}C_{org}$ record is similar to modern biomass from methanogens (Schidlowski, 2001), supporting molecular clock data which could indicate that methanogenesis had developed by 3.6 Ga (Battistuzzi et al., 2004; Walker, 1997).

Preservation of Carbon isotope biosignatures in the rock record

An important factor to evaluate when interpreting rock-record $\delta^{13}C$ potential biosignatures like the previously described, is the capability of diagenesis to alter $\delta^{13}C$ values (Cochran et al., 2010). The main diagenetic processes affecting rock-record $\delta^{13}C$ are chemically evolved porewaters, meteoric fluids, dolomitizing fluids, and brine fluids (Richardson et al., 2019). As an example, meteoric diagenesis alters carbonate towards

a more negative $\delta^{13}C$ value, with the introduction of isotopically light carbon from meteoric waters. The incorporation of ^{12}C from meteoric oxidised organic matter needs to be evaluated when observing a negative $\delta^{13}C$ excursion, as it can be masking the signal, which is typical of sediments with low concentrations of $CaCO_3$ (Zachos et al., 2005).

C isotope biosignatures in modern hydrothermal systems

$\delta^{13}C_{Org}$ is studied in modern hydrothermal environments in order to understand biogeochemical dynamics (e.g. carbon cycling during microbial metabolisms, Zhang et al., 2004). Similarly, is used to examine the potential for preservation of $\delta^{13}C_{Org}$ as a biosignature in different types of hydrothermal deposits (Bradley, 2008). These studies suggest that $\delta^{13}C_{Org}$ measurements are a potent tool that can be used to identify functional metabolisms and changes in microbial community structure within modern hydrothermal systems (Zhang et al., 2004).

For example, total $\delta^{13}C_{Org}$ and $\delta^{13}C$ of lipid biomarkers (fatty acids) were previously examined in hot springs of Yellowstone National Park, US, in an attempt to understand the dynamics of C cycling during microbial metabolisms in different environments of travertine precipitation (Zhang et al., 2004). The total $\delta^{13}C_{Org}$ biomass values (-15 ‰) suggested the TCA pathway was the dominant pathway for CO_2 fixation in this environment. However, distinct $\delta^{13}C$ values in fatty acids from the same environment implied the involvement of other biosynthetic pathways in the system (Zhang et al., 2004). A different study, also in Yellowstone National Park, was done to aid the interpretation of fossil stromatolites and microbial mats (Schuler et al., 2017). In this study, $\delta^{13}C_{Org}$ values were similar to the ones found in the fossil stromatolites (-11 to 24.3 ‰). Lastly, a study of $\delta^{13}C_{Org}$ from the ocean floor Lost City Hydrothermal Field system by Bradley et al. (2009) revealed that $\delta^{13}C_{Org}$ varies from -21.5 to -2.8 ‰. The different lipid assemblages and $\delta^{13}C$ values here indicate fatty acids were likely produced by hydrogen-consuming methanogens that are in conditions of CO_2 limitation. An important discovery of this study was that under limited conditions of CO_2, biotic production is not differentiated from abiotically produced $\delta^{13}C_{Org}$ (Bradley et al., 2009). Overall, $\delta^{13}C_{Org}$ studies in hydrothermal springs have helped to identify the main metabolisms performing carbon fixation pathways, even though in the case for Lost City

Hydrothermal Field, the biotic signatures are not necessarily distinct from abiotic values.

2.3.3 Sulfur isotope biosignatures

Sulfur (S) has 4 stable isotopes, with mass 32, 33, 34 and 36 respectively. S is one of the most abundant elements on Earth. The S biogeochemical cycle is important on Earth, due to the large range of oxidation states that S offers (Figure 2-13). Microorganisms benefit from these redox states to perform: i) metabolic dissimilatory microbial sulfate reduction (MSR), ii) microbial sulfur disproportionation of intermediate compounds (MSD), and iii) sulfide and S oxidation (Sox) (Figure 2-13). MSR and MSD produce H_2S largely depleted in ^{34}S during their metabolisms, leaving an isotopic composition of metal FeS_2 in the sediment with a distinctively negative $\delta^{34}S$ composition (e.g. Canfield, 2001a, 2001b; Fike & Grotzinger, 2008; Johnston et al., 2008b).

Sulfur can be assimilated into biomass or used in energy yielding reactions during dissimilatory processes in microorganisms. S is used as an essential element for building molecules, but also in respiratory oxidation-reduction processes to produce energy for growth (Zehnder & Zinder, 1980). Both of these processes can leave a chemical imprint within the environment (Canfield, 2001a). When S is used for assimilatory purposes, S is incorporated into the structure of amino acids such as cysteine and methionine, but it also can play a role in electron transport complexes (Fe-S) and in the coenzymes (Zehnder & Zinder, 1980).

Dissimilatory S transformations are those where S is used for respiration in geomicrobiology processes. In these reactions, in order to produce energy there is a transfer of electrons that happens inside the cell (Rabus et al., 2013). This transfer of electrons produces energy that is used for growth (Pereira et al., 2011). In order to perform this transfer, the S species need to donate or receive electrons, depending on the reaction. Usually oxidised forms of S (S^0, SO_4^{2-}) are used as electron acceptors. Then, the reduced forms of S (as H_2S, or HS^-) are used as electron donors, and they are coupled to oxidation of compounds such as hydrogen (H_2) (Dahl & Trüper, 1994).

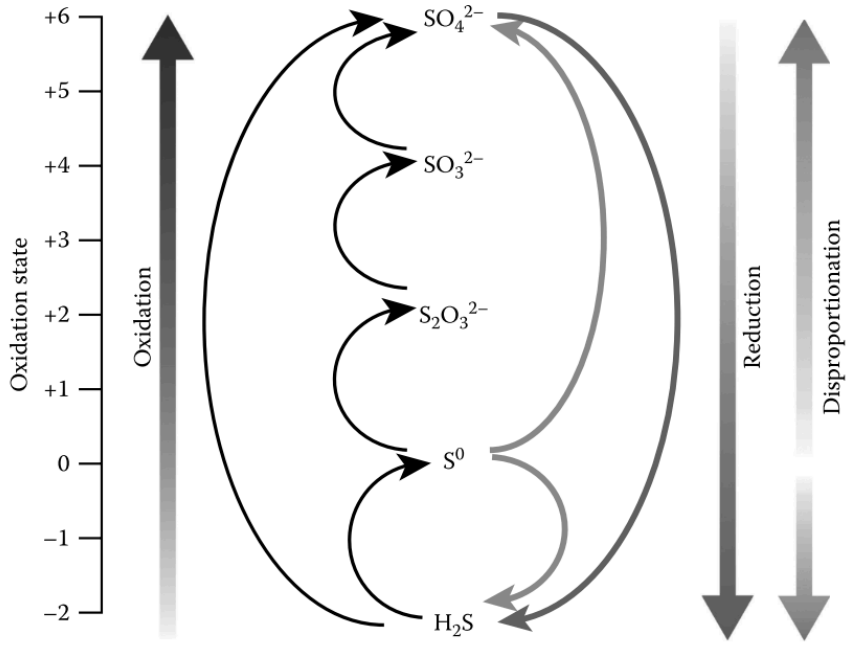

Figure 2-13. Schematic of redox transformations related with the microbial sulfur-cycling: Sulfate Reduction, Sulfide Oxidation and Disproportionation, from Fike et al. (2015).

Microbial Sulfate Reduction (MSR)

MSR pathways are performed by microorganisms in both the Archaea and Bacteria, and are significant contributors to the Earth's biogeochemical cycles (Pereira et al., 2011). In Earth's ocean, MSR is coupled to the oxidation of organic compounds, playing a large role in both C and S cycles (Rabus et al., 2013). The majority of cultured and identified MSR are strict anaerobes. They are mainly heterotrophs as they prefer organic electron donors, such as lactate, pyruvate, fumarate, malate, and ethanol, even though they can also grow autotrophically (Detmers, 2001; Rabus et al., 2016). Most of the MSR autotrophs discovered to date are mesophilic and thermophilic (Widdel & Pfenning, 1977. Autotrophic MSR use H_2 as an electron donor: for example *Desulfovibrio* and *Desulfotmaculum* have been grown autotrophically with H_2 (Klemps et al., 1985). Some autotrophic MSR assimilate CO_2 by TCA cycle with H_2 and SO_4^{2-} (Lovley et al., 1982). MSR grown in pure cultures have been observed to produce S isotope fractionations larger than >65 ‰ between SO_4^{2-} and H_2S (Detmers, 2001; Sim et al., 2011a). The extent on the S isotope fractionations depending on the strain, and environmental parameters such

as the abundance and type of organic carbon source, sulfate concentrations, and temperature (e.g. Detmers, 2001; Hoek et al., 2006; Sim et al., 2011b).

Oxidative Sulfur Cycling (Sox)

Oxidation of reduced H_2S or S is coupled to the reduction of O_2 (Friedrich et al., 2001). These processes typically happen in oxic environments, including marine sediments and hydrothermal systems. Bacteria performing Sox are usually autotrophs, that oxidise H_2S or S to SO_4^{2-} to assimilate CO_2 (Friedrich et al., 2005; Ghosh & Dam, 2009). Some of them can also oxidise sulfur species to intermediate compounds, like S^0 or thiosulfate ($S_2O_3^{2-}$). Within Sox, some can also perform anaerobic oxidation of H_2S with NO_3^{2-} (Kamp et al., 2006). The majority of anaerobic bacteria that oxidise H_2S or S^0 to perform CO_2 reduction are photolithotrophs (Holt, 1984),represented by photosynthetic purple and green bacteria and certain cyanobacteria (Pfenning, 1977). The S isotope fractionations performed between H_2S and SO_4^{2-} are smaller than MSR, but vary between -3 and -12‰ (Fry et al., 1988; Pellerin et al., 2019; Zerkle et al., 2009).

Microbial Sulfur disproportionation (MSD)

As well as MSR and S oxidation, some S cycling microorganisms are capable of performing Microbial Sulfur Disproportionation (MSD) (Bak & Pfenning, 1977). MSD reduces and oxidise species (S^0, SO_3^{2-}, or $S_2O_3^{2-}$) to produce both sulfate and sulfide (e.g. Frederiksen & Finster, 2003). The disproportionation of $S_2O_3^{2-}$ or S^0 is done anaerobically assimilating carbon from CO_2 or acetate (Bak & Pfenning, 1977). In order for S^0 disproportionation to support growth, sulfide concentrations must be kept low at less than 1mM (Thamdrup et al., 1993). Large S isotope fractionations are associated with MSD, related with the recycling of reduced components during metabolic processes (Reviewed in Canfield et al., 2001a). Fractionations up to -33.9 ‰ have been measured during elemental S^0 disproportionation (S^0 oxidation to SO_4^{2-}) by pure cultures at cellular level (Habicht et al., 1998). The earliest S isotope fractionations are larger than 50 ‰ and have been credited to a combination of MSD and MSR (Canfield & Thamdrup, 1994; Habicht et al., 1998; Johnston et al., 2005b). It is thought MSR could not provide fractionations large enough alone (Johnston et al., 2005a). This theory has been

challenged as MSR are shown to produce by themselves fractionations large enough (Sim et al., 2011a).

$\Delta^{33}S$ and $\Delta^{36}S$ biosignatures

$\Delta^{33}S$ ($\Delta^{33}S = \delta^{33}S - 0.515 * \delta^{34}S$) has been used to detect S-Mass Independent Fractionations (S-MIF) processes that happened on the early Earth and in the Martian atmosphere (Farquhar et al., 2000b, 2000a; Farquhar & Wing, 2003). Biology is a mass dependent process, but records small magnitude anomalies in $\Delta^{33}S$ due to mass conservation effects during redistribution of sulfur between sulfur pools, at both the cellular and ecosystem levels (e.g. Farquhar & Wing, 2003; Farquhar et al., 2007). These variations can be preserved in the rock record in the same way as $\delta^{34}S$ (e.g. Johnston et al., 2008b). Unlike $\delta^{34}S$, $\Delta^{33}S$ has been shown to produce distinctive variations as a result of biological processes, even when $\delta^{34}S$ values are small or indistinguishable from abiotic processes (Ono et al., 2007).

Preservation of sulfur isotope biosignatures in the rock record

Once S isotope biosignatures from sulfate and pyrite have deposited, the S isotope rock record has the potential to be altered by diagenetic processes. These diagenetic processes are similar to the ones altering C isotopes (e.g. meteoric fluids, basinal brines) (Richardson & Hanssen, 1991). For example, signatures from $\delta^{34}S_{pyrite}$ can be over printed during late-stage diagenesis if sulfide-bearing fluids migrate through the sedimentary record that contains reduced iron (Xiao et al., 2010). These diagenetic alteration can be distinguished based on morphology and major element geochemistry characteristics (Fisher et al., 2014).

2.4 S metabolisms on Mars

Chemolithotrophic microorganisms are the most likely organisms to have existed on the Martian surface, as to thrive and grow they only require inorganic C sources, such as CO_2 (Boston et al., 1992; Fisk & Giovani, 1999). Furthermore, Mars was thought to have reducing conditions during the Noachian-late Hesperian, which is considered the habitable window, meaning that any potential metabolisms must have been anaerobic

(Michalski et al., 2018).The availability of S in many redox states on Mars makes S-based biogeochemical pathways appealing for any life that could have arisen there.

The Martian surface is dominated by basaltic rocks containing S^{2-}, and SO_4^{2-} , and sulfate has been detected on wide extensions forming extended evaporitic deposits (Bibring, 2006; Meyer, 2012; Scott, 1999) As explained, S can act as electron donor or electron acceptor depending on the redox state. MSR could have used electrons donors from organic substrates (detected by Curiosity Rover), inorganic CO_2 and H_2, or S^0 with SO_4^{2-} and NO_3^{2-} as electron acceptors. Hydrogen is present on Mars through photochemical origins, and it is likely that serpentinsation and other water-rock interaction processes happening on earlier Mars would have produced H_2 (Ehlmann et al., 2010; Viviano et al., 2013). There is also the likely possibility that inorganic H_2S, CO_2, and H_2 degassed from volcanoes (e.g. Ramirez et al., 2014) when Mars was more active, as observed for Earth. Microbial sulfide oxidation could have used H_2S produced from volcanic gasses and in the absence of molecular O_2, could have used NO_3^{2-}, which has been found to be present on the Martian surface by the Curiosity Rover (Stern et al., 2015). The only redox state of sulfur that has not yet been found on Mars from the above inventory is S^0.

2.5 The knowledge gap

The literature review has outlined the importance of Martian hydrothermal systems for microbial habitability during the Noachian and early Hesperian. This period is when life would have been able to arise on the Martian surface or within the subsurface. The presence of liquid water, redox reactions and nutrients for microbial life makes hydrothermal environments a high priority target for exploration. Widespread volcanism and release of S on the surface, together with the variety of S species found on Mars, point towards a S cycle being implicated in any putative Martian biogeochemistry. Future rover missions NASA 2020 and ExoMars 2020 launching in 2020 will join Curiosity in the search for habitability and biosignatures on the Martian surface, and also store samples for a future Mars Sample Return Mission. One of the priorities for the Sample Return Mission is to perform stable isotope analysis of carbon and sulfur (Goudge et al., 2017). The study of metabolic biosignatures such as carbon

and sulfur isotopes evidencing microbial activity such as MSR, MSD or Sox is extremely important for these exploration purposes. Thanks to the new discoveries by the NASA Curiosity mission, we know that Mars contains the electron donors and acceptors required for sulfide oxidation and sulfate reduction, which makes S metabolisms central in the search for life on Mars. In order to understand the habitability of Mars analogue hydrothermal systems and study their carbon and sulfur isotopic biosignature preservation, these are the questions that will be addressed:

Question 1: What are the main controls on the geochemistry and mineralogy of Mars analogue hydrothermal environments? This question will be addressed in Chapter 4 by characterising the water geochemistry and sediment mineralogy of Kerlingarfjöll and Kverkfjöll, two hydrothermal Mars-analogue environments.

Question 2: Which chemolithotrophic communities inhabit Mars analogue hydrothermal environments and what are their main metabolisms? Chapter 5 will answer this question with a DNA-based investigation into the environments explored for Question 1, to understand what microorganisms could inhabit Martian hydrothermal systems. A culturing experiment presented at Chapter 6 will help understand the main environmental variables affecting Microbial Sulfate Reducing (MSR) communities in these systems.

Question 3: Can $\delta^{13}C$ and $\delta^{34}S$ biosignatures be preserved in hydrothermal environments? Chapter 5 will investigate this question by coupling $\delta^{34}S$ and $\delta^{13}C$ with the DNA results from Question 2.

Question 4: Could a Mars analogue hypersaline spring be a better environment to find evidence of $\delta^{34}S$ biosignatures? $\delta^{34}S$ from Lost Hammer hypersaline spring (Canada) is compared to Kerlingarfjöll and Kverkfjöll hydrothermal analogue systems, taking into account the different environmental variables (Chapter 7).

Question 5:Can $\Delta^{33}S$ evidence preservation of life in the sediments? $\Delta^{33}S$ is analysed here for Kerlingarfjöll, Kverkfjöll and Lost Hammer (LH). It is used as a tool to identify metabolism activity even in circumstances were biotic $\delta^{34}S$ is difficult to distinguish from abiotic processes.

3 General Methodology

3.1 Sampling sites

All samples used for this PhD research were obtained from hydrothermal Mars analogues Kerlingarfjöll and Kverkfjöll (Chapter 4 Figure 4-1). Research permits, access, and sample export permits were granted by Orkustofnun (Reference OS2016120056/50.44), sampling permission was given by Vatnajökulsþjóðgarður, and the sample export licence granted by the Icelandic Institute of Natural History. The fieldwork expedition to collect the samples lasted from the 30th of July to the 9th of August of 2017. Kverkfjöll was accessed via helicopter approach to the Hveratagl ridge while Kerlingarfjöll was accessed by 4x4 vehicle. A second follow-up trip to Kverkfjöll was conducted at the beginning of September 2017, as part of a Deep Carbon Observatory (DCO) expedition in collaboration with Oxford University and the University of Iceland. Axel Heiberg brine samples were collected in the Canadian Arctic by Dr. Mark Fox-Powell in July 2017 to provide an environmental contrast to the Icelandic volcanic systems for the study of S isotopes.

Kerlingarfjöll and Kverkfjöll were selected as sites as they encompassed the interaction of volcanic hydrothermal systems with the glaciers that overlie these volcanoes. Within these main systems, the aim was to focus on sampling hydrothermal pools, produced from the interaction of the heat from the volcanic systems, and the cold water from the glaciers and snow melt. These systems have been previously studied (Cousins & Crawford, 2011; Cousins et al., 2013, 2018), and attested to be relevant for astrobiological implications, mainly as Mars analogues. Samples were collected firstly to characterise a volcanic-ice Mars analogue (water and sediment samples, characterised in Chapter 4), secondly to conduct microbiological studies (sediment

samples for DNA), and thirdly to investigate the plausible preservation of isotopic carbon and sulfur as biosignatures (water and sediment samples) for these systems to inform future Mars exploration (Chapter 5, 6 and 7).

3.2 Sample collection

Water and sediment samples were collected from pools with visible and absent fumarole steam input, capturing a range of sizes and colour variations indicative of compositional differences. Three pools and one stream were sampled at Kerlingarfjöll Hveradallir valley, and three more pools at Kverkfjöll Hveratagl ridge. Snow pack was sampled close to the pools at both Kerlingarfjöll (KR-ice) and Kverkfjöll (KV-ice) for SO_4^{2-} and Cl^- measurements. Sediment sample are shown in Chapter 4 Figure 4-2, Figure 4-3, Figure 4-4, and were taken from the sediment-water interface as much as possible to capture the authigenic alteration environment, up to 2-5 cm depth (circles in pool pictures indicate the exact point were the samples were taken). Only one sample was taken to represent the activity occurring at this pools as the pool sizes were small: only from 30 cm to 1 m of diameter.

Temperature, pH, and Dissolved Oxygen (DO) were measured in-situ using a Mettler Toledo meter (+/- 0.02 pH error, +/- 1% DO), calibrated in the field. Thermal imaging was achieved using Testo 882 thermal camera. Waters from pools were filtered through 0.2 µm Surfactant-free Cellulose Acetate (SFCA) filters, and after filtering stored in polypropylene 15 mL tubes at ~ 4 ºC. Duplicates were acidified in the field with 1 % HNO_3 taken for analysis of (i) dissolved major cations (Ca, Fe, Si, Al, Mg, Na, K, Pb, Zn, Cr, Mn, P), and (ii) H-O isotope and Cl^- analyses.

Water samples for dissolved SO_4^{2-} and H_2S were collected by filtering the water through 0.2 µm SFCA filters into 15 mL tubes and fixing immediately to 0.5 % $ZnCl_2$. The addition of $ZnCl_2$ fixes the aqueous H_2S as ZnS, at Zn concentrations low enough to allow for ion chromatography without dilution. For measurements of S isotopes ($\delta^{34}S$, $\Delta^{33}S$, and $\Delta^{36}S$) of dissolved SO_4^{2-} and H_2S, water samples were filtered with 0.22 µm filters and collected in 15 mL tubes with $ZnCl_2$ to a final concentration of 2 % to sequester the dissolved H_2S as ZnS and isolate it from dissolved SO_4^{2-}.

Sediment samples for Total Organic Carbon (TOC) weight % and $\delta^{13}C$ analysis were collected in 10 mL furnaced glass vials with furnaced spatulas and collected from sediment mid-way into each of the pools. Sediment samples for S isotope analysis were collected in 50 mL tubes and fixed to 2 % $ZnCl_2$. Sediment samples were also collected for DNA analysis using ethanol-flamed sterile spatulas and introduced in 50 mL sterile Falcon tubes subsequently stored with ice-packs until end of field campaign. Once in the laboratory, these were frozen to -20 ^oC until DNA analysis.

3.3 Sediment compositional analyses

Each sediment sample (from the different pools) was freeze-dried and subsequently homogenised to <500 µm grain size using a pestle and mortar. Sediments from Kerlingarfjöll were more coarse and darker, and Kverkfjöll were finer and lighter.

3.3.1 Visible–Short Wave Infrared (Vis-SWIR)

Visible-Short Wave Infrared (Vis-SWIR) reflectance spectroscopic measurements were made using a Spectral Evolution RS-3500 spectrometer, calibrated with a 99 % Labsphere Spectralon® standard, at Aberystwyth University, UK. Vis-SWIR spectroscopy measures the reflected light from 350 to 2500 nm to detect absorption bands that can indicate the different minerals within the analysed material. When the incident light interacts with the material, certain wavelengths are absorbed, while other wavelengths are reflected or transmitted. Each mineral has a characteristic pattern of absorption related to the crystal and chemical structure of the material. This is based on molecular vibrations (bonds) and electronic transitions that produce key spectral features that have unique position, shapes, depth and width parameters (Van der Meer & Jong, 2011). Vis-SWIR is sensitive to bonds and transition metals, such as OH, H-O-H bond, Al-OH, Fe-OH, Mg-OH Fe^{2+}, and Fe^{3+}, which are the most common absorption bands that help the identification of the minerals (Hunt, 1977).

3.3.2 X-Ray Diffraction (XRD)

XRD analysis was done at the Australian Synchrotron, Victoria (AU). For the XRD technique, samples are bombarded with X-rays that are refracted depending on the

composition of the mineral in the sample. The refraction pattern results in peaks that define the crystal structure of the minerals that compose the sample (Ulery & Drees ,2008). Samples were further hand ground to <5 µm in a mortar and pestle, mixed with a NIST SRM ZnO 674b internal standard, loaded into 0.7 mm diameter borosilicate glass capillaries and mounted onto the powder diffraction beamline. The diffraction patterns were determined using NIST SRM LaB6 660b to be 0.7769787 (5) Å. Data were collected using the Mythen II microstrip detector from 1.5 to 76° in 2 q. To cover the gaps between detector modules, two data sets, each of 5 minutes in duration, were collected with the detector set 0.5° apart and these were then merged to give a single data set. Merging was performed using the in-house software PDViPER. The capillary was rotated at ~1Hz during data collection to aid powder averaging. Mineral phases present were determined using Panalytical highscore with the ICDD PDF4+ database. Semi quantitative phase analysis was carried out in Topas version 6 (Bruker AXS), using the internal standard method to determine relative amounts of the crystalline material. The composition or quantification of the amorphous content wasn't identified.

3.3.3 X-Ray Fluorescence (XRF)

Particulate samples (<150 µm) were analysed for major element composition by Energy-Dispersive (ED) X-Ray Fluorescence (XRF) using a Spectro XEPOS HE at the University of St Andrews. The XRF analysis excites the sample with a primary X-ray source, and subsequently measures the fluorescent X-ray emitted (Lozano & Bernal, 2005). Characteristic fluorescent X-rays are produced by certain elements present in the sample. XRF analysis was carried out by charring the samples at 1000°C for 8h prior to fusion in Pt-Au crucibles. This removes sulfides and volatile phases, which is recorded as loss on ignition (LOI). Samples were fused in glass discs prepared by fusing 0.5 g of sample with 5 g of flux (50:50 mix), and mix of lithium tetraborate and lithium metaborate. Elemental abundances are reported as oxides and then stoichiometrically converted to elemental abundances using atomic masses.

3.4 Dissolved water chemistry analysis

3.4.1 ICP-OES

Major and trace elements concentrations in aqueous samples (Si_{TOTAL}, Ca^{2+}, Na^{+}, K^{+}, Fe_{TOTAL}, Mg^{2+}, Mn^{2+}, Al^{2+}, Pb^{2+}, Cr^{2+}, P_{TOTAL}, Zn^{2+}) were measured in triplicate using a Teledyne-Leeman Prodigy7 high dispersion ICP-OES (Inductively Coupled Plasma Atomic/Optical Emission Spectrometer) at the Open University, UK. Samples were diluted by factors of x20, x200, x1000 and x2000 in dH_2O (higher factors for Al, Fe and Ca due to higher concentrations) prior to analysis, to fall within the emission intensity ranges of the standard curves. Standards were prepared with certified stock solution of 100 ppm multi element standard (Fisher Scientific). Inside the ICP-OES, diluted samples were injected as mist directly into a stable argon plasma (at ~7200 ^{o}C) where they are instantaneously ionised radiate at wavelengths diagnostic of the atomic mass of the element (Hou & Jones, 2000). The optical spectrometer was operated in axial view (head on to the plasma torch) recording the radiation projected from the different elements. The strength of the electron radiation from the different elements was then compared to the standard curves of known concentrations. Mean values were taken from three replicate analyses per sample, and a standard was measured every 5th measurement to assess the drift of the ICP-OES.

3.4.2 Ion Exchange Chromatography for SO_4^{2-} and Cl^{-}

SO_4^{2-} and Cl^{-} anions were measured in triplicate using Ion Chromatography with a Metrohm 930 Compact IC Flex coupled to a Metrohm 919 autosample. Element specific calibration curves were fitted depending on the range of concentrations identified using Metrohm MagIC Net software. Based on this range, a set of standards were analysed in triplicate. Instrument blanks and procedural blanks were checked for unidentified peaks (to assess contamination). The lowest concentrations measured assessed the limits of detection (LODs). Standard deviations of measurements were ⩽ 0.1 % for all anions.

3.4.3 Quantification of dissolved hydrogen sulfide

Dissolved hydrogen sulfide ($\Sigma H_2S = H_2S + HS^- + S^{2-}$) concentrations for natural samples and microbial cultures were measured photometrically using the methylene blue method (± 2 % precision with 95 % confidence; Cline, 1969) with a Thermo Scientific Aquamate 8000 U-Vis Spectrophotometer. The method is applicable to natural waters containing 1-1000 µmol/L of H_2S (0.03-32 ppm). For this, the mixed diamine reagent was made for different concentrations and dilutions. The diamine reagent contained N,N dimethyl-*p*-phenylenediamine sulfate and ferric chloride ($FeCl_3 \bullet 6H_2O$), in 500 mL of 50 % (v/v) reagent grade HCl. Two different diamine reagents were made (as indicated by the Cline method) to detect concentrations of ΣH_2S: 1) for 1-3 µmol/L range (containing 0.5 g of Diamine/500 mL, 0.75 g Ferric/500 mL) and 2) for 3-40 µmol/Litre range (containing 2 g of Diamine/500 mL, 3 g ferric/500 mL). N,N dimethyl diamine reacts with ΣH_2S in presence of an oxidizing agent (ferric ion) to form methylene blue, which is a blue colour dye (Reese et al., 2011) as presented in reaction (1).

$$2[(CH_3)_2\,NCH_4NH_2\,H_2SO_4] + 6FeCl_3 + H_2S \rightarrow$$

$$(CH_3)_2\,2NC_6H_3N,S,\,C_6H_3N(CH_3)_2Cl + 2H_2SO_4 + NH_4Cl + 6FeCl_2 + 4HCl \qquad (1)$$

Standards with sodium sulfide ($Na_2S \bullet 9H_2O$) were carefully prepared anaerobically to establish the calibration curves (F in equation 2) for the 1-3 and 3-40 µmol/L concentrations. Standards with H_2S concentrations of 1, 2, 5, 10, 25, 30, 40, 50 µmol/L were prepared in a Coy anaerobic chamber (oxygen-free N_2 with 2-3 % H_2) and after the headspace was filled with N_2. One 25 µmol/L standard was run as a reference in every set of analyses. For each sulfide concentration analysis, 1 mL of each sample was extracted from the natural sample or microbial culture and fixed with 100 µL of 20 % Zn-Acetate in an Eppendorf tube. Next, 0.08 mL of diamine reagent was added and incubated at 4 °C for 20 minutes to await reaction (1). All the samples were analysed in triplicate, and the necessary dilutions were made after the colour development time. After that, the samples were transferred to cuvettes and mounted in the U-Vis Spectrophotometer, and measured at single points at 670 nm wavelength. In the U-Vis Spectrophotometer, two beams of light from a visible or UV light source are sent to the reference cuvette, and another one to the sample cuvette. The intensities of these are

measured by electronic detectors and compared (Worsfold & Zagatto, 2017). The concentrations of sulfide in the sample were calculated from Cline 1969 following equation (2):

$$C_S = F\ (A - A_b) \quad (2)$$

C_S= Total sulfide concentration, F= standard slope, A= Absorbance sample, A_b= Absorbance blank (Cline, 1969)

3.4.4 Water δD and $\delta^{18}O$

Water-bound oxygen (^{16}O, ^{18}O; $\delta^{18}O_{WATER}$) and hydrogen (^{1}H, ^{2}H; δD_{WATER}) isotopes were measured. Isotopic results are given as δ-values (‰) with respect to V-SMOW (Vienna-Standard Mean Ocean Water). Water oxygen and hydrogen isotopes were measured simultaneously by CRDS using a L2140-i Picarro water isotope analyser, interfaced with an A0211 high-precision vaporizer (Picarro, Santa Clara, US). The instrument uses N_2 gas as the carrier. Each sample was injected ten times into the vaporizer, which was heated to 110°C. Values for the final 7 injections were averaged with a typical mean instrumental precision (±1 SD) of ±0.02 ‰ for $\delta^{17}O$, ±0.03 ‰ for $\delta^{18}O$ and ±0.19 ‰ for $\delta^{2}H$, as observed from repeated analysis of an in-house water standard (n=127) over one year. The results were normalized against V-SMOW by analysing internal standards before and after each set of fifteen to twenty samples. To this end, three internal water standards (JRW, BOTTY, SPIT) were calibrated against the international standards V-SMOW, GISP and SLAP.

3.5 Stable Isotope measurements

3.5.1 Sample preparation for isotope analyses

A split of the sediment samples were freeze-dried, powdered and homogenized prior to analyses.

Removal of carbonate from samples

For Total Organic Carbon (TOC) and $^{12}C/^{13}C$ analysis, samples were treated with 2M HCl in pre-combusted Pyrex centrifuge tubes prior to analysis to remove any potential carbonate. The residue was three times centrifuged and washed with DI-H_2O and dried at 60 °C in a closed oven.

Sulfur extraction

For S isotope analysis dissolved hydrogen sulfide ($\Sigma H_2S=H_2S+HS^-+S^{2-}$) fixed as ZnS during sampling was captured on 0.2 µm filters. Dissolved SO_4^{2-} was precipitated as $BaSO_4$ from the filtered solution by acidifying and adding an overabundance of 1M $BaCl_2$, and subsequently captured on a second set of 0.2 µm filters. Both sets of filters were subsequently dried at 25°C overnight. The ZnS powder resulting from the dissolved ΣH_2S and sedimentary samples containing solid S phases (e.g. pyrite and elemental S) were transformed to Ag_2S for isotopic analysis through sequential distillation with AVS (Acid Volatile Sulfides) and CRS (Chromium Reducible Sulfides) following the methods described in (Canfield et al., 1986).

For the sulfur distillations, acidified chromium (II) chloride solution ($CrCl_2$), silver nitrate solution ($AgNO_3$) and 50 % (vol/vol) hydrochloric acid (HCl) were prepared. To make the acidified $CrCl_2$ solution, 533 g of chromium (III) chloride ($CrCl_3 \cdot 6H_2O$) was mixed with 2 L of Milli-Q H_2O. The acidified solution was transferred to a beaker containing Zn pellets to reduce the Cr(III) to Cr(II), and purged for 2-3 h with oxygen-free N_2 gas to prevent oxidation of the solution by contact with O_2. The reduced solution was stored in capped 60 mL syringes stored at 4 °C. A one molar silver nitrate solution ($AgNO_3$) was prepared by dissolving 17 g $AgNO_3$ in 100 mL of 18.2 Milli-Q water. The solution was covered in aluminium foil in order to prevent photoreaction, and stored in the fume cupboard at room temperature.

Around 2 g of homogenised sample powder was weighed in a tri-neck flask and assembled as seen in Figure 3-1, with 6 samples run in series during distillation. As it can be seen in Figure 3-1, an individual set of distillation apparatus consists of a tri-neck flask on a stirring hotplate, under constant stream of oxygen-free N_2 gas, and connected to a water-cooled condenser and subsequently a $AgNO_3$ trap. A magnetic

stirrer is placed inside the tri-neck so that the sample and the reagents are homogenised during the distillation.

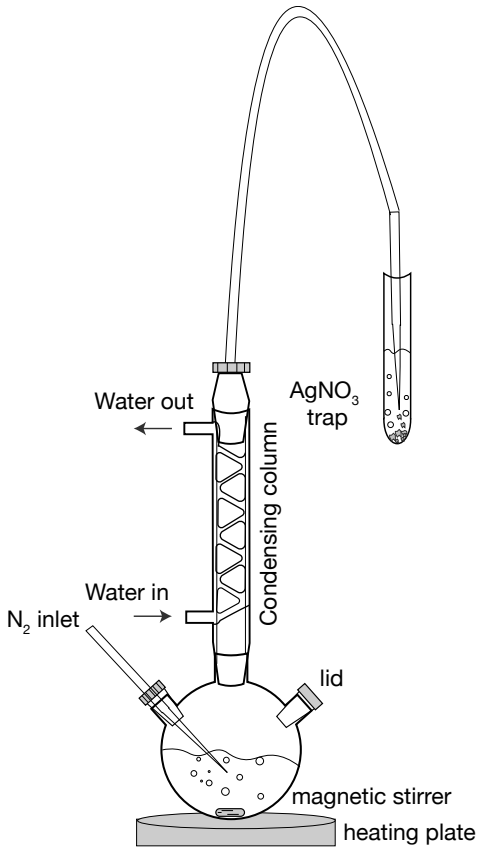

Figure 3-1. Drawing of a single sulfur distillation line, consisting of a tri-neck flask with magnetic stirrer, N_2 gas entry, condensing column, $AgNO_3$ trap, and heating plate.

After the distillation lines were assembled, magnetic stirrers were placed in the tri-neck flask with some ethanol (C_2H_6O) to prevent organic matter creep. For the $AgNO_3$ trap, 7 mL of Milli-Q water was added to 1 mL of 1M $AgNO_3$. The N_2 gas was turned on and after assuring a gentle but constant flow into the traps, 7 mL of HCl 50 % (v/v) was added to the tri-neck before heating to 150°C. After 5-10 minutes a dark precipitate (Ag_2S) was formed in the trapping tubes, indicating HCl liberating Acid Volatile Sulfur (AVS) from the samples as H_2S gas, which was carried on a stream of N_2 and trapped as Ag_2S in the trap. AVS comprises $\Sigma H_2S = H_2S + HS^- + S^{2-}$ and Fe-mono-sulfides. This reaction was run for 1h to ensure full conversion of all AVS to Ag_2S. After 1h new trapping tubes were prepared in order to proceed with the Chromium Reducible Sulfur extraction (CRS), by adding 15 mL of acidified chromium chloride solution into the tri-neck. $CrCl_2$ solution, unlike HCl, is a stronger acid that is capable to liberate H_2S from sedimentary pyrite

(FeS_2) and elemental sulfur (S°). When precipitation ceased, Ag_2S tubes were filtered in 0.22 µm cellulose filters and dried overnight at 30 °C. The filters were weighed before and after drying, in order to calculate pyrite abundances. Ag_2S samples were stored in aluminium foil envelopes, placed in glass vials for future isotope analysis.

Sulfate reduction, Thode method

In order to measure S isotopes in sedimentary sulfates, a Thode solution was made following methods from Thode et al. (1961) with adaptations from Forrest and Newman (1977) and Arnold et al. (2014). This is a strongly acidic solution used to reduce SO_4^{2-} to H_2S, for capture as Ag_2S. To make a total volume of 520 mL of Thode solution, 272 mL of HCl (conc hydrochloric acid, 37 %) , 166.66 mL of HI (pure hydriodic acid, 48 %), 81.66 mL of HP (pure hydrophosphorus acid, 50 %) were measured in volumetric flasks and mixed in a 1 L beaker for 10 minutes and transferred to a 1 L Strauss flask. To boil the Thode mixture to get rid of any S impurities, the Strauss flask was attached to a similar N_2-flushed condensing system, and attached to two subsequent water traps to neutralise the acid vapours produced during boiling. The mixture was brought to boil for 3-4 h, observing a colour change from yellow to dark brown to clear brown. After boiling, the Strauss flask was covered with aluminium foil to prevent photoreaction over time.

For the sulfate samples, between 20-40 mg of precipitated $BaSO_4$ from water or sediments were weighed. The samples were introduced in the tri-necks and followed the same procedure when running the pyrite line for AVS/CRS extraction, with the following variations: i) Water traps were added between the condensers and the $AgNO_3$ traps to neutralise any additional acid vapours, ii) a blank was always included to verify purity of the Thode solution, and iii) 20 mL of Thode solution was added to initiate the reaction, and the reaction was run for ≥ 3 hours as needed until completion.

3.5.2 Isotope notation and analyses

Isotopic values are reported in standard delta notation (δ), where X is an element (e.g. carbon or sulfur), a is the heavier isotope and b the light isotope (e.g. $^{34}S/^{32}S$). Showing per mil (‰) deviations from international standards as follows:

$$\delta^{a}X(‰) = (({}^{a}X/{}^{b}X)\ \text{sample} / ({}^{a}X/{}^{b}X)\ \text{standard} - 1) \times 1000 \quad (3)$$

Fractionation factors are given in $\varepsilon_{A\text{-}B}$ between the reactant (A) and the product (B). Carbon isotope fractionations ($\varepsilon^{13}C$, calculated with equations 4 and 5) are calculated for Chapter 5 between the $\delta^{13}C$ of volcanic CO_2 gas as the dominant substrate for autotrophy (Kerlingarfjöll values from Barry et al., 2014, Kverkfjöll from Poreda et al., 1992), and the $\delta^{13}C$ of product biomass (TOC) from the sediments.

$$\alpha_{CO2\text{-}TOC} = (\delta^{13}C_{CO2} + 1000)/(\delta^{13}C_{TOC} + 1000) \quad (4)$$

$$^{13}\varepsilon_{CO2\text{-}TOC} = \ln \alpha_{CO2\text{-}TOC} \times 1000 \quad (5)$$

S isotope fractionations ($^{34}\varepsilon$, calculated with equations 6 and 7) are calculated for Chapter 5 between the $\delta^{34}S$ values of reactant aqueous SO_4^{2-} and the $\delta^{34}S$ of product sulfide preserved as sedimentary CRS (CRS includes sedimentary pyrite and elemental S). $\delta^{34}S$ CRS is used here for the calculations of S isotope fractionations instead of water $\delta^{34}S$ H_2S for three reasons. First, water H_2S concentrations were too low in all the pools, hence $\delta^{34}S$ was only measurable at KR-P1 and KR-P3. Second, CRS is the preservation of H_2S in the rock record, and used to investigate the preservation of biosignatures. Third, to allow comparison between LH , Kerlingarfjöll and Kverkfjöll. In the Kverkfjöll KV-P5 pool the water could not be sampled for $\delta^{34}S$ aqueous SO_4^{2-} measurements; therefore, KV-P5 is not plotted when comparing $^{34}\varepsilon_{SO4\text{-}CRS}$.

$$\alpha_{SO4\text{-}CRS} = (\delta^{34}S_{CRS} + 1000)/(\delta^{34}S_{SO4} + 1000) \quad (6)$$

$$^{34}\varepsilon_{SO4\text{-}CRS} = (\alpha_{SO4\text{-}CRS} - 1) \times 1000 \quad (7)$$

Quadruple sulfur isotope ratios ($^{33}S/^{32}S$, $^{34}S/^{32}S$, $^{36}S/^{32}S$) are reported in standard delta notation (δ) showing per mil (‰) deviations from international standard V-CDT. For mass dependent processes, deviations from the predicted reference lines (RL, $\Delta^{33}S$ and $\Delta^{36}S$) are expressed in the form of $\Delta^{33}S$ and $\Delta^{36}S$ notations (Ono et al., 2003, 2006) as:

$$\Delta^{33}S = \delta^{33}S - 0.515 * \delta^{34}S \quad (8)$$

$$\Delta^{36}S = \delta^{36}S - 1.9 * \delta^{34}S \quad (9)$$

where:

$$\delta^{33,34,36}S = 1000\ (\delta^{33,34,36}S/1000 + 1) \quad (10)$$

Organic carbon $\delta^{13}C_{org}$ and $\delta^{34}S$ isotopes

Between 0.05 mg and 2 mg of sample material (for C isotopes), $BaSO_4$ or Ag_2S (for S isotopes) mixed with 1-2 mg of V_2O_5, was analysed in Thermo-Fisher 8 x 5 mm tin capsules. All samples were analysed in duplicate by flash combustion with an EA Isolink (Thermo Fisher) coupled to a MAT253 isotope-ratio mass spectrometer via a Conflo IV (Thermo Finnigan). The data were calibrated with USGS-40 and USGS-41 for organic carbon isotopes, and IAEA-S1, IAEA-S2, IAEA-S3 for sulfur. Stable isotope values are reported in standard delta notation as ‰ variations relative to the VPDB standard for $\delta^{13}C$, and VCDT for $\delta^{34}S$ with analytical precision of 0.09 ‰ and 0.24 ‰ respectively

Minor sulfur isotopes $\Delta^{33}S$, $\Delta^{36}S$

For minor S isotope analyses ($\Delta^{33}S$ and $\Delta^{36}S$, as defined in equation 1 and 2), 0.3-0.5 mg of Ag_2S was weighed in an iron-nickel-cobalt alloy pyrofoil with ≥ 50 times excess CoF_3, and placed in a 10 cm long borosilicate glass tube with ~ 1 g of optical NaF crystals, which help to consume HF during the reaction. The reaction tube was placed in a Curie-point pyrolyser (JHP-22, Japan Analytical Industry), evacuated to vacuum, and flash heated to 590 °C for 297 seconds to fluorinate solid Ag_2S to SF_6 gas, following methods modified from Ueno et al. (2015). The product gas was introduced into a bespoke vacuum line, and purified through sequential cryogenic capture at -190 °C and -110 °C to remove residual F_2 and other condensable contaminants (e.g., HF). The gas was then passed through an SRI 8610C gas chromatograph equipped with a 12 ft HayeSep Q packed column (1/8″ OD, 80–100 mesh) and a 12 ft Molecular Sieves 5Å packed column (1/8″ OD, 60–80 mesh) operating at a He flow rate of 24 ml/min and at a temperature of 80 °C (Ono et al., 2006). The SF_6 peak was monitored by a thermal conductivity detector (TCD), and captured in an additional liquid N_2 trap after 27-31 minutes. The final purified SF_6 was frozen in the microvolume inlet system of a Finningan MAT 253 dual inlet mass spectrometer. Isotopic abundances were analysed at m/e values of 127, 128, 129 and 131 ($^{32}SF_5^+$, $^{33}SF_5^+$,$^{34}SF_5^+$,$^{36}SF_5^+$) and compared to reference SF_6 gas calibrated to V-CDT (Warke et al., *in revision*). The $\Delta^{33}S$ and $\Delta^{36}S$ values for IAEA-S1 produced by this method (n=78) are 0.115 ± 0.015 ‰ and -0.581 ± 0.172 ‰ (mean ± 1σ), respectively. These values are within uncertainty of standard values reported in other studies (e.g. Defouilloy et al., 2016; Johnston et al., 2008a; Ono et al., 2006; Ueno et al., 2015). The

precision of a single measurement was typically in the range of 0.01 ‰ for $\Delta^{33}S$ and 0.1 ‰ for $\Delta^{36}S$.

3.6 Anaerobic microbial culturing techniques

Anaerobic culturing was performed for experiments described in Chapter 6. The main culture media recipe used was from Widdle and Bak (1992), to target the growth of microbial sulfate reducers. The media was adapted by increasing the SO_4^{2-} concentrations to a range matching the hydrothermal sites, and the sodium sulfide ($Na_2S \bullet 6H_2O$) solution was substituted by Na-thyoglycolate solution to avoid masking H_2S microbial production. The composition of the modified media was: 2 g NaCl, 0.4 g $MgCl_2 \bullet 6H_2O$, 0.1 g $CaCl_2 \bullet 2H_2O$, 4 g Na_2SO_4, 0.25 g NH_4Cl, 0.2 g $KHPO_4$, 0.5 g KCl, 10 mL Na-thyoglycolate solution (0.1 g Na-thyoglycolate powder, 0.1 g ascorbic acid, topped with Milli-Q water up to 10 mL) and 1 mL/L Trace Elements Solution. The Trace Element Solution containing: 12.5 mL of 100 mM of HCl, 2100 mg $FeSO_4 \bullet 7H_2O$, 30 mg $\bullet H_3BO_3$, 100 mg $MnCL_2 \bullet 4H_2O$, 190 mg $CoCl_2 \bullet 6H_2O$, 24 mg $NiCl_2 \bullet 6H_2O$, 2 mg $CuCl_2 \bullet 2H_2O$, 144 mg $ZnSO_4 \bullet 7H_2O$, 144 mg $ZnSO_4 \bullet 7H_2O$, 36 mg $Na_2MoO_4 \bullet 2H_2O$). After mixing the reagents were added to 900 mL Milli-Q water in a measuring column, and topped up with Milli-Q water up to 1 L mark. The media was subsequently divided into two bottles, and in one of the bottles resazurin was added as an oxygen indicator control. Then both bottles (one with media, one with media plus resazurin) were purged with oxygen-free N_2 gas for 30 minutes/L. These were transferred into a Coy anaerobic chamber and 50 mL of media was distributed into 100 mL serum bottles and sealed with butyl rubber stoppers. Once outside the anaerobic chamber, the rubber stoppers were crimped, and the serum bottles flushed with oxygen-free N_2 gas for 5 minutes, and subsequently autoclaved at 121°C for 20 minutes. Following this, for every 50 mL of media, 0.05 mL of selenite were added to each serum bottle to boost the growth, and 1 mL of acetate to the required bottles. pH was checked and adjusted to replicate pool conditions by introducing 10% HCl or 1 M NaOH (reagents made in an anoxic atmosphere). For the final step, the media was inoculated with 1 mL of sample. For each inoculated batch there were always oxygen control media with resazurin, plus blanks (media with no resazurin and no inoculation).

The aseptic technique was used to ensure sterile conditions were maintained after autoclaving. In order to ensure sterile conditions during sampling, N_2 was passed through heated copper column to remove any O_2 and filtered through 0.22 µm pore filter to remove any impurity present. Syringes and needles were flushed with filtered N_2 before being introduced into the anaerobic serum bottles, through a flame-sterilised canula. The rubber tops from serum bottles were always kept under a Bunsen flame, and sterilised by ethanol flaming before introducing a needle. Serum bottles with media were stored horizontally in a dark cupboard at room temperature.

3.7 DNA extraction and PCR

Total genomic DNA was extracted from sediment samples using the Qiagen DNAeasy PowerMax Soil Kit (Qiagen laboratories, Germany) following the manufacturer's instructions, modified with the addition of 1M phosphate buffer (method adapted from Direito et al., 2012). To mitigate against extraction bias, duplicate extractions comprising a 'soft' and 'hard' method were conducted, and extractions for each sample pooled. For each, 1 g of sample was used for the extraction, with 4 mL of 1M phosphate buffer added to the bead-beating tubes, and then the mix was gently inverted twice and incubated for 30 minutes at 60 °C prior to continuing with the DNA isolation protocol. Each sample was done in duplicate and extracted for soft. For the soft extraction, the bead-beating step was replaced with a 30 minute incubation at 60 °C temperature. After the extraction the DNA was concentrated from 5 mL to a final volume of 1 mL following the protocol for DNA concentration from the DNAeasy powerMax Soil Kit Handbook with 5M NaCl and 100 % cold ethanol. Throughout

For DNA extraction from microbial cultures, cells were gathered by filtration into sterile 25 mm diameter 0.22 um pore filters. Once the cells were collected, DNA extraction was performed using the DNeasy Ultra Clean Microbial Kit (Qiagen laboratories, Germany).

Polymerase chain reaction (PCR) DNA amplification was used to screen for 16S rRNA bacteria and archaea prior to sending for sequencing (Figure 3-2). For each sample 1 µL of DNA template was added to a 50 µL PCR tube containing 25 µL of REDTaq Ready Mix PCR reaction Mix with $MgCl_2$ (Sigma-Aldrich), 0.5 µL of reverse primer (UN1492R-GGT

TAC CTT GTT ACG ACT T), 0.5 µL forward primer (either 21F- TTC CGG TTG ATC CYG CCG G or 27F-AGA GTT TGA TYM TGG CTC AG), and 23 µL of nuclease free water. PCR conditions as follows: denaturing stage at 94 °C for 3 minutes, annealing stage at 53 °C for 40 seconds, and elongating stage at 72 °C for 90 seconds, with a final elongation of 72 °C extended for 90 seconds. The PCR cycle was repeated 30 times and PCR products verified with gel electrophoresis (primers and PCR conditions from DeLong (1992). For the gel electrophoresis, 2 % of agarose gel was stained with 8 µL of SYBR safe stain, and 10 µL of PCR product was loaded into the gel wells, along with 5 µL 1 kb hyper ladder for reference(Figure 3-2). The gel was run at 60 mV for 1h.

3.8 PCR for APSr gene

PCR screening was also done for the gene that encodes the APSr enzyme (adenosine-5'-phosphosulfate reductase) of the extracted DNA. APSr is present in all Sulfate Reducing Prokaryotes (Friedrich, 2002). PCR master mix was done in the same way described above with REDTaq Read Mix, and only substituting reverse and forward primers for APSr forward APSF-TGGCAGATMATGATYMACGG and reverse APSR-GGGCCGTAACCGTCCTTGAA, Sigma-Aldrich primers. PCR conditions as follows: denaturing stage at 94 °C for 2 minutes, annealing stage at 60 °C for 1 minute, and elongating stage at 72 °C for 3 minutes, with a final elongation of 72 °C extended for 10 minutes (Primers and PCR conditions from Friedrich, 2002). The PCR cycle was repeated 30 times.

3.9 DNA sequencing

Bacterial and Archaeal 16S rRNA amplicons were sequenced using Pacific Biosciences (PacBio) Sequel single-molecular long-read technology conducted by MR DNA Laboratories (MR DNA, Shallowater, Texas, USA) using bacteria (27F-AGAGTTTGATCCTGGCTCAG and 519R-GTNTTACNGCGGCKGCTG) and archaea (21F-TCCGGTTGATCCYGCCGG and 505R- CCR TGC TTS GGR CCV GCC TGV CCG AA) specific primers. A depth of 5000 reads per sample was achieved for each 16S rRNA assay

with an average postprocessing read length of 1400 bp. Sequence trimming, denoising, and chimera checking were carried out by MR DNA (MR DNA, Shallowater, Texas, USA) using CCS, OTUs generated and chimeras removed. Operational Taxonomic Units (OTUs) were defined by clustering at 3 % divergence (97 % similarity). Final OTUs were taxonomically classified using BLASTn against a curated database derived from RDPII and NCBI.

3.10 Sequence processing

Sequences generated by PacBio Sequel were analysed and processed after the Mr. DNA trimming, denoising and chimera checking. OTU clustering and taxonomic identification was done using the MOTHUR programme (Schloss et al., 2009). Sequences that were less than 200 bases or longer than 1600 bases in length were removed from downstream analysis, to keep quality scores above threshold. Different statistical commands in MOTHUR were used to extract information about the similarity OTU level between the pools: a Venn diagram, phylogenetic tree were produced from it. From the trimmed file, FAPROTAX (Functional Annotation of Prokaryotic Taxa, Louca et al. 2016), database was used to cluster OTUs in microbial metabolic functions based on the literature, converting taxonomic microbial community profiles into functional profiles. Bootstrap cut-off values used were >80 %, but classification was typically at 100 % confidence. Phylogenetic trees were drew using the interactive Tree of Life version 5.3 (Letunic & Bork, 2019).

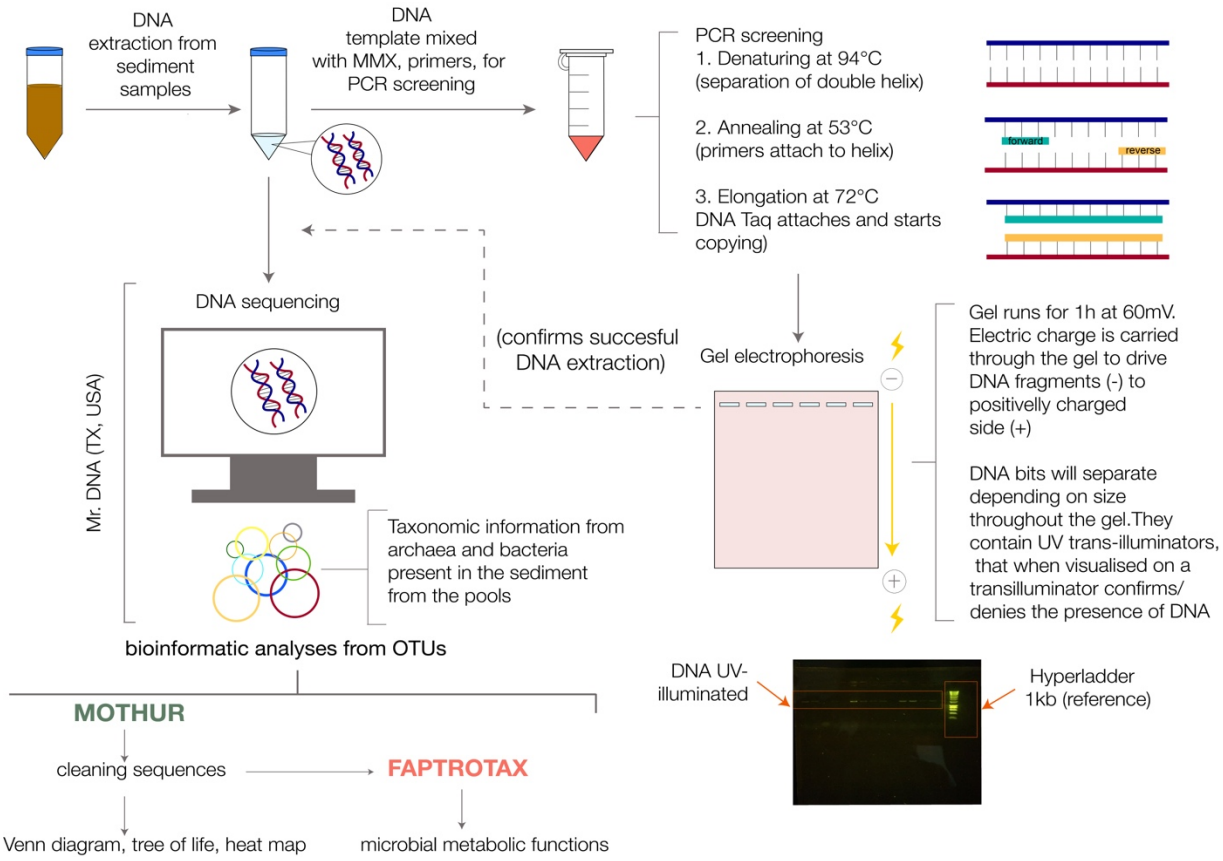

Figure 3-2. Diagram representing the different DNA analyses performed. From DNA extraction, followed by PCR and gel electrophoresis, then DNA sequencing and bioinformatics.

4 Characterisation of two hydrothermal Mars- analogues: Kerlingarfjöll and Kverkfjöll

This is an expanded version of:

A. Moreras-Marti, C.R. Cousins, M. Fox-Powell, A.L. Zerkle, F. Gazquez, H.E.A. Brand, (in review). Volcanic controls on the microbial habitability of Mars analogue hydrothermal environments, *Geobiology*.

Data analysed and manuscript written by A. Moreras-Marti

4.1 Introduction

This chapter investigates the relationship between aqueous geochemistry and syn-depositional bulk sediment mineralogy in two hydrothermal systems in Iceland: Kerlingarfjöll and Kverkfjöll. These systems serve as direct analogues to snow and ice-fed hydrothermal habitats on Mars such as Sisyphi Montes (Ackiss et al., 2018) or Arsia Mons (Scanlon et al., 2014). Due to the potential biological relevance of these systems, is necessary to understand the hydrothermal geochemical dynamics and the major volcanic controls. This valuable information will direct future exploration of Mars, and in particular the interpretation of the reflectance spectral properties of the resulting sediments produced by these environments. Six hydrothermal pools in Iceland were used to assess: i) what controls the dominant aqueous geochemistry in Mars-analogue

hydrothermal pools; ii) how aqueous geochemistry is reflected by sediment authigenic mineralogy; and iii) whether host lithology is a major control on the aqueous geochemistry of these systems.

4.2 Kerlingarfjöll- Hveradallir, the geothermal valley

Kerlingarfjöll volcano (64°38'32.61"N, 19°17'44.43"W) is situated 12 km SW of Hosfjökull glacier (Figure 4-1 A). It covers an area of 200 km^2, with the highest peaks (1000 to 1488 m) partially covered by the Hosfjökull glacier. The volcanic complex formed subglacially between 331 Ka and 65 Ka and has a rhyolitic composition (20-27 % of the volcano) underlain by basalt (Flude et al., 2010; Gronvold, 1972). The northern part of the complex experiences higher geothermal activity (Flude et al., 2010; Humlum, 1936). Our area of study is at the north of Kerlingarfjöll, at the Hveradallir valley (Hvera- geothermal, dallir- valley in Icelandic) valley, where two geothermal sites (Site 1 and Site 2; Figure 4-1 A) were sampled. Here, meltwater from the glacier interacts with fumaroles downstream (Humlum, 1936;Figure 4-2 and Figure 4-3).

Three pools were sampled at Site 1 at the Kerlingarfjöll Hveradallir valley, these are:

(i) KR-P1 - water with gas input (Figure 4-2 D);

(ii) KR-P2 - no visible gas input (both about 2m downslope from the glacier) (Figure 4-2 E); and located on a different slope

(iii) KR-P3 - gas input and black sediments (Figure 4-2 F).

Lastly, a meltwater stream was sampled at Site 2, 500 m SE (KR-Bio stream; Figure 4-3). Both KR-P3 and KR-Bio presented high rates of fumarole gas and were not close to the glacier.

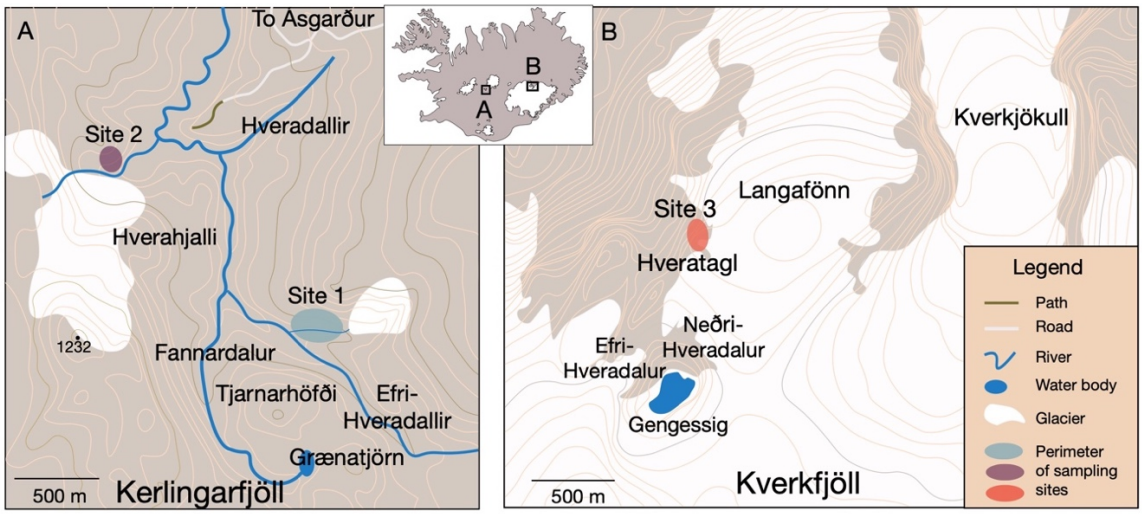

Figure 4-1. Map of Kerlingarfjöll (a) and Kverkfjöll (b). (a) Kerlingarfjöll, Site 1 where three hydrothermal pools were sampled: KR-P1, KR-P2, KR-P3, and Site 2 a small stream, KR-Bio.(b) At Kverkfjöll site 3, three pools were sampled (KV-P4, KV-P5, and KV-P6).

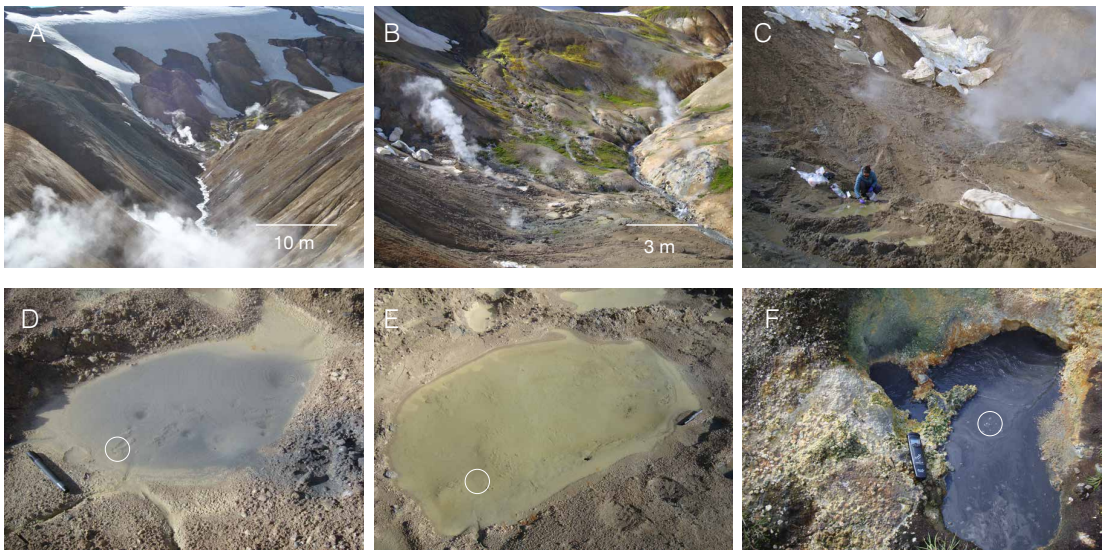

Figure 4-2. Kerlingarfjöll Hveradallir valley Site 1. (a-c) are contextual views of Site 1. In them, it can be seen how the glacier interacts with fumaroles and heat from the geothermal areas on the slope of the valley, and the molten sections of glacier form the hydrothermal pools. (d) KR-P1 pool, with pen for scale. (e) KR-P2 pool, with pen for scale. (f) KR-P3, with pH meter for scale. White circle indicates location within the pools where sediment and water samples were taken.

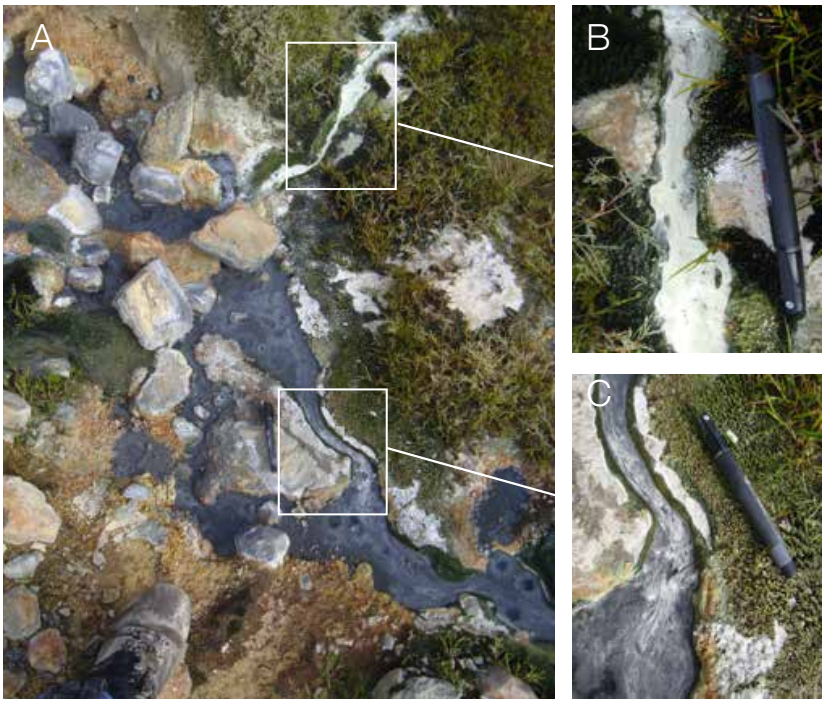

Figure 4-3. Kerlingarfjöll Hveradallir valley Site 2. (a) Kerlingarfjöll Bio-stream (KR-Bio), with walking boot for scale. (b) Stream with yellow crust (small tributary), with pen for scale. (c) main part of KR-Bio stream, with pen for scale. Sub-locality C is where the sample was taken. It can be seen how there are filament-looking material, hypothesised during sampling as biofilms.

4.3 Kverkfjöll-Hveratagl, the geothermal ridge

The Kverkfjöll volcano (64°41'22.28" N, 16° 40'43.01"W) underlies the northern margin of the Vatnajökull glacier (Figure 4-1 B, Figure 4-4) and eruptions date back to ~7.6 ka (Óladóttir et al., 2011a). It rises 1000 m above the local area and has two calderas with an associated NW-extending fissure swarm (Björnsson & Pálsson, 2008). The volcanic complex hosts a high-temperature geothermal area at the glacier margin, covering 25 km^2, with a surface manifestation of pools, mudpots and fumaroles (Figure 4-4). Most of the exposed geothermal areas lie within the northern caldera (Ármannsson 2016; Cousins et al., 2013; Cousins et al., 2018; Olafsson et al., 2000). Eruptive materials are tholeiitic basalts (Jakobsson et al., 2008) including hyaloclastite, pillow lava and fine-grained tuff sequences (Óladóttir et al. 2011b). The study area, Hveratagl (Hvera- geothermal, tagl- ridge in Icelandic) is situated on the northern caldera ridge. Here, as with Kerlingarfjöll, the geothermal features investigated comprise snow/ice-fed

meltwater pools interacting with fumarolic ground (Figure 4-5). Previous work identified pools with a pH of 3-4 and temperatures ranging from 10-20 °C (Cousins et al., 2013) and identified alteration phases including zeolites (heulandite), sulfates (gypsum, jarosite, alunogen), crystalline Fe-oxides (goethite, hematite), smectite (montmorillonite, saponite) and ferric oxides.

At Kverkfjöll three pools were selected:

(i) KV-P4, with visible gas input and grey sediment (Figure 4-4 D)

ii) KV-P5 with no gas influx (Figure 4-4 E)

iii) KV-P6 with no visible gas input (Figure 4-4 F), and suspended red particles.

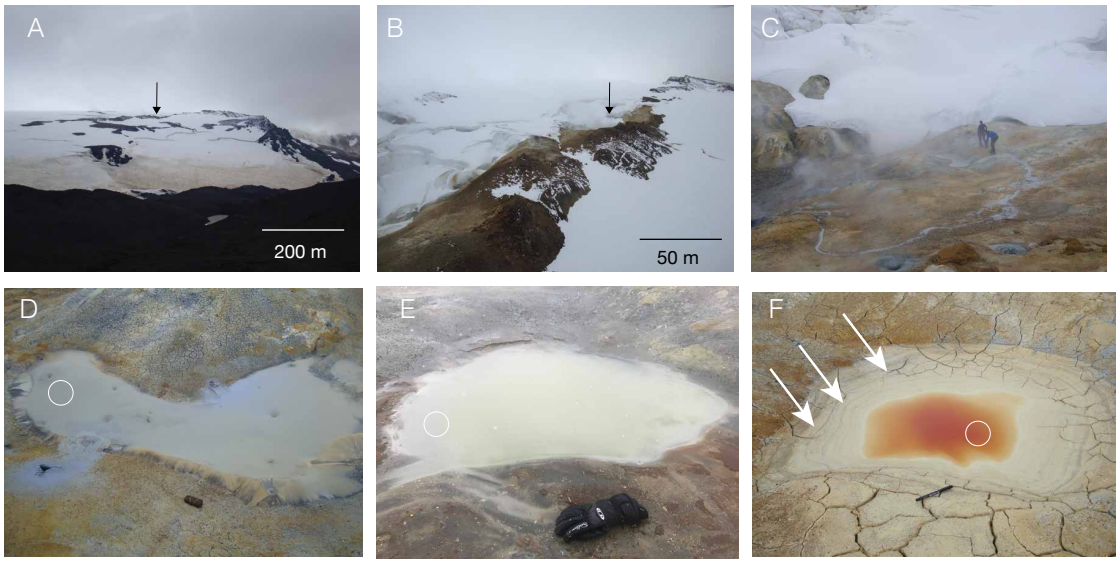

Figure 4-4. Kverkfjöll Hveratagl ridge site 3. (a-c), are a contextual photos of the geothermal ridge, looking south. (a) Photo taken of the north side of the glacier, when approaching the ridge with helicopter. (b) Hveratagl ridge, and (c) Hveratagl geothermal area, with geologists for scale standing in front of KV-P4 pool. The different sampled pools were (with circle where the sample was taken): (d) KV-P4 pool with camera case for scale. (e) KV-P5 pool with glove for scale. (f) KV-P6 pool, with pen for scale and arrows indicating evaporation marks.

4.4 Results

4.4.1 Water geochemistry

Rhyolite- (Kerlingarfjöll) and basalt- (Kverkfjöll) hosted pools show clear physicochemical distinctions (Figure 4-6, Table 4-1). Kerlingarfjöll (KR) pools have

temperatures from 21.6 to > 60 °C with circum-neutral pH, whereas Kverkfjöll (KV) pools have a lower temperature range (16.8 to 23.6 °C), and an acidic pH from 1.7 to 2.7 (Figure 4-6 A). Dissolved ion compositions are shown in Figure 4-6 E. Both sites are dominated by SO_4^{2-} (>70 % of total ions) but clear geochemical water composition differences can be seen on the other dominant ions: Kerlingarfjöll is dominated by Ca^{2+}, Mg^{2+} and K^+, and Kverkfjöll by Fe_{TOTAL}, Na^{2+} and Al^{2+} (Figure 4-6 F). In particular, Kerlingarfjöll pools have undetectable levels of Fe (Fe < 0.03 ppm), in contrast to Kverkfjöll where Fe_{TOTAL} ranges from 7.10 ppm (KV-P4) to 4156.32 ppm (KV-P6). No trends between Dissolved Oxygen, temperature, or pH were identified either within each site, or across sites. All pools have some ppm-level dissolved heavy metal component - Mn^{2+} in all pools, with Kerlingarfjöll pools also having ppm-levels of Zn^{2+}, and KV-P5 and KV-P6 Cr^{2+}.

At Kerlingarfjöll, dissolved SO_4^{2-} ranges from 108.28 to 937.75 ppm, and 13.11 ppm for nearby snow-pack values (KR-ice). SO_4^{2-} concentrations are highest in Kverkfjöll pool waters (21001.12 ppm), similarly distinct from nearby snow-pack SO_4^{2-} (6.16 ppm; KV-ice) that was observed feeding into the pools. Cl^- concentrations at both sites are typically low, ranging from 0.81 to 2.64 ppm for Kerlingarfjöll pools, similar to the nearby snow-pack (2.32 ppm). Cl^- concentrations for the Kverkfjöll pools (0.21 to 2.99 ppm) are lower than that of the snow-pack (3.97ppm; Figure 4-6 B). Aqueous H_2S concentrations from both sites are also low (0.05 to 2.57 ppm for pools at Kerlingarfjöll; <0.05 ppm H_2S in Kverkfjöll pools), with the highest H_2S measured for the higher temperature pools (Figure 4-6 C). Dissolved cations in all samples comprise highly mobile elements. Kerlingarfjöll pools are characterised by dominant Ca^{2+}, Mg^{2+}, K^+ and Si concentrations, whereas Kverkfjöll pools are characterised by Fe, Al^{2+}, Na^+, and Si.

All pools show $\delta^{18}O_{WATER}$ and δD_{WATER} values (Figure 4-6 D) deviating from the Icelandic Water Meteoric Line (IWML; MacDonald et al., 2016). The isotopically heaviest waters are KR-P1 and KV-P6, for which pools have no visibly apparent active water inlets or outlets at the time of sampling. Kverkfjöll values are heavier in δD and $\delta^{18}O$ than a previous study that measured steam from fumaroles and water from the same area (Olaffson et al., 2000).

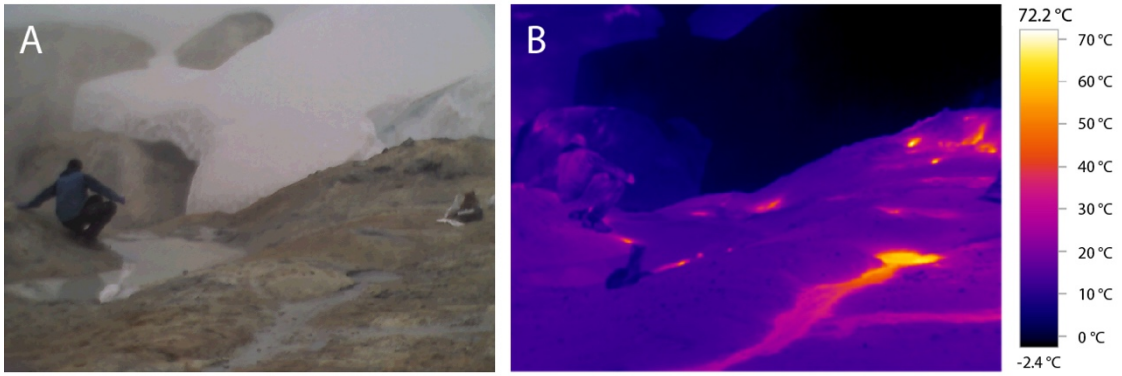

Figure 4-5. Thermal image from Hveratagl, Kverkfjöll, with geologist for scale in front of pool KV-P4. It shows the spatial association between fumarole clusters (72.2 °C) and compacted snow (-2.4 °C), the thermal end-members within this environment. The meltwater pool of the photo (KV-P4) displays an intermediate temperature (20.3 °C).

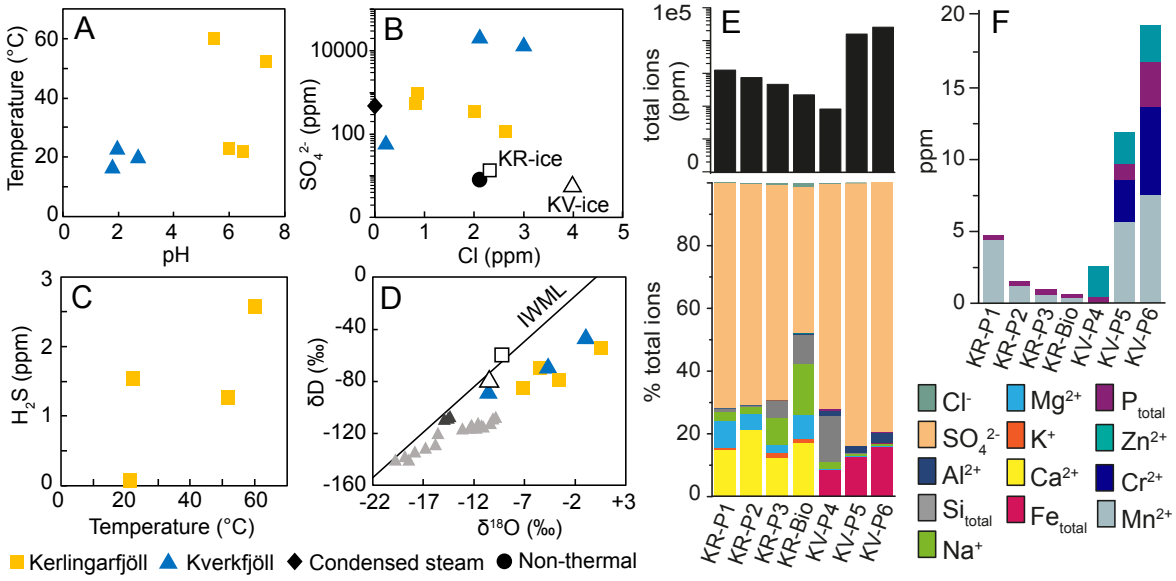

Figure 4-6. Water chemistry for Kerlingarfjöll and Kverkfjöll pools. a) Temperature vs pH, presenting Kerlingarfjöll with circum-neutral values and Kverkfjöll acidic, temperatures around 20 °, KR-Bio and KR-P3 with higher temperatures; b) SO_4^{2-} vs. Cl^-; condensed steam and non-thermal shown for comparison (values from Stefánsson et al., 2016), Kverkfjöll has high SO_4^{2-} concentrations compared with other pools. (c) H_2S concentrations vs Temperature, Kerlingarfjöll concentrations increasing with temperature, Kverkfjöll H_2S concentrations are below detection. (d) δD_{WATER} vs $\delta^{18}O_{WATER}$. Icelandic Water Meteoric Line (IWML) data from MacDonald et al., (2016). Grey triangles show previous data from Kverkfjöll steam (light grey) and water (black) (Olaffson et al., 2000). (e) Total ion concentration in solution (log scale) and relative percentage of dissolved anions and cations. (f) Expanded plot for ions <2 % abundance (Mn^{2+},Cr^{2+}, P_{total}, Zn^{2+}) in ppm.

Table 4-1. Geochemical parameters of pools. BD = below detection. DO = Dissolved Oxygen. All values reported as ppm unless otherwise stated.

Site	Kerlingarfjöll	Kerlingarfjöll	Kerlingarfjöll	Kerlingarfjöll	Kverkfjöll	Kverkfjöll	Kverkfjöll	Kerlingarfjöll	Kverkfjöll
ID	KR-P1	KR-P2	KR-P3	KR-Bio	KV-P4	KV-P5	KV-P6	KR-ice	KV-ice
Temperature (°C)	22.30	21.60	> 60	52.0	20.30	23.60	16.80	-	-
pH	6.00	6.50	5.50	7.35	2.70	1.94	1.76	-	-
DO	0.06	0.93	0.80	2.47	0.26	2.00	1.57	-	-
Si_{total}	13.25	4.13	27.52	20.87	12.55	54.38	78.27	-	-
Ca^{2+}	195.73	162.24	60.46	39.27	0.21	79.60	54.38		
Na^{+}	36.89	15.70	41.45	37.96	2.03	100.54	98.84	-	-
K^{+}	6.48	1.84	6.62	3.68	0.22	0.35	0.27	-	-
Fe_{total}	0.55	BD	BD	BD	7.10	2050.91	4156.32	-	-
Mg^{2+}	113.79	38.73	13.51	17.41	BD	72.05	92.89	-	-
Mn^{2+}	4.43	1.19	0.58	0.30	0.04	5.53	7.37	-	-
Al^{2+}	0.07	0.21	0.49	0.54	1.33	386.00	910.65	-	-
Pb^{2+}	BD	BD	BD	BD	BD	BD	BD	-	-
Cr^{2+}	BD	BD	BD	BD	BD	2.88	5.95	-	-
P_{total}	0.29	0.32	0.36	0.35	0.33	1.01	3.08	-	-
Zn^{2+}	BD	BD	BD	BD	BD	2.170	2.488	-	-
Cl^{-}	0.85	0.81	2.01	2.64	0.21	3.00	2.10	2.32	3.97
SO_4^{2-}	937.75	542.47	333.87	108.28	61.71	13888.82	21001.12	13.11	6.16
Total ions	1310.13	767.69	486.91	231.34	85.76	16608.50	26438.99	-	-
H_2S	1.54	0.05	2.57	1.25	BD	-	BD	-	-
$\delta^{18}O$ (‰)	0.55	-5.39	-3.54	-7.07	-10.63	-4.65	-0.95	-9.16	-10.50
error std	0.06	0.03	0.02	0.03	0.01	0.07	0.08	0.04	0.03
δD(‰)	-55.29	-70.00	-79.92	-86.11	-87.15	-68.36	-45.35	-60.44	-78.66
error std	0.16	0.29	0.09	0.19	0.13	0.19	0.27	0.16	0.15

4.4.2 Sediment mineralogy and geochemistry

Bulk mineralogy derived from XRD analysis is in Table 4-2. XRD patterns for Kerlingarfjöll sediments have sharper peaks and a lower background than those measured from Kverkfjöll sediments, indicating more crystalline phases (Figure 4-7, Table 4-2). Phases detected by XRD in Kerlingarfjöll sediments include quartz, pyrite, calcite, kaolinite, montmorillonite, and anatase, while pyrite dominates the KR-P3 and KR-Bio sediment. Kverkfjöll sediment XRD patterns have less pronounced peaks and higher background, indicating more poorly crystalline and amorphous phases, with peaks for kaolinite, pyrite, anatase and montmorillonite. The abundance of kaolinite distinguishes the two field areas, whereby kaolinite in Kerlingarfjöll pools accounts for ~10 – 25 % crystalline material compared to ~60 – 70 % in Kverkfjöll pool sediments. Fe/Mg smectites were not identified by XRD in any sediments.

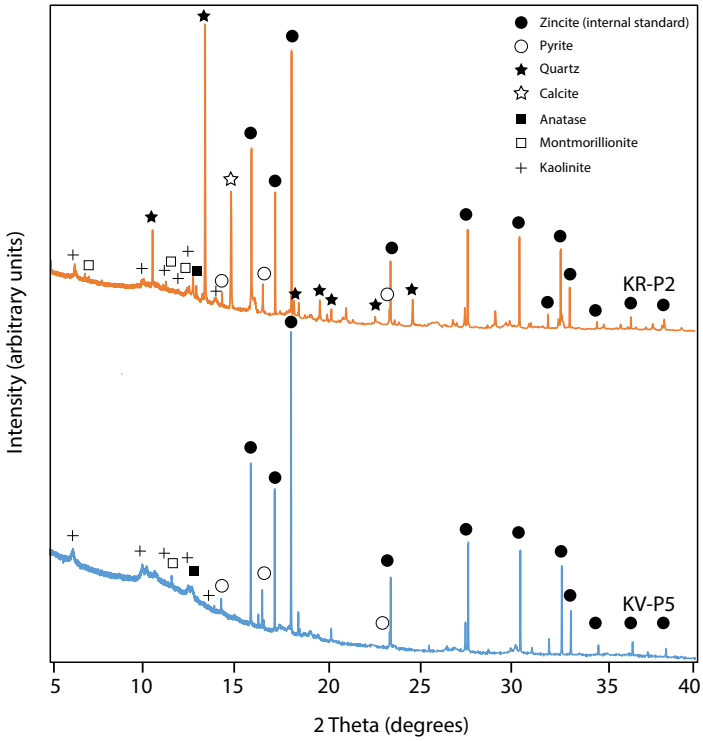

Figure 4-7. Example XRD patterns from Kerlingarfjöll (KR-P2) and Kverkfjöll (KV-P5). Major peaks for mineral phases marked with symbols. Kerlingarfjöll presents calcite, quartz, montmorillonite, kaolinite, pyrite, anatase where Kverkfjöll presents kaolinite, montmorillonite, pyrite, anatase.

Table 4-2. Table shows XRD results with percentages (+- 5 %) of each phase present on the sediment sample. n/a = not applicable.

Site	Sample ID	Quartz	Pyrite	Calcite	Anatase	Kaolinite	Montmorillonite
Kerlingarfjöll	KR-P1	65	5	15	n/a	10	5
Kerlingarfjöll	KR-P2	60	5	10	5	15	5
Kerlingarfjöll	KR-P3	30	30	n/a	10	25	5
Kerlingarfjöll	KR-Bio	55	25	5	5	5	5
Kverkfjöll	KV-P4	n/a	20	n/a	15	60	5
Kverkfjöll	KV-P5	n/a	15	n/a	10	70	5
Kverkfjöll	KV-P6	n/a	15	n/a	15	65	5

Vis-SWIR reflectance spectra of bulk sediments are shown in Figure 4-8. Kverkfjöll pool sediment, KR-P1 sediment, and KR-Bio precipitates, exhibit strong H-O-H and OH^- absorptions in their reflectance spectra at 1.4 and 1.9 μm (Figure 4-8 A,B), and all Kverkfjöll and Kerlingarfjöll sediment spectra have a prominent ~2.2 μm Al-OH absorption band (Figure 4-8 C). Sediments from KR-P1, KV-P4, KV-P5, and KV-P6 have doublet features at 2.1 and 2.2 μm, typical for kaolinite (Ehlmann et al., 2009; Figure 4-8 C), consistent with XRD analysis. These pools (excluding KV-P5), also show weak Mg-OH and Fe-OH overtones between 2.3 and 2.4 μm (Figure 4-8 C), indicating a hydrated Fe/Mg phase, but not necessarily a crystalline smectite clay. KR-P3 sediment has a flat, low-albedo spectrum, with absent hydration features observed in the other sediments from both sites. Electronic transition features associated with Fe-oxidation state vary across sediments (Figure 4-8 D), with pool sediment from KR-Bio, KR-P1, KR-P2, KV-P5, and KV-P6 exhibiting Fe^{3+} absorptions at 0.48, 0.66, and 0.9 μm, which are absent from KR-P3 and KV-P4 sediment. KR-P3 and KV-P4 sediment spectra indicate Fe^{2+} phases, consistent with XRD detection of pyrite, and do not have the distinctive Fe^{3+} absorption bands seen in KV-P5 and KV-P6 (pH <2) or KR-P1, KR-P2 and KR-Bio (pH >6).

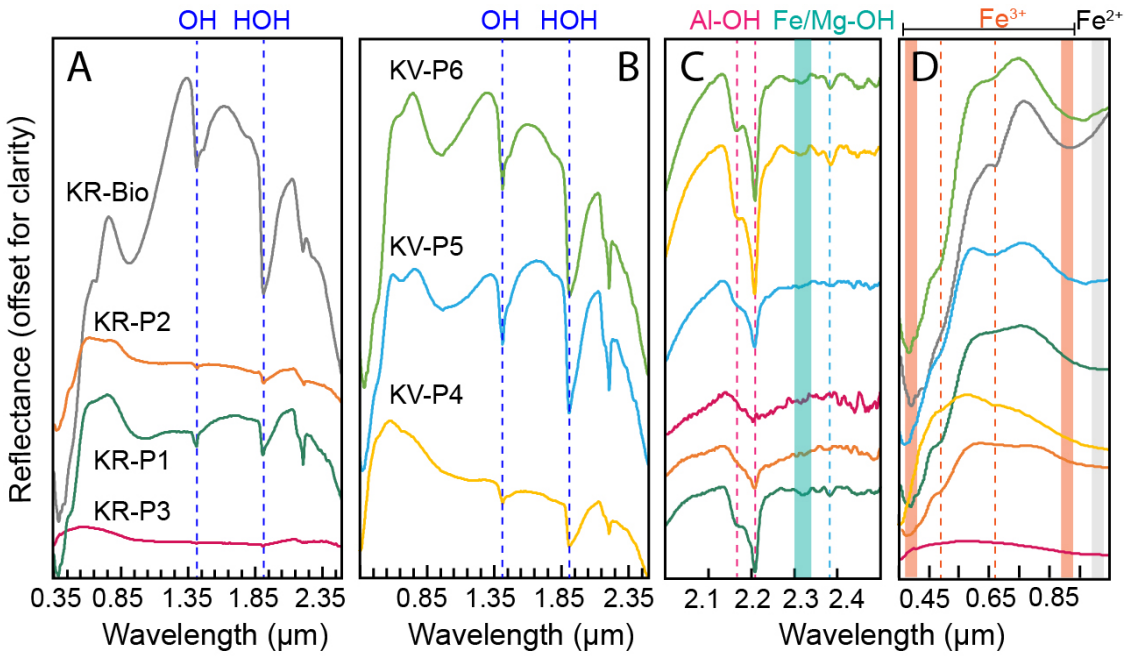

Figure 4-8. Vis-SWIR reflectance spectra from Kerlingarfjöll (a) and Kverkfjöll (b), both showing strong O-H and H-O-H absorptions a part from KR-P2 and KR-P3. (c) Continuum-removed spectra from 2.0 to 2.5 µm; (d) 0.35 – 1.05 µm region. Dashed lines and colour bands highlight absorption features. All Kerlingarfjöll and Kverkfjöll sediment spectra have a prominent ~2.2 µm Al-OH dashed line, and Kerlingarfjöll KR-P1 and Kverkfjöll KV-P4, KV-P6 Fe/Mg-OH absorption band. KR-Bio, KR-P1, KR-P2, KV-P5, and KV-P6 show Fe^{3+} absorptions at 0.48, 0.66, and 0.9 µm and KR-P3 and KV-P4 sediment spectra indicate Fe^{2+} phases.

XRF bulk elemental composition data show Kerlingarfjöll and Kverkfjöll sediments to all be depleted in SiO_2, Na_2O and K_2O, and Kverkfjöll sediments enriched in Al_2O_3 and TiO_2 (Figure 4-9 A,C and Table 4-3), with respect to their host lithologies. Kerlingarfjöll sediments are also enriched in MgO and CaO (Figure 4-9 D), consistent with the XRD detection of calcite. Open-system Chemical Index of Alteration (CIA = Al_2O_3 /(Al_2O_3 +CaO +K_2+Na_2O); Nesbitt and Young, 1982) values at Kerlingarfjöll range from 52-78 %, and 96 to 98 % at Kverkfjöll indicating high levels of chemical alteration compared with the parental rock (Figure 4-9 B). The ternary AFK plot (Figure 4-9 E) supports this, with Kverkfjöll sediments becoming enriched in Al_2O_3 progressing on the path of argillic weathering, compared with Kerlingarfjöll, which instead is slightly enriched in Fe_2O_3 and MgO, following a more typical terrestrial weathering profile (Hurowitz et al., 2006; Nesbitt and Young, 1984).

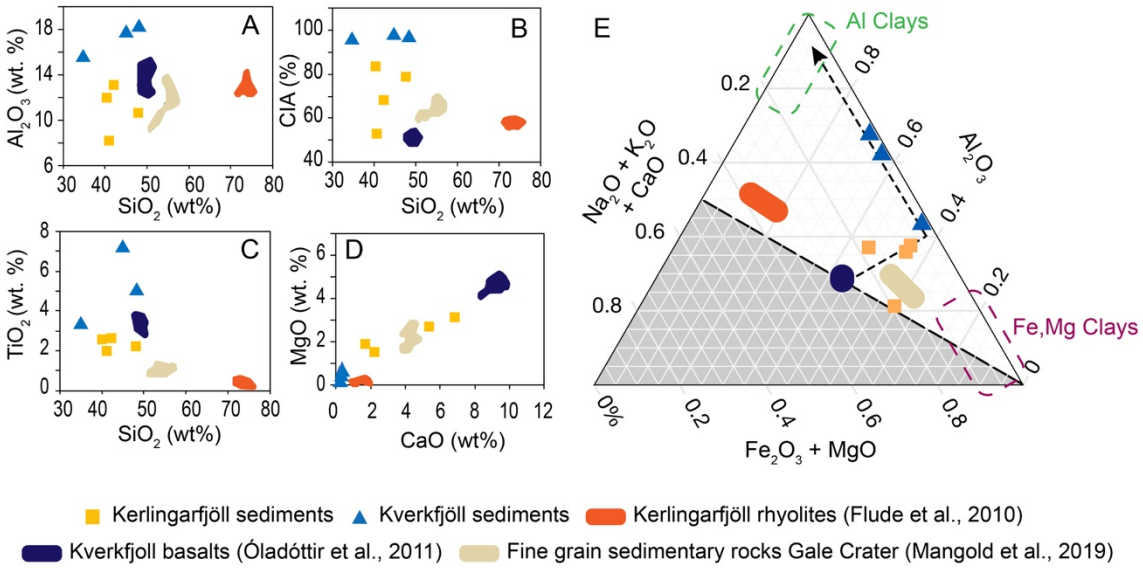

Figure 4-9. Elemental composition data for Kverkfjöll and Kerlingarfjöll pools sediments. (a) Al_2O_3 vs SiO_2 (wt. %). (b) CIA weathering index vs SiO_2 (wt. %). (c) TiO_2 vs SiO_2 (wt. %). (d) MgO vs CaO (wt. %). Both sites show distinctive elemental abundances compared with parental rocks. (e) Ternary AFK diagram, adapted from Hurowitz et al., (2006) and Ehlmann et al. (2011). Dashed black arrow indicating main basalt alteration pathway. Data for Kerlingarfjöll rhyolites and Kverkfjöll basalts from Flude et al., (2010) and Óladóttir et al., (2011b) respectively; Mars Gale Crater geochemistry data of fine-grained sedimentary rocks from Mangold et al. (2019).

*Table 4-3. Table with elemental chemistry data results for both sites. *Sulfates measured (total S in the sample, part of LOI) semiquantitative measurement. This is not volatised sulfides. **CIA = $Al_2O_3/(Al_2O_3+CaO+K_2O+Na_2O))x100$ Average values for parental rhyolitic rock from Flude et al., 2010, average values for parental basaltic rock from Oladottir et al., 2011b.*

Site	Kerlingar-fjöll	Kerlingar-fjöll	Kerlingar-fjöll	Kerlingar-fjöll	Kverk-fjöll	Kverk-fjöll	Kverk-fjöll	absolute deviation (avg)	relative deviation (%)	Kerlingar-fjöll	Kverk-fjöll
Major elements (wt%)	KR-P1	KR-P2	KR-P3	KR-Bio	KV-P4	KV-P5	KV-P6			average parental rhyolite	average parental basalt
SiO_2	42.36	41.0	40.38	48.03	44.9	34.65	48.24	0.05	0.1	74.41	49.62
TiO_2	2.57	1.82	2.52	2.23	7.24	3.36	5.04	0.00	0.0	0.22	3.25
Al_2O_3	13.03	8.08	11.94	10.56	17.83	15.55	18.36	-0.20	-1.6	12.78	13.41
Fe_2O_3	14.51	18.86	14.52	13.57	9.99	19.98	7.43	0.01	0.4	2.90	14.33
MnO	0.23	0.31	0.14	0.17	0.02	0.04	0.03	0.00	-1.2	0.08	0.23
MgO	2.68	3.17	1.93	1.53	0.33	0.91	0.72	-0.04	-2.4	0.08	4.82
CaO	5.38	6.87	1.7	2.17	0.18	0.36	0.22	-0.03	-0.6	1.12	9.18
Na_2O	0.43	<0.13	0.18	0.26	<0.11	<0.12	0.11	0.11	6.7	4.83	2.82
K_2O	0.41	0.31	0.49	0.47	0.06	0.18	0.19	0.02	0.8	3.54	0.61
P_2O_5	0.34	0.27	0.29	0.34	0.38	0.43	0.42	0.00	-1.8		
SO_3*	1.92	3.22	0.81	0.90	0.04	0.14	0.17				
CIA (%)**	67.6	52.9	83.4	78.4	98.6	96.6	97.2				
Na_2O+K_2O	0.84	0.31	0.67	0.73	0.06	0.18	0.30				
LOI (%)	15.95	15.73	24.91	19.58	18.83	24.24	18.92				
SUM	97.89	96.53	99	98.92	99.74	99.7	99.67				

4.5 Discussion

4.5.1 Volcanic gas and surface water controls

Kverkfjöll pool geochemistry is typical of acid-SO_4^{2-} waters (Markússon & Stefánsson, 2011), with the concentration of SO_4^{2-} and Cl^- in surface geothermal waters dependent on the depressurisation, boiling and vapour generation in the upwelling fluid (Arnorsson et al. 2007; Giggenbach & Stewart 1982; Gysi & Stefánsson 2012; Markússon & Stefánsson 2011). Here, Cl^- separates to the liquid phase and concentrates underground after boiling. On the other hand, H_2S goes into the vapour phase, encounters oxidising waters, condenses and becomes oxidised to H_2SO_4. The product is then acidic surface waters with low Cl^- and high SO_4^{2-} concentrations (Figure 4-6 B; Arnorsson & Andresdottir 1995; Stefánsson et al. 2016). Cl^- concentrations are close to the KV-ice value, indicating mixing with surface meteoric water (as snow-pack), also evidenced by the low temperatures (16.8 to 23.6 °C) of the pools (Figure 4-5). The thermal image (Figure 4-5) reveals the spatial association between the thermal end-members within this environment, with fumarole clusters (72.2 ºC) and compacted snow (-2.4 ºC), and the three meltwater pools intermediate temperature (e.g. KV-P4, 20.3 ºC). Kerlingarfjöll pool geochemistry conversely is consistent with steam-heated CO_2 buffered waters, with pH between 5-7 and lower SO_4^{2-} concentrations (Björke et al. 2015; Björke, 2010; Kaasalainen & Stefánsson 2012 ; Markússon & Stefánsson 2011). As at Kverkfjöll, steam mixes with snow/ice-melt, indicated by similar low Cl^- concentrations for KR-ice (2.32 ppm) and water from the pools (0.85 to 2.64 ppm).

The $\delta^{18}O_{WATER}$ and δD_{WATER} values of pool waters from both sites also reveal condensed steam mixing with surface waters. The isotopic values of pool waters follow a typical evaporation trajectory with a lower slope for both Kerlingarfjöll (3.5, R^2=0.7) and Kverkfjöll (4.2, R^2 = 0.9), compared with the IMWL (Icelandic Meteoric Water Line; 6.5), suggesting the pools underwent different degrees of evaporation (highest degree of evaporation for smaller size/closed pools like KR-P1 and KV-P6, Figure 4-6 D). The origin of the evaporation trajectory for Kverkfjöll, estimated from the intersection with the IMWL, differs from the ice-melt values and Icelandic rainwaters (MacDonald et al.,

2016). Instead, the Kverkfjöll intersection with the meteoric line is close to the water and steam values measured here by Olaffsson (2000; Figure 4-6 D). This indicates that the source of water for the pools here is isotopically depleted with respect to the meteoric input, with additional contribution by steam condensation from boiling groundwater at depth, that is isotopically depleted in $\delta^{18}O_{WATER}$ and δD_{WATER} (Olaffsson, 2000). As a result, two evaporation trends form for Kerlingarfjöll and Kverkfjöll.

4.5.2 Bedrock-water interaction and alteration mineralogy

Phase segregation of geothermal aquifer fluids upon ascent to the surface affects the extent of acid supply to the water, which in turn affects the leaching of bedrock (Kaasalainen & Stefánsson, 2012). This is reflected by the circum-neutral Kerlingarfjöll pools with lower total ion concentrations and the acidic Kverkfjöll pools KV-P5 and KV-P6 that have the highest total ion concentrations. Conversely, KV-P4 (pH 2.7), and KR-Bio (pH 7.35) each show low dissolved ion concentrations due to dilution by the observed influx and outflow of meltwater, representing a more open-system alteration environment. Sediment vis-SWIR spectra support low pH, high argillic alteration within the Kverkfjöll pools, also observed at other Icelandic geothermal sites (e.g. Black & Hynek, 2018).

The mineral alteration assemblages observed are largely specific to their immediate environment, with no complete assemblage broadly representing either basalt- or rhyolite-hosted pools. The exception to this is the quartz present within the low temperature (~ 20°C) Kerlingarfjöll pools KR-P1 and KR-P2. The quartz is likely detrital, weathered from surrounding quartz-bearing bedrock (rhyolite) or sediment derived from a higher-temperature region. The elemental geochemistry supports this theory, where both Kerlingarfjöll and Kverkfjöll sediments are considerably depleted in SiO_2 and Na_2O+K_2O compared with their parental rhyolite and basalt. Furthermore, Kverkfjöll is enriched in Al_2O_3 and both in TiO_2, indicative of hydrothermal alteration.

Kerlingarfjöll KR-P1, KR-P2 and Kverkfjöll pools KV-P4 and KV-P6 all have similar SWIR Al-OH and Fe/Mg-OH absorption bands, despite pH varying significantly from 1.8 to 6. Instead, sub-meter scale mineral assemblages identified from both XRD analysis and vis-SWIR spectra are primarily controlled by: (i) the intensity of the surface activity

and temperature, (ii) ratio of geothermal steam to meteoric water, and (iii) the oxidation front of geothermal waters and resulting acid supply. All of these result from the geothermal surface activity rather than host lithology (Markússon & Stefánsson, 2011). At Kerlingarfjöll, the presence of dissolved H_2S in all pools and reducing waters shows the oxidation front is restricted to the water-atmosphere interface, resulting in surface sedimentary pyrite (Figure 4-10). CO_2 input from the vent buffers the circum-neutral pH here through precipitation and dissolution of calcite (seen in KR-P1 and KR-P2). Kverkfjöll pools lack detectable H_2S in the water column, including reducing pool KV-P4, and all have visibly lower steam activity. This lack of H_2S is likely due to the acidic pH of the waters, which causes it to degas (KV-P4), or mix with meteoric water, quickly oxidising H_2S to SO_4^{2-} (KV-P6 and KV-P5). For both scenarios, the oxidation front is restricted to the sediment-water interface.

Overall, Kerlingarfjöll and Kverkfjöll pool water environments are primarily controlled by acid supply, that in turn causes rock leaching. At low pH the major elements Ca^{2+}, Mg^{2+}, K^+ and Na^+ are mobile, with Fe and Al mobility subject to their secondary-mineral solubility (Kaasalainen & Stefánsson, 2012). Water pH and redox conditions are the primary controls for Fe^{2+} and Fe^{3+} speciation reported in Icelandic hydrothermal waters study (Kaasalainen et al., 2017). Above circum-neutral pH, Fe^{2+} and Fe^{3+} precipitation is controlled by redox equilibrium with low-solubility Fe minerals (typically Fe^{3+}-OH and Fe^{2+}-S). For the acidic pool waters at Kverkfjöll, Fe is more soluble, with the relative distribution of Fe^{2+}/Fe^{3+} controlled by the underlying basaltic bedrock, Fe^{2+} oxidation kinetics, and potentially microbial Fe cycling (Kaasalainen et al., 2017).

4.5.3 Implications for past aqueous hydrothermal environments and habitability on Mars

Overall, acid supply and surface activity - resulting from deeper volcanic processes – and top-down redox conditions create two distinct aqueous environments that are largely independent of bedrock lithology. Hydrothermal volcanic environments on Mars could have maintained reduced conditions and circum-neutral pH through the delivery of reduced volcanic gases, even when surface conditions on Mars became more oxidised. Lakes and other non-volcanic systems conversely would have become oxidised, as demonstrated by the paleolake sediments within Gale crater (Hurowitz et al., 2017).

The elemental geochemistry of Kerlingarfjöll and Kverkfjöll can be directly compared to the elemental geochemistry from the hydrothermal site Home Plate, Gusev Crater, on Mars. Specifically, SiO_2 and TiO_2 concentrations (~ 45 % wt for SiO_2 and between 0.5-2.0 % wt TiO_2) on Gusev soils indicate hydrothermal alteration, product of the reaction between the pre-existing soils with acidic hydrothermal sulfate waters in a closed system, in low water to rock ratios (Morris et al, 2008). Similar SiO_2 and TiO_2 concentrations are found in Kerlingarfjöll (between 40- 48 % wt of SiO_2 and 1.8 to 2.5 % wt of TiO_2) and Kverkfjöll (between 34- 48 % wt for SiO_2 and 3.3 to 7.2 % wt TiO_2). The similar TiO_2 concentrations between Kerlingarfjöll and Gusev soils could suggest that concentrations of TiO_2 between 1.8 and 2.5 % wt can also be obtained in circum-neutral pH waters such as Kerlingarfjöll. Kverkfjöll presents greater TiO_2 concentrations than Gusev crater soils, up to 7 %. They are similar to TiO_2 concentrations from a different Mars analogue, Hawaii's Sulfur Bank samples from Morris et al., 2008, which were found to be a product of hypogene alteration at elevated temperatures.

The detection of hydrated Fe/Mg phases co-forming with Al-phyllosilicates within acidic alteration environments (pH <3) at Kverkfjöll show that ~2.3 and 2.4 μm absorption features do not necessarily indicate a broadly circum-neutral pH aqueous environment, but can indicate Al^{3+} and Fe^{3+} saturation within naturally occurring argillic alteration systems, noting that the solubility of Al^{3+} and Fe^{3+} differs by several orders of magnitude between pH 6 (Kerlingarfjöll) and pH ~2 (Kverkfjöll) (Hurowitz et al., 2006). As a result, the SWIR spectra for pool KR-P1 (pH 6), and pools KV-P4/P6 (pH ~2) are markedly similar (Figure 4-8 C) despite the different pH environments for each. These observations differ from the observed stratification of Fe/Mg smectites overlain by Al smectites on Mars, interpreted to represent circum-neutral alteration followed by increasingly acidic alteration environments, either by direct precipitation or through Fe and Mg being replaced by Al and Si (Bristow et al., 2018). Other recent studies have also challenged this interpretation by demonstrating that Fe/Mg smectites can be formed, for instance, under laboratory settings mimicking hydrothermal acidic conditions (Perethyazhko et al., 2014), or in Mars analogue acidic saline lake sediments (Story et al., 2010). Kerlingarfjöll and Kverkfjöll data then support the theory that Fe/Mg smectites can be formed in acidic water conditions.

Similarly, despite the comparable volcano-ice geologic setting, the bulk mineral assemblages observed at Kverkfjöll and Kerlingarfjöll differ to those observed at Sisyphi Montes, which are dominated by smectites, sulfates, zeolites and iron oxides (Ackiss et al., 2018). They also differ from the mineral alteration assemblages previously identified at Hveratagl and the neighbouring geothermal area of Hveradalur at Kverkfjöll, which were dominated by zeolite and smectite clays in addition to gypsum, iron hydroxides, and pyrite (Cousins et al., 2013). This reflects the highly dynamic nature of these hydrothermal environments, particularly at the meter-scale, with implications for extrapolating a given mineral assemblage back to the original paleoenvironment. This observation has also been made on the Martian Home Plate hydrothermal system, where the chemical compositions was found to be highly variable over centimetre scales by the rover MER Spirit (Wang et al., 2008; Yen et al., 2008). Finally, while pyrite has not been detected *in situ* on Mars, its widespread presence in terrestrial hydrothermal sediments suggests Fe-sulfides could have likely formed in Martian hydrothermal settings, since altered by oxidative weathering. Spirit Rover found the Home Plate soils dominated by salts, with a majority of ferric sulfates, silica and magnesium sulfates (Yen et al., 2008). Fe-sulfides could have been oxidised and altered to form ferric sulfates at Home Plate (Yen et al., 2008, Squyres et al., 2007), although they are yet to be found in such environments.

Interaction between volcanic fumaroles and meteoric water-ice creates a mix between deep subsurface high temperature fluids, steam, and gas, and low surface temperatures, resulting in liquid water with moderate temperatures (around 16-20 ºC). This creates a hydrothermal alteration environment that is controlled more by localised redox and pH changes than temperature. Where these types of ice-fed hydrothermal systems existed on Mars in the past, similar processes would potentially operate. More broadly, the pool waters with reducing conditions at Kerlingarfjöll serve as an analogue for aqueous environments on early Mars (4.1–3.7 Ga; Carr & Head, 2010). Here, CH_4 and H_2S delivered via volcanism (Sholes et al., 2017) would result in reduced Fe-S species at the sediment-water interface. Conversely, the geochemical conditions identified in KV-P5 and KV-P6 at Kverkfjöll are representative of oxidising surface aqueous conditions on Mars, with an active oxidation front within the water column itself, and a similar process of oxidised gas delivery through oxidation of H_2S or SO_2 to SO_3 through interaction with

water, exposure to O_2, and photochemical oxidation. KV-P6 typifies this, with concentrated aqueous SO_4^{2-}, acid pH waters, and sedimentary Fe-oxyhydroxides, with pyrite only existing deeper within the sediment, beneath the oxidation front. Such redox transitions are particularly relevant for the preservation of organic biosignatures under reduced conditions, and further necessitates the search for organic molecules within subsurface sediments (Eigenbrode et al., 2018).

Finally, reduced or oxidised Fe or S species in these hydrothermal environments are an ideal localised source of metabolic redox pairs for chemolithotrophic microorganisms, while all pool environments provide accessible trace heavy metals leached from the bedrock (Figure 4-6 F), fundamental for microbial metabolism (Havig et al, 2015; Kee et al., 2013), and potentially prebiotic chemistry (Rimmer & Shortle, 2019). The widespread presence of Fe and S phases at the Martian surface suggests S and Fe-driven metabolisms are plausible in Martian hydrothermal systems (Grotzinger et al., 2014; Nixon et al., 2013; Skok et al., 2010). The pools investigated here however suggest Fe-driven metabolisms face challenges due to pH-driven speciation of Fe. Fe^{2+} oxidation could be challenging in acidic conditions like Kverkfjöll which could only be feasible on Mars with nitrate as an electron acceptor, requiring circum-neutral waters (Price et al., 2018). Fe-oxidation metabolisms could use S^0 as an electron acceptor, with H_2 as an electron donor under anaerobic conditions. Sulfur-driven redox metabolisms however are more plausible: both sites have pools with high concentrations of SO_4^2, available for SO_4^{2-} reducing microorganisms using CO_2 or H_2, and sulfide-oxidation possible within Kerlingarfjöll pools (H_2S was only detected in Kerlingarfjöll, but potentially possible as well in Kverkfjöll sediment under redox front). Sulfur redox metabolisms can produce distinct variable carbon and sulfur stable isotope fractionation values, than can be preserved on the rock record (Johnston et al., 2007; Zerkle et al., 2005; Zerkle et al., 2016).

The Sample Analysis at Mars instrument on board the NASA Curiosity rover (MSL) has measured sulfur isotope compositions in Gale crater sediments, with $\delta^{34}S$ values varying between -47 ‰ to +28 ‰. They have been explained by sulfate-sulfide equilibrium fractionation in a long-term hydrothermal system from the impact crater (Franz, et al., 2017). It is therefore of particular importance to constrain how $\delta^{34}S$ biosignatures would

manifest within relict Martian hydrothermal systems, and how these can be differentiated between abiotic signatures. This will be explored in the following chapters.

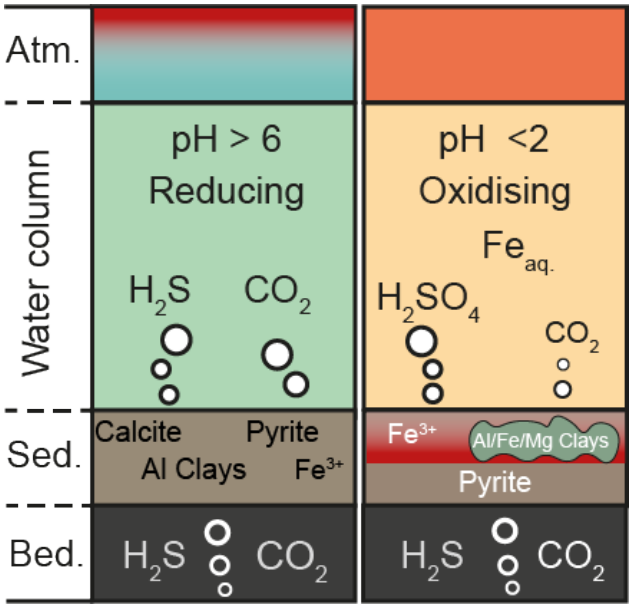

Figure 4-10. Conceptual profile of two environmental Mars scenarios produced by different oxidation fronts (red line), one maintained above the water column (left; KR-P1 or KR-P2), and one maintained within the subsurface sedimentary layer (right; KV-P5 or KV-P6). The reduced environment sustains elevated pH, with dissolved H_2S, and reduced minerals present in the sediment. Where the oxidised scenario has acidic pH, elevated concentrations of dissolved Fe, and an oxidation front present in the sediment that divides the sediment into an oxidised upper layer where there are Fe-oxides minerals and Al/Fe/Mg clays, and reduced layer with reduced minerals.

4.6 Conclusions

The geochemical alteration environments and resulting mineral phases within geothermal pools were investigated at the rhyolitic Kerlingarfjöll volcano and basaltic Kverkfjöll volcano in Iceland. Kerlingarfjöll pools have circum-neutral CO_2-rich waters with reduced conditions and dissolved H_2S, captured as authigenic calcite, pyrite, and kaolinite sediments. Kverkfjöll pool waters are the result of acid-SO_4^{2-} processes, resulting in poorly crystalline Fe-, Mg-phases and Al-phyllosilicates, and subsurface pyrite beneath the sedimentary oxidation front. Dissolved SO_4^{2-} and Cl^- at both sites reveal mixing between surface meteoric water with volcanic steam, with the ephemeral

pools undergoing continual evaporation and dry-wet cycles. Overall, the primary controls on dissolved ion chemistry are acid supply, redox conditions, and secondary-mineral solubility, with underlying lithology playing a minor role in the precipitation of authigenic phases. This study demonstrates how these hydrothermal pools are relevant for understanding past Martian alteration environments on a small scale, and how these are represented in the resulting sedimentary alteration minerals and redox-sensitive phases. Finally, this sensitivity of water chemistry to local redox conditions significantly affects the viability of different S- and Fe-cycling chemolithotrophic microbial metabolisms, with implications for the nature of feasible geochemical biosignatures that can be preserved within the geological record. This is the subject of the research presented in Chapter 5.

5 Are $\delta^{13}C$ and $\delta^{34}S$ robust biosignatures in Mars-analogue hydrothermal systems?

5.1 Introduction

The exploration for life on Mars and other planets is based on the search for biosignatures, as relic evidence for life (Hays et al., 2017). Life requires three vital mechanisms based on universal laws of physics and chemistry. These are: i) an energy source for metabolic reactions, ii) liquid medium to facilitate the reactions, iii) nutrients to build biomass and enzymes that control the metabolic reactions (Cockell et al., 2016; Schwieterman et al., 2018). Biosignatures are usually described as an object, substance or pattern that in order to be produced, needs the mediation of a biological agent (Des Marais et al., 2002). Biosignatures can occur as organic biomarkers (Simoneit et al., 1998, Summons 2011), gases in atmospheres (Rugheimer & Kaltenegger, 2018; Seager et al., 2013), sedimentary structures (e.g. stromatolites, Westall, 2008), microbial material captured within minerals in sedimentary or metamorphic rocks (Cousins et al., 2020; Stueeken 2016), or chemical or isotopic fingerprints of microbial metabolic processes preserved in ancient sediments (Cady et al., 2003; Pilcher et al., 2003; Summons et al., 2008; Westall et al., 2015). These latter geochemical biosignatures can also provide evidence for specific metabolic reactions.

The recent targeted landing sites on Mars for surface exploration have been sedimentary environments such as lakes (NASA Curiosity Rover), or delta/clay-rich deposits (future rover missions NASA 2020 will land at Jezero Crater and ExoMars 2020 on Oxia Planum). The hunt for habitability at these ancient lakes and deltas is justified by the diversity of

environmental niches that these settings support, which includes a large water column offering protection from UV exposure, chemical gradients, a supply of nutrients (Westall et al., 2015) and large input of clays, offering preservation potential for organic biosignatures (Ehlmann et al., 2008). Hydrothermal environments are another setting where life could likely have flourished and been preserved (Des Marais & Walter, 2019a; Michalski et al., 2018; Westall et al., 2018), and as such relic hydrothermal systems are significant in the search for evidence of past microbial life on Mars (e.g. Ruff & Farmer, 2016a). Hydrothermal systems on Earth are known to support chemolithotrophic life, and can preserve evidence of early life as far back as 3.7 Ga (Dodd et al., 2017). Furthermore, they can provide basic elements for life and redox couples for metabolisms, and traces of these processes can be recorded in the geologic record through stable isotope ratios (Banfield et al., 2001).

Carbon (C) and sulfur (S) preserved in the rock record are influenced by metabolic processes driven by life; C isotopes are fractionated by the specific CO_2 fixation pathways used by autotrophic microorganisms, with larger or smaller fractionations depending upon the different pathways (Zerkle et al., 2005). Sulfur isotope values in the environment are influenced by S-cycling microbes, in particular microbial sulfate reducers (MSR). MSR produce significant S isotope effects by producing sulfide (H_2S) that is depleted in heavy isotopes with respect to the reactant sulfate (SO_4^{2-}) through enzymatic processes that happen inside the cell (Bradley et al., 2016). These compounds can be incorporated in the sedimentary record as sulfate minerals (e.g., barite or carbonate-associated-sulfate) (Perry et al., 1971; Rose et al., 2019) or sulfide minerals (e.g., pyrite) that can be preserved in the rock record and record the resulting sulfur isotope values (Berner et al., 1984; Canfield et al., 2001a; Hurtgen et al., 2005; Johnston et al., 2007).

Importantly, abiotic processes can mask the C and S isotope biosignatures, making it difficult to discriminate between abiotic and biologic sources. Results from laboratory experiments synthetising organic compounds mimicking hydrothermal conditions at 250 ^{o}C, found $\delta^{13}C$ from organic products were depleted up to -50 ‰, typically attributed to biological effects (McCollom & Seewald, 2006). After deposition, $\delta^{13}C$ isotopic biosignatures in the rock record can be altered through diagenetic processes, as

mentioned in Chapter 2. The main processes are fluids such as meteoric, brine or porewaters, that percolate through the sediments altering the $\delta^{13}C$ (Richardson et al., 2019). Sulfide can react abiotically with oxygen, producing an increase in sulfide $\delta^{34}S$ up to 5 ‰ (Fry et al., 1988). Sulfate reduction can happen abiotically through thermochemical conditions, at high-temperatures (between 100- 200 ^{o}C) and produces fractionations <20 ‰ (Watanabe et al., 2009). Diagenetic processes can also alter $\delta^{34}S$ by diagenetic processes, such as meteoric or brine fluids (Fisher et al., 2014).

Sulfur phases have been detected on Mars in the form of sulfide in shergottites, but mostly in the form of sulfates on the surface (Aubrey et al., 2006; Burns & Fisher, 1990; Gaillard et al., 2013; Gendrin et al., 2005).These deposits, likely volcanogenic, suggest that the S cycle played a significant role in modifying the Martian surface. Microbial life could have taken advantage of these sulfur compounds by obtaining energy through their oxidation and reduction (Nixon & Cousins, 2013). Sulfur deposits are dominant on the Martian surface, but C-bearing deposits are rare. This is one of the main differences between Earth and Mars: Mars is dominated by the S cycle and Earth is dominated by the C cycle (Gaillard et al., 2013). Still, carbon is found on the Martian surface in the form of Fe/Mg carbonates present in small magnitudes, in relation with clays underlying sulfate deposits (Ehlmann et al., 2008b; Wray et al., 2016). It has also been suggested that C deposits could exist deep within the subsurface (Michalski et al., 2013). Furthermore, the Gale Crater paleolake hosts 3.5 Ga mudstones with preserved organic matter (Eigenbrode et al., 2018).

Given the occurrence of carbon and sulfur on Mars' surface, and their suitability to provide stable isotope biomarkers, this chapter evaluates the utility of $\delta^{13}C$ and $\delta^{34}S$ values as microbial biosignatures in hot spring pool sediments, by comparing two geochemically distinct hydrothermal Mars analogue systems in Iceland with different pH. Kerlingarfjöll has circum-neutral pH and Kverkfjöll acidic pH, both characterised and detailed in Chapter 4. As Chapter 4 concludes, the pH of the hydrothermal pools from Kerlingarfjöll and Kverkfjöll is controlled by deep volcanic processes. Then, it is important to understand what's the influence of pH to the microbial communities in these systems. By contextualising the $\delta^{13}C$ and $\delta^{34}S$ isotope values with the chemolithotrophic communities present in the pools, this study allows for organic $\delta^{13}C$

and mineral $\delta^{34}S$ values to be assessed as potential isotopic biosignatures in analogous systems on Mars. The challenges of distinguishing abiotic from biotic signatures in these settings are also explored, and potential strategies for future missions.

5.2 Results

5.2.1 Water geochemistry, carbon and sulfur isotopes

Kerlingarfjöll and Kverkfjöll have key water geochemical differences (as described in Chapter 4). The main differences are the pH and Fe_{total} concentrations of these two sites: Kerlingarfjöll is circum-neutral with low/undetectable Fe_{total}, and Kverkfjöll is acidic with high Fe_{total} concentrations. Water geochemistry at both sites is consistently dominated by dissolved SO_4^{2-} (up to 937.7 ppm in Kerlingarfjöll, and up to 21000 ppm in Kverkfjöll), followed in Kerlingarfjöll by high concentrations of dissolved Ca^{2+}, Mg^{2+}, K^{+}, Na^{2+}. Kerlingarfjöll also has detectable H_2S (0.05-2.5 ppm) and almost no dissolved total Fe (<0.03 ppm, and 0.5 ppm in KR-P1). Conversely, Kverkfjöll acidic waters are dominated by high concentrations of Al^{2+} and total Fe values (7.1 to 2050.9 ppm of total Fe), with no detectable H_2S. Dissolved oxygen concentrations are variable across Kerlingarfjöll and Kverkfjöll: Kerlingarfjöll pools are micro-oxic (0.06 ppm KR-P1, 0.93 ppm KR-P2, 0.8 ppm P3) as is Kverkfjöll pool KV-P4 (0.2 ppm). Oxic conditions are found in Kerlingarfjöll stream KR-Bio (average of 2.47 ppm), and at Kverkfjöll pools KV-P5 (2.0 ppm) and KV-P6 (1.5 ppm). Temperatures in Kerlingarfjöll pools KR-P1 and KR-P2 are 21 and 22 °C respectively and KR-P3 60°C. Kerlingarfjöll stream (KR-Bio) has an average temperature of 52 °C, and Kverkfjöll pools range between 16-23 °C.

Total Organic Carbon (TOC) concentrations and associated $\delta^{13}C$ values from sediments ($\delta^{13}C_{TOC}$) of the pools are presented in Table 5-1 and Figure 5-1. TOC concentrations range from 0.10 to 0.32 wt. % at Kerlingarfjöll and 0.29 to 0.42 wt. % at Kverkfjöll. There is a minor difference between both sites, with generally lower TOC values at Kerlingarfjöll, and higher TOC values at Kverkfjöll. Kverkfjöll KV-P6 has the highest wt. % of TOC. $\delta^{13}C_{TOC}$ values vary from -23.5 to -16.8 ‰ at Kerlingarfjöll, and from -23.5 ‰ to -20.97 ‰ at Kverkfjöll (Figure 5-1 A). KV-P4 exhibits the lowest $\delta^{13}C_{TOC}$ value overall

(-23.5 ‰). Figure 5-1 B shows the fractionations between $\delta^{13}C_{CO2}$ (volcanic CO_2, literature values from Barry et al., 2014 and Poreda et al., 1999: -4.01 ‰ at Kerlingarfjöll -2.83 ‰ at Kverkfjöll) and $\delta^{13}C_{TOC}$ ($^{13}\varepsilon_{CO2\text{-}TOC}$), as a function of temperature. High temperature pool KR-P3 and stream KR-Bio (52 and 60 °C respectively), show smaller fractionations in $\delta^{13}C$ (16.29 and 15.64 ‰) than lower temperature (16-23 °C) KR-P1 and Kverkfjöll pools (18.4- 21.0 ‰).

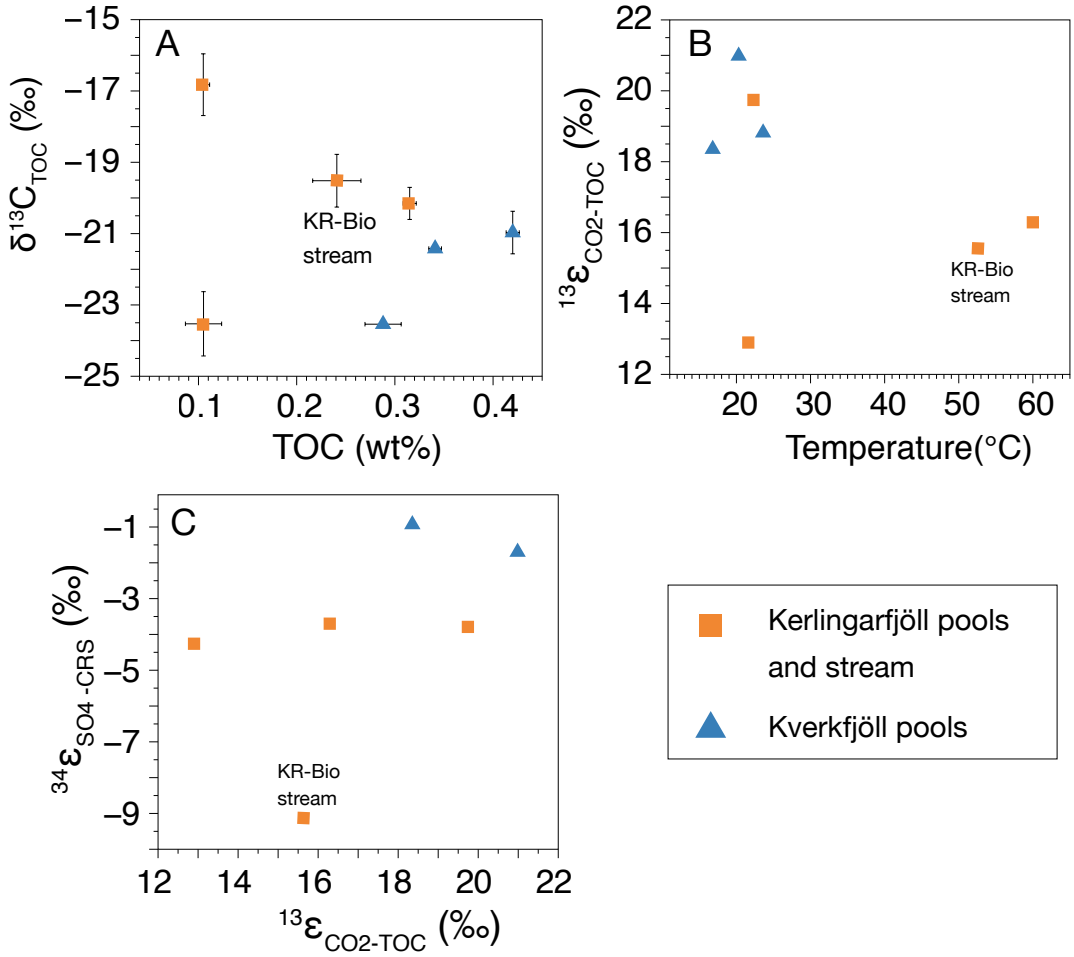

Figure 5-1. Relationships for a) $\delta^{13}C$ vs TOC, b) C isotope fractionations ($^{13}\varepsilon_{CO2\text{-}TOC}$). vs temperature, c) S isotope fractionations ($^{34}\varepsilon_{SO4\text{-}CRS}$) vs C isotope fractionations ($^{13}\varepsilon_{CO2\text{-}TOC}$).

Table 5-1. TOC and $\delta^{13}C$ TOC values. $\delta^{13}C$ CO_2 Kerlingarfjöll values from Barry et al., 2014, and Kverkfjöll values average of Barry et al., 2014 values and Poreda et al., 1992 values.

ID	SITE	TOC	STDEV TOC	$\Delta^{13}C_{TOC}$	STDEV $\Delta^{13}C_{TOC}$	$\Delta^{13}C_{CO2\text{-}TOC}$	$^{13}E_{CO2\text{-}TOC}$
		wt%		‰			‰
KR-P1	Kerlingarfjöll	0.11	0.018	-23.5	0.901	1.019	19.7
KR-P2	Kerlingarfjöll	0.10	0.006	-16.8	0.866	1.013	12.9
KR-P3	Kerlingarfjöll	0.31	0.007	-20.2	0.450	1.016	16.3
KR-Bio	Kerlingarfjöll	0.24	0.025	-19.5	0.739	1.016	15.6
KV-P4	Kverkfjöll	0.29	0.013	-23.5	0.049	1.021	21.0
KV-P5	Kverkfjöll	0.34	0.046	-21.4	0.597	1.019	18.8
KV-P6	Kverkfjöll	0.42		-21.0		1.019	18.4

-4.06 *1 $\delta^{13}C$ CO_2 Kerlingarfjöll

-2.83 *2 $\delta^{13}C$ CO_2 Kverkfjöll

The S isotope values ($\delta^{34}S$) measured are listed in Table 5-2 . They were measured for aqueous SO_4^{2-} ($\delta^{34}S_{SO4}$), aqueous H_2S ($\delta^{34}S_{H2S}$), sedimentary AVS ($\delta^{34}S_{AVS}$) and sedimentary CRS ($\delta^{34}S_{CRS}$). Aqueous $\delta^{34}S_{H2S}$, was measurable in two Kerlingarfjöll pools KR-P1 and KR-P3 (1.2 ‰ and 1.3 ‰ respectively). $\delta^{34}S_{SO4}$ values are heavier in Kerlingarfjöll (from 0.2 ‰ to 4.7 ‰) than Kverkfjöll pools (-1.4 to 1.0 ‰). Sedimentary $\delta^{34}S_{AVS}$ was only measurable at KR-P2 (2.2 ‰). Sedimentary $\delta^{34}S_{CRS}$ values are lighter at Kerlingarfjöll (-4.5 to -2.3 ‰) compared with Kverkfjöll pools (-2.4 ‰ to -0.7 ‰). Carbon isotope fractionations ($\varepsilon^{13}C_{CO2\text{-}TOC}$) are compared to S isotope fractionations ($^{34}\varepsilon_{SO4\text{-}CRS}$) in Figure 5-1 C. For both Kerlingarfjöll and Kverkfjöll, the fractionations for $^{34}\varepsilon_{SO4\text{-}CRS}$ (- 9.1 to -0.9 ‰) are smaller than $\varepsilon^{13}C_{CO2\text{-}TOC}$ (12.9 to 19.7 ‰).

.

Table 5-2. $\delta^{34}S$ values for water H_2S, SO_4^{2-} and sediment samples AVS and CRS. Fractionations shown as $^{34}\varepsilon_{SO4\text{-}CRS}$ between reactant water SO_4^{2-} and product sedimentary CRS (including pyrite and elemental S).

		H_2S (AQ)		**SO_4^{2-} (AQ)**		**AVS SEDIMENTS**		**CRS SEDIMENTS**		**CRS-SO_4^{2-} (AQ)**	
	SITE	**$\Delta^{34}S$**	**STDEV**	**$\Delta^{34}S$**	**STDEV**	**$\Delta^{34}S$**	**STDEV**	**$\Delta^{34}S$**	**STDEV**	**$\Delta^{34}S$**	**$^{34}E_{SO4\text{-}CRS}$**
ID		‰	‰	‰	‰	‰	‰	‰	‰	‰	‰
KR-P1	Kerlingarfjöll	1.2	-	1.5	0.00	-	-	-2.3	0.18	1.00	-3.8
KR-P2	Kerlingarfjöll	-	-	1.8	0.37	2.2	-	-2.4	0.28	1.00	-4.3
KR-P3	Kerlingarfjöll	1.5	0.86	0.2	0.08	-	-	-3.5	0.05	1.00	-3.7
KR-Bio	Kerlingarfjöll	-	-	4.7	0.34	-	-	-4.5	0.55	0.99	-9.1
KV-P4	Kverkfjöll	-	-	1.0	0.06	-	-	-0.7	0.07	1.00	-1.7
KV-P5	Kverkfjöll	-	-			-	-	-1.7	0.18		
KV-P6	Kverkfjöll	-	-	-1.4	0.04	-	-	-2.4	0.20	1.00	-0.9

5.2.2 Archaeal communities

The archaeal communities at genus level in the Kerlingarfjöll pools and KR-Bio stream are dominated by sequences that affiliate with the *Thermofilum* (between 38 and 65 % of relative abundance of the genus profile; Figure 5-2, Table 5-3). The Kerlingarfjöll pools at archaeal genus level are also dominated by methanogens (*Methanobrevibacter, Methanomassiliicoccus, Methanosaeata, Methanothermobacter, Methanococcus, Methanocaldococcus, Methanocella,* and *Methanotorris*). Between them they make up the following % of genus profile on each pool: 44.98 % at KR-P1, 40.99 % at KR-P2, and 25.54 % at KR-P3. Apart from mostly *Thermofilum*, KR-Bio genus population also includes *Candidatus caldiarcheum* (12.18 %) and *Ignisphaera* (4.48 %) and low presence of methanogens (*Methanotorris*, 1.5 %). *Candidatus nitroscaldus* is the only archaea genus existing across different sites. At Kverkfjöll KV-P5, *Candidatus nitroscaldus* is up to 50.85 % of the genus profile. The other 50 % of the KV-P5 archaeal genus profile is comprised by *Aciduliprofundum* (Figure 5-2). At Kverkfjöll, archaea were not detected with universal or archaea-specific primers in KV-P4 and KV-P6.

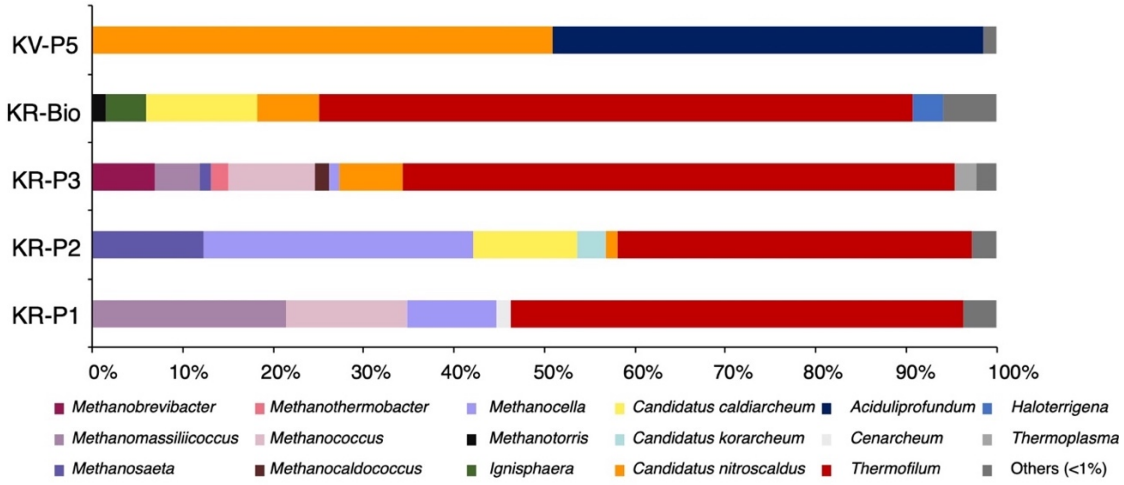

Figure 5-2. Phylogenetic affiliation of 16S rRNA results for archaea at the genus level. Kverkfjöll pools KV-P4 and KV-P6 are not represented as archaea were not detected.

The Venn diagram for archaeal OTUs across all sites (Figure 5-3) supports Figure 5-2, as it shows how KR-P3 and KR-Bio have a similar archaeal community profile. They both share the highest numbers of archaea OTUs (10) between pools at Kerlingarfjöll. KR-P3

has the highest number of OTUs (88), followed by KR-Bio (81), KR-P2 (19) and KR-P1 (9). The number of OTUs shared between all groups is 15. Table 5-4 describes the optimum environmental parameters (temperature, pH, C source, O_2 conditions for growth) and potential metabolic pathways for the most dominant archaea taxa at genus level at Kerlingarfjöll and Kverkfjöll. The dominant metabolic pathways are S^0 reduction and methanogenesis (a majority hydrogenotrophic). Most of them grow at circum-neutral pH and anoxic conditions, apart from *Candidatus nitroscaldus* (which grows aerobically). Carbon sources are varied with no general preference for Organic C or CO_2. *Aciduliprofundum* is the only one with pH range from 3 to 6.

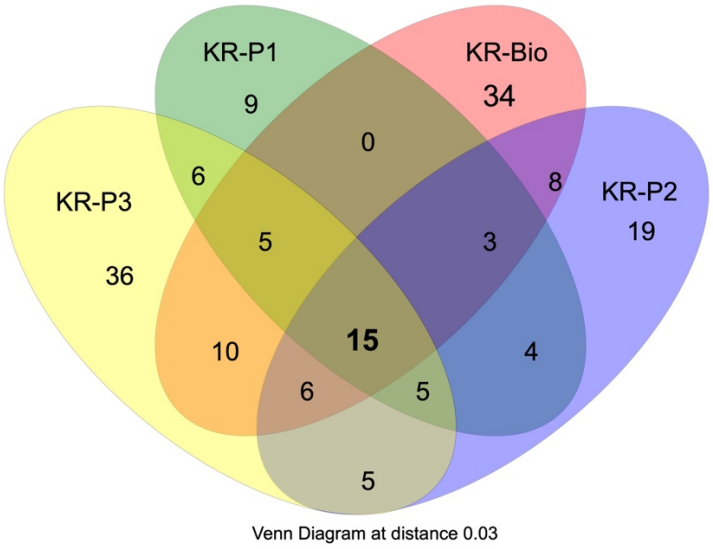

Figure 5-3. Venn diagram plots for archaea OTU's at Kerlingarfjöll only.

The phylogenetic archaeal tree is presented in Figure 5-4 with Kerlingarfjöll and Kverkfjöll pool OTUs (127 sequence reads). Included in it are the names of the most similar cultured or uncultured archaeal relatives identified using BLASTn and GenBank (see Appendix A). In Figure 5-4 the phylogenetic relationships between archaeal groups in Kerlingarfjöll pools and Kverkfjöll pool KV-P5 reveal many shared OTUs between both sites, with few novel OTUs for any one pool. Specifically, KR-P3, KR-Bio and KV-P5 are most prevalent across the tree. Most of the archaeal OTUs share higher similarity (>95 %) to uncultured archaeon strains rather than cultured strains.

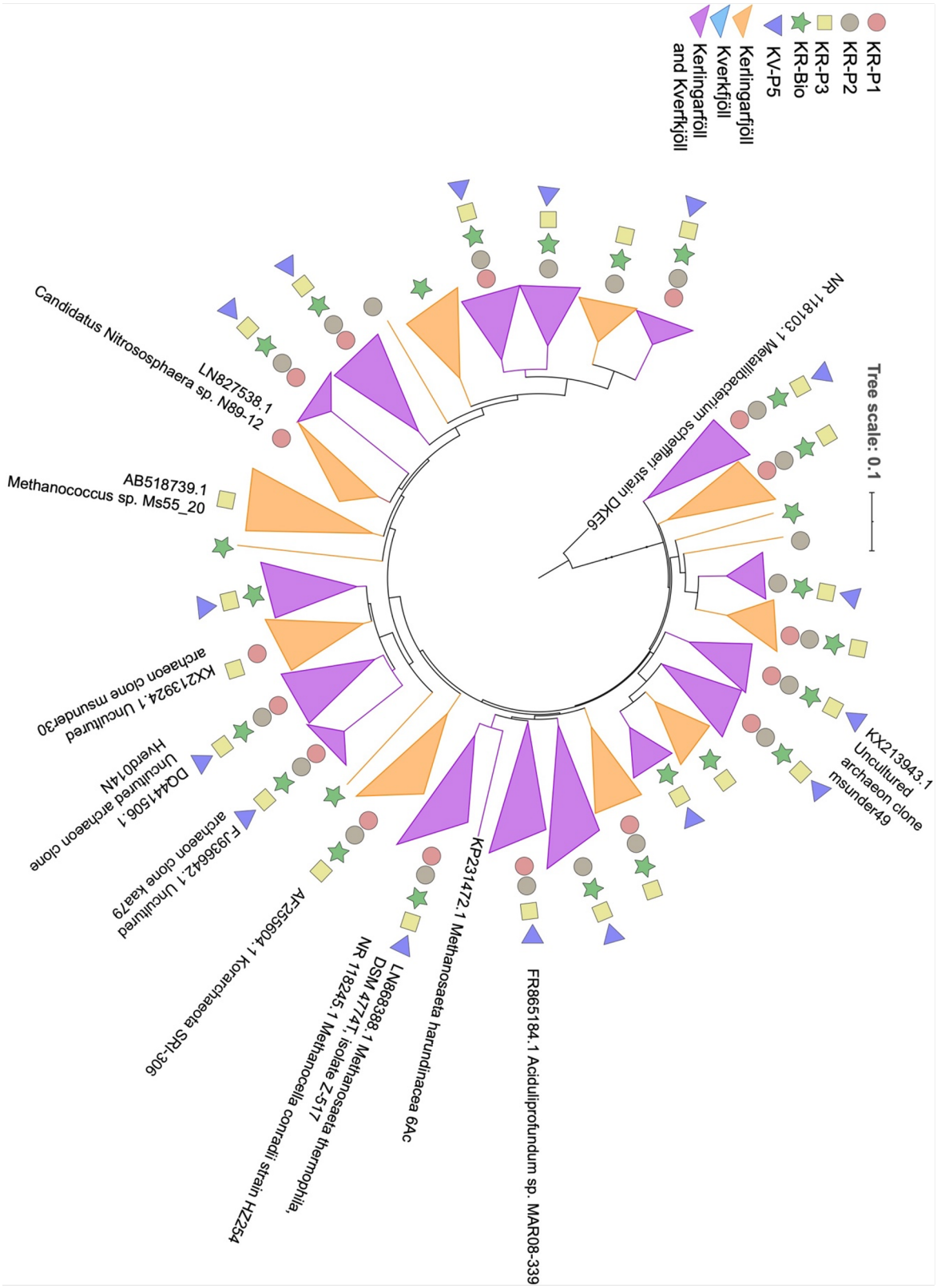

Figure 5-4. Phylogenetic tree from Kerlingarfjöll and Kverkfjöll representative archaea species. NB: GenBank species are indicated, where they have their closest relatives. Bacteria Metallibacterium cheffleri strain DKE6 is used as the outgroup.

Table 5-3. Phyllogenetic affiliation of 16s rRNA results for Archaea for the most abundant at genus level for Kerlingarfjöll and Kverkfjöll (KV-P5).

KR-P1	KR-P2	KR-P3	KR-Bio	KV-P5
Thermofilum	*Thermofilum*	*Thermofilum*	*Thermofilum*	*Candidatus nitroscaldus*
(50.29%)	(38.20%)	(57.27%)	(65.66%)	(50.85%)
Methanomassiliicoccus	*Methanocella*	*Methanococcus*	*Candidatus caldiarcheum*	*Aciduliprofundum*
(21.56%)	(29.03%)	(9.04%)	(12.18%)	(47.70%)
Methanococcus	*Methanosaeta*	*Candidatus nitroscaldus*	*Candidatus nitroscaldus*	Others
(13.51%)	(11.96%)	(6.71%)	(6.99%)	(1.45%)
Methanocella	*Candidatus*	*Methanobrevibacter*	*Ignisphaera*	
(9.91%)	*caldiarcheum*	(6.46%)	(4.48%)	
	(11.22%)			
Others	*Candidatus*	*Methanomassiliicoccus*	*Haloterrigena*	
(3.71%)	*korarcheum*	(4.65%)	(3.28%)	
	(3.13%)			
	Candidatus	*Methanothermobacter*	Others	
	nitroscaldus	(1.71%)	(5.94%)	
	(1.28%)			
	Others	*Methanosaeta*		
	(2.61%)	(1.22%)		
		Methanocaldococcus		
		(1.43%)		
		Methanocella		
		(1.04%)		
		Others		
		(2.09%)		

Table 5-4. Description of optimal growth parameters for the dominant archaeal taxa present in Kerlingarfjöll and Kverkfjöll pools

Genus **Phylum**	**An/aerobic**	**C Source**	**pH R**	**pH Op**	**T R**	**T Op**	**Metabolic pathway**	**Reference**
Thermofilum Crenarcheota	ChemoOrg Anaerobe	Corg	4-6.5	6-6.5	67-95	85	sulfur reduction formate hydrogen lyase $nS^o + nH^+ + Corg \rightarrow nH_2S + CO_2$ $nH_2 + Corg + nH^+ \rightarrow Corg + nH_2O$	Dominova et al., 2013 Zeikus et al., 1983 Anderson et al., 2008 Zillig et al., 1981
Candidatus caldiarcheum Thaumarcheota	ChemoLitho Anaerobic	CO_2		5.1		70	$2H_2 + O_2 \rightarrow 2\ H_2O$	Nunoura et al., 2011 Hirayama 2005
Candidatus nitroscaldus Crenarcheota	ChemoLitho Aerobic	CO_2	3-7.5		25-84	68	$NH_3 + O_2 \rightarrow NO_2^- + 3H^+$	Abby et al., 2018 Jung et al., 2014
Ignisphaera Crenarcheota	ChemoOrg Anaerobic	Corg	5.4-7	6.4	85-98	92-95	N/A	Niederberg et al., 2006
Methanomassiliicoccus Euryarcheota	ChemoOrg Anaerobic	Corg		7.6		37	methanogenesis from methanol $CH_3OH + H_2 \rightarrow CH_4$	Dridi et al., 2012 Kroninger et al., 2017
Methanocella Euryarcheota	ChemoOrg Anaerobic	Corg	6.4-7.2	6.8	37-60	50-55	hydrogenotrophic methanogenesis, but acetate as C source $CO_2 + H_2 \rightarrow CH_4 + H_2O$	Lu et al., 2012
Methanococcus Euryarcheota	ChemoLitho Anaerobic	CO_2	5.5-7.5		20-55		hydrogenotrophic methanogenesis $CO_2 + H_2 \rightarrow CH_4 + H_2O$	Kendall et al., 2006
Methanosaeta thermophila Euryarcheota	ChemoOrg Anaerobic	Corg		7	55-60	55	methanogenesis from acetate degradation $CH_3COOH \rightarrow CH_4 + CO_2$	Kamagata et al., 1992 Berger et al., 2012
Methanobrevibacter Euryarcheota	ChemoLitho Anaerobic	CO_2	5-7.5	6		35	hydrogenotrophic methanogenesis $CO_2 + H_2 \rightarrow CH_4 + H_2O$	Savant et al., 2002.
Aciduliprofundum Euryarcheota	ChemoOrg Anaerobic	COrg	3.3-5.8	4.5	55-75	70	$nS^o + nH^+ + Corg \rightarrow nH_2S + CO_2$ $Fe^{3+} + H_2O \rightarrow Fe^{2+} + O_2 + 4H^+$	Reysenbach et al., 2006 Schouten et al., 2008

5.2.3 Bacterial communities

16S rRNA results identify *Proteobacteria* as the most abundant bacterial phylum across Kerlingarfjöll (KR-P1 and KR-P2) and Kverkfjöll pools (46 to 77 % of the phylum profile relative abundance Figure 5-5 A, Table 5-5). At phylum level, the remaining community profiles within KR-P1 and KR-P2 are similar with varying % (see Figure 5-5 A). These are *Actinobacteria* (1-5 %), *Nitrospirae* (3-5 %), *Firmicutes* (2-6 %), *Acidobacteria* (1-3 %), *Spirochaetes* (1-3 %), and *Chloroflexi* (2-29 %). At Kverkfjöll pools after *Proteobacteria* the remaining phylum profiles have likewise similar taxonomic profiles than KR-P1 and KR-P2. They are dominated by *Actinobacteria* (13- 26 %), *Nitrospirae* (8-20 %) and *Firmicutes* (12- 21 %). On more detail within *Proteobacteria, Desulfurivibrio* represents 35% of the profile at genera level in KR-P1, and 21 % in KR-P2 (Figure 5-5 B). KR-P2 *Proteobacteria* also presents *Desulfocapsa* (24 %) and *Thiobacillus* (14 %). Within *Proteobacteria* phylum at Kverkfjöll pools are dominated by genera profiles of *Syntrophus* (7- 25 %), *Acidithiobacillus* (9-24 %) and *Acidiferrobacter* (6-12 %) (Figure 5-5 B).

Kerlingarfjöll pool KR-P3 and KR-Bio stream are distinct, as they are not dominated by *Proteobacteria*. At KR-Bio *Protebacteria* make up less than 1 % of the bacterial phylum community profile, and only 22 % for KR-P3 (Figure 5-5 A). Instead, KR-Bio is dominated by *Aquificae* (82 %). KR-P3 genus composition is dominated by *Dehalococcoides* (19 %) (from phylum *Cloroflexi*), *Caldisericum* (15 %) (phylum *Caldiserica*) and *Sulfurihydrogenibium* (7 %, phylum A*quificae*). The KR-Bio community affiliates predominantly with *Sulfurihydrogenibium* (75 %).

In the Venn diagram for Kerlingarfjöll bacteria (Figure 5-6 A), KR-P1 and KR-P2 share the highest number of bacterial OTUs (66), and KR-P3 and KR-Bio share 48 OTUs at a similarity cut-off of 0.03. The total OTUs shared between Kerlingarfjöll pools is 2. The Kverkfjöll OTU Venn diagram (Figure 5-6 B) shows the highest number of shared OTUs are between KV-P4 and KV-P6 (47), while 11 OTUs are common to all three pools. The main metabolic pathways identified at genus level at Kerlingarfjöll are S oxidation and SO_4^{2-} reduction, with a preference for circum-neutral pH for growth (*Table 5-6*). The main metabolic pathways identified at genus level at Kverkfjöll are Fe reduction and oxidation, and S oxidation (Table 5-7). The pH preference is all below 4 at Kverkfjöll.

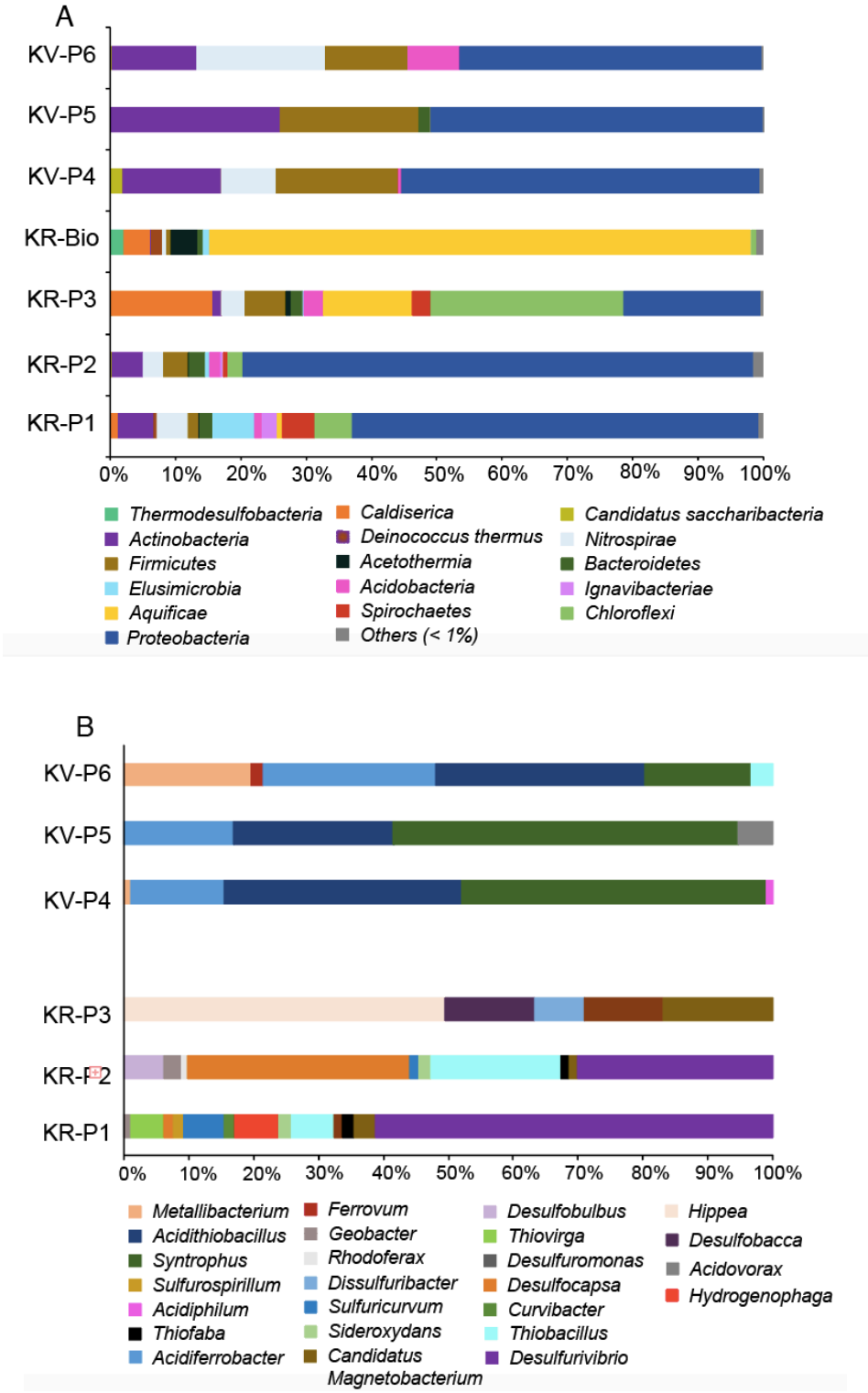

Figure 5-5. Phylogenetic affiliation of 16S rRNA results for Bacteria on 100% stacked bars for the different pools and stream (a) at phylum level, it can be seen how Proteobacteria phylum dominates the communities (22-77 %) of the pools. (b) Only comprising genus level from Proteobacteria. KR-Bio are not featured as Proteobacteria make up only 1% of the profile.

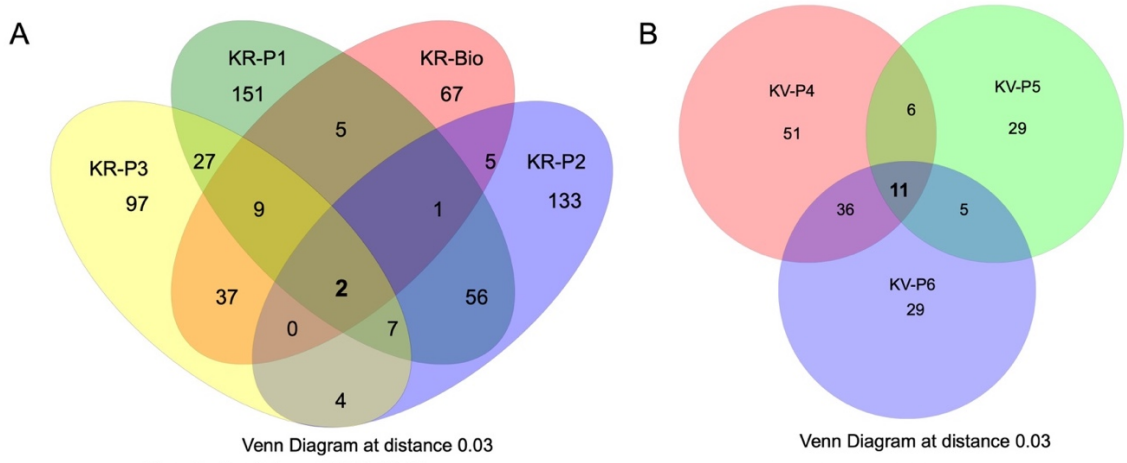

Figure 5-6 Venn diagram plots for bacteria OTU's at (a) Kerlingarfjöll, and (b) Kverkfjöll. The cut-off is 0.03, and the total number of species shared between all samples in Kerlingarfjöll is 2, and at Kverkfjöll 11.

A bacterial phylogenetic tree is presented in Figure 5-7 comprising Kerlingarfjöll and Kverkfjöll pool OTUs (822 sequence reads). Also included are the names of the most similar relatives (cultured and uncultured) identified using BLASTn and downloaded from GenBank (see Appendix A). Overall, there are fewer shared OTUs between Kerlingarfjöll and Kverkfjöll, with unique clades particularly for KR-P1 and KR-P2. Conversely to the archaeal tree, the majority of closest relatives are cultured relatives. Closest cultured relatives are *Caldisericum, Thermodesulfobacterium, Desulfurivibrio, Desulfobacca*, and *Hippea* are present only in Kerlingarfjöll. Whereas closer cultured relatives are *Acidiferrobacter, Metallibacterium, Aciditerrimonas* and *Ferrimicrobium* are present only in Kverkfjöll. Shared closer cultured relatives are *Leptospirillum, Thiomonas, Thiobaciullus, Desulfofcapsa, Sulfobacillus, Sulfurihydrogenibium.*

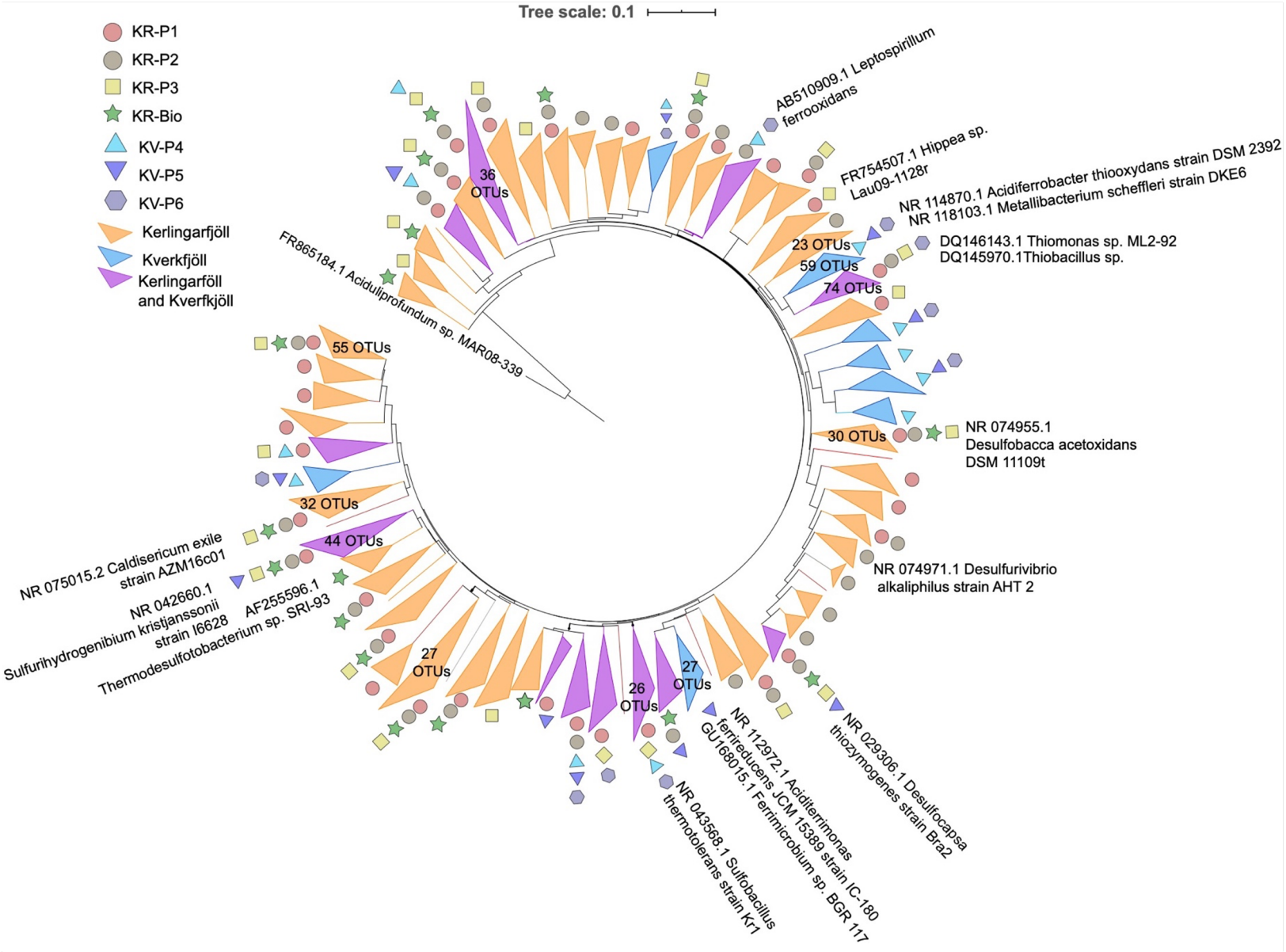

Figure 5-7. Phylogenetic tree from Kerlingarfjöll and Kverkfjöll OTUs (97%) and representative bacteria species. Tree branches with more than 20 OTUs collapsed have the number indicated. NB: GenBank species are indicated, where they have their closest relatives. Archaea Aciduliprofundum sp. MAR08-339 is used as the outgroup.

Table 5-5. Phylogenetic affiliation of 16S rRNA results for Bacteria for the most abundant at genus level of the different pools at Kerlingarfjöll and Kverkfjöll

KR-P1	KR-P2	KR-P3	KR-Bio	KV-P4	KV-P5	KV-P6
Desulfurivibrio	*Desulfocapsa*	*Dehalococcoides*	*Sulfurihydrogenibium*	*Syntrophus*	*Syntrophus*	*Leptospirillum*
(35.03%)	(24.33%)	(18.82%)	(74.54%)	(25.44%)	(15.68%)	(19.56%)
Elusimicrobium	*Desulfurivibrio*	*Caldisericum*	*Hydrogenobacter*	*Acidithiobacillus*	*Pseudomonas*	*Acidithiobacillus*
(6.15%)	(21.39%)	(15.39%)	(6.97%)	(19.78%)	(11.98%)	(14.12%)
Hydrogenophaga	*Thiobacillus*	*Sulfurihydrogenibium*	*Candidatusacetothermum*	*Sulfobacillus*	*Sulfobacillus*	*Acidiferrobacter*
(3.79%)	(14.15%)	(7.43%)	(4.13%)	(14.47%)	(10.54%)	(11.66%)
Thiobacillus	*Nitrospira*	*Hyppea*	*Caldisericum*	*Ferrimicrobium*	*Acidithiobacillus*	*Metallibacterium*
(3.67%)	(2.15%)	(6.87%)	(4.06%)	(8.59%)	(8.60%)	(8.62%)
Sulfuricurvum	*Geobacter*	*Thiomonas*	*Thermodesulfobacterium*	*Leptospirillum*	*Acidiferrobacter*	*Acidobacterium*
(3.52%)	(1.85%)	(6.82%)	(1.90%)	(8.40%)	(5.56%)	(7.72%)
Nitrospira	Others	*Hydrogenobacter*	Others	*Acidiferrobacter*	Others	*Sulfobacillus*
(2.86%)	(14.59%)	(5.60%)	(7.24%)	(7.70%)	(23.0%)	(7.30%)
Thiovirga		*Acidobacterium*		*Aciditerrimonas*		*Syntrophus*
(2.92%)		(2.46%)		(5.95%)		(7.20%)
Candidatus		*magnetobacterium*		*Candidatus*		*Ferrimicrobium*
magnetobacterium		(2.39%)		*saccharimonas*		(4.46%)
(1.88%)				(1.88%)		
Dehalococcoides		*Desulfobacca*		Others		*Aciditerrimonas*
(1.67%)		(1.86%)		(2.31%)		(2.94%)
Others		*Desulfuromonas*				*Thiobacillus*
(13.94%)		(1.64%)				(1.52%)
		Candidatus				Others
		Others				(9.45%)
		(30.72%)				

Table 5-6. Description of preferred growing parameters for main bacteria of Kerlingarfjöll.

Genus Phylum	**Anaerobic or aerobic**	**C Source**	**pH R**	**pH Op**	**T R**	**T Op**	**Metabolic pathway**	**Reference**
Sulfurihydrogenibium Aquificae	ChemoLitho ChemoOrg Aerobic	CO_2 Corg	5.3-7.8	6.6	40-73	68	Sulfur oxidising $2H_2 + O_2 \rightarrow 2H_2O$ $nS^o + H_2O \rightarrow 2H^+ + SO_4^{2-}$ $S_2O_3^{2-} + O_2 + H^+ \rightarrow SO_4^{2-} + H_2O$	Flores et al., 2008
Hydrogenobacter Aquificae	ChemoOrg Aerobic	Corg	5.5-9	7.5	60-85	78	Sulfur oxidising $S_2O_3^{2-} + nO_2 + nH^+ \rightarrow SO_4^{2-} + H_2O$; $2H_2 + O_2 \rightarrow 2H_2O$; $H_2S^+ \rightarrow SO_4^{2-}$; $nS^o + nH^+ + Corg \rightarrow nH_2S + CO_2$	Takai et al., 2001
Thermodesulfobacterium Thermodesulfobacteria	ChemoOrg Anaerobic	Corg	6.3-6.8	6.5	50-80	70-75	Sulfate reduction SO_4^{2-}; $+ nH^+ + Corg \rightarrow nH_2S + CO_2$ $S_2O_3^{2-} + 4H^+ + Corg \rightarrow nH_2S + CO_2$	Zeikus et al,. 1983 Bhantnagar et al., 2015
Caldisericum Firmicutes	ChemoOrg Anaerobic	Corg	5.5-7.5	6.5	55-70	65	Sulfur reduction $nS^o + nH^+ + Corg \rightarrow nH_2S + CO_2$ $S_2O_3^{2-} + nH^+ + Corg \rightarrow nH_2S + CO_2$ SO_4^{2-}; $+ nH^+ + Corg \rightarrow nH_2S + CO_2$	Mori et al., 2009
Thiobacillus Proteobacteria	ChemoLitho Anaerobic Aerobic	CO_2	6.3-8.7	7.5-8.3	-2-30	25-30	Fe and S oxidising $nS^o + H_2O \rightarrow H^+ + SO_4^{2-}$ $S_2O_3^{2-} + 4H^+ + Corg \rightarrow nH_2S$ $Fe^{2+} + O_2 + 4H^+ \rightarrow Fe^{3+} + H_2O$	Rao and Berger, 1971 Kellermann and Griebler, 2009
Desulfurivibrio Deltaproteobacteria	ChemoLitho Anaerobic	CO_2	8.5-10.3	9.5	30-50	37	S^o disproportionation $4S^o + 4H_2O \rightarrow SO_4^{2-} + 3H_2S + 2H^+$ $S_2O_3^{2-} + H_2O \rightarrow SO_4^{2-} + H_2S$ $4SO_3^{2-} + 2H^+ \rightarrow 3SO_4^{2-} + H_2S$	Poser et al.,2013 Sorokin et al., 2008
Desulfocapsa Deltaproteobacteria	ChemoLitho Anaerobic	CO	6-8.2			30	disproportionating S^o, sulfite or thiosulfate with CO $4S^o + 4H_2O \rightarrow SO_4^{2-} + 3H_2S + 2H^+$ $S_2O_3^{2-} + H_2O \rightarrow SO_4^{2-} + H_2S$ $4SO_3^{2-} + 2H^+ \rightarrow 3SO_4^{2-} + H_2S$	Finster et al., 2013
Dehalococcoides Chloroflexi	ChemoOrg Anaerobic	Corg		7.2		30	$nH_2 + Corg + nH^+ \rightarrow C_6H_{12}O_6 + nH_2O$	Cheng, 2009

Table 5-7. Description of preferred growing parameters for main bacteria of Kverkfjöll.

Genus Phylum	Anaerobic or aerobic	C Source	pH R	pH Op	T R	T Op	Metabolic pathway	Reference
Sulfobacillus *Firmicutes*	ChemoOrgChemoLitho Anaerobic Aerobic	Corg CO_2	0.8-2.2	1.7	30-47	38-39	Fe and S oxidising $Fe^{2+} + O_2 + 4H^+ \rightarrow Fe^{3+} + H_2O$ $S_2O_3^{2-} + nO_2 + nH^+ \rightarrow SO_4^{2-} + H_2O$ $nS^o + H_2O \rightarrow 2H^+ + SO_4^{2-}$ $H_2S \rightarrow SO_4^{2-}$	Johnson et al., 2008 Norris et al., 1996
Syntrophus *Deltaproteobacteria*	ChemoOrg Anaerobic	Corg		6.5	25-42	35	$Corg + nH_2O \rightarrow Corg + HCO3^- + nH^+ + nH_2$	Jackson et al., 1999 Mountfort et al., 1984 McInerney et al., 2007
Acidithiobacillus *Proteobacteria*	ChemoLitho Aerobic	CO_2	0.5-5.5	2.5	10-37	30-37	S and Fe oxidising $nS^o + H_2O \rightarrow H^+ + SO_4^{2-}$ $S_2O_3^{2-} + 4H^+ + Corg \rightarrow nH_2S$ $Fe^{2+} + O_2 + 4H^+ \rightarrow Fe^{3+} + H_2O$	Kelly et al., 2000
Ferrimicrobium *Actinobacteria*	ChemoOrg Anaerobic	Corg		2		35	Fe oxidising/reduction and FeS_2 oxidation $Fe^{2+} + O_2 + 4H^+ \rightarrow Fe^{3+} + H_2O$ $Fe^{3+} + H_2O \rightarrow Fe^{2+} + O_2 + 4H^+$ $FeS_2 + 14Fe^{3+} + 8H_2O \rightarrow 15Fe^{2+} + 2SO_4^{2-} + 16H^+$	Johnson et al., 2009
Acidiferrobacter *Proteobacteria*	ChemoLitho Anaerobic	CO_2	1.2-2.5	2	20-47	38	S and Fe oxidising $Fe^{2+} + O_2 + 4H^+ \rightarrow Fe^{3+} + H_2O$ $nS^o + H_2O \rightarrow H^+ + SO_4^{2-}$ $S_4O_6^{2-} + 4H^+ + Corg \rightarrow nH_2S$	Hallberg et al., 2011
Leptospirillum *ferrooxidants*	ChemoLitho Aerobic	CO_2	1.3-2.0	1.4	45 max	30-37	Fe oxidising $Fe^{2+} + O_2 + 4H^+ \rightarrow Fe^{3+} + H_2O$	Coram et al., 2002 Schrenk et al., 1998
Metallibacterium *Proteobacteria*	ChemoOrg Anaerobic	Corg	2.5-6.5	5.5		25-30	Fe reduction $Fe^{3+} + H_2O \rightarrow Fe^{2+} + O_2 + 4H^+$	Ziegler et al., 2013
Acidobacterium *Acidobacteria*	ChemoOrg Aerobic Anaerobic	Corg	3-6			20-45	Iron oxidation and Nitrification $Fe^{2+} + O_2 + 4H^+ \rightarrow Fe^{3+} + H_2O$ $NH_4^+ + O_2 \rightarrow NO_3^- + 2H^+ + H_2O$	Kishimoto et al., 1991 Eichorst et al., 2018
Aciditerrimonas *ferrireducens* *Actinobacteria*	ChemoOrgChemoLitho Aerobic Anaerobic	Corg CO_2	2-4.5	3	35-58	50	Fe reduction and Dissimilatory Fe reduction $Fe^{3+} + H_2O \rightarrow Fe^{2+} + O_2 + 4H^+$	Itoh et al., 2011

Bacterial communities are grouped by the different S metabolisms identified by FAPROTAX in Figure 5-8. For S metabolisms, sulfur and sulfate respiration are important in KR-P1 and KR-P2. Whereas dark thiosulfate and sulfur oxidation dominate KR-P3 and KR-Bio, followed by respiration of sulfur compounds and sulfate respiration (in lesser proportions). The S metabolisms potentially operating in the Kverkfjöll pools are mainly oxidation of sulfur, through dark oxidation of sulfur compounds. The S metabolisms operating in Kerlingarfjöll confirmed with the detection of a positive Aps PCR product for KR-P1, KR-P2, KR-P3 and KR-Bio.

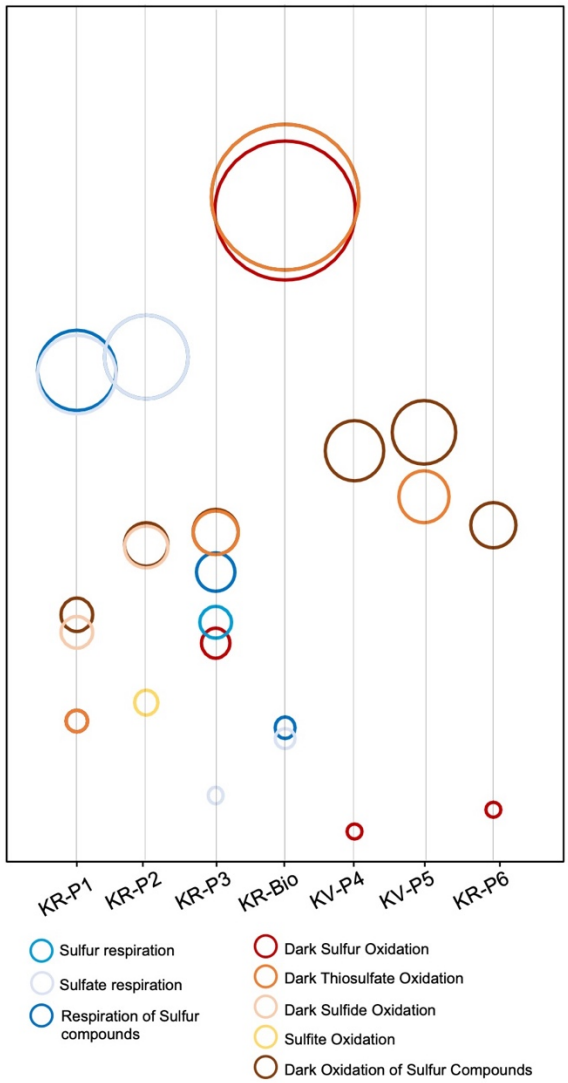

Figure 5-8. FAPROTAX bubble plot with different S metabolisms indicated for different pools. Sizes are proportional to number of OTUs.

5.3 Discussion

5.3.1 Phylogenetic differences of Kerlingarfjöll and Kverkfjöll pools

Archaeal communities are dominated by methanogens and *Thermofilum* at genus level, and the main metabolic pathways are methanogenesis (hydrogenotrophic and acetate degradation), and sulfide reduction. Most of the archaeal communities are widespread across pools and sites, at both Kerlingarfjöll pools and Kverkfjöll KV-P5, regardless of temperature, pH and electron donors/acceptors. Archaeal *Thermofilum*, *Candidatus nitroscaldus,* and *Aciduliprofundum* seem to have a wide range of pH of growth (between 3 to 8, Table 5-4). On the other hand, bacterial communities are well differentiated between both sites as seen in the phylogenetic tree (Figure 5-7): higher diversity at Kerlingarfjöll than Kverkfjöll pools with very few OTUs shared.

Bacteria communities at Kerlingarfjöll and Kverkfjöll are controlled by deep volcanic processes, which determine the pH and availability of electron donors and acceptors, as has been previously observed in Yellowstone (Colman et al., 2016, 2019) and is described in detail in Chapter 4. There is a strong pH control on community structure of the pools from both sites, particularly for bacteria (seen at Table 5-6 and Table 5-7). Conversely to archaea, the pH range in which the bacteria are found to grow is narrower and very differentiated: either acidic (at Kverkfjöll) or circum-neutral (Kerlingarfjöll). Deep volcanic processes also determine the availability of electron donors and acceptors such as Fe and S. For example, Kverkfjöll waters have high Fe water concentrations (between 7.1 to 2050.9 ppm), allowing the dominance of Fe cycling bacterial taxa in the Kverkfjöll pools. Similarly, at Kerlingarfjöll, the presence of MSR/ S oxidation can be explained by the presence of SO_4^{2-}. MSR are also known to prefer circum-neutral pH and anoxic conditions, which Kerlingarfjöll pools offer (Widdel & Pfenning, 1977). The main metabolic pathways in Kerlingarfjöll pools are sulfur/sulfate reduction, and sulfide oxidation; and at Kverkfjöll, sulfide oxidation, and Fe reduction/oxidation.

5.3.2 Carbon cycling and associated biosignatures

$\delta^{13}C$ values are influenced by biological processes, and therefore are useful biosignatures that could potentially be preserved in the organic matter of the Martian rock record. Autotrophic microorganisms preferentially incorporate ^{12}C from CO_2 into their biomass, producing different degrees of fractionation between CO_2 and the resulting organic C, generally depending on their CO_2 fixation pathway (Havig et al., 2017; Zerkle et al., 2006).

It is important to consider the abiotic production of $\delta^{13}C_{TOC}$, as the general $\varepsilon^{13}C_{CO2\text{-}TOC}$ seen in this chapter are relatively small for biological fractionations (<25 ‰, Zerkle et al., 2005). Values for $\delta^{13}C_{TOC}$ as low as -50 ‰ for organic compounds have been produced by abiotic synthesis under laboratory hydrothermal conditions (McCollom & Seewald, 2006). An important circumstance for these abiotic fractionations, is that they happen at temperatures significantly greater (250 °C) than Kerlingarfjöll or Kverkfjöll hydrothermal pools (16-60 °C). Subsequently, low temperature hydrothermal environments are key for exploration of $\delta^{13}C_{TOC}$ in order to differentiate between biotic or abiotic organic carbon produced in hydrothermal systems.

High temperature hydrothermal springs have been associated with small C isotope fractionations (Havig et al., 2011). These are suggested to be produced as a result of hot temperatures favouring the TCA pathway. Conversely, lower temperatures favour C pathways that produce larger or more variable C isotope fractionations (Havig et al., 2011). This temperature control can be observed here (Figure 5-1 B): small $^{13}\varepsilon_{CO2\text{-}TOC}$ for high temperature (KR-Bio, KR-P3) and large $^{13}\varepsilon_{CO2\text{-}TOC}$ for low temperature pools (KR-P1 and Kverkfjöll pools). High temperature Kerlingarfjöll pool KR-P3 and stream KR-Bio (52-60 °C) have similar, relatively small C isotope fractionations (16.3 and 15.6 ‰, Figure 5-1 B). Carbon isotope fractionations observed for KR-Bio ($^{13}\varepsilon_{CO2\text{-}TOC}$= 15.6 ‰) are consistent with fractionations observed for the reductive tricarboxylic acid cycle (TCA) C fixation pathway (TCA < 20 ‰; House et al., 2003) The TCA pathway is used by the bacteria genus *Sulfurhydrogenibium* (phylum *Aquificae)*, which comprises 82% of the bacterial community at KR-Bio (Figure 5-5 A, Table 5-5). Furthermore, the KR-Bio archaeal community is dominated by *Thermofilum* (65 %) (phylum *Crearchaeota*, Figure

5-2). *Thermofilum* is also known to produce fractionations smaller than 20 ‰, through either TCA or 3-HP (3-hydroxypropionate pathway, < 10 ‰; Zerkle et al., 2005 and references therein). KR-P3 microbial communities are also related to CO_2 pathways producing small fractionations. The KR-P3 bacterial community consists of *Dehalococcoides* (29 %) (phylum *Chloroflexi* (Figure 5-5 A, Table 5-5) which use the 3-HP pathway (3-HP pathway, < 10 ‰ House et al., 2003). The KR-P3 archaeal community is dominated by *Thermofilum* (57 %, Figure 5-2), as mentioned before for KR-Bio (*Thermofilum* uses either TCA or 3-HP).

The low temperature Kerlingarfjöll pool KR-P1 and Kverkfjöll pools (16-23 °C) present the largest fractionations (18.4- 21.0 ‰, Figure 5-1 B), where the Kerlingarfjöll pool KR-P2 (22 °C) has the lowest fractionation (12.9 ‰). It is challenging to elucidate the differences in C isotope fractionations between KR-P1 and KR-P2, since they have very similar communities in both archaea and bacteria. The bacterial communities are dominated by genus *Desulfurivibrio* in KR-P1 (35%), and *Desulfocapsa* at KR-P2 (24 %), (both TCA or AP (acetyl-CoA pathway) , $^{13}\varepsilon_{CO2\text{-}TOC}$ <20 ‰, House et al., 2003), (Figure 5-5 B). The Archaeal communities from KR-P1 and KR-P2 are dominated by *Thermofilum* (50.29 and 38.20 % respectively), but also methanogens (KR-P1 KR-P2; Figure 5-2). The differences in C isotope fractionations between KR-P1 and KR-P2 could be due to the difference in volcanic activity affecting the active communities. KR-P1 at the time of sampling was observed to be actively bubbling gas (likely composed of CO_2) and was suboxic, which is preferential for anaerobic microbes such as methanogens. On the other hand, pool KR-P2 was visually quiescent and more oxidised (0.93 ppm O_2 concentrations). The suboxic conditions in KR-P1could have supported more methanogenesis, leading to larger C isotope fractionations (microbial methanogenesis $\delta^{13}C$ values are observed from 21 to 80 ‰, when using H_2 (Whiticar, 1999) and 21 to 35 ‰ with acetate (Valentine et al., 2004).

5.3.3 Sulfur cycling and associated biosignatures

Sulfur isotope effects produced by microbial processes, notably microbial sulfate reduction (MSR) and oxidative sulfur (re)cycling, have been used to reconstruct the evolution of S-based metabolisms and trace the oxygenation of Earth's surface through

time (Canfield & Teske, 1996; Luo et al., 2016; Scott et al., 2008). The largest S isotope fractionation effects are generally produced by MSR, although oxidative recycling of sulfur species can increase these fractionations further (e.g. Canfield, 2001a).

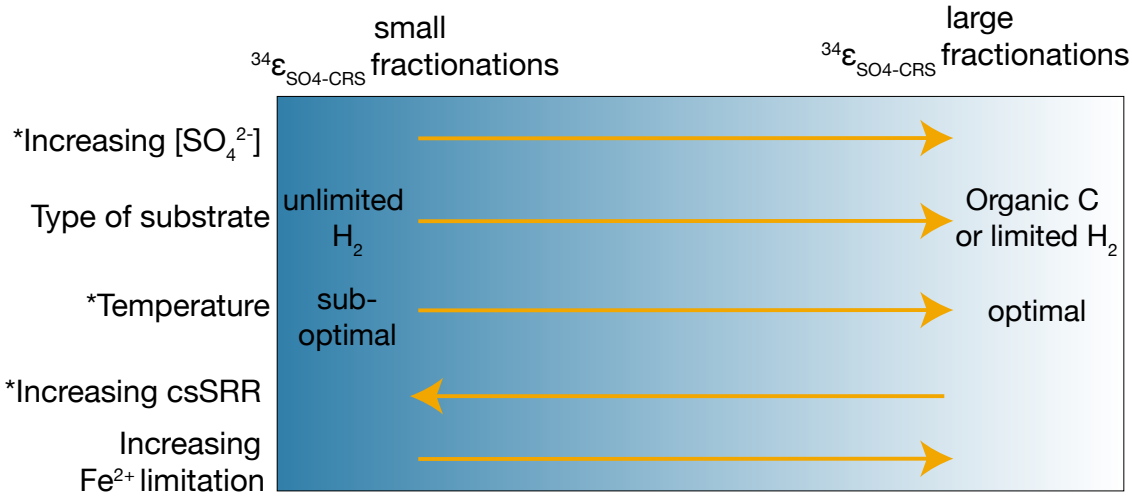

*Figure 5-9. Main environmental controls on S isotope fractionation during MSR, modified from Fike et al., (2009), with updated parameters. Arrows indicate the direction of the fractionation (larger or smaller) for the indicated parameter. * indicated for parameters that are strain-specific (SO_4^{2-} concentrations, temperature, cell specific sulfate reduction rates(csSRR). References are: for SO_4^{2-} concentrations (Bradley et al., 2016; Canfield et al., 2001 a, 2001b; Habicht et al., 2002). Substrate (Hoek et al., 2006; Sim et al., 2011b), temperature (Canfield et al., 2006; Hoek et al., 2006), increasing csSRR (Chambers et al., 1975; Habicht & Canfield, 1997; Sim, 2012), Fe limitation (Sim et al., 2011b).*

Sulfur isotope fractionations produced by MSR in natural environments are influenced by several environmental parameters, such as SO_4^{2-} and Fe concentrations, type and abundance of electron donors, and temperature (Figure 5-9). The variation of SO_4^{2-} concentration plays a big role on the S fractionations produced as SO_4^{2-} is the terminal electron acceptor for MSR (Sim, 2012). It is recognised that for SO_4^{2-} concentrations less than 200 µM, MSR tend to produce fractionations smaller than 5 ‰ (Habicht et al., 2002) and larger fractionations are generally only produced above those concentrations. Moreover, S isotope fractionations during MSR have been shown to be dependent on strain-specific physiological parameters, such as affinity for SO_4^{2-} and electron donors (Bradley et al., 2016). When MSR are limited by low concentrations of electron donors, the fractionations produced are generally larger (Chambers et al., 1975; Hoek et al., 2016; Sim et al., 2011b). Additionally, when MSR use organic electron donors the

fractionations produced tend to be larger (Figure 5-9; 6-44 ‰, Sim *et al*., 2011) than when they have an excess supply of inorganic electron donors, such as H_2 (Figure 5-9; 1-6 ‰, Hoek *et al*., 2006). Fe concentration also acts as a limiting factor, reducing the growth rate, causing a decrease in cell specific sulfate reduction rates (csSRR) and subsequently larger S isotope fractionations (Figure 5-9, Sim et al., 2011b). csSRR (moles of SO_4^{2-} reduced/cell/time) is a metabolic rate measurement that responds to environmental parameters such as SO_4^{2-} concentration and source of electron donors. MSR usually produces largest fractionations for the lowest csSRR (Chambers et al., 1975; Habicht & Canfield, 1997; Kaplan & Rittenberg, 1964). This is similar to the effects seen for organic limitation, as they are both key controllers of the proportions at which electrons are supplied to the MSR pathway (Sim, 2012). Finally, the relationship between temperature and fractionation is not straight forward. The differences in fractionations due to temperature are associated with responses of internal enzyme kinetics together with the flux of SO_4^{2-} going in and out the cell (Canfield et al., 2006; Hoek et al., 2006). Depending on the responses of individual organism strains to temperature, the magnitudes of those two paths are different. These responses seem to be variable for different microbial strains, with generally larger fractionations for optimal temperatures, and smaller fractionations for suboptimal temperatures (Figure 5-9, Canfield et al., 2006).

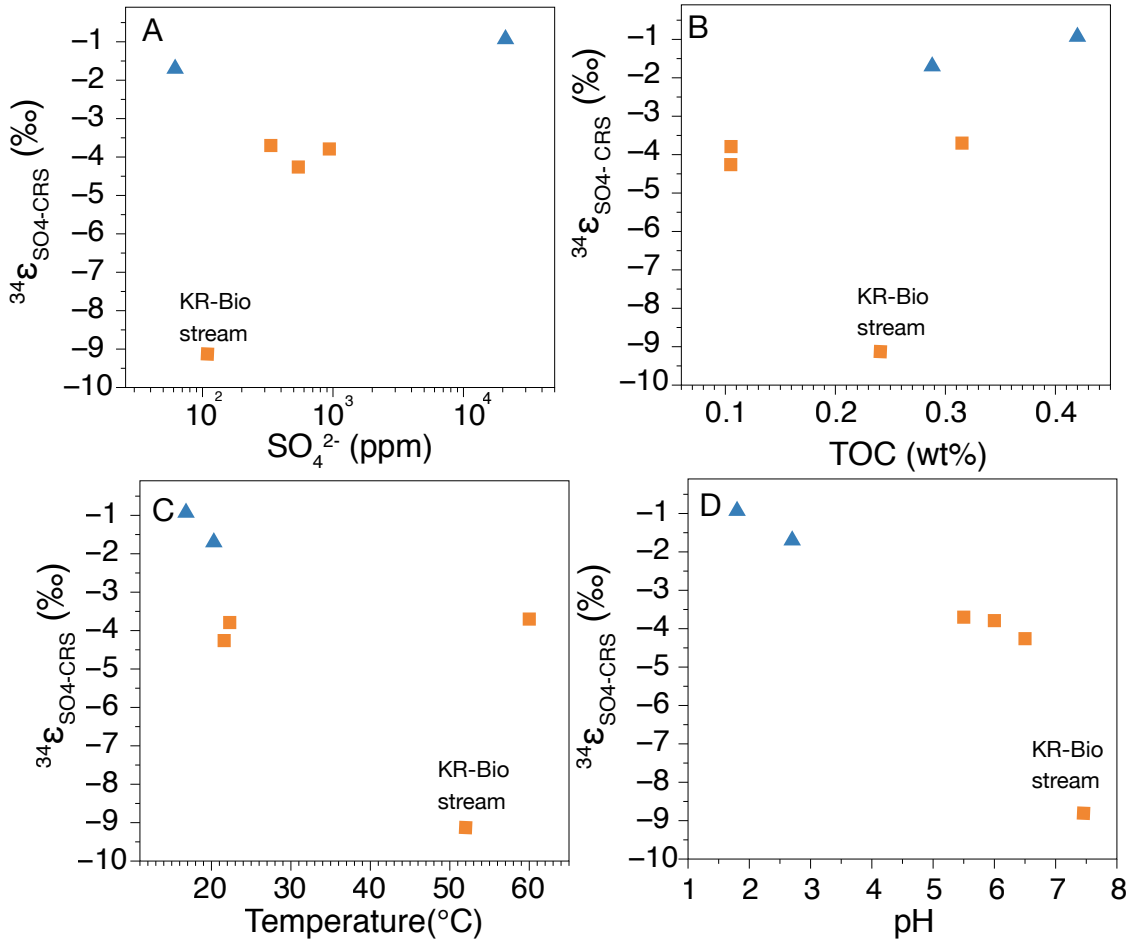

Figure 5-10. Figure showing S isotope fractionations ($^{34}\varepsilon_{SO4\text{-}CRS}$) against environmental parameters: a) vs SO_4^{2-} concentrations; b) vs TOC; c) vs temperature; d) vs pH

When comparing with the environmental variables from the hydrothermal sites, only sulfur isotope fractionations and pH show a clear negative trend (Figure 5-10 D), which suggests that this could be an important, but as-yet unexplored environmental variable for controlling S isotope fractionations. A major finding of this work is that S isotope fractionations show only a weak relationship with SO_4^{2-} concentration, TOC wt. % and temperature (Figure 5-10 A, B, C). Instead, S isotope fractionations vary as a function of pH, with larger fractionations observed for higher pH (Figure 5-10 D). Largest $^{34}\varepsilon_{SO4\text{-}CRS}$ fractionations are observed at Kerlingarfjöll KR-Bio (-9.1 ‰) for pH of 7, followed by the Kerlingarfjöll pools (-4.3 to -3.7 ‰) for pH between 5-6. Smaller $^{34}\varepsilon_{SO4\text{-}CRS}$ are observed in Kverkfjöll pools (-1.7 to -0.9 ‰) with acidic pH (1 to 3). pH could be a primary variable affecting csSRR in these populations, and therefore S isotope fractionations. It is known that pH controls the availability of dissolved Fe due to Fe

solubility under different pH conditions; Fe is more soluble at low pH than at circum-neutral pH. This trend is observed in these hydrothermal systems: Fe concentrations are high in Kverkfjöll (7.10 to 4156 ppm, pH <3), where in Kerlingarfjöll waters (pH 5-7) only KR-P1 presents detectable Fe (>0.03 ppm). Fe could therefore be acting here as a limiting factor reducing the growth rate, causing a decrease in cell specific sulfate reduction rates (csSRR) and subsequently larger fractionations (Sim et al., 2011b). However, the pH/Fe control alone cannot fully explain why KR-Bio presents larger S isotope fractionations than KR-P2 or KR-P3. This is likely due to KR-Bio exhibiting an additional oxidative S recycling, increasing the overall fractionations between SO_4^{2-} and H_2S/CRS, as discussed below.

The small S isotope values preserved in Kverkfjöll ($\delta^{34}S_{CRS}$ -2.4 to -0.7 ‰, $\delta^{34}S_{SO4}$ -1.4 to 0.1 ‰) are not discernible from abiotic volcanic S isotope values reported in the literature. Icelandic basalt $\delta^{34}S_{S\text{-}II}$ ranges from -2 to +0.4 ‰ (Torssander, 1989), and the $\delta^{34}S$ values of H_2S in the liquid and vapor phases of Icelandic volcanic fumaroles range from -2.5 to 2 ‰, and -2 to +3.4 (Stefansson et al., 2015). $\delta^{34}S$ values of aqueous sulfate range from +3.6 to +15 ‰. The fractionations between these aqueous and gaseous species (HS^-, H_2S and SO_4^{2-}) are due to purely abiotic processes, such as boiling, fluid-rock interaction and associated changes between liquid and vapor phases (Gunnarson-Robin et al., 2017; Stefansson et al., 2015, 2016).

The biological processes responsible for controlling S isotope values in these pools are further informed by molecular identification of the relevant microbial communities inhabiting them. The small S isotope fractionations observed in Kverkfjöll (-1.7 to -0.9 ‰) are consistent with 16S rDNA results indicating an absence of MSR, with S related metabolisms dominated instead by sulfide or sulfur oxidising organisms, Including *Acidithiobacillus, Sulfobacillus,* and *Acidiferrobacter* (Figure 5-5 A). Sulfur oxidising organisms typically produce small S fractionations in their resulting products (-5 to 12 ‰; Zerkle et al., 2009, Pellerin et al., 2019 and references) which can be easily overprinted by volcanic processes. Furthermore, Kverkfjöll, acidic pools are dominated by $SO_4^{2-}$and Fe. In acidic waters, Fe is more soluble with the relative distribution of Fe^{2+}/Fe^{3+} controlled by a combination of the underlying basaltic bedrock, Fe^{2+} oxidation kinetics, and microbial Fe cycling (Kaasalainen et al., 2017). This Fe availability allows

the dominance of Fe cycling bacterial taxa at the Kverkfjöll pool sediments, including *Sulfobacillus, Acidithiobacillus, Ferrimicrobium and Acidobacter*. These bacteria can perform both dark iron oxidation and dark sulfur oxidation (Coupland et al., 2008, Druschel et al., 2004). At the same time, they could be contributing to the high concentrations of SO_4^{2-} and Fe (e.g. KV-P6), and maintaining the low pH of the pools by oxidising sulfur and iron (Colman et al., 2019). At low pH, sulfate reduction and methanogenesis are typically inhibited when they are amongst the presence of very electropositive electron acceptors, such as Fe^{3+} (Bodegom et al., 2004, Sanchez-Andrea et al., 2011).

Conversely, S isotope fractionations in Kerlingarfjöll pools ($^{34}\varepsilon_{SO4\text{-}CRS}$ of -4.3 to -3.7 ‰) are significantly smaller than what would be expected, given that S cycling bacteria and archaea communities identified in these pools are dominated by MSR taxonomic groups. For example, KR-P1 and KR-P2 bacteria communities are dominated by *Desulfurivibrio* (35 %) and *Desulfocapsa* (24 %) respectively, while he archaeal communities in the Kerlingarfjöll pools are dominated by *Thermofilum* (35-57 %, Figure 5-2). *Thermofilum* obtains energy from S^0 reduction with hydrogen and formate as electron donors, or independently on formate with formate hydrogen lyase (Anderson et al., 2008). The small S isotope fractionations and absence of a trend between TOC and $^{34}\varepsilon_{SO4\text{-}CRS}$ from the pools (Figure 5-10 C), could be indicating that the preferred pathway for MSR and S^0 reduction is via inorganic electron donors like H_2 instead of organic C. As mentioned before, fractionations observed for limited H_2 flux conditions revealed large fractionations (24- 37 ‰), compared with unlimited H_2 supply (1-6 ‰) (Hoek et al., 2006). Hydrogen gas (H_2) was not measured on this study but H_2 is a typical gas from hydrothermal environments, and has been detected at Kverkfjöll by Ólaffson et al., 2000. Hydrothermal settings could therefore provide an effectively unlimited H_2 electron donor supply, explaining the generally small fractionations. An enrichment culture feasibility study to test this idea is presented in Chapter 6.

KR-Bio shows the largest S isotope fractionations ($^{34}\varepsilon_{SO4\text{-}CRS}$ of -9.1 ‰), but these are still smaller than most sulfate-rich ecosystems. The KR-Bio bacterial community is dominated by the $S_2O_3^{2-}$ or S^0 oxidiser *Sulfurihydrogenibium* (74.54 %,Table 5-5) which visibly dominates the stream forming grey filamentous biofilm streamers (Chapter 4,

Figure 4-3). Furthermore, it has also been identified in other Icelandic hydrothermal locations (Flores et al., 2008) and Mammoth Hot Spring in Yellowstone National Park, USA (Dong et al., 2019). *Sulfurihydrogenibium* is an evolutionarily primitive taxon found dominating filamentous microbial mat communities in shallow fast flowing aqueous systems world-wide (Dong et al., 2019). Biofilms facilitate stabilisation of diverse microbial communities and could provide the ideal setting for biological recycling of sulfur through the close contact of the S reducing and oxidising communities (Fike et al., 2009). However, the fractionations produced at KR-Bio (-9.1 ‰) are smaller than those usually seen for such S recycling systems (20-40 ‰, Fike et al., 2009). Instead, KR-Bio *Sulfurihydrogenibium* could be the main active organism dominating the S cycle in this stream with $S_2O_3^{2-}$/ S^0 oxidation and with little S reduction happening.

In summary, Kverkfjöll S isotope values are not discernible from volcanic S isotope values reported in the literature, and Kerlingarfjöll S isotope values only marginally so. It is likely the case that in these hydrothermal systems biological sulfur inputs are overwhelmed by the volcanic H_2S, which dominates the resulting $\delta^{34}S$ of sedimentary pyrite over the biologically controlled $\delta^{34}S$ values. Moreover, the environmental selection for chemolithoautotrophic MSR using H_2 instead of organic compounds can further diminish the biological $\delta^{34}S$ signatures produced during MSR. These ideas are explored in more detail in Chapter 7, by investigating these same metabolisms in a high-sulfur, non-volcanic environment.

5.3.4 Comparison with other Mars hydrothermal analogue studies

Relatively small S isotope variations have also been found elsewhere in similar hydrothermal systems. At Los Alamos (New Mexico, US), hydrothermal pools had pH values ranging from 2 to 8, and temperatures between 3 to 50 °C. Here, similarly small $\delta^{34}S_{CRS}$ variations (-2.3 to 2.2 ‰) are attributed to prevailing forms of volcanic sources (Szynkiewicz et al., 2012). Similar conclusions were drawn by a study of a nearby hydrothermal stream at Hveradalur, Kverkfjöll, by Cousins et al., (2018). This stream presented a pH range of 4 to 5 (between the pH's of Kerlingarfjöll and Kverkfjöll), and sedimentary pyrite $\delta^{34}S$ ~0 ‰ interpreted as the product of volcanic sulfide. The microbial community was also dominated by taxa that utilise sulfide and sulfur

oxidation metabolisms. Carbon isotope values from this hydrothermal stream were similar to those measured for both Kverkfjöll and Kerlingarfjöll pools with $\delta^{13}C_{TOC}$ values becoming more negative with decreasing temperature. This negative trend of C isotopes was also evidenced in a different study at Yellowstone National Park by Havig et al., (2011), where microorganisms from low temperature pools favoured C pathways coupled to large variations in C isotope compared to high temperature pools. Overall, S isotope measurements in Mars analogue hydrothermal systems are challenging to discern from volcanic S isotope signatures while C isotopes in this and two studies cited above show large fractionations for lower temperature hydrothermal systems.

5.3.5 Implications for C and S biosignatures in Mars hydrothermal systems

For any stable isotope system, the most robust form of biosignature would require at least two distinct pools such that a fractionation effect can be calculated. Kerlingarfjöll and Kverkfjöll show evidence of biological processes when $\delta^{13}C_{TOC}$ is compared with $\delta^{13}C_{CO2}$ from the volcanic gases input in these pools (Figure 5-11). On Mars, $\delta^{13}C$ has been measured for reduced and oxidised carbon phases in meteorites and in the current Martian atmosphere. The total range for Martian $\delta^{13}C$ is very broad, from -24 to + 60 ‰ (Grady et al., 2004.; Wright et al., 1992). $\delta^{13}C_{CO2}$ of magmatic origin has been measured in basaltic Martian shergottites, varying between -24 to -14 ‰ (Grady et al., 2004.; Wright et al., 1986). This negative $\delta^{13}C_{CO2}$ range encompasses the $\delta^{13}C$ range produced by microorganisms (Grady & Wright, 2006). In order to find evidence for biological $\delta^{13}C_{TOC}$ on Mars, hydrothermal environments would need to host microorganisms likely to produce larger C isotopic fractionations, such as methanogens. It has been shown in this study together with others (e.g. Havig et al., 2011 and Cousins et al., 2018) that low temperature hydrothermal systems could be prospective environments to preserve $\delta^{13}C_{TOC}$ biosignatures in Martian sediments. Low temperature hydrothermal environments would: i) select for microorganisms performing larger C isotope fractionations, and ii) distinguish organic carbon values from those with an abiotic origin.

This study shows the search for $\delta^{34}S$ biosignatures is best suited to hydrothermal terrains with a limited influx of volcanic H_2, and where circum-neutral and reduced waters were once present, as they are more likely to produce and preserve S isotopic biosignatures. Hydrothermal environments are rich in electron donors, acceptors and volcanic H_2 which can be used by MSR. This is significant for potential MSR present on early Mars: due to the low abundance of organics on the Martian surface, H_2 driven metabolisms would have been more feasible, potentially reducing S isotope fractionations. It is suggested that early Martian volcanoes outgassed CO_2 and H_2 vigorously from a reduced mantle (Ramirez et al., 2014; Wadhwa, 2018). MSR is also thought to be one of the most primitive metabolisms on Earth, and a central microbial metabolism of the Paleoarchean and Eoarchean era (equivalent to Mars' late Noachian-Hesperian) (Roerdink et al., 2012). The early appearance of MSR is linked to the availability of metals around hydrothermal vents during that period, as Fe is present in the main protein required for MSR (Moore et al., 2017).

This study also illustrates the importance of pH on S isotope biosignatures, which can influence $\delta^{34}S$ fractionations during MSR, either directly or indirectly through its control on Fe availability. Early Mars is suggested to have dominant circum-neutral-alkaline waters, generated from the reaction between basalts and water (Vaniman et al., 2014). In a case study for Gale Crater by Tosca et al. (2018), it is shown that Fe^{2+} is liberated from the basalts, and its solubility controlled by pH and CO_2 fugacity. For a pH lower than 7 with low CO_2 fugacity, Fe^{2+} would have remained in solution. At pH > 8 for low and high CO_2 fugacity, Fe^{2+} would precipitate generating green rust or Fe-carbonates. In this scenario, limiting Fe^{2+} conditions would only be possible at alkaline pH >8, were Fe^{2+} is not in solution but precipitated in authigenic minerals. For Martian hydrothermal environments, it is quite likely that water pH would have been instead controlled by the immediate hydrothermal acid/alkaline volcanic gases delivered, and less controlled by surface processes.

Lastly, large S isotope fractionations for MSR (>55 ‰) are typically linked with MSR cells metabolising at very slow rates. This has been observed on Earth for environments with limited concentrations of electron donors and acceptors (energy limited or low-energy) (Bowles et al., 2014; Hoehler & Jørgensen, 2013; Jørgensen & Marshall, 2016;

Wenk et al., 2018). These metabolic energy-limited niches on Earth include intertidal mudflats, coastal environments, continental shelves, deep sea sediments, and euxinic water columns. The adaptations observed for such environments involve using electron carriers with modest negative reduction potentials, requiring less energy to grow (Wenk et al., 2018). These energy-efficient electron carriers subsequently cause large S fractionations (Wenk et al., 2018). Hydrothermal environments present abundant electron donors and acceptors (unlimited-energy). For such geochemically metabolic energy-unlimited environments, MSR present strongly negative reduction potential electron carriers (e.g., ferredoxin). When ferredoxin is used, S isotope fractionations have been observed to be smaller than 22 ‰ (Wenk et al., 2018). For Mars exploration this implies that the search for evident S isotopic biosignatures (>55 ‰) will be more fruitful at metabolic energy-limited paleo environments. For example, paleo-lakes that had euxinic water-columns (e.g. Gale Crater), or sea basins with coastal environments (e.g. Eridiana Basin). These paleo-environments would have provided limited concentration of electron donors or acceptors, causing low metabolic rates, and larger fractionations.

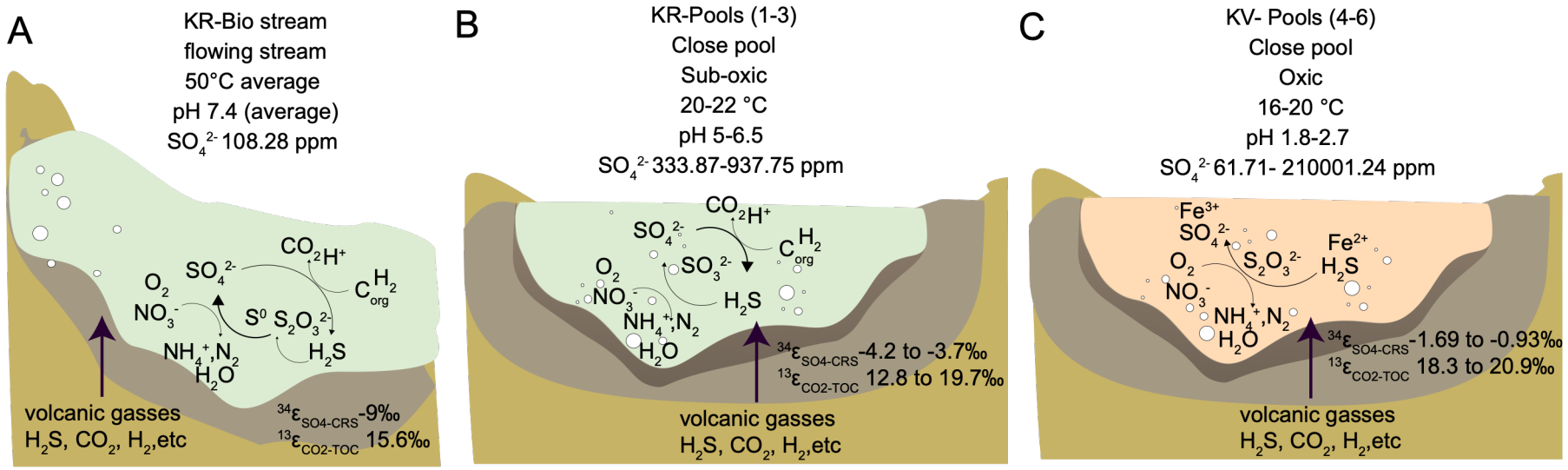

Figure 5-11. Conceptual figure for a) Kerlingarfjöll stream, b) Kerlingarfjöll pools, and c) Kverkfjöll pools. Illustrated in them the different C and S isotope fractionations produced, and main biological S cycling happening.

5.4 Conclusions

In this study C and S isotope fractionations were combined with microbial community studies, to provide an evaluation of these two isotope systems as biosignatures for hydrothermal Mars analogue environments. Kerlingarfjöll and Kverkfjöll microbial communities are found to be controlled by deep volcanic processes, determining pH and the availability of electron donors and acceptors. Kerlingarfjöll and Kverkfjöll have distinct geochemical properties, including different pH (acidic vs circum-neutral). Consequently, Kerlingarfjöll sites are dominated by methanogens, MSRs, and S oxidisers, whereas the Kverkfjöll microbial communities are dominated by microorganisms utilising S oxidation and Fe oxidation/reduction Figure 5-11. Carbon isotope fractionations from this study seem to be controlled in these systems by temperature, consistent with previous results from other studies of $\delta^{13}C$ in hydrothermal sites. $\delta^{34}S$ isotope biosignatures, however, are not conclusive of biosignature preservation at Kverkfjöll due to potential prevalence of volcanic $\delta^{34}S$ over biological $\delta^{34}S$, and on the low range of fractionation effects during biological S cycling at Kerlingarfjöll. At Kerlingarfjöll pools the small fractionations are likely caused by the hydrothermal setting providing an unlimited H_2 electron donor supply. Largest fractionations observed at Kerlingarfjöll for KR-Bio can be a combination between S oxidation dominating the stream and limitation of Fe. A major finding of this work is the effect of pH on S isotope fractionations, through the control of Fe solubility and hence its limitation on the csSRR. In order to find evidence of S isotope biosignatures produced by sulfur cycling on Mars, priority should be given to environments with limited H_2 input that impose low metabolising rates.

6 Influence of pH, electron donors, and C source on hydrothermal microbial sulfate reduction: a cultivation approach

6.1 Introduction

Cultured-based techniques are used to decipher the microbial ecology of natural environments, by allowing the importance of environmental variables that drive microorganisms growth and activity to be assessed. In fact, it is through enrichment cultures and pure strain experiments, that MSR biological S-isotope effects have been constrained (e.g. Canfield & Teske, 1996; Chambers et al., 1975; Hoek et a., 2006; Sim et al., 2011b). One of the best examples is the discovery of the effect of electron donor limitation on pure cultures of strain DMSS-1 *Desulfovibrio sp* (Sim et al., 2011b), where lactate provided in continuous culture produces a larger isotope effect than lactate-limited batch cultures (Sim et al., 2011b). The effects of other environmental variables (temperature, variable organic C, SO_4^{2-} concentration) have also been investigated for natural populations of MSR from a marine lagoon (e.g. Denmark marine lagoon, from Canfield, 2001b). The MSR were studied in a flow-through reactor, were the largest fractionations were seen for temperatures between 15 and 25 ^{o}C and indigenous organic substrate (Canfield, 2001b).

In Chapter 5, pH was demonstrated as an important environmental parameter controlling S isotope fractionations in Kerlingarfjöll and Kverkfjöll pools. It was hypothesised that pH regulates the levels of Fe available for microbial communities in

the pools, thus affecting the extent of S isotope fractionations (Sim et al., 2011b). As discussed in Chapter 5, the preference for H_2 as an inorganic electron donor in these pools may also be responsible for smaller fractionations (Hoek et al,. 2006). The aims for this chapter are i) to successfully enrich Microbial Sulfate Reducers (MSR) from two representative Kerlingarfjöll and Kverkfjöll pool inoculations: KR-P2 (henceforth P2) and KV-P6 (henceforth P6), ii) quantify the effect of variable pH on the activity of MSR communities of the pools, iii) discern the preferred C source for growth, from either organic C (acetate/lactate) or CO_2, iv) discern the preferred electron donor source, either organic (acetate/lactate) or inorganic (H_2).

6.1.1 Anaerobic culturing, Widdle and Bak media for MSR

The culture media recipe used to target the growth of MSR was taken from Widdle and Bak (1992). The media recipe was adapted by increasing the SO_4^{2-} concentrations to a range matching the hydrothermal field sites. Sodium sulfide ($Na_2S\bullet 6H_2O$) solution was substituted by Na-thyoglycolate solution, to avoid masking H_2S microbial production. The composition of the modified media is in Table 6-1.

*Table 6-1. Composition of the modified Widdle and Bak media. *Trace Element Solution containing: 12.5 mL of 100 mM of HCl, 2100 mg $FeSO_4 \bullet 7H_2O$, 30 mg $\bullet H_3BO_3$, 100 mg $MnCL_2 \bullet 4H_2O$, 190 mg $CoCl_2 \bullet 6H_2O$, 24 mg $NiCl_2 \bullet 6H_2O$, 2 mg $CuCl_2 \bullet 2H_2O$, 144 mg $ZnSO_4 \bullet 7H_2O$, 144 mg $ZnSO_4 \bullet 7H_2O$, 36 mg $Na_2MoO_4 \bullet 2H_2O$).*

Composition of modified media	For 1L of media
NaCl	2 g
$MgCl_2\bullet 6H_2O$	0.4 g
$CaCl_2\bullet 2H_2O$	0.1 g
Na_2SO_4	4 g
NH_4Cl	0.25 g
$KHPO_4$	0.2 g
KCl	0.5 g
Na-thyoglycolate solution	10 mL
Na-thyoglycolate powder	*0.1 g*
ascorbic acid	*0.1 g*
Trace Element Solution*	1 mL/L

The reagents were mixed in a measuring column with Milli-Q water and topped up to 1 L. Once completely dissolved, the media was divided into two bottles, one of which was used to make resazurin controls. Resazurin is an oxygen indicator control necessary for anaerobic cultures, such as MSR, as they are intolerant to oxygen and it can affect their growth. It was not possible to add resazurin directly to the cultures, as it becomes pink when it reacts with oxygen, and the colour interferes with UV-spec H_2S measurements. Both bottles were purged with oxygen-free N_2 gas for 30 minutes/L, and transferred into a Coy anaerobic chamber. The media was then distributed into 100 ml serum bottles and sealed with butyl rubber stoppers. Once outside the anaerobic chamber the tops were crimped, and the serum bottles flushed with oxygen-free N_2 gas for 5 minutes. They were all subsequently autoclaved at 121 °C for 20 minutes. For every serum bottle containing 50 mL of media, 0.05 mL of selenite-tungstate solution was added to each serum bottle to boost the growth, and 1 mL of acetate to the required bottles. pH was checked and adjusted to the desired values at each stage of the experiment by introducing 10 % HCl or 1M NaOH (reagents made in an anoxic atmosphere and sterilised via autoclaving). For the final step, the media was inoculated with 1 mL of sample (mixture of sediment and liquid). For each inoculated batch there were always corresponding oxygen control media with resazurin, plus blanks (media with no resazurin and no inoculation). As explained in Chapter 3 general methodology, an aseptic technique was used throughout to ensure sterile conditions.

6.1.2 Quantification of growth

Growth of MSRs was determined using the Cline method described in Chapter 3. In brief, 1 mL of each sample was extracted from the microbial culture and fixed with 100 µL of 20 % Zn-Acetate in an Eppendorf tube. Next, 0.08 mL of diamine reagent was added and incubated at 4 °C for 20 minutes. All the samples were analysed in triplicate, and the necessary dilutions were made after the colour development time. After that, the samples were transferred to cuvettes and mounted in the UV-Vis Spectrophotometer.

6.1.3 DNA extraction and sequencing

DNA was extracted from cultures using methods detailed in the Chapter 3. For DNA extraction from microbial cultures, cells were gathered by filtration into sterile 25 mm

diameter 0.22 µm pore filters. Once the cells were collected, DNA extraction was performed using the DNeasy Ultra Clean Microbial Kit (Qiagen laboratories, Germany).

6.1.4 Experimental set-up

Two pools - Kerlingarfjöll KR-P2 and Kverkfjöll KV-P6 - were selected for the set of experiments. For the experiments (summarised in Figure 6-1), three stages were created in order to achieve isolation of the MSR community, and track growth under the different variables.

At stage 1 (T1), replicate cultures were initiated from P2 and P6 with organic and inorganic C and electron donor sources. For the organic conditions, acetate was used as both the C source and electron donor. For inorganic conditions, CO_2 was used as the carbon source and H_2 as the electron donor (introduced in the headspace as 50 % H_2 and 50 % CO_2/N_2). The pH for stage T1 was designed to mimic the pH from the pools: P2 at 5.5 and P6 at 1.7. The goal of stage T1 was solely to enrich for the MSR communities, no growth curve was tracked at this stage. For the following stage T2, T1 cultures were transferred to freshly made media. This time, media spanned a range of different pH values: P2 was transferred into for pH 4, 5.5 and 6; P6 into pH 1, 1.7 and 3 (Figure 6-1). For T2 the growth was tracked by measuring the H_2S production. For stage T3, T2 cultures were transferred again to a new batch of freshly made media. At stage T3, it was decided to proceed only with the organic C source, and focus on the most successful cultures (P2 pH 5.5 and pH 6). The goal at T3 was to understand which organic C sources (acetate and lactate) would promote the most successful growth. DNA was extracted at stage T2 for: A) P2 CO_2/H_2 pH 6, B) P2 acetate pH 6, and B.2) for T3 P2 lactate pH 6. An attempt was made to extract from T2 acetate pH 5.5 and T3 acetate pH 5.5, but there was insufficient DNA material, implying no growth in these cultures.

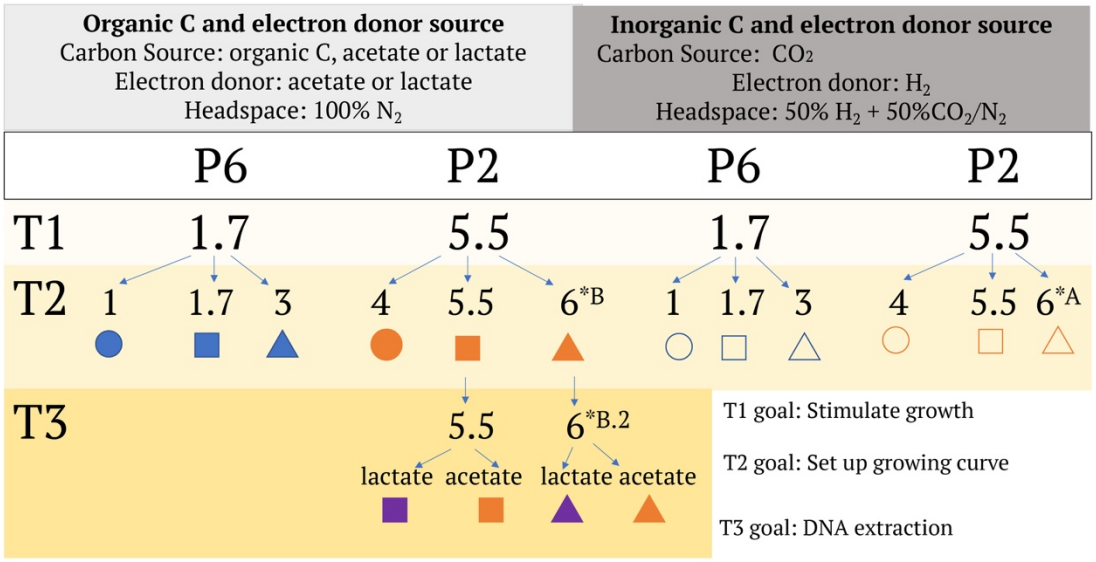

*Figure 6-1. Flow chart from the culturing experiments performed for selected pools P2 and P6. The experiment was divided into two sets for the cultures: organic C (acetate) and inorganic (CO_2). Organic electron donor (acetate) and inorganic (H_2). For Stage 1 (T1) cultures were grown on the pH from the pools, to stimulate the growth of the microbial communities present in the inoculated sediment. For Stage 2 (T2) T1 was inoculated in a range of different pH and growth monitored through production of H_2S. For stage 3 (T3), the pool that presented more growth was inoculated to the same pH but with different organic C source, lactate or acetate, and growth monitored. DNA extractions were done from samples marked with *: A, B, and B.2.*

6.2 Results

6.2.1 MSR culturing results for T2

Growth dynamics varied substantially between P2 and P6, and between organic and inorganic cultures (Table 6-3). Organic acetate cultures supported a faster but smaller magnitude growth (measured by H_2S production) than their inorganic CO_2/H_2 counterparts. Even though the CO_2/H_2 counterparts took longer, their growth reached the highest levels of H_2S produced at T2 (Figure 6-2).

For CO_2/H_2 enrichments, cultures grew over 100 days, with a peak of H_2S production between day 70 and 90. P2 at pH 5.5 CO_2/H_2 supported the highest growth overall (1660 µM of H_2S) (Figure 6-3 A). P2 pH 6 CO_2/H_2 peak growth produced almost 100 µM of H_2S, where P2 pH 4 CO_2/H_2 growth was lower (22 µM of H_2S at day 20). Kverkfjöll cultures were generally not successful in their growth, only P6 pH 3 CO_2/H_2 showed a production

of H_2S higher than 1 µM. All the cultures exhibited a significant dip in growth around day 35, 5 days after the renewal of the headspace. It is possible that some oxygen percolated through and affected the MSR growth of the cultures. At the same time, after the second renewal of the headspace P2 pH 5.5 CO_2/H_2 shows extremely rapid growth; within 10 days reaching levels of 1600 µM H_2S production. Acetate cultures grew over 100 days (Figure 6-3 B). None of the P2 cultures seemed to enhance growing apart from pH 6 acetate, and none at P6. P2 pH 6 shows a clear peak of 36 µM of H_2S at day 50.

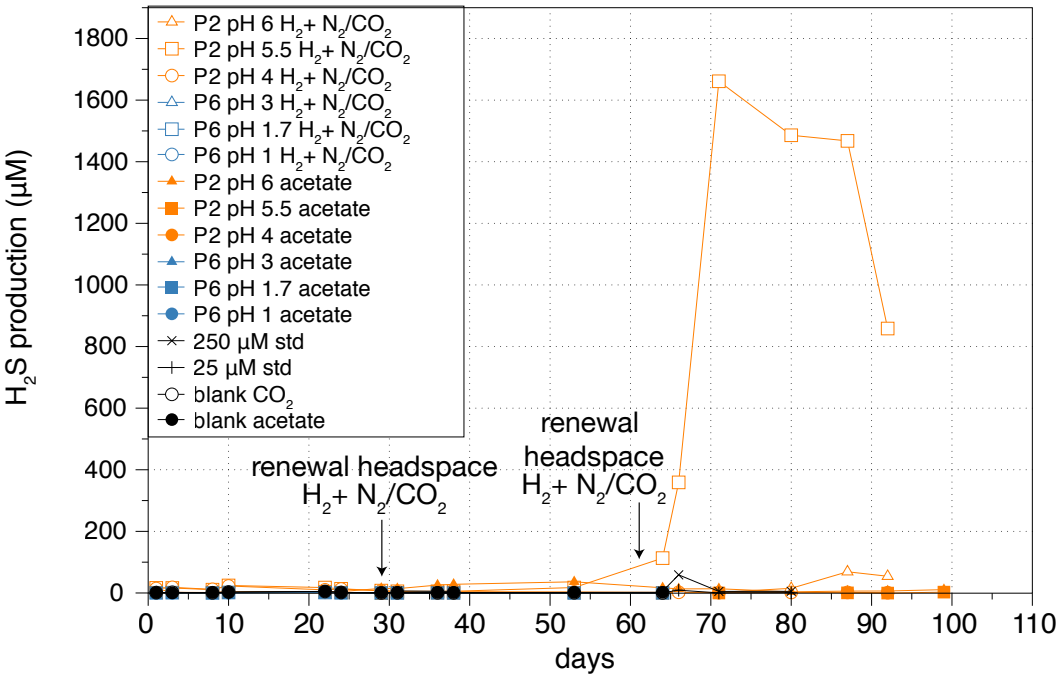

Figure 6-2. Growth curve from H_2S production (µM) for over 100 days of T2 of the culturing experiment. It can be seen how P2 at pH 5.5 with headspace of H_2+ N_2/CO_2 shows the highest production of H_2S over time. Figure 6-3 shows expanded plots for growth on acetate, and H_2/CO_2. Shapes refer to symbols in Figure 6-1.

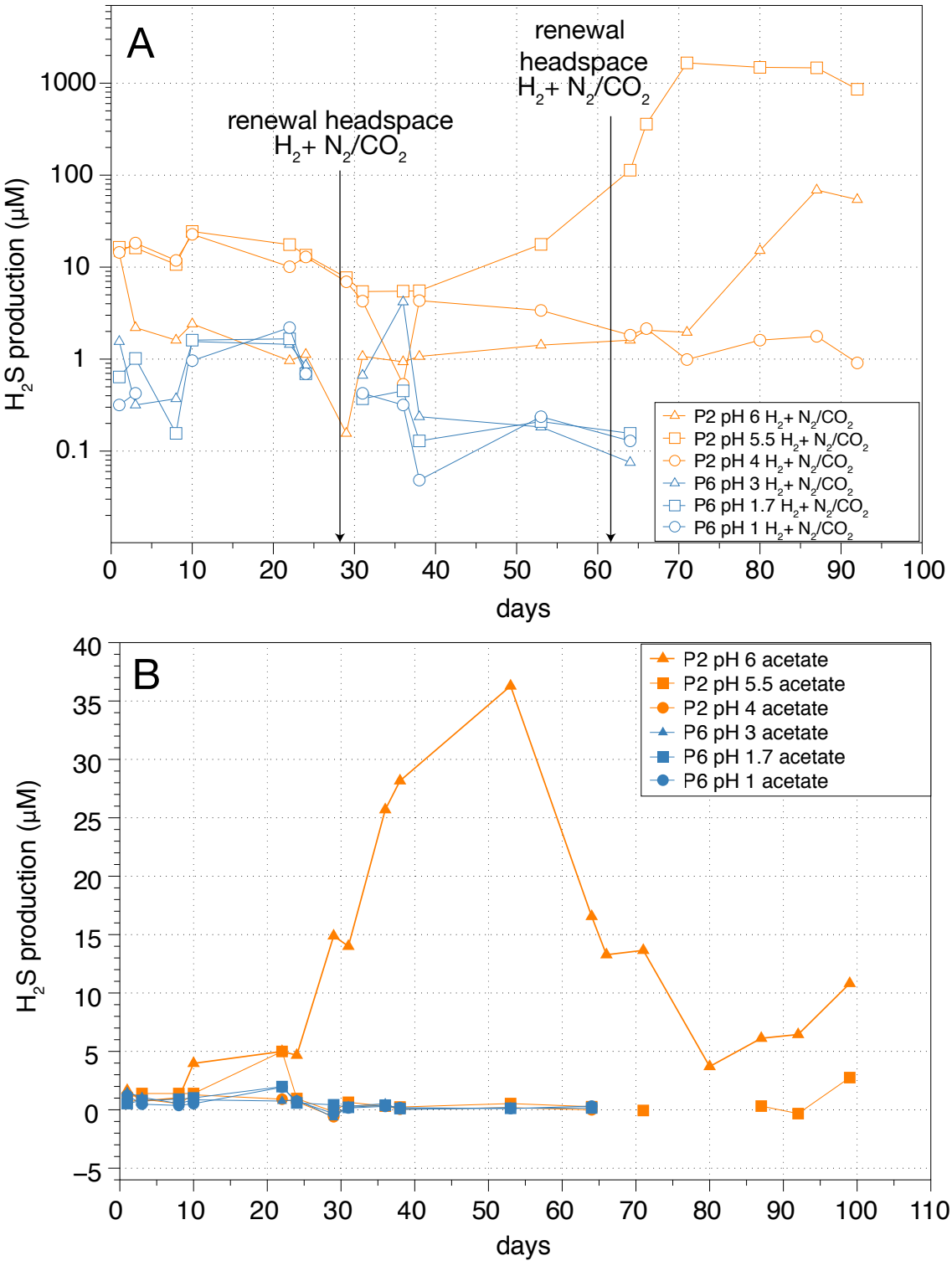

Figure 6-3. Growth curve from H_2S production (µM) for over 100 days of T2 of the culturing experiment. a) H_2+ N_2/CO_2; and b) acetate for different pH (different shapes, orange colour sample from P2 (KR-P2), and blue colour sample from P6 (P6).

6.2.2 MSR culturing results for T3

T3 was carried out only for P2, with acetate and lactate and only two pH variables, pH 5.5 and pH 6 (Table 6-4, Figure 6-4 A). These conditions proved to be more successful in terms of growth for T2 organic conditions, and therefore selected for T3. At T3 growth was observed for 53 days, with the highest point at day 53 (Figure 6-4 B). Cultures exhibiting highest growth were at pH 6, with preference for lactate over acetate. P2 pH 6 lactate exhibited a gradual growth from day 10 to day 30 (27 µM of H_2S production at day 30), and a very quick growth from day 30 to 53 (24947 µM of H_2S production at day 53). This is related to the fact that an extra 2 mL of acetate and lactate were added to respective cultures to enhance growth at day 20. Curiously, only one culture from pH 6 lactate reacted to this by increasing growth.

6.2.3 16s rRNA results from cultures

Only three of the cultures generated sufficient cellular material to perform DNA extraction (Table 6-2). The media (50 mL) from the three cultures was filtered to try to obtain maximum biomass. The 16s rRNA results at genus level show that only one genus of MSR dominates the culture, *Desulfovibrio*. At T2, *Desulfovibrio* is between 64- 67 % of the culture community, with very similar matched identify % between the CO_2/H_2 and acetate cultures at pH 6. For T3, *Desulfovibrio* represents 99 % of the community, nearing a monoculture. DNA results from the sediments of the hydrothermal pools showed *Desulfovibrio* being only 0.03 % of the total OTUs for both P2 and P6, as described in Chapter 5.

Table 6-2. 16s rRNA results from DNA extractions of three cultures at different stages: Stage 2 (T2): P2 pH 6 H_2 +N_2/CO_2, P2 pH 6 acetate, and stage 3: (T3) P2 pH 6 lactate. As Desulfovibrio turned out to be only 0.03 % of all genus in P2 , and not playing an important role in P2 community, the experiment was stopped.

Sample/ DNA match	**A T2 P2-pH 6 H_2 +N_2/CO_2**	**B T2 P2-pH 6 acetate**	**B.2 T3 P2pH 6 lactate**
Genus *Desulfovibrio*	64 %	67 %	99 %
99.46 % match with cultured *Desulfovibrio* sp. 6-71 (AB596886.1), optimal growth pH 7.0 (Ise et al., 2011).			
99.73 % match with uncultured bacterium clone 53c (FJ461941.1). mesophilic anaerobic reactor fed with effluent from the chemical industry. Unpublished study by Hernanandez-Eugenio,G. et al. (2008).			
	Desulfovibrio is 0.03 % of OTUs in P2 and P6		

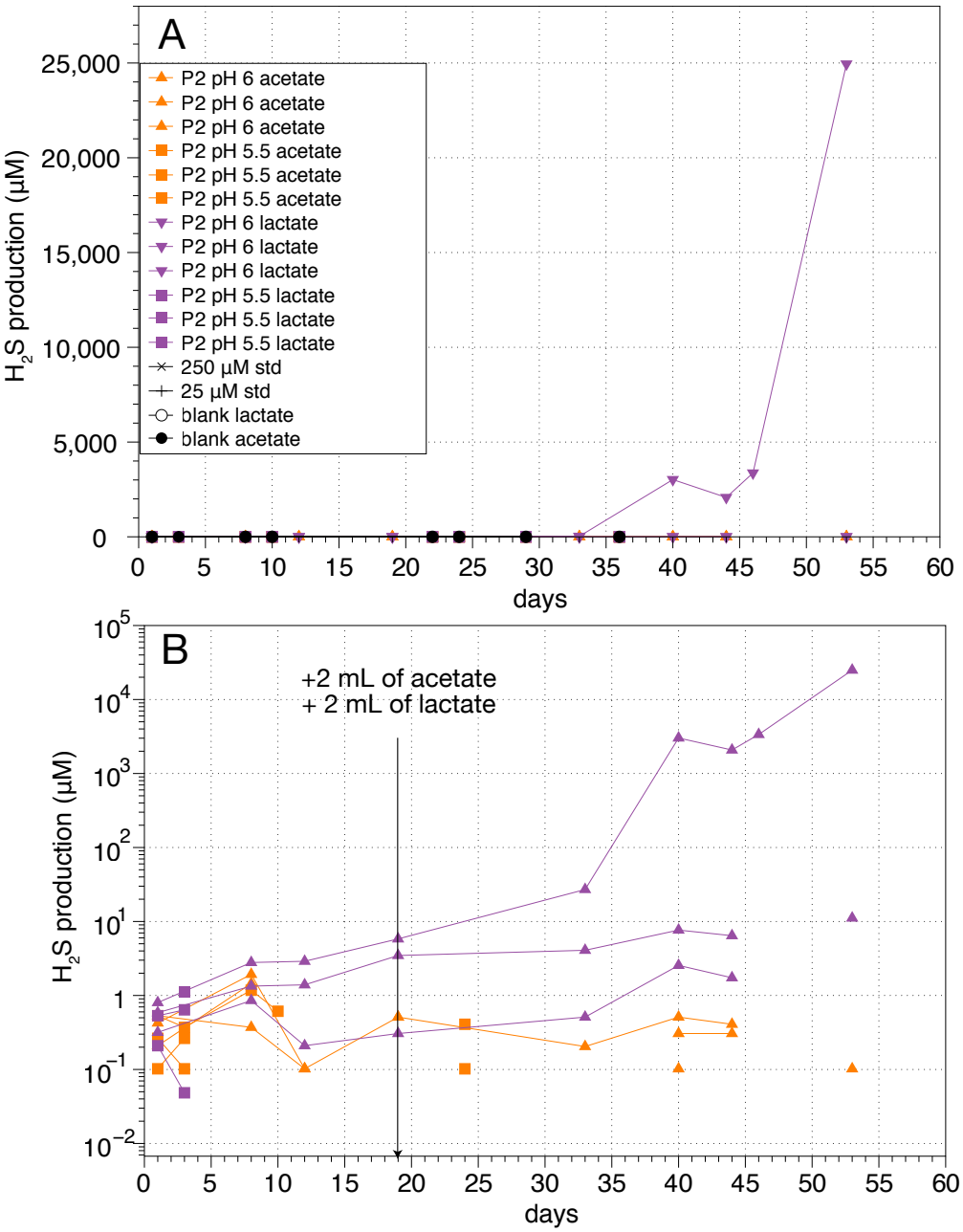

Figure 6-4. Growth curves from H_2S production (µM) for over 55 days of T3 of the culturing experiment a) pH 6 with acetate and lactate, pH 5.5. acetate and lactate, stds and blanks; b) log scale for acetate and lactate (with some zero-values omitted).

Table 6-3. Results from H_2S production (μM) from the cultures at stage 2 (T2) during the different days that they were monitored.

	H_2 +N_2/CO_2							acetate								
days	P2 pH6	P2 pH5.5	P2 pH4	P6 pH3	P6 pH1.7	P6 pH1	blank	P2 pH6	P2 pH5.5	P2 pH4	P6 pH3	P6 pH1.7	P6 pH1	blank	std 250	std 25
1	14.13	16.45	14.46	1.55	0.64	0.32	1.12	1.66	1.02	0.64	1.50	0.53	1.23	1.23		
3	2.20	16.18	18.27	0.32	1.02	0.42	2.09	0.75	1.39	0.91	1.07	0.80	0.48	0.64		
8	1.61	10.69	11.82	0.37	0.16	-0.01	0.59	1.02	1.39	0.53	0.53	0.91	0.37	1.39		
10	2.41	24.40	22.74	1.55	1.61	0.96	3.11	3.97	1.39	1.28	0.85	1.02	0.52	2.52		
22	0.96	17.58	10.10	1.45	1.66	2.20	4.99	4.99	4.99	0.91	0.75	1.98	1.93	5.16		
24	1.12	13.49	12.90	0.85	0.69	0.69	1.61	4.67	0.96	0.69	0.85	0.59	0.75	1.82		
29	0.16	7.68	6.93	-0.54	-0.38	-0.49	-0.01	14.89	-0.17	-0.60	-0.65	0.42	-0.33	1.12		
31	1.07	5.42	4.27	0.67	0.37	0.42	0.69	14.00	0.64	0.34	0.29	0.21	0.16	1.39	6.45	0.83
36	0.94	5.48	0.53	4.19	0.45	0.32	0.67	25.69	0.32	0.32	0.53	0.40	0.29	1.58	5.24	0.53
38	1.07	5.53	4.32	0.24	0.13	0.05	0.40	28.17	0.24	0.05	0.02	0.10	0.18	1.28	5.18	-0.11
53	1.42	17.68	3.38	0.18	0.21	0.24	0.85	36.28	0.53	0.18	0.18	0.13	0.10	1.66		
64	1.61	113.22	1.82	0.08	0.16	0.13	0.24	16.55	0.26	-0.01	0.16	0.16	0.32	2.12	5.69	0.59
66	2.06	359.03	2.15					13.27	-						58.81	9.11
71	1.96	1661.18	0.99					13.65	-0.06						5.10	0.21
80	15.16	1485.91	1.61					3.70	-						5.32	0.96
87	68.87	1467.63	1.77					6.12	0.32							
92	54.30	858.49	0.91					6.45	-0.33							
99								10.82	2.76							

Table 6-4. Results from H_2S production (µM) from the cultures at stage 3 (T3) during the different days that they were monitored.

	acetate							lactate								
days	P2 pH6	P2 pH6	P2 pH6	P2 pH5.5	P2 pH5.5	P2 pH5.5	blank	P2 pH6	P2 pH6	P2 pH6	P2 pH5.5	P2 pH5.5	P2 pH5.5	blank	std 250 uM	std 25 uM
1	0.21	0.42	0.53	0.53	0.32	0.80	0.59	0.32	0.53	0.21	-0.04	0.75	5.32	0.53		
8	1.45	1.93	0.37	0.26	0.10	0.37		2.79	1.34	0.85	0.64	0.05	1.12	0.69	5.69	1.02
12	-0.22	0.10	0.10	0.10	0.26	1.18	-0.33	2.90	1.39	0.21	-0.27	-0.38	-0.27	-0.11	5.16	0.37
19	0.51	0.51	0.00	-0.11	-0.49	0.61	0.51	5.82	3.47	0.31	0.00	-0.51	-0.10	1.12	24.80	5.31
33	0.20	-0.31	-0.41	-0.71	-0.41	-0.41	-0.41	27.04	4.08	0.51	-0.82	-1.02	-0.20	-0.71	10.92	3.78
40	0.51	0.31	0.10	-0.61	-0.82	0.10	-0.20	3019.39	7.65	2.55	-0.20	-0.20	0.00	-0.31	0.10	3.57
44	0.41	0.31	-0.51	-0.41	0.41	-0.20	-0.61	2076.53	6.43	1.73	-1.22	-0.61	-0.51	-0.41	0.00	0.00
46				-0.51	-0.61			3366.33								
53	-0.61	-0.61	0.10	-0.82	-1.12	-0.71	-1.22	24947.96	11.12	-0.71	-0.41	-1.02	-0.71	0.92		

6.3 Discussion

6.3.1 T2 and *Desulfovibrio* growth

A modified Widdle and Bak media recipe was used to enrich for the growth of MSR from Kerlingarfjöll and Kverkfjöll pools. The goal was to understand the preference of their MSR community with respect to pH, inorganic or organic C and electron donor, which are all factors known to influence microbial S isotope fractionation. *Desulfovibrio* was the main genus that dominated the growth in the cultures. Importantly, *Desulfovibrio* was not representative of either the Kerlingarfjöll or Kverkfjöll pool sediment communities (only 0.03 % of the total community in both P2 and P6).

Investigations into how pH range affects growth showed that from the two pools explored in this study, only P2 yielded substantial growth. This suggests that MSR from these habitats are limited to a specific pH range. Based on culture-independent methods (Chapter 3), S oxidisers dominate the microbial community for Kverkfjöll acidic waters (pH 1 – 2). The narrow circum-neutral pH range at which MSR grew in this experiment, could imply that MSR prefer alkaline environments over acidic. Studies have shown how MSR are found to thrive in acidic mines and lakes down to a pH of 3 (Gyure et al., 1990; Praharaj & Fortin, 2004; Sanchez-Andrea et al., 2014). Kverkfjöll pH is between 1 and 3, which is lower than these environments and perhaps too extreme for MSR. This suggestion is consistent with findings from previous chapters. Environmental pH, which is controlled by deep volcanic processes (shown in Chapter 1), dictates the presence of MSR at Kerlingarfjöll (circum-neutral pH), and the near absence of MSR at the highly acidic Kverkfjöll (as seen in Chapter 2).

Results for the different organic/inorganic C source and electron donor experiments show that at stage T2 inorganic CO_2/H_2 was preferred over organic acetate for P2 cultures. The exponential growth for CO_2/H_2 was likely due to the presence of the H_2 electron donor in the headspace, more than CO_2 as a C source. H_2 is an electron donor for which *Desulfovibrio* species exhibits a maximum growth rate (Widdle & Bak,1988). It has also been reported as the most effective substrate utilisation at limiting concentration, even more efficient than H_2-consuming methanogenic bacteria (Zellner

& Winter, 1987). *Desulfovibrio* species seem to be important H_2 scavengers in the anaerobic degradation of organic matter in sediments (Widdle, 1988). When comparing the growth with CO_2/H_2 versus acetate in T2, a longer low-growth lag phase was observed with CO_2/H_2. However, as increases in H_2S began to be detected, CO_2/H_2 growth became exponential very shortly afterwards, producing significantly more H_2S than the acetate cultures. If, at Kerlingarfjöll,H_2 is being delivered into the pools from volcanic gas input, this volcanic H_2 would be the primary choice of electron donor over natural organic carbon sources for the MSR residing within the sediments. Furthermore, a number of other studies have reported methanogens and MSR competing for H_2 and acetate as electron donors (Lovley et al., 1982). Some of them report MSR outcompeting methanogens (Karhadkar et al., 1987; Lovley & Klug1983). The presence of methanogens at Kerlingarfjöll pools was observed from the 16s data for KR-P1, P2 and KR-P3. As such, it is possible that methanogens and MSR are competing for electron donors in the sediments of these pools.

As discussed in Chapter 5, when MSR are offered an unlimited H_2 supply, they produce smaller fractionations ($^{34}\varepsilon_{SO4\text{-}CRS}$ = 1- 6 ‰) than with a limited H_2 supply ($^{34}\varepsilon_{SO4\text{-}CRS}$ = 24-27 ‰). If, as suggested here, Kerlingarfjöll MSR prefer H_2, and volcanic H_2 is not limited in the pools, the S isotope fractionations produced would be small. Despite the fact that the cultures were enriched for a genus (*Desulfovibrio*) that may not represent the wider community, this inference explains observations made in Chapter 5 at Kerlingarfjöll, where $^{34}\varepsilon_{SO4\text{-}CRS}$ = -2 to -4 ‰.

6.3.2 T3 growth on acetate vs lactate

For T3 experiments investigating acetate vs lactate, lactate was clearly preferred over acetate at pH of 6. The growth from lactate at pH 6 showed the highest H_2S production of any culture (23949 µM) overall. This result shows how once *Desulfovibrio* was isolated at T3 from the T2 transfer (*Desulfovibrio* being 99 % of the community at T3), they grew exceptionally well with lactate as the electron donor and carbon source.

It has been shown in the literature how the use of lactate as an electron donor produces a larger S isotope effect ($^{34}\varepsilon_{SO4\text{-}CRS}$ = 37 – 47 ‰) than with other organic electron donor sources. These large S isotope fractionations are related to starvation in environments

that receive very little organic matter (Sim et al., 2011, Goldhaber and Kaplan 1975). Sedimentary Total Organic Carbon values are low in Kerlingarfjöll pools (0.10 – 0.33 wt %). This could indicate that if MSR were using lactate, larger fractionations than those observed should be expected. Together, these results further support the use of H_2 over acetate/lactate at Kerlingarfjöll pools.

6.3.3 Limitations

This study demonstrates the challenges in using culture-based experiments to investigate the stable isotope fractionations, especially when they are set up for heterogeneous microbial communities inhabiting natural environments. The lack of a constant but controlled flow of H_2 /N_2+CO_2 in the culture bottles limited the experiments. In order to progress with the inorganic CO_2/H_2 experiments, the delivery of H_2 to the cultures had to be controlled to be able to regulate growth. This was concluded after observing exponential growth when the headspace was renewed. Control of the flow and rates with reactors inside the cultures (H_2 and CO_2) is key for experiments monitoring S isotope fractionations (Hoek et al., 2006; Sim, 2012). Because of not being able to control the growth with CO_2/H_2, this was an added reason to stop the inorganic experiments after T2.

6.4 Conclusions

This chapter demonstrates how MSR from the pools were unable to grow at pH 1-3, reticently grew at pH 4, and thrived at pH 5.5 and 6 (for P2). The genus *Desulfovibrio* dominated all cultures. The results here suggest *Desulfovibrio,* and therefore potentially MSR at Kerlingarfjöll prefer H_2 over acetate. This conclusion is based on quick growth in culture with CO_2/H_2, and the small S isotope fractionations, consistent with H_2 utilisation, observed for these pools in Chapter 5. It may be easier for them to consume H_2 as it is likely readily available due to fumarole activity in the vicinity of the pools.

Future studies would benefit from research that addresses i) how MSR grow under different CO_2/H_2 conditions under a continuous flow, and ii) is H_2 or lactate a preferred electron donor? Experiments can also be set up with media enriching for the most

dominant species from the pool (known from DNA data: MSR *Desulfurivibrio, Desulfocapsa, Thermofilum* and S oxidisers *Sulfurihydrogenibium*). A fourth transfer stage (T4) could be set once the growing curves are known in order to measure the $\delta^{34}S$ from SO_4^{2-}- H_2S from the cultures. These results would help to understand the fractionations produced and compare them to those measured in the sediments from the environment.

7 Minor S isotope biosignatures and the search for life: results from terrestrial Mars analogue systems

7.1 Introduction

The S isotope system has been proposed as a diagnostic tool for evidence of life on Earth and on Mars (e.g. Farquhar et al., 2000b; Franz et al., 2014, 2017; Johnston et al., 2008a). A number of studies in the last two decades have focused specifically on the quadruple S isotope system, which couples standard ^{32}S and ^{34}S measurements with measurements of the minor isotopes ^{33}S and ^{36}S (e.g. Ono et al., 2007; Pellerin et al., 2015; Zerkle et al., 2009). ^{33}S and ^{36}S values preserved in sulfur compounds in the environment and in the rock record provide evidence of mass-dependent fractionation from biological processes (Farquhar et al., 2000a; Farquhar & Wing, 2003; Johnston et al., 2005a; Ono et al., 2006). Notably, these minor isotopes show small deviations that are quantifiable through systematic variations produced in the mass-dependent relationships of $\Delta^{33}S$ ($\Delta^{33}S \approx \delta^{33}S - 0.515 * \delta^{34}S$) and $\Delta^{36}S$ ($\Delta^{36}S \approx \delta^{36}S - 1.9 * \delta^{34}S$), even when $\delta^{34}S$ ($\delta^{34}S = 1000 \times ({}^{34}R_{sample}/{}^{34}R_{reference} - 1)$) values are almost identical. These variations in $\Delta^{33}S$ and $\Delta^{36}S$, termed mass conservation effects, are caused by the redistribution of sulfur between pools, at both the cellular and ecosystem levels (Farquhar & Wing, 2003; Farquhar et al., 2007). At cellular levels, $\Delta^{33}S$ and $\Delta^{36}S$ are produced due to the kinetic complexity of the multi-step enzymatic reactions that cycle sulfur inside the cell (Farquhar & Wing, 2003; Farquhar et al., 2007). Each enzymatic reaction inside the cell has i) a

fractionation effect and ii) an intrinsic mass flow rate (Brunner & Bernasconi, 2005; Farquhar et al., 2005; Rees, 1973). Due to the reversibility of many of the reactions between enzymes, small variations in $\Delta^{33}S$ and $\Delta^{36}S$ are associated with the transfer between different S pools inside the cells (Farquhar et al., 2007).

This chapter examines the utility of quadruple S isotopes (QSI: ^{32}S,^{33}S,^{34}S,^{36}S) as biosignatures in Mars analogue systems. Two very distinct Mars analogue environments are studied: the hydrothermal Icelandic pools discussed in previous chapters (Kerlingarfjöll and Kverkfjöll), and a Lost Hammer (LH) hypersaline spring from Axel Heiberg Island, Nunavut, Canada. These two environments are distinct in many ways (geochemistry, volcanic activity, salinity, and temperatures), allowing this chapter to investigate the preservation of potential QSI biosignatures under different Mars analogue environments: hydrothermal versus brine conditions. First, $\delta^{34}S$ data from LH is presented, followed by $\Delta^{33}S$ and $\Delta^{36}S$ data from Kerlingarfjöll, Kverkfjöll and LH. Trends in QSI data between the three sites are discussed and compared to the results of two steady-state box models of microbial sulfur cycling. These models allow us to quantitatively constrain the biogeochemical processes producing these signatures in both sites. Last, $\delta^{34}S$ values from LH, Kerlingarfjöll and Kverkfjöll are compared to Martian surface, and to QSI data measured from Martian meteorites, to evaluate their potential relationship with known Mars S isotope data. Overall, this chapter demonstrates the strong potential for QSI values to be used as biosignatures in the search for life in both hydrothermal and hypersaline environments on Mars.

7.2 Axel Heiberg Island, Canadian Arctic

Axel Heiberg Island (AHI) is located in the Canadian Arctic. The thick permafrost is underlain by Carboniferous evaporitic diapirs (Harrison & Jackson, 2014). These diapirs have associated surface representations in the form of hypersaline springs, covering parts of the island surface (Figure 7-1; Fox-Powell et al., 2019). The hypersaline springs from AHI are reduced and maintain low temperatures (-5 to 8 °C) and an alkaline to neutral pH (5-7) throughout the year (Fox-Powell et al., 2019). The waters have a briny composition, with high SO_4^{2-} and Cl^- concentrations that form $NaSO_4$ and NaCl salts

when dry (Battler et al., 2013; Fox-Powell et al., 2019; Pollard et al., 1999). The spring discussed here, Lost Hammer spring (LH), was sampled in July 2017 by Dr. Fox-Powell. The following sample description and site characterisation is modified from Fox-Powell et al., (2019), summarised in Table 7-1. The LH spring source is composed by a large salt dome where the spring flows out (Figure 7-1 A). One sample was taken from inside the dome at the origin (LH-Vent sample, Figure 7-1 B), and two were taken from downstream sites (LH-Out-1, Figure 7-1 C and LH-Out-2). The LH spring temperatures vary from -3.6 °C at the LH-Vent, to -3.3 °C and 1.8 °C for LH-Out-1 and LH-Out-2 respectively. The pH is maintained around circum-neutral conditions along the stream (from 5.8 to 6.0). The oxygen conditions transition from suboxic to oxic downstream, from 0.1 ppm O_2/L at LH-Vent to 7.7 ppm at LH-Out-2. The aqueous geochemistry of the stream resembles a brine composition, as it contains high concentrations of salts (>10 % w.t). The SO_4^{2-} concentrations are between 5531 to 6130 ppm in the spring, and Cl^-concentrations are between 141628 to 143142 ppm.

Table 7-1. Main in situ measurements (temperature, pH, Dissolved Oxygen) and water geochemical composition (SO_4^{2-}, Cl^-) of LH spring. Total Organic Carbon measurements in weight % from sediments for the three locations. Temperature, pH, DO, SO_4^{2-}, Cl^- from Fox-Powell, (2019). TOC measurements conducted by undergraduate Ms. Toni Galloway.

ID	T (°C)	pH	DO (ppm)	SO_4^{2-} (ppm)	Cl^- (ppm)	TOC (wt %)
LH-VENT	-3.6	6.0	0.1	5930.9	141628.6	0.01
LH-OUT-1	-3.3	5.8	2.3	5531.0	142511.8	0.44
LH-OUT-2	1.8	6.0	7.7	6130.4	143142.7	1.09

LH spring is a non-volcanic but high-sulfur system that contrasts with the Icelandic Kerlingarfjöll and Kverkfjöll hydrothermal sites investigated so far. The LH hypersaline spring (with environmental arctic cold and dry conditions) serves as a direct analogue for the Martian late Noachian to Hesperian period. This period is dominated by increasingly cold and dry surface conditions, including the formation of evaporites (Pollard et al., 2009). Despite the low air temperatures on LH, the saline springs are maintained in liquid state, allowing for the presence of microorganisms (Colangelo et al., 2019; Magnuson et al., 2020). Martian-like polygonal terrains have also been found within the surroundings of the hypersaline springs (Pollard et al., 2009). The chlorine

salts that dominate LH are less common than sulfate brines on Mars, although they also exist in local deposits, or associated with sulfate evaporites that were deposited during the late Noachian to mid Hesperian (McLennan et al., 2005). Martian brines were also present in smaller scale systems, such as Gusev Crater (Wang et al., 2006) and Columbus Crater (Murchie et al., 2008).

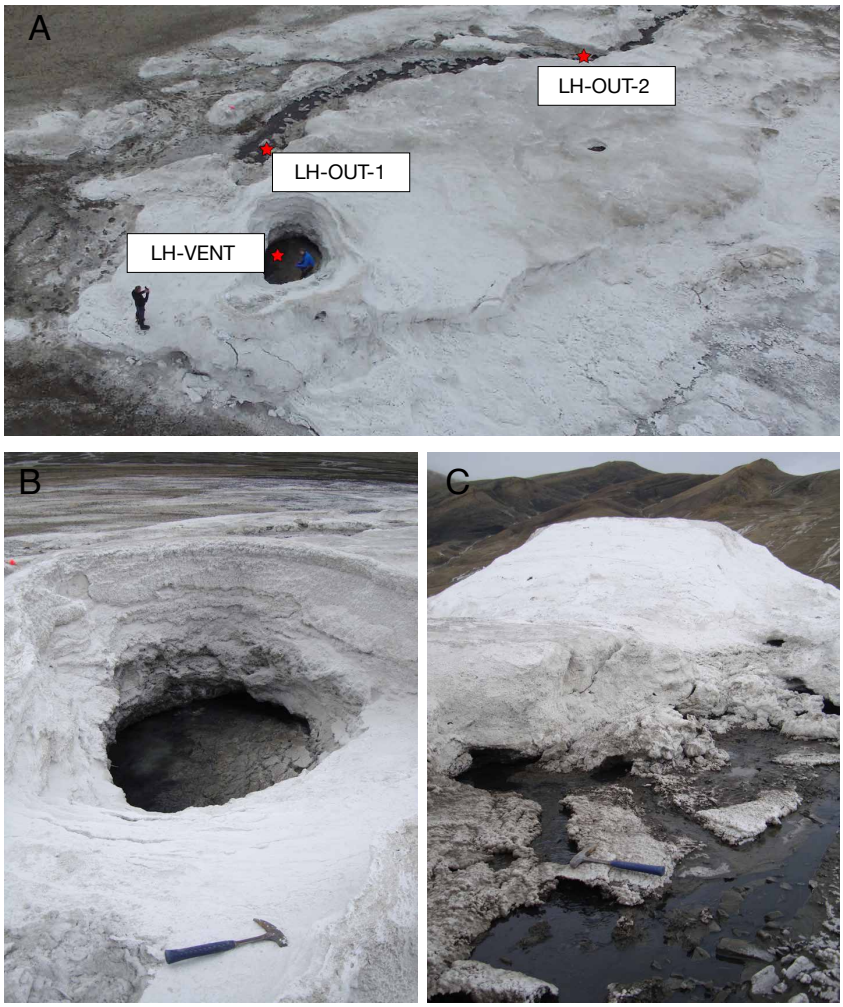

Figure 7-1. a) Lost Hammer spring seen from a drone view. The photo shows the outlet and salt apron, with sampling sites indicated by red stars. Two geologists for scale. b) Closer view from the LH-Vent, surrounded by the salt apron. Hammer for scale. c) View of LH-Out-1, looking upstream towards the salt apron. Hammer for scale. Photographs taken by Dr. Fox-Powell when sampling the site in 2017.

7.3 Results

7.3.1 $\delta^{34}S$ values from LH hypersaline springs (Canadian Arctic)

The $\delta^{34}S_{SO4}$ values of aqueous SO_4^{2-} are, from the top of the spring to the bottom: 22.2 ‰ at LH-Vent, 22.4 ‰ at LH-Out-1, and 22.3 ‰ at LH-Out-2. The mean value of $\delta^{34}S_{SO4}$ is 22.3 +/- 0.33 ‰ (1σ) (Table 7-2). The $\delta^{34}S_{CRS}$ values of CRS extracted from the sediments range from -28.4 ‰ at LH-Vent, -25.0 ‰ at LH-Out-2 and -22.2 ‰ at LH-Out-2. The mean value of $\delta^{34}S_{CRS}$ is 22.2 +/- 0.75 ‰ (1σ) (Table 7-2).

Chapter 5 describes the S isotope fractionations ($^{34}\varepsilon_{SO4\text{-}CRS} = (\alpha_{SO4\text{-}CRS} - 1) \times 1000$) identified at Kerlingarfjöll and Kverkfjöll between aqueous $\delta^{34}S_{SO4}$ and sedimentary $\delta^{34}S_{CRS}$. As discussed in Chapter 5, S isotope fractionations in these pools are generally small compared to most S-cycling environments. The largest $^{34}\varepsilon_{SO4\text{-}CRS}$ fractionations are observed at Kerlingarfjöll KR-Bio (-9.1‰), followed by the Kerlingarfjöll pools (-4.3 to -3.7 ‰). Even smaller $^{34}\varepsilon_{SO4\text{-}CRS}$ are observed in Kverkfjöll pools (-1.6 to -0.9 ‰). Much larger fractionations are found in the LH system. S isotope fractionations ($^{34}\varepsilon_{SO4\text{-}CRS}$) are as large as -49.5 ‰ at the LH-Vent, and decrease as the stream progresses downstream, to -43.5 ‰ at LH-Out-2.

7.3.2 QSI results from hydrothermal and hypersaline Mars analogues

The $\Delta^{33}S$ and $\Delta^{36}S$ results for Kerlingarfjöll and Kverkfjöll hydrothermal samples and LH brine samples are listed in Table 7-2 and shown in Figure 7-2. For $\Delta^{33}S$ (Figure 7-2 A, B), sedimentary CRS ($\Delta^{33}S_{CRS}$) from Kerlingarfjöll ranges from the lowest value of 0.014 ‰ (at KR-P1), to the highest value of 0.135 ‰ (at KR-Bio). Kverkfjöll $\Delta^{33}S_{CRS}$ ranges from 0.017 ‰ (at KV-P5) to 0.034 ‰ (at KV-P4). LH $\Delta^{33}S_{CRS}$ ranges from 0.081 ‰ (at LH-Out-2) to 0.140 ‰ (at LH-Vent). The $\Delta^{33}S_{SO4}$ of aqueous SO_4^{2-} from Kerlingarfjöll is 0.031 ‰ at KR-P1, and 0.054 ‰ at KR-P2. For Kverkfjöll, $\Delta^{33}S_{SO4}$ is 0.018 ‰ at KV-P6. For LH, $\Delta^{33}S_{SO4}$ ranges from 0.045 ‰ (at LH-Out-2) to 0.070 ‰ (at LH-Out-1).

For $\Delta^{36}S$ results (Figure 7-2 C), sedimentary CRS ($\Delta^{36}S_{CRS}$) from Kerlingarfjöll ranges from -0.658 ‰ (at KR-Bio) to 0.131 ‰ (at KR-P2). Kverkfjöll $\Delta^{36}S_{CRS}$ ranges from -0.208 ‰ (at KV-P4) to 0.146 ‰ (at KV-P5). LH $\Delta^{36}S_{CRS}$ ranges from -0.799 ‰ to 0.406 ‰ at LH-

Out-1 and LH-Out-2 respectively. $\Delta^{36}S_{SO4}$ from Kerlingarfjöll is from -0.208 ‰ (at KR-P2) to 0.419 ‰ (at KR-P1). For Kverkfjöll, $\Delta^{36}S_{SO4}$ is 0.077 ‰ at KV-P6. At LH, $\Delta^{36}S_{SO4}$ values ranges from -0.387 (at LH-Out-1) to -0.085 (at LH-Vent).

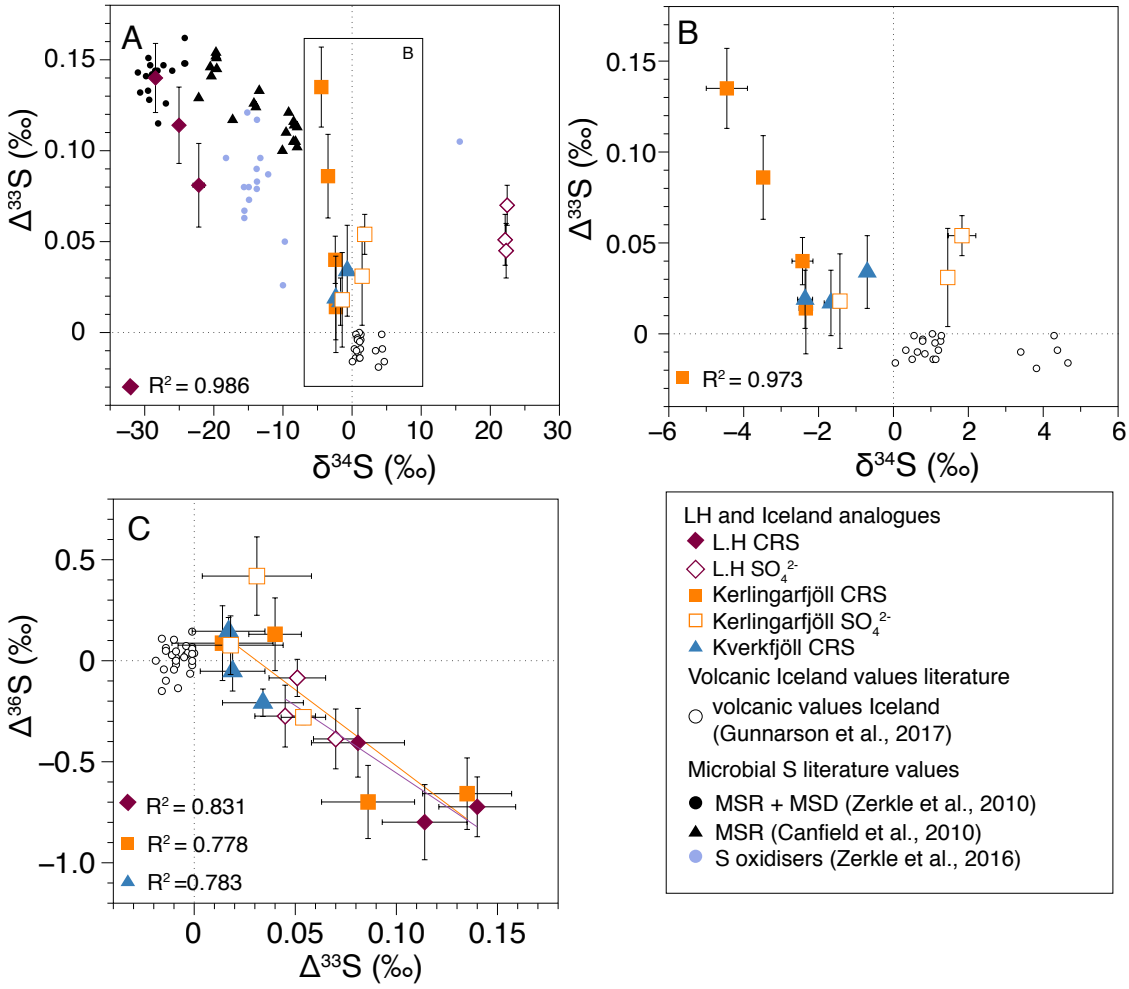

Figure 7-2. a) $\delta^{34}S$ vs $\Delta^{33}S$ systematics for all samples from LH, Kerlingarfjöll and Kverkfjöll. Rectangle highlights the data range for plot B.. Literature values shown for MSR from euxinic Lake Cadagno (Canfield et al., 2010), MSR+MSD (MSD: Microbial Sulfur Disproportionation) from euxinic Fayetteville Green Lake (Zerkle et al., 2010), and for S oxidisers from sulfidic Frasassi caves (Zerkle et al., 2016). b) Zoom-in of the Kerlingarfjöll and Kverkfjöll values compared to volcanic values. Values from vapor and liquid H_2S from Icelandic volcanoes plotted here and in plot C, are from Gunnarsson et al. (2017). c) $\Delta^{36}S$ vs $\Delta^{33}S$ for LH, Kerlingarfjöll and Kverfkjoll samples. LH $\Delta^{36}S/\Delta^{33}S$ slope is -6.6, Kerlingarfjöll $\Delta^{36}S/\Delta^{33}S$ slope is -7.5, Kverkfjöll $\Delta^{36}S/\Delta^{33}S$ slope is -17.

7.3.3 Trends in QSI

When plotting $\delta^{34}S$ against $\Delta^{33}S$ (Figure 7-2 A, B), a steep negative trend appears for CRS values from LH (R^2= 0.986, slope -0.009) and Kerlingarfjöll (R^2= 0.973, slope -0.053). It

can be observed that $\delta^{34}S_{CRS}$ and $\Delta^{33}S_{CRS}$ from LH-Vent and LH-Out-1 plot within the range of values for MSR + MSD (MSD: Microbial Sulfur Disproportionation) measured in other natural environments (Zerkle et al., 2010: $\delta^{34}S$ from -30 to -20 ‰, and $\Delta^{33}S$ from 0.155 ‰ to 0.160 ‰). LH CRS values are largely depleted in $\delta^{34}S$ compared to Icelandic Kerlingarfjöll and Kverkfjöll CRS values. The steep trend for Kerlingarfjöll is produced as a result of the small range of $\delta^{34}S_{CRS}$ (-4.5 ‰ to -2.3 ‰, Figure 7-2 B) and a larger range for $\Delta^{33}S_{CRS}$ (0.014 ‰ to 0.135 ‰). The highest Kerlingarfjöll $\Delta^{33}S_{CRS}$ values, 0.135 ‰ and 0.084 ‰ (from KR-Bio, and KR-P3 respectively), plot similarly to $\Delta^{33}S_{CRS}$ values from LH and natural populations of S oxidisers, MSR, and MSR+MSD (Canfield et al., 2010; Zerkle et al., 2010, 2016). Kverkfjöll pools plot on a smaller range ($\delta^{34}S_{CRS}$ from -2.4 ‰ to -0.7 ‰; $\Delta^{33}S_{CRS}$ 0.017 to 0.034 ‰), closer to Icelandic $\Delta^{33}S_{H2S}$ volcanic values. Kerlingarfjöll and Kverkfjöll $\Delta^{33}S_{SO4}$ values also plot lower than 0.05 ‰, close to volcanic $\Delta^{33}S$. $\Delta^{33}S_{SO4}$ results from LH plot lower than 0.05 ‰ but $\delta^{34}S_{SO4}$ values are clearly distinct (22.2-22.4 ‰, Figure 7-2 A).

Samples from the three sites plot on a negative trend for $\Delta^{33}S$ versus $\Delta^{36}S$ that is consistent with mass dependent processes: for CRS results LH R^2= 0.83, slope -5.6 $\Delta^{36}S/\Delta^{33}S$; Kerlingarfjöll R^2= 0.77, slope -7.5 $\Delta^{36}S/\Delta^{33}S$; Kverkfjöll R^2= 0.78, slope -17 $\Delta^{36}S/\Delta^{33}S$ (Figure 7-2 A). The three sites present distinct positive $\Delta^{33}S$ values compared with $\Delta^{33}S$ Icelandic volcanic aqueous and vapour phases, as the volcanic $\Delta^{33}S$ range is narrow and negative (from -0.016 ‰ to 0.000 ‰, from Gunnarsson-Robin et al., 2017). On the other hand, the $\Delta^{36}S$ values from KV-P6 overlap with the volcanic values ($\Delta^{36}S$ volcanic values from -0.136 to 0.144 ‰ (Gunnarsson-Robin et al., 2017). The negative correlation with high $\Delta^{33}S$ and low $\Delta^{36}S$ with a negative slope has been observed before in previous studies: the $\Delta^{36}S/\Delta^{33}S$ slope relation measured for MSR is between $\Delta^{36}S/\Delta^{33}S$ -10 and -5 (Johnston et al., 2007), and theoretical predictions for mass dependent processes $\Delta^{36}S/\Delta^{33}S$ = -6.85 (e.g. Johnston et al., 2008b; Ono et al., 2007). The three slopes for LH (-5.6), Kerlingarfjöll (-7.5) and Kverkfjöll (-17), deviate from the equilibrium slope (Johnston et al., 2006). The $\Delta^{36}S/\Delta^{33}S$ slope for LH and Kerlingarfjöll are consistent with mass-dependent S cycling processes (Farquhar et al., 2007).

Table 7-2 Multiple S isotope compositions of LH, Kerlingarfjöll and Kverkfjöll sediment CRS and water SO_4^{2-}. $\delta^{34}S$ values for Kerlingarfjöll and Kverkfjöll from Chapter 5

Sample ID	$\Delta^{33}S$ (‰)	1σ (‰)	$\Delta^{36}S$ (‰)	1σ (‰)	$\delta^{34}S$ (‰)	1σ (‰)	λ^{33}	λ^{36}	$^{34}\varepsilon_{SO4\text{-}CRS}$ (‰)
KR-P1 CRS	0.014	0.025	0.087	0.185	-2.3	0.18	0.515	1.861	-3.8
KR-P2 CRS	0.040	0.013	0.131	0.180	-2.4	0.28	0.511	1.839	-4.3
KR-P3 CRS	0.086	0.023	-0.699	0.181	-3.5	0.05	0.510	1.934	-3.7
KR-Bio CRS	0.135	0.022	-0.658	0.177	-4.5	0.55	0.500	1.950	-9.1
KV-P4 CRS	0.034	0.020	-0.208	0.068	-0.7	0.07	0.512	1.893	-1.7
KV-P5 CRS	0.017	0.018	0.146	0.068	-1.7	0.18	0.515	1.857	-
KV-P6 CRS	0.019	0.016	-0.052	0.098	-2.4	0.20	0.514	1.879	-0.9
KR-P1 SO_4^{2-}	0.031	0.027	0.419	0.194	1.5	0.00	0.513	1.831	
KR-P2 SO_4^{2-}	0.054	0.011	-0.280	0.036	1.8	0.37	0.506	1.913	
KV-P6 SO_4^{2-}	0.018	0.026	0.077	0.145	-1.4	0.06	0.514	1.860	
LHVENT CRS	0.140	0.019	-0.723	0.148	-28.4	0.05	0.511	1.924	-49.5
LHOUT-1 CRS	0.114	0.021	-0.799	0.186	-25.0	0.43	0.510	1.935	-46.4
LHOUT-2 CRS	0.081	0.023	-0.406	0.170	-22.2	0.83	0.511	1.919	-43.5
LHVENT- SO_4^{2-}	0.051	0.014	-0.085	0.092	22.2	0.22	0.517	1.896	
LHOUT-1- SO_4^{2-}	0.070	0.011	-0.387	0.148	22.4	0.32	0.517	1.888	
LHOUT-2- SO_4^{2-}	0.045	0.015	-0.274	0.153	22.3	0.47	0.518	1.881	

7.4 Discussion

7.4.1 Comparison of $\delta^{34}S$ values between hypersaline and hydrothermal Mars analogues

The LH spring is characterised by circum-neutral pH, hypersaline conditions (more than 10 wt. % salt) and low temperatures from (-3.6 °C to 1.8 °C). The SO_4^{2-} comes from the underlying Carboniferous evaporite diapirs, as $\delta^{34}S$ values are similar to those measured for Carboniferous evaporites ($\delta^{34}S$ of ~20 ‰, Wu et al., 2010) The S isotope fractionations calculated between aqueous SO_4^{2-} in LH ($\delta^{34}S_{SO4}$) and sedimentary CRS ($\delta^{34}S_{CRS}$) vary from $^{34}\varepsilon_{SO4\text{-}CRS}$ = -49.5 to -43.5 ‰, consistent with isotope effects produced via MSR (e.g. Farquhar et al., 2003; Johnston et al., 2005b, 2007), with or without MSD (e.g. Johnston et al., 2005b; Zerkle et al., 2010). The largest fractionation between aqueous SO_4^{2-} and sedimentary CRS is found at the origin of the spring (LH-Vent sample), and fractionations decrease downstream. The fractionations from the LH spring are considerably larger than the ones reported in the Chapter 5 for hydrothermal Kerlingarfjöll and Kverkfjöll. The S isotope fractionations from Kerlingarfjöll, Kverkfjöll and new $^{34}\varepsilon_{SO4\text{-}CRS}$ LH data are plotted in Figure 7-3 against main environmental parameters that are expected to control biological S isotope fractionation effects (temperature, Total Organic Carbon (TOC), Dissolved Oxygen, pH, SO_4^{2-} and Cl^- concentrations).

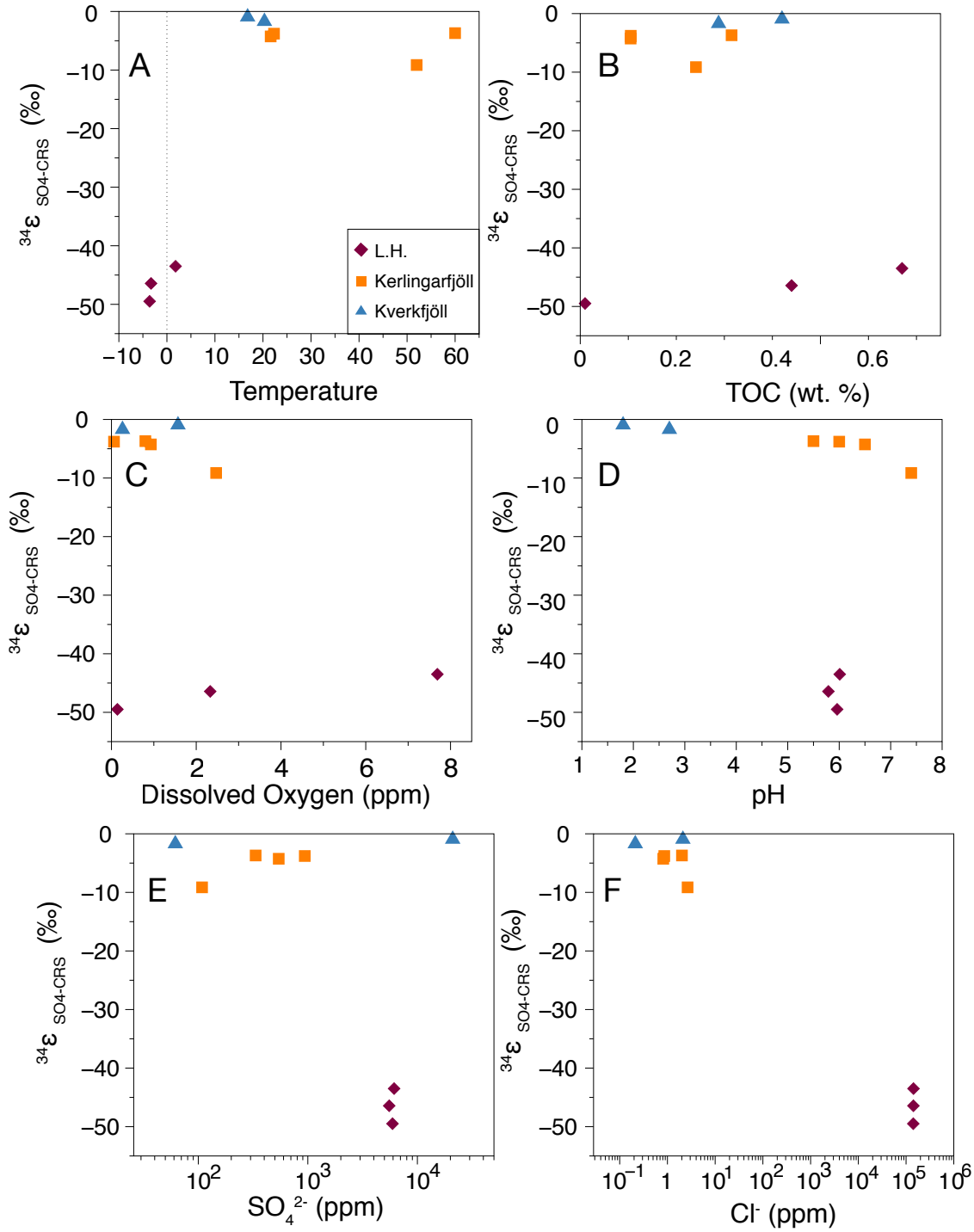

Figure 7-3. Plots showing S isotope fractionations ($^{34}\varepsilon_{SO4\text{-}CRS}$) presented in a previous chapter for Kerlingarfjöll and Kverkfjöll compared with new LH results. $\varepsilon^{34}{}_{SO4\text{-}CRS}$ are plotted against environmental parameters: a) vs temperature; b) vs TOC; c) vs Dissolved Oxygen (DO); d) vs pH; e) vs SO_4^{2-} concentration; f) vs Cl^- concentrations.

The environmental differences, such as Cl^- and temperature between the hypersaline LH spring and the hydrothermal Kerlingarfjöll and Kverkfjöll could be the cause for the differences in S isotope fractionation effects. S isotope fractionations from both systems

are compared in Figure 7-3 against the main environmental parameters known to affect S isotope fractionations during biological S cycling in natural environments (e.g., see discussion in Chapter 5). No clear differences or trends between sites are observed between S isotope fractionations and TOC, Dissolved Oxygen, SO_4^{2-} concentrations, or pH. On the other hand, S isotope fractionations show a relationship with temperature and salinity (salinity defined by Cl^- concentrations). Namely, the larger S isotope fractionations at LH are associated with lower temperatures (around 0 ^oC; Figure 7-3 E) and significantly higher Cl^- values (from 141628 to 143142 ppm) than at the hydrothermal spring sites (Figure 7-3 F). Taken together with observations for Kerlingarfjöll and Kverkfjöll from Chapter 5, these trends suggest that the main environmental parameters allowing for large magnitude S isotope fractionations in LH include: i) a lack of volcanic (abiotic) H_2S input, ii) environmental stress (high salinity, low temperature), and iii) the electron donor/acceptor limitation of the environment. These possibilities will be subsequently examined.

First, as mentioned in Chapter 5, the small S isotope fractionations seen at Kerlingarfjöll and Kverkfjöll would provide a challenge in detection of $\delta^{34}S$ biosignatures in hydrothermal environments. These small apparent fractionations are primarily due to the prevalence of volcanic (abiotic) H_2S input and resulting $\delta^{34}S$ values overprinting MSR and microbial $\delta^{34}S$ signatures. On the other hand, LH has no volcanic inputs, with the majority of S sourced as SO_4^{2-} from evaporites. Thus, the dominant source of H_2S in the environment is from MSR, such that fractionation effects during MSR are preserved in Fe-sulfides without being swamped by abiotic H_2S inputs.

Second, high salinity and low temperatures are linked to larger fractionations at LH compared to Kerlingarfjöll and Kverkfjöll. LH Cl^- concentrations are 10^5 times greater than Kerlingarfjöll and Kverkfjöll concentrations. The elevated salinity of the LH spring could be causing osmotic stress to the MSR cell, and slowing down the metabolism (i.e., resulting in lower cell-specific sulfate reduction rates) producing larger fractionations (Chambers et al., 1975; Habicht & Canfield, 1997; Kaplan & Rittenberg, 1964). Hypersaline environments are colonised by halotolerant microorganisms and by hyperhalophiles. Halophiles are observed to perform sulfate reduction at their optimum rate in elevated salt concentrations (Brandt et al., 2001; Howarth & Teal, 1979; Porter

et al., 2007). Stress response genes were found to be abundant in nearby LH spring in a metagenomic study from Lay et al, (2013). These genes provide stress responses for adapting to cold and osmotic stresses in the hypersaline and cryogenic conditions at LH spring. However, a drop in sulfate reduction rates has been observed in different studies with hyperhalophiles occurring at salt concentrations higher than 60 g/L of Cl^-, similar to LH (141 to 143 g/L of Cl^-) (Brandt et al., 2001; Porter et al., 2007). Above these high salt concentrations, cells are no longer able to regulate salt balance, therefore reducing their cell specific sulfate reduction rates (Cypionka, 1995).

Low temperatures could also play a role in cellular stress and lowered metabolic rates at LH. As mentioned in Chapter 5, the relationship between temperature and S isotope fractionation is strain-specific. The S isotope fractionations during MSR are directly related to temperature via the responses of internal enzyme kinetics and the SO_4^{2-} flux into the cell (Canfield et al., 2006). Larger fractionations were observed at low temperatures when the flux of SO_4^{2-} into the cell was kept at medium flow, where the reduction of sulfite to sulfide between S pools in the cell was low (Canfield et al., 2006). Similar cellular responses could be happening at LH. The large fractionations observed at LH (even though the temperatures are sub-zero), could indicate that specific adaptations to cryogenic stress allowed MSR at LH to have a regular SO_4^{2-} flux into the cell, but a sluggish exchange of S between the S pools inside the cell.

Lastly, the limited amount of available metabolic energy (electron donors and acceptors) in this hypersaline environment could also contribute to small S isotope fractionation effects during MSR. As pointed out in Chapter 5, enzymes favouring large S isotope fractionations are present in electron donor/acceptor limited environments (Wenk et al., 2018). Kerlingarfjöll and Kverkfjöll resemble a comparably unlimited-metabolic energy environment for microbial sulfur-based metabolisms, as hydrothermal systems provide abundant volcanic CO_2 and H_2, Fe, SO_4^{2-}, and other components able to support metabolic reactions. Conversely, LH resembles a limited-metabolic energy environment, as it has high SO_4^{2-} concentrations, but limited organic C as a C source, and no inorganic CO_2 or H_2 to serve as an electron donor/acceptor and undetectable dissolved Fe_{total} (Fox-Powell et al., 2019). Overall, the saline stress and metabolic energy-limited conditions of LH might be favouring electron carriers with

weak negative reduction potentials. These electron carriers would use efficient pathways to exploit the little energy available in this hypersaline-cold environment, with large associated S isotope fractionations (Wenk et al., 2018).

Additional S cycling processes, e.g., oxidative recycling of sulfur compounds, could also contribute to the large S isotope fractionations at LH. In particular, oxidation of sulfide followed by microbial sulfur disproportionation (MSD) can increase apparent S isotope fractionations between sulfate and sulfide in natural systems. MSD uses intermediate redox state sulfur species such as S^0, SO_3^{2-}, and $S_2O_3^{2-}$ to produce both sulfate and sulfide at the same time (e.g. Frederiksen & Finster, 2003). Large $\delta^{34}S$ fractionations of up to ~21 ‰ are associated with MSD (e.g. Böttcher & Thamdrup, 2001). The ability to generate larger fractionations is associated with branching within these metabolic transformations, and the fractionations linked to the recycling of reduced components (reviewed in Canfield, 2001a).

7.4.2 Open-system steady-state S isotope ecosystem models

Comparison with previously published data from natural environments (Figure 7-2) suggests that QSI values from LH are consistent with S oxidisers, MSR, and MSR+MSD values. Kerlingarfjöll KR-P3 and KR-Bio QSI results are not conclusive of microbial S cycling due to the small fractionations $^{34}\varepsilon_{SO4\text{-}CRS}$. Therefore, a model will be explored here in order to diagnose the potential biogenic production of these values.

In order to further constrain the input of these biogeochemical processes (using $\delta^{34}S$ and $\Delta^{33}S$) from LH, Kerlingarfjöll and Kverkfjöll systems, two open-system steady-state S isotope mass balance models are used here. Model A is an open-ocean-type model system, as described in Johnston et al. (2005b), used to interpret the LH data, and Model B is adapted with modified S inputs to interpret the Kerlingarfjöll and Kverkfjöll data. The models are based on traditional geochemical box models (Garrels and Lermann, 1981), following derivations of Johnston et al. (2005b, 2006, 2008), and Zerkle et al. (2009). Models A and B are represented conceptually in Figure 7-4, and Figure 7-5 shows the produced results. For both, the model produces results for open-system steady-state isotope mass-balance calculations ($^{34}S/^{32}S$ and $^{33}S/^{32}S$). They are done for different fluxes of material (arrows) between reservoirs (boxes) (Figure 7-4) (Johnston et al., 2005b;

2008b; Zerkle et al., 2009). The fluxes represent the interaction between reservoirs, and each flux has a fractionation associated with the transformation (Johnston et al., 2005b; 2008b). As the model is run in steady-state open-system conditions, the flux terms represent a relative flux of material. Furthermore, the model is used to calculate values for the resulting isotopic composition of sulfate and sulfide pools (preserved as CRS in the sediments) in the water column (Figure 7-5, sulfate and sulfide shown for model A, sulfide shown for model B) (Johnston et al., 2005b).

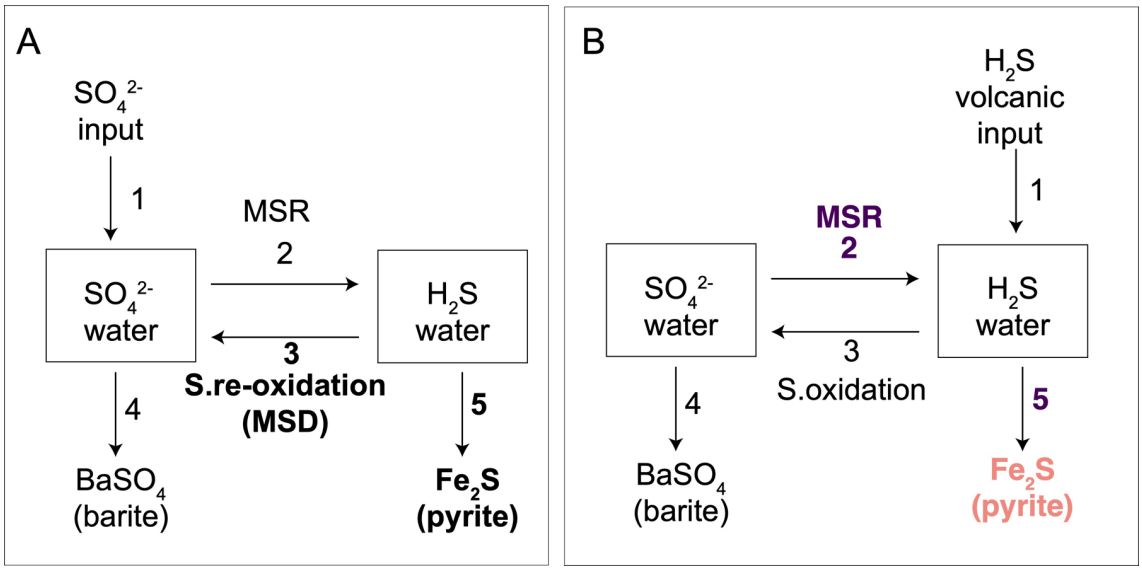

Figure 7-4. Illustration of the two open-system steady-state S isotpe mass-balance models used to calculate the model fields presented in Figure 7-5 A, B. The boxes represent the different sulfur reservoirs. The fluxes leaving or entering the sulfur reservoirs linked to each pathway are represented with an arrow and a correlated number. Each flux has an isotopic fractionation associated with the transfer of material along the pathway. a) Illustrates the box model A from Johnston et al. (2005b), from a marine sulfur cycle. The main flux terms explored (variables) within the model are shown in bold, and are the relative pyrite burial and re-oxidation of sulfide (MSD). The variables explored produce the fields observed in Figure 7-5 A for sulfide and sulfate. b) Illustrates the model adjusted for Kerlingarfjöll and Kverkfjöll conditions, with MSR and volcanic H_2S as the main inputs of H_2S to the water column pool. The variables in this model are a function of relative pyrite burial and MSR. The variables explored produce the field in Figure 7-5 B for sulfide in the water column.

Model A was adapted from the Johnston et al. (2005b) marine sulfur cycle model to examine S isotope values from LH, as it considers similar inputs, outputs, and sulfur reservoirs to the LH system. The inputs for Model A are: 1) the isotopic composition of SO_4^{2-} entering the SO_4^{2-} water pool, shown as the origin in Figure 7-5 A, and 2) experimental $^{34}S/^{32}S$ and $^{33}S/^{32}S$ fractionations associated with sulfur transformations

(MSR, and MSD). Johnston's model explores the different fractionations associated with MSR and MSD as a function of two flux (*f*) terms: fluxes for pyrite burial and re-oxidation of H_2S. The pyrite burial flux (f_{py}, flux 5 in Figure 7-5 A), represents the relative flux of material leaving the S cycle as pyrite, while the re-oxidation flux ($f_{r\text{-}o}$, flux 3, Figure 7-5 A) represents re-oxidation of H_2S to SO_4^{2-} relative to the original flux of SO_4^{2-} to H_2S in the water column. For example, when $f_{py} = 0$, no sulfur is removed as pyrite from the system, and all is removed as sulfate minerals. For this model, re-oxidation is used as a proxy for the presence of MSD, and the model predicts fields for $\delta^{34}S$ and $\Delta^{33}S$ of water column H_2S and SO_4^{2-}, as shown in Figure 7-5 A). The starting $\delta^{34}S$ composition for SO_4^{2-} in LH is estimated to be ~20 ‰, from underlying Carboniferous evaporites (Wu et al., 2010). Hence, three different model fields using initial $\delta^{34}S$ values between 18 and 22 ‰, and $\Delta^{33}S$ between 0.00 and 0.05 ‰ are shown (Figure 7-5 A squares).

Model B required some adaptation from this original model, since input of sulfur into the Kerlingarfjöll and Kverkfjöll hydrothermal systems is dominantly as volcanic H_2S rather than as aqueous sulfate (calculations for model B are found in Appendix B. Model B has two inputs to the aqueous H_2S pool: isotopic composition of 1) volcanic H_2S and 2) MSR, and the $^{34}S/^{32}S$ and $^{33}S/^{32}S$ fractionations associated with sulfur transformations (MSR). The starting isotopic composition of volcanic H_2S is an average of $\delta^{34}S$ and $\delta^{33}S$ values from the literature (Gunnarsson-Robin et al., 2017), where $\delta^{34}S$ is 3.63 ‰ and $\delta^{33}S$ is 1.84 ‰. For the MSR fractionations, a range of fractionation factors (α) for MSR were explored. The fractionation factor used to generate the final model field is the largest reported in the literature ($^{34}\alpha = 0.94088$ and $^{33}\alpha = 0.9692$, from Sim et al., 2011). The main goal of model B is to explore the different S isotope values produced in the system as a function of two flux terms: the flux of pyrite burial (f_{py}, flux 5 Figure 7-5 B) and the flux of MSR (f_{MSR} , flux 2 Figure 7-5 B). This is overall expressing the proportion of sulfide that is coming from biological production instead from abiotic sources, to produce large S isotope fractionations/biosignatures. The predicted model field for the water column H_2S is presented in Figure 7-5 B. The purple colour represents the predicted f_{MSR}, and the red colour, f_{py}. For example, for $f_{MSR} = 1$, all the flux going into the H_2S aqueous pool is introduced from MSR, and 0 from volcanic H_2S.

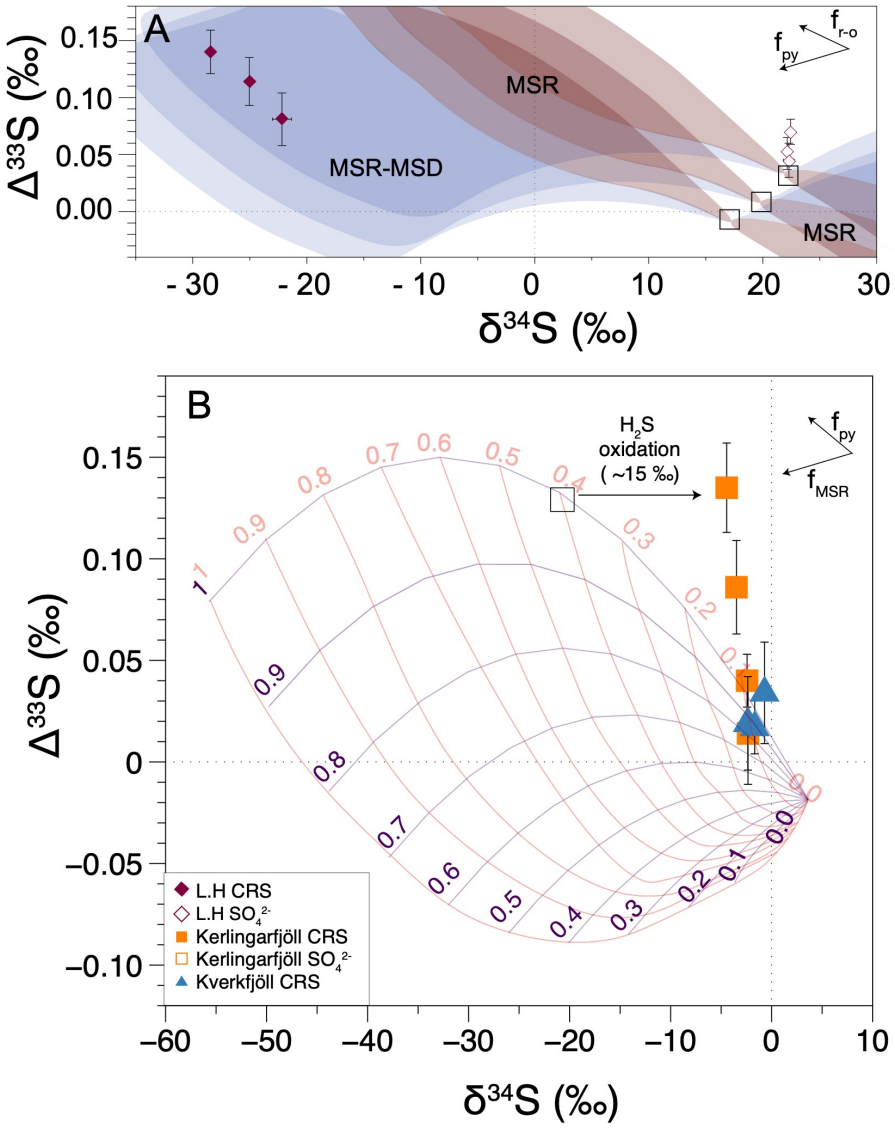

Figure 7-5. a) plot of $\delta^{34}S$ versus $\Delta^{33}S$ for the LH results of CRS and water column SO_4^{2-}, including predicted fields for model A for the composition of sedimentary sulfides (left side) and water column sulfates (right side). The red field encompasses resulting compositions that can only be described with MSR, whereas the blue field requires additional MSD. The model was made by Johnston et al., (2005b) as a function of the relative fraction of pyrite burial and sulfide re-oxidation. The three squares represent three different starting SO_4^{2-} compositions with $\delta^{34}S$ between 18-20 ‰ and $\Delta^{33}S$ between 0.00 and 0.05 ‰. b) $\delta^{34}S$ versus $\Delta^{33}S$ for the Kerlingarfjöll and Kverkfjöll CRS, also including the sedimentary sulfides generated with model B as a function of relative fraction of pyrite burial (red lines) and MSR (purple lines). The proportion of the flux is indicated (from 0 to 1). The model shown was generated using the largest MSR fractionation factor (α) reported in the literature ($^{34}\alpha$ = 0.94088 and $^{33}\alpha$ = 0.9692 from Sim et al., (2011)).

The $\delta^{34}S$ and $\Delta^{33}S$ results are presented in Figure 7-5 A for sedimentary CRS and water column SO_4^{2-} from LH, plotted on top of fields for the predicted S isotope composition of sedimentary pyrite (left) and water column SO_4^{2-} (right) computed with model A. The model A field is sub-divided into two regions, one for MSR only (shown in red), and one for MSR-MSD (shown in blue). Figure 7-5 A illustrates how the LH CRS data can be satisfied with the model, for both $\delta^{34}S$ and $\Delta^{33}S$. For all three model fields, the LH CRS data plot within the MSR-MSD field. This suggests that LH $\delta^{34}S$ and $\Delta^{33}S$ values are likely produced by MSR with additional MSD cycling in the spring.

The $\delta^{34}S$ and $\Delta^{33}S$ results for sedimentary CRS at Kerlingarfjöll and Kverkfjöll results are plotted with the predicted composition of sedimentary pyrite calculated from model B in Figure 7-5 B. KR-P1 and KR-P2 and Kverkfjöll pools plot within fields predicted by the model, but only at the extreme edge of the calculation. To reproduce the majority of these data the model requires a variable flux of sulfide from MSR (between 0.5 to 1), and low fluxes of pyrite burial (between 0.3 and 0.1). These results are consistent with a potential volcanic H_2S flux up to 0.5 compared to MSR in these pools. These results agree with the conclusions from Chapter 4, which suggested that the $\delta^{34}S$ values of KR-P1, KR-P2 and Kverkfjöll pools are closer to volcanic values than biologically produced values.

On the other hand, sedimentary CRS from Kerlingarfjöll pools KR-P3 ($\delta^{34}S$ -3.48 ‰ and $\Delta^{33}S$ 0.086 ‰) and KR-Bio ($\delta^{34}S$ -4.45 ‰ and $\Delta^{33}S$ 0.135 ‰) fall outside the S isotope fields predicted by model B. This discrepancy suggests a more complex biogeochemical S cycle than what was included in the model. For example, S recycling in these pools could involve oxidation of H_2S to S^0 or other intermediate S species, followed by further oxidation or reduction. S oxidation could be driven either by microorganisms (Pellerin et al., 2015; Zerkle et al., 2016) or abiotically with oxygen or nitrate (Fry et al., 1984). As indicated in Figure 7-5 B, sedimentary CRS from pools KR-P3 and KR-Bio can be explained by taking model predictions for sulfide (MSR flux of 1 and pyrite burial flux of 0.4) and including a positive shift in $\delta^{34}S$ of ~15‰ through additional oxidative sulfur (re)cycling.

The 16S rRNA microbial community studies presented in Chapter 5 affirm the use of S^0 and other intermediate S species for reduction and oxidation at KR-Bio and KR-P3. The

archaeal community at both KR-Bio and KR-P3 is dominated by *Thermofilum*, whose metabolic pathway is S^0 reduction through formate hydrogen lyase. The bacterial community is dominated by *Sulfurhydrogenibium* in KR-Bio, which oxidises S^0 or $S_2O_3^{2-}$ to SO_4^{2-}, and *Caldisericum*, *Hydrogenobacter*, and *Sulfurhydrogenibium* at KR-P3. The *Caldisericum* metabolic pathway can reduce S^0 or $S_2O_3^{2-}$ to H_2S, and *Hydrogenobacter* oxidises $S_2O_3^{2-}$, S^0 or H_2S to SO_4^{2-}. The S isotope fractionations produced during S cycling by these specific organisms are unknown, but microbial oxidation of H_2S to S^0 generally only produces very small S isotope fractionations of < 3 ‰ (see review in Pellerin et al., 2019). It is more likely that the abiotic oxidation of H_2S, that produces intermediate S products (S^0, $S_2O_3^{2-}$, SO_3^{2-}) depleted in $\delta^{34}S$ by an average of 5.2 ‰, is what is driving $\delta^{34}S$ values of H_2S heavier (Fry et al., 1988). The specific abiotic oxidation of H_2S to S^0 had an associated isotopic fractionation up to -7.5± 6.2 ‰ (Fry et al., 1988). Furthermore, abiotic sulfide oxidation does not require elevated temperatures, as the abiotic oxidations reported by the literature were carried out at 22-25 °C (Fry et al., 1988). Overall, the combined $\delta^{34}S$ and $\Delta^{33}S$ values from KR-P3 and KR-Bio support a complex biological S-cycle recycling S intermediates, with additional abiotic oxidation of H_2S, shifting the $\delta^{34}S$ for a given $\Delta^{33}S$.

7.4.3 QSI in Martian meteorites and $\delta^{34}S$ data from Gale Crater

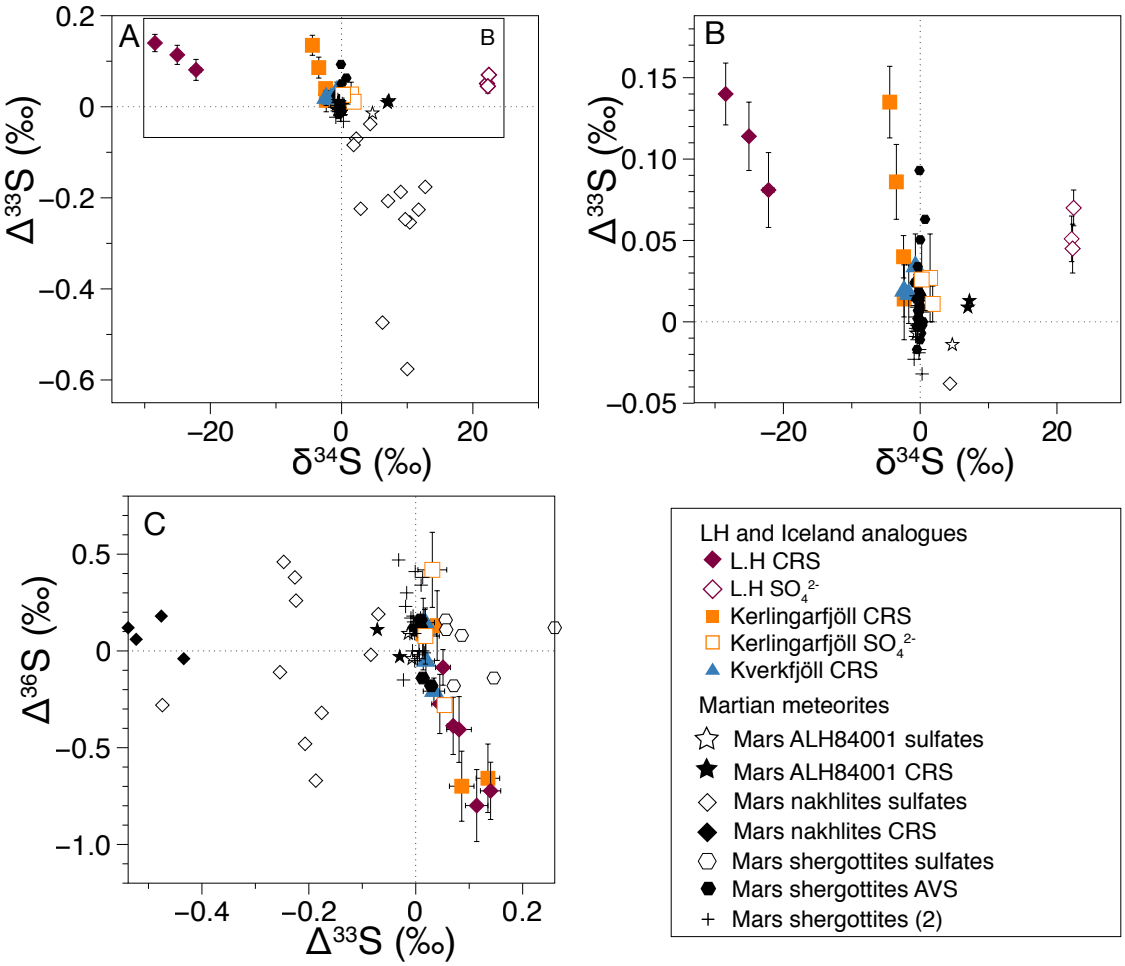

Figure 7-6. $\delta^{34}S$ vs $\Delta^{33}S$ for LH, Kerlingarfjöll, and Kverkfjöll samples, and Martian meteorites from Franz et al., 2014, 2019a,2019b. The square area corresponds to plot b. b) zoom in of Kerlingarfjöll and Kverkfjöll samples compared with Martian meteorites. c) $\Delta^{36}S$ vs $\Delta^{33}S$ for LH, Kerlingarfjöll, and Kverkfjöll samples, and Martian meteorites.

The S isotope values measured for sulfide (CRS, AVS) and sulfates from igneous Martian meteorites are shown in Figure 7-6 (Franz et al., 2014, 2019a,2019b). These $\Delta^{33}S$ and $\Delta^{36}S$ values reveal evidence of sulfur mass independent fractionation (S-MIF), proposed to result from photochemical processes in the Martian atmosphere. Martian meteorite $\Delta^{33}S$ values suggest that volcanic eruptions released SO_2 into the Martian atmosphere, which underwent photochemical transformations, producing S-MIF. Sulfur from the atmosphere was then assimilated into the magmas, capturing the large $\Delta^{33}S$ variations (Farquhar et al., 2000b; Franz et al., 2014).

S isotope data from the LH, Kerlingarfjöll and Kverkfjöll samples compared to the Martian meteorite values are shown in Figure 7-6. These plots illustrate how biologically-influenced values for $\Delta^{33}S$ are distinctive from Martian MIF values recorded by the meteorites. Martian meteorites show a larger range of $\Delta^{33}S$ (from -0.454 to 0.260‰), outside the range of values produced during mass conservation effects and mass dependent processes (Franz et al., 2014). Biologically-influenced samples from LH and Kerlingarfjöll plot on a small concrete range, from 0.05 to 0.15 ‰, with no negative values. Furthermore, when combining $\Delta^{36}S$ /$\Delta^{33}S$, LH and Kerlingarfjöll values plot in a different field, with negative $\Delta^{36}S$ (from -0.5 to -1.0 ‰), distinctive from meteorite values.

This comparison illustrates how paired analysis of S isotopes (QSI) can be useful in recognising biological S isotope effects on Mars' surface. Very large fractionations in $\delta^{34}S$ (up to 40 ‰) have been measured at Gale crater between sulfate and sulfide (Franz et al., 2017). These large fractionations are hypothesised to have been produced by equilibrium fractionation between sulfate and sulfide at high temperatures (~150 ^{o}C) over 4,000 years (Franz et al., 2017). By also measuring $\Delta^{33}S$ on the Martian surface, these values could be unpaired from biological S-cycling. This is demonstrated on Earth, as large $\delta^{34}S$ isotope fractionations (up to 58 ‰) are equally related to equilibrium fractionations (Johnston et al., 2011). The associated $\Delta^{33}S$ changes during equilibrium fractionations are small, between -0.02 and 0.03 ‰ (Johnston et al., 2011), smaller than values observed for biologically produced signals (> 0.05 ‰).

If S-cycling microorganisms were present on the Martian surface, two scenarios emerge for their potential contribution and interaction with the Martian S cycle, and resulting S isotope signatures. In the first one, S cycling microorganisms could interact with atmospherically-derived sulfur bearing a S-MIF signal. Preservation of a S-MIF signal requires two distinct exit channels for S from the atmosphere. Once deposited, these two distinct S species have to remain separate to preserve the S-MIF signal in the resulting sediments. S-cycling by microorganisms on Mars' surface could mix these pools, diluting the S-MIF signal (Farquhar et al., 2003).

In the second scenario, S cycling organisms would interact with MIF-free reservoirs, such as volcanic or hydrothermally-sourced sulfur derived directly from the mantle. The

meteorites with a S-MIF signal preserved could only be a small representation of all the S surface and subsurface processes going on Mars. Thus, it is reasonable to assume that certain S reservoirs were free of S-MIF contamination from the atmosphere. For example, S delivered directly from inputs of volcanic sources will have a near zero S isotope value reflecting mantle values and no MIF. These volcanic inputs could be delivered to hydrothermal systems, which could further avoid the interaction with S-MIF if they were subglacial. From these two scenarios, a clearer biosignature of biological sulfur cycling would be detected in the MIF-free systems.

Overall, the combination of $\delta^{34}S$, $\Delta^{33}S$ and $\Delta^{36}S$ seems to provide a rigorous approach for future biosignature Mars exploration purposes in S rich systems on the Martian surface. Our data suggest that $\delta^{34}S$ and $\Delta^{33}S$ values could support evidence of S cycling biosignatures on the Martian surface. However, there is a need to look in the sediments from the Martian surface in order to observe the types of biological signals observed here. Future studies involving modelling of how this signal could have been recycled are necessary in order to understand $\Delta^{33}S$ and $\Delta^{36}S$ biosignatures on Mars.

This chapter demonstrates the potential for QSI as a biosignature tool on Mars, which is more conclusive than $\delta^{34}S$ alone for future explorations. The preservation of $\Delta^{33}S$ biosignatures in the Kerlingarfjöll hydrothermal environment is a significant outcome. It demonstrates how $\Delta^{33}S$ values can record complex S cycling processes in KR-Bio and KR-P3 pools, even when $\delta^{34}S$ are not clearly distinct from volcanic values. The study of $\Delta^{33}S$ in brine analogue locations such as LH should be continued in the future in more detail, as sulfate has a high potential to preserve biosignatures on Mars (Foster et al., 2010). This higher potential is due to the rapid precipitation of sulfate minerals, which can capture organics and biosignatures inside the crystals, in fluid inclusions or along the boundaries, protecting them from UV radiation (Foster et al., 2010; Franz et al., 2019a). The large S fractionations found in this hypersaline analogue opens the door for more studies into the microbial community and deeper understanding of the S cycling at this site, to help understand the potential microbial life that could have lived in Martian brines. Of particular relevance, Jezero crater landing site for Mars 2020 mission, presents chloride and sulfate rich sediment layers from late Noachian-early Hesperian ages (Ehlmann & Mustard, 2012).

7.5 Conclusions

$\delta^{34}S$ values from the LH hypersaline spring exhibit large fractionations typical of MSR or MSD ($^{34}\varepsilon_{SO4\text{-}CRS}$ from -49.49 to -43.50 ‰), contrary to the small S isotope fractionations reported for the Icelandic hydrothermal sites. The environmental differences between hypersaline LH and hydrothermal Kerlingarfjöll and Kverkfjöll control this disparity. The main environmental distinctions that make LH an ideal environment for the preservation of S isotope biosignatures are a dominantly biological source of sulfide, metabolic stress due to highly saline conditions, and the limited electron donor/acceptor environment.

S isotope values from LH can only be reproduced with a steady-state mass balance sulfur box model including both MSR and MSD, suggesting that MSD could be aiding the production of large S isotope fractionations in this system. On the other hand, low S isotope values at Kerlingarfjöll and Kverkfjöll can be reproduced with a model including an abiotic supply of volcanic H_2S. Samples KR-P3 and KR-Bio fall outside this model, suggesting that these streams support a more complex biological S cycle with further abiotic or biological recycling of sulfur species. The combination of $\delta^{34}S$, $\Delta^{33}S$ and $\Delta^{36}S$ seems to provide a rigorous approach for future biosignature for Mars exploration These results are encouraging and foreshadow the use of QSI as a diagnostic tool for finding evidence of life on future Mars missions, especially Mars sample return from brine environments. It is necessary for future missions to include QSI measurements in order to discern and investigate the potential for QSI biosignature preservation in hypersaline and hydrothermal environments.

Overall, LH provided clear evidence for $\delta^{34}S$ and $\Delta^{33}S$ preserving biological S cycling processes, and demonstrated that hydrothermal environments are more challenging for S isotope biosignatures. The LH analogue presents an ideal setting for the study of Martian brines, with similar conditions to the late Noachian and early Hesperian. Sulfate salts present a higher potential for the preservation of biosignatures, due to their quick formation and therefore the capture of biosignatures inside or along the crystals. A greater understanding of these brine systems is needed to elucidate how microbial

communities could have lived in Martian brines, what kinds of biomarkers they may have preserved, and which techniques will be required for their discovery.

8 Conclusions

The purpose of this thesis was to understand and characterise the stable isotope biosignatures produced in Mars-analogue hydrothermal environments. This aim has been addressed through a comprehensive interdisciplinary study analysing Kerlingarfjöll and Kverkfjöll hydrothermal pools. Additionally, these results have been contextualised through a comparison with those from LH hypersaline spring. The data presented here demonstrate that:

i) Deep volcanic processes are a critical influence on the preservation of biosignatures in Mars hydrothermal pools. The deep volcanic processes control the geochemistry of the system, which select the microbial communities inhabiting the hydrothermal pools and the electron acceptors available.

ii) Priority should be given to hypersaline over hydrothermal systems for the search of S isotope biosignatures on Mars. The $\delta^{34}S$ from volcanic origin can overwhelm the biological $\delta^{34}S$ values in hydrothermal systems.

iii) C isotopes and QSI can be an effective tool for identifying biosignatures on Mars. C isotopes are an effective tool on hydrothermal environments, and QSI in hypersaline or hydrothermal environments.

This final chapter summarises the main findings of the individual studies, and discusses the implications for Mars future exploration. An updated knowledge gap is included, with a final outlook and identification of the future work of isotopic biosignatures and their application to Mars.

8.1 Main findings

This study presents the first comprehensive investigation of stable isotope biosignatures (C isotopes and QSI) coupled with microbial community DNA analyses in Mars analogue hydrothermal systems. $\Delta^{33}S$ and $\Delta^{36}S$ are measured for the first time in a natural Mars analogue environment, which opens promising new avenues of research. Previous work on microbial isotopic biosignatures measured on modern and also ancient natural systems has laid the foundations of this project (such as Zerkle et al., 2009), Des Marais 1997). Here, these approaches were adapted and combined to characterise the hydrothermal Mars analogue environments, in order to help aid the interpretation of future isotopic signatures on Mars by either future landers or return mission explorations.

The core result of this thesis is that the geochemical composition of hydrothermal systems drive the fundamental differences observed in the type of microbial communities they support. Therefore, it has an effect on the isotopic biosignatures produced. $\delta^{34}S$ is not a conclusive biosignature by itself in hydrothermal systems as they are not distinctive from volcanic $\delta^{34}S$ signals (e.g. Kverkfjöll). Therefore, $\delta^{34}S$ coupled to $\Delta^{33}S$ and $\Delta^{36}S$ can help to provide conclusive evidence of microbial metabolisms acting in hydrothermal environments. Furthermore, sulfur-rich hypersaline systems such as LH, seem to be better environments for the detection of microbial S isotope biosignatures. This is due to the environmental stressors placed on the microbial community, which tend to enhance biological fractionation effects. Specific findings are summarised below.

The geochemistry of hydrothermal systems are driven by deep processes, which drive the acid supply, redox conditions, and secondary-mineral solubility, with the lithology of each site playing a minor role (Chapter 4). Kerlingarfjöll and Kverkfjöll hydrothermal pool geochemistry is controlled by deep volcanic processes. The deep volcanic processes leads to the pools to have very distinct pH environments, circum-neutral and acidic for Kerlingarfjöll and Kverkfjöll, respectively. The pH difference is the basis for the observed disparity in water geochemistry and sediment mineral phases between sites. The results from Chapter 4 indicate how hydrothermal

redox variations happen on a small scale, affecting the mineralogy and dissolved S and Fe species present. Chapter 4 results observe Fe-Mg-phyllosilicate phases in acidic environments in Kverkfjöll. Usually, they are associated with circum-neutral environments, and used to interpret palaeoenvironments on Mars as such. The observation of Fe-Mg phyllosilicate phases in acidic environments, indicates how processes ongoing in hydrothermal systems are controlled on a small scale by the hydrothermal fluids, independent from larger scale processes happening on the surface.

Microbial communities in hydrothermal systems are controlled by deep volcanic processes (Chapter 5 and 6). The redox variability determines the different S and Fe species present, and therefore the electron donors or acceptors available in the pools for microorganisms. The 16S rRNA microbial community results indicate the dominant communities growing in Kerlingarfjöll or Kverkfjöll pools are different based on the pH range in which they grow. The pH also controls the electron donors and acceptors geochemically-available in these environments. For example, Kverkfjöll waters have high Fe water concentrations that can be linked with the dominance of Fe reduction/oxidation bacterial taxa in the Kverkfjöll pools.

$\delta^{13}C$ values are controlled in these systems by temperature, consistent with previous results from other studies in hydrothermal sites (Chapter 5). C isotope fractionations preserved as organic carbon (TOC) from this study are controlled in Kerlingarfjöll and Kverkfjöll systems by temperature. This is consistent with previous $\delta^{13}C$ studies in hydrothermal systems. In the hydrothermal systems investigated, low temperature pools (16 to 23 ^{o}C) favour carbon CO_2 fixation pathways that produce larger or more variable C isotope fractionations, whereas high temperature hydrothermal pools (50 to 60 ^{o}C) favour CO_2 fixation pathways (such as the TCA pathway) with small C isotope fractionations.

$\delta^{34}S$ values alone do not provide strong evidence for microbial activity in hydrothermal systems at Kverkfjöll, and are minimally-distinct from abiotic values at Kerlingarfjöll. Despite the presence of S-metabolising microorganisms (Chapter 5 and 7). $\delta^{34}S$ isotope values in sediments are not conclusive of biosignature preservation at Kverkfjöll due to abundant H_2S with abiotic $\delta^{34}S$ values seemingly overwhelming the biological $\delta^{34}S$ values. This result is consistent with previous

literature measurements and is corroborated by the model results. The model shows how Kverkfjöll values are likely produced by volcanic H_2S with abiotic $\delta^{34}S$ values. At Kerlingarfjöll, $\delta^{34}S$ isotope values are on the low range of fractionation effects produced during biological S cycling. The small fractionations observed at Kerlingarfjöll pools are likely caused by the preference of unlimited H_2 as the inorganic electron donor with a continual volcanic supply, over locally-available organic carbon sources. An important outcome is the relationship with pH, regulating the availability of dissolved Fe in hydrothermal systems. This relation outlies how pH and redox processes control the solubility of Fe. This effect is key on the S isotope fractionations for MSR, and extremely relevant for past Mars conditions.

$\delta^{34}S$ data from a hypersaline environment reveals S isotope biosignatures are better preserved here than in hydrothermal environments (Chapter 7). LH sediments preserve $\delta^{34}S$ and $\Delta^{33}S$ values that show clear evidence for S cycling microbiological processes. Larger fractionations in $\delta^{34}S$ are found in LH are typical of MSR-MSD, demonstrated by the steady state box model. LH hypersaline spring is more ideal than the hydrothermal environments explored for the preservation of S isotope biosignatures due to: i) no volcanic input masking the potential biosignatures produced; ii) salinity stress potentially causing larger fractionations during biological sulfur cycling, iii) limitation of electron donors and acceptors in the environment. The limitation of electron donors/acceptors in the saline spring favours the presence of enzymes that cause larger S isotope fractionations to make the most of the limited energy available. Furthermore, the LH analogue site presents an ideal setting for the study of Martian brines, with similar conditions to the late Noachian and early Hesperian.

The most robust form of S isotope biosignature is a combination of QSI (Chapter 7). Chapter 7 demonstrates the potential for QSI as a geochemical biosignature tool on Mars, by combining $\delta^{34}S$ with $\Delta^{33}S$ and $\Delta^{36}S$. The preservation of QSI biosignatures in the Kerlingarfjöll environment is an important outcome, as $\delta^{34}S$ alone does not provide strong evidence of biological cycling. $\Delta^{33}S$ and $\Delta^{36}S$ values in combination with $\delta^{34}S$ can record complex S- cycling processes in KR-Bio and KR-P3 pools, even when $\delta^{34}S$ are not clearly distinct from volcanic values.

8.2 Updating the knowledge gap

Following the work presented in this thesis, the knowledge gaps outlined in Chapter 2 are updated here.

Question 1: What are the main controls on the geochemistry and mineralogy of Mars analogue hydrothermal environments?

As discussed in Chapter 4, deep volcanic processes determine the primary controls on dissolved ion chemistry are acid supply, redox conditions, and secondary-mineral solubility. The underlying lithology plays a minor role in the precipitation of authigenic phases. The main geochemical characteristics between these two sites are the pH and redox conditions driving the differences in the main ions dissolved in the water. The sensitivity of water chemistry to local redox conditions observed in Chapter 4 affects the presence of different S and Fe species on the hydrothermal pools. S and Fe are also the main species dominating these environments. The main differences between environments are that Kerlingarfjöll pools have circum-neutral CO_2-rich waters with reduced conditions and dissolved H_2S, captured as authigenic calcite, pyrite, and kaolinite sediments. Kverkfjöll pool waters are the result of acid-SO_4^{2-} processes, resulting in poorly crystalline Fe-, Mg-phases and Al-phyllosilicates. Trends in SO_4^{2-} and Cl^- additionally indicate mixing between surface meteoric water with volcanic steam.

Question 2: Which chemolithotrophic communities inhabit Mars analogue hydrothermal environments and what are their main metabolisms?

The archaeal and bacterial community in these environments are dominated by S-cycling chemolithotrophic metabolisms. The archaeal communities at Kerlingarfjöll are dominated by methanogens and *Thermofilum* at genus level, where archaeal communities at Kverkfjöll are dominated by *Aciduliprofundum*. The archaeal communities seem to be more widespread across pools and sites than bacteria, since some taxa are found at both Kerlingarfjöll and Kverkfjöll regardless of temperature, pH and electron donors/acceptors. The bacterial communities at Kerlingarfjöll are dominated by *Sulfurihydrogenibium*, *Desulfurivibrio*, *Desulfocapsa, Hydrogenobacter* and

Thiobacillus. The main metabolisms of these organisms are sulfide oxidation and sulfur/sulfate reduction. The Kverkfjöll bacterial community is dominted by S*ulfobacillus, Syntrophus, Acidithiobacillus, Ferrimicrobium*, and *Acidiferrobacter*. The main metabolic pathways are Fe reduction/oxidation and sulfur oxidation. The composition of bacterial communities at Kerlingarfjöll and Kverkfjöll seem to be controlled by deep volcanic processes, as they control the pH that determines the main bacterial communities living in these environments.

Question 3: Can $\delta^{13}C$ and $\delta^{34}S$ biosignatures be preserved in hydrothermal environments?

C isotopes measured in organic carbon at Kerlingarfjöll and Kverkfjöll show relatively small fractionations from source CO_2, compared to the majority of biological CO_2 fixation pathways (<25 ‰). Values as low as -50 ‰ for abiotic organic compounds have been produced through laboratory synthesis, although only at high temperatures, of around 250 ^{o}C. Subsequently, low temperature hydrothermal environments become key for Mars exploration of $\delta^{13}C_{TOC}$, in order to differentiate between biotic or abiotic organic carbon produced in hydrothermal systems. Furthermore, these low temperature hydrothermal systems also evidence larger C isotopic fractionations. Small C isotopic fractionations are suggested to be produced as a result of hot temperatures favouring the TCA carbon pathway. Conversely, lower temperatures favour carbon pathways that produce larger or more variable C isotope fractionations (Havig et al., 2011).

S isotope fractionations between sulfate and sulfide in Kerlingarfjöll and Kverkfjöll pools are generally small compared to most S cycling environments. The small $\delta^{34}S$ values in Kverkfjöll are not discernible from abiotic volcanic $\delta^{34}S$ values reported in the literature. At Kerlingarfjöll, the $\delta^{34}S$ values measured would become a challenge in the detection of $\delta^{34}S$ biosignatures in hydrothermal environments. These small apparent S isotope values are primarily due to the prevalence of volcanic (abiotic) H_2S input and resulting $\delta^{34}S$ values over MSR and microbial $\delta^{34}S$ signatures in a hydrothermally active environment.

Question 4: Could a Mars analogue hypersaline spring be a better environment to find evidence of $\delta^{34}S$ biosignatures?

LH provides clear evidence for $\delta^{34}S$ and $\Delta^{33}S$ preserving biological- S cycling processes, and demonstrates how hydrothermal environments are more challenging for the detection of S isotope biosignatures. The LH hypersaline spring is a more suitable environment for the preservation of S isotope biosignatures than hydrothermal environments. This is inferred from the unique input of $\delta^{34}S$ from H_2S produced by MSR-MSD processes, hypersaline stress and limitation of electron donors and acceptors.

Question 5: Can $\Delta^{33}S$ help the evidence of life in the sediments?

As proven in Chapter 7, QSI helps to distinguish biotic from abiotic signatures at hydrothermal environments. Kerlingarfjöll pools QSI results demonstrate how $\Delta^{33}S$ values can record complex S cycling processes in KR-Bio and KR-P3 pools, even when $\delta^{34}S$ is not clearly distinct from volcanic values. The other Kerlingarfjöll and Kverkfjöll pools QSI values can be reproduced with a model, including an abiotic supply of volcanic H_2S. The QSI values from LH suggests MSR-MSD metabolisms, reproduced with a steady-state mass balance sulfur box model.

8.3 Impact on future Mars exploration

Overall, this work constitutes a solid foundation for using isotopic biosignatures to understand evidence of microbial metabolisms in Mars hydrothermal and hypersaline, systems. The different chapters build on data and methods from isotope and analogue work, and combine their use for applications to Mars future explorations.

8.3.1 Environmental targeting

Hydrothermal volcanic environments on Mars could have maintained locally-independent conditions, such as reduced waters and circum-neutral pH, at the time when lakes and other surface water bodies became oxidised towards the Noachian – Hesperian. This is caused by the dependence of hydrothermal systems on their immediate delivery of volcanic fluids and gases (CO_2, H_2S, H_2, etc), controlling the pH and redox conditions. The resulting hydrothermal mineralogical alteration assemblages observed are also controlled by the volcanic system at a small scale. The redox transitions observed in both volcanic systems investigated are important for the

preservation of organic molecules within the subsurface sediments (Eigenbrode et al., 2018). Furthermore, the unusual low temperatures in some of the hydrothermal environments are controlled by the mixing of low temperature meltwater (glacial and snowpack) with hydrothermal fluids. The larger $\delta^{13}C_{TOC}$ values observed in these lower-temperature systems make these volcano-ice interaction settings strong candidates for the detection of hydrothermally-hosted microbial communities on Mars. Evidence of these systems are found in the already mentioned Sysphi Montes and Arsia Mons. $\delta^{13}C_{TOC}$ values larger than the -24 ‰, would be needed in order to demonstrate biological processes on Mars. The most likely microorganisms to produce such fractionations are methanogens: $\delta^{13}C$ from 21 to 80 ‰, when using H_2 (Whiticar, 1999) and 21 to 35 ‰ with acetate (Valentine et al., 2004).

This work also illustrates the importance of pH on S isotope biosignatures, which can influence $\delta^{34}S$ fractionations during MSR, either directly or indirectly through its control on Fe availability. Dissolved Fe^{2+} on the Martian surface was controlled by pH and CO_2 fugacity (Tosca et al., 2008). This study suggested that Fe^{2+} limitation in such environment would only be possible with at a pH higher than 8 (Tosca et al., 2008). Then, if hydrothermal systems on Mars become part of future exploration plans and use S isotope as a biosignature tool, priority should be given to hydrothermal terrains with limited influx of volcanic H_2 and alkaline waters. Due to the low abundance of organics on the Martian surface, S cycling metabolisms would preferentially use H_2. It's only when H_2 is limited that S isotope fractionations become larger (Hoek et al., 2006). The pH in hydrothermal systems would be controlled by the immediate volcanic input rather than general surface processes.

Lastly, LH hypersaline spring material presents a better evidence of QSI biosignature preservation compared with hydrothermal systems. The search for QSI biosignatures on Mars should therefore be prioritised in hypersaline systems over hydrothermal systems. For example, Gale Crater presents an euxinic water column and circum-neutral pH within deeper parts of the lacustrine sequence (Grotzinger & Milliken, 2012). Likewise, Eridania Basin shows chlorine salt deposits on high elevations, and deep sea sediments typical of hydrothermal circulation (Michalski et al., 2017). Large S isotope fractionations from microbial sulfur cycling are typically linked with these

environments producing fractionations larger than 55 ‰ between sulfate and sulfide (Wenk et al., 2018).

On the other hand, hydrothermal sub-glacial systems could offer a S reservoir for MSR free of S-MIF atmospheric signal, that would make the MSR biosignature more clear. If S-cycling microorganisms were present on the Martian surface, they could be interacting with S-MIF signal S reservoirs or S-MIF free S reservoirs. On the first scenario the S-cycling by microorganisms on Mars' surface could mix these pools, diluting the atmospheric S-MIF signal (Farquhar et al., 2003). The second scenario would be MIF free reservoirs, such as inputs of volcanic sources having a near zero S isotope value reflecting mantle values and no MIF. Volcanic inputs could be delivered to hydrothermal systems, which could further avoid the interaction with S-MIF if they were subglacial. A handicap for this scenario is that hydrothermal systems would need specific chemical conditions, as pointed earlier, in order to preserve S isotope biosignatures (limited H_2, limited Fe^{2+}, etc). From these two scenarios, a clearer biosignature of biological sulfur cycling would be detected in the MIF-free systems.

8.3.2 Upcoming Mars exploration

Jezero crater and Oxia Plannum are the landing sites for two upcoming rover missions, NASA 2020 and ExoMars 2020, that will launch in 2020 to search for potential biosignatures. Jezero crater is an open lake basin acting as a catchment for two rivers that drained waters from the area of Nilli Fossae (Goudge et al., 2015). The rivers created fan deltas that delivered sedimentary materials, including hydrous minerals such as smectites clays that reveal several episodes of water activity on early Mars (Ehlmann et al., 2008; Goudge et al., 2015, 2017). These deltaic deposits are thought to be ideal for the sequestration and preservation of organic material (Ehlmann et al., 2008). The Jezero paleolake could be relevant as environment with limited electron donor/acceptor, for QSI biosignatures. C isotope biosignatures could be preserved in the organic material in the smectite clays within the deltaic fans. Little is known yet about the content of the groundwater that percolated also through the deltaic sediments (Lakdawalla, 2019), but that could have also influenced the potential microbial communities delivering different electron donors/acceptors, and changing the chemistry of these sediments. Jezero crater also presents chloride and sulfate deposits

(Ehlmann et al., 2008; Ehlmann & Mustard et al., 2012). The chlorides are associated to paleolake deposits, and the sulfate deposits indicate a transition towards low pH and highly oxidising conditions. The proposed origin for these acidic and oxidising conditions is a volcanic-hydrothermal scenario (Ehlmann & Mustard, 2012). If these settings are compared with the studied analogues here, only Kverkfjöll reassembles this conditions. As explained in Chapter 5, the environmental conditions at Kverkfjöll are not favourable for preservation of S isotope biosignatures, so perhaps for this specific deposits C isotopes could be a more appropriate biosignature tool.

The ExoMars 2020 mission will land on Oxia Planum, and is focused on Noachian materials in order to maximise the potential for the preservation of organic biosignatures from some of the earliest geological terrains on Mars (Quantin et al.,2015). Oxia Planum is a clay-dominated plain likewise located in a wide catchment basin. There is evidence of Noachian phyllosilicates and a fluvio-deltaic deposits (Quantin et al., 2015; Mandon et al., 2019). The phyllosilicate deposits suggest a neutral pH environment but, as seen in the work presented in Chapter 4, local pH-variability could have occurred. The ExoMars Rosalind Franklin rover will be able to drill up to 2m (De Sanctis et al., 2017), which will be an advantage for the discovery of subsurface microbial life. The availability to drill is particularly relevant where localised redox interfaces can exert a strong control on the preservation of biosignatures.

Finally, as exposed in this thesis, both hydrothermal and hypersaline environments present positive and negative sides as potential landing sites for the future. Neither is better than the other, they offer different conditions and one of the goals of this study has been to point the most appropriate tools for biosignature detection in each particular environment. The hydrothermal environments studied here present a range of electron donors and acceptors for life, which creates a diverse microbial community. Carbon isotopes from sedimentary organic carbon in these sites provide evidence of different metabolic carbon pathways when the temperatures in the hydrothermal pools are around 20 ^{o}C. On the contrary, δ^{34}S becomes challenging when was used as a biosignature tool by itself in these systems, but the use of QSI can help distinguish biotic from abiotic signatures at hydrothermal environments. Hydrothermal environments present the handicap of being difficult to detect due to being very localised, and as

observed in this study they present a large variation of mineralogy in a small scale. Many of the hydrothermal systems on Mars are shown to be covered by thick ice deposits, which could have sheltered any life through long periods of time from the harsh surface conditions that Mars experienced. In comparison, the hypersaline spring is a more extreme environment for life due to high salinity and low temperatures. These environmental conditions could narrow the diversity of microbial communities active in the hypersaline springs. At the same time, the hypersaline stress and limitation of electron donors and acceptors favours the presence of enzymes in the cell that causes larger S isotope fractionations to make the most of the limited energy available. S isotope biosignatures combined with QSI in the hypersaline spring studied here provided evidence of MSR-MSD microbial processes. On Mars, the surface exposure of hypersaline deposits could difficult the preservation of biosignatures.

8.4 Future work

In terms of progress from here and future work, several potential avenues of research can be identified. Future studies should focus on understanding the preservation of organics and biogenic pyrite captured inside sulfate salts at hypersaline springs, and how this gets preserved in the rock record. Specially, how the process of sulfurisation can aid the preservation of organic matter underlined by Eigenbrode et al., 2018, but also looking at biogenic pyrite. The study of relic hydrothermal environments and hypersaline springs preserved on Earth's rock record reassembling Mar's environments could provide valuable information. This study can help understand the preservation of C and QSI isotope biosignatures from these environments on a longer time-scale, and how post-depositional events (e.g. diagenesis) could modify or erase these biosignatures through time. It can also be expanded to other type of environments perhaps more relevant to current lander missions on Mars, such as relic deltaic sediments.

Based on the QSI results, there is a need to further explore the potential for this tool to detect life on Mars, but also on other exoplanets. On Mars, it is relevant to understand through modelling how microorganisms could have potentially interacted with Martian

atmospheric S-MIF, and how they would have processed the S-MIF signal. At the same time, research should be focused on detecting likely MIF-free deposits on Mars to perform QSI analyses in the future. Potential studies should be done on experimental work understanding the S isotope fractionations for natural hydrothermal environments using continuous culture experiments. In particular, understanding the preference of either H_2 or organic carbon for S-driven metabolisms could be key for Mars exploration. Hydrothermal environments have proven to be a challenging setting to differentiate abiotic from biotic biosignatures. Then, it can be then of special interest and not only relevant to Mars, to study and compare hydrothermal sites across the world with different conditions, to understand why, when and how do C isotope and QSI biosignatures are preserved. At the same time, the study of other hypersaline environments could also help understand the conditions and settings in which these environments become relevant for biosignature preservation and aid on targeting future landing sites.

Appendix A

Appendix A displays Archaea and Bacteria closest environmental isolate relatives and closest cultured species of the most predominant OTUs. Data from BLAST database.

Appendix A Table 1. Archaea predominant OTUs, selected BLAST database closest environmental isolate relatives and closest cultured species based on 16S rRNA similarity (%) with Kerlingarfjöll and Kverkfjöll samples.

OTU number and OTU name	Cultured relative (+ID number)	% of match	Uncultured relative (+ID number)	% of match
OTU_1 thermofilum sp. 1910b ;k__archaea;p__crenarchaeota;c__thermoprotei;o__thermoproteales;f__thermofilaceae;g__thermofilum;s__thermofilum sp.;superkingdom__archaea OUT_83 uncultured thermofilum sp. ;k__archaea;p__crenarchaeota;c__thermoprotei;o__thermoproteales;f__thermofilaceae;g__thermofilum;s__thermofilum sp.;superkingdom__archaea	Thermofilum adornatus 1505 chromosome, complete genome CP007493.1	84.66%	Uncultured archaeon clone msunder30 16S ribosomal RNA gene, partial sequence KX213924.1	98.43%
OTU_3 methanocella conradii hz254 ;k__archaea;p__euryarchaeota;c__methanomicrobia;o__methanocellales;f__methanocellaceae;g__methanocella;s__methanocella conradii;superkingdom__archaea	Methanocella conradii HZ254, complete genome CP003243.1	97.39%	Uncultured archaeon clone OPA-GC-16SrRNA-157 16S ribosomal RNA gene, partial sequence	98.24%

OTU_5 aciduliprofundum sp. mar08_339 ;k__archaea;p__euryarchaeota;c__euryarchaeota;o__euryarchaeota;f__euryarchaeota;g__aciduliprofundum;s__aciduliprofundum sp.;superkingdom__archaea	Aciduliprofundum sp. MAR08-339, complete genome CP003168.1	86.83%	Uncultured archaeon gene for 16S rRNA, partial sequence, clone: NasMA74 LC158428.1	98.29%
OTU_6 nc_008553.1 methanosaeta thermophila str. pt;k__archaea;p__euryarchaeota;c__methanomicrobia;o__methanosarcinales;f__methanosaetaceae;g__methanosaeta;s__methanosaeta thermophila;superkingdom__archaea	Methanosaeta thermophila partial 16S rRNA gene, type strain DSM 4774T, isolate Z-517 LN868388.1	98.89%	Uncultured archaeon clone 11H_P2 16S ribosomal RNA gene, partial sequence KC682096.1	99.69%
OTU_11 candidatus caldiarchaeum subterraneum ;k__archaea;p__thaumarchaeota;c__thaumarchaeota;o__thaumarchaeota;f__thaumarchaeota;g__candidatus caldiarchaeum;s__candidatus caldiarchaeum subterraneum;superkingdom__archaea	Candidatus Caldiarchaeum subterraneum DNA, fosmid clone: No.10-H-08 AB201309.1	83.41%	Uncultured archaeon clone msunder49 16S ribosomal RNA gene, partial sequence KX213943.1	98.52%

OTU_42 candidatus caldiarchaeum subterraneum ;k__archaea;p__thaumarchaeota;c__thaumarchaeota;o__ thaumarchaeota;f__thaumarchaeota;g__candidatus caldiarchaeum;s__candidatus caldiarchaeum subterraneum;superkingdom__archaea	Candidatus Caldiarchaeum subterraneum clone PNG_TBR_A55 16S ribosomal RNA gene, partial sequence JN881579.1	91.33%	Uncultured archaeon clone kuc012 16S ribosomal RNA gene, partial sequence HM150466.1	98.18%
OTU_184 unclutured candidatus nitrosocaldus sp. ;k__archaea;p__crenarchaeota;c__crenarchaeota;o__cren archaeota;f__crenarchaeota;g__candidatus nitrosocaldus;s__unclutured candidatus nitrosocaldus	Candidatus Nitrososphaera sp. N89-12 partial 16S rRNA gene, strain clone N89-12 LN827538.1	90.06%	Uncultured relative (+ID number) Uncultured archaeon clone Hverd014N 16S ribosomal RNA gene, partial sequence DQ441506.1	98.87%

Appendix A Table 2. Bacteria predominant OTUs, selected BLAST database closest environmental isolate relatives and closest cultured species based on 16S rRNA similarity (%) with Kerlingarfjöll and Kverkfjöll samples.

OTU number and OTU name	Cultured relative (+ID number)	% of match	Uncultured relative (+ID number)	% of match
OTU_3 sulfurihydrogenibium kristjanssonii ;k__bacteria;p__aquificae;c__aquificae;o__aquificales;f__hydrogenothermaceae;g__sulfurihydrogenibium;s__sulfurihydrogenibium kristjanssonii;superkingdom__bacteria	Sulfurihydrogenibium kristjanssonii strain I6628 16S ribosomal RNA, partial sequence NR_042660.1	99.79%	Uncultured Sulfurihydrogenibium sp. clone HV-6 16S ribosomal RNA gene, partial sequence GU233839.1	99.57%
OTU_5 desulfurivibrio sp. ames2 ;k__bacteria;p__proteobacteria;c__deltaproteobacteria;o__desulfobacterales;f__desulfobulbaceae;g__desulfurivibrio;s__desulfurivibrio sp.;superkingdom__bacteria;subphylum__delta/epsilon subdivisions	Desulfurivibrio alkaliphilus strain AHT 2 16S ribosomal RNA, partial sequence NR_074971.1	91.93%	Uncultured bacterium clone SEAA1AF041 16S ribosomal RNA gene, partial sequence KC432093.1	98.12%
OTU_8 acidiferrobacter sp. spiii_3 ;k__bacteria;p__proteobacteria;c__gammaproteobacteria;o__chromatiales;f__ectothiorhodospiraceae;g__acidiferrobacter;s__acidiferrobacter sp.;superkingdom__bacteria	Acidiferrobacter sp. SPIII_3 chromosome, complete genome CP027663.1	99.39%	Uncultured bacterium clone RT9-ant05-g12-S 16S ribosomal RNA gene, partial sequence JF737871.1	99.39%

OTU_10 uncultured sulfobacillus sp. ;k__bacteria;p__firmicutes;c__clostridia;o__clostridiales;f__clostridiales family xvii. incertae sedis;g__sulfobacillus;s__sulfobacillus spp.;superkingdom__bacteria	Sulfobacillus thermotolerans strain Kr1 chromosome, complete genome CP019454.1	98.21%	Uncultured bacterium clone RI_Dun_a11 16S ribosomal RNA gene, partial sequence EU376020.1	99.86%
OTU_13 uncultured desulfurivibrio sp. ;k__bacteria;p__proteobacteria;c__deltaproteobacteria;o__desulfobacterales;f__desulfobulbaceae;g__desulfurivibrio;s__desulfurivibrio spp.;superkingdom__bacteria;subphylum__delta/epsilon subdivisions	Desulfurivibrio alkaliphilus strain AHT 2 16S ribosomal RNA, partial sequence NR_074971.1	90.89%	Uncultured bacterium clone EMIRGE_OTU_s3t2d_674 16S ribosomal RNA gene, partial sequence JX222667.1	99.00%
OTU_14 uncultured desulfocapsa sp. ;k__bacteria;p__proteobacteria;c__deltaproteobacteria;o__desulfobacterales;f__desulfobulbaceae;g__desulfocapsa;s__desulfocapsa spp.;superkingdom__bacteria;subphylum__delta/epsilon subdivisions	Desulfocapsa thiozymogenes strain Bra2 16S ribosomal RNA, partial sequence NR_029306.1	95.97%	Uncultured bacterium clone UA_19 16S ribosomal RNA gene, partial sequence JX120389.1	99.47%

OTU_16 ef446268.1 prokaryotic and ecology floating macroscopic filaments extreme acidic river rio tinto (sw spain) floating macroscopic filaments acidic river clone placa4_g3 ;k__bacteria;p__nitrospirae;c__nitrospira;o__nitrospirales;f__nitrospiraceae;g__leptospirillum;s__leptospirillum ferrooxidans;superkingdom__bacteria;species group leptospirillum sp. group i	Leptospirillum ferrooxidans C2-3 DNA, complete genome AP012342.1	99.80%	Uncultured bacterium clone placa4_g3 16S ribosomal RNA gene, partial sequence EF446268.1	99.80%
OTU_19 dehalococcoides sp. bhi80_15 ;k__bacteria;p__chloroflexi;c__dehalococcoidia;o__dehalococcoidales;f__dehalococcoidaceae;g__dehalococcoides;s__dehalococcoides sp.;superkingdom__bacteria	Dehalococcoides sp. BHI80-15 16S rRNA gene, strain BHI80-15 AJ431246.1	87.20%	Uncultured bacterium clone HMTAb180 16S ribosomal RNA gene, partial sequence KM373100.1	98.76%
OTU_20 metallibacterium scheffleri ;k__bacteria;p__proteobacteria;c__gammaproteobacteria;o__xanthomonadales;f__xanthomonadaceae;g__metallibacterium;s__metallibacterium scheffleri;superkingdom__bacteria	Metallibacterium scheffleri strain DKE6 16S ribosomal RNA, partial sequence NR_118103.1	100.0%	Uncultured bacterium clone CEM_Eug_c3 16S ribosomal RNA gene, partial sequence EU370273.1	100.0%

OTU_36 uncultured acidithiobacillus sp. ;k__bacteria;p__proteobacteria;c__gammaproteobacteria;o__acidithiobacillales;f__acidithiobacillaceae;g__acidithiobacillus;s__acidithiobacillus spp.;superkingdom__bacteria	Acidithiobacillus ferrooxidans strain 3 16S ribosomal RNA gene, partial sequence DQ909078.1	98.78%	Uncultured bacterium clone RT9-ant04-c09-S 16S ribosomal RNA gene, partial sequence JF737865.1	99.12%
OTU_83 uncultured thiobacillus sp. ;k__bacteria;p__proteobacteria;c__betaproteobacteria;o__hydrogenophilales;f__hydrogenophilaceae;g__thiobacillus;s__thiobacillus spp.;superkingdom__bacteria	Thiobacillus sp. ML2-16 16S ribosomal RNA gene, partial sequence DQ145970.1	92.78%	Uncultured beta proteobacterium clone 6_40_10|23|Lib6 16S ribosomal RNA gene, partial sequence KJ650693.1	99.86%
OTU_21 hippea sp. lr3_dr ;k__bacteria;p__proteobacteria;c__deltaproteobacteria;o__desulfurellales;f__desulfurellaceae;g__hippea;s__hippea sp.;superkingdom__bacteria;subphylum__delta/epsilon subdivisions				

Appendix B

Appendix B presents the calculations used for model B in Chapter 7 and the results for f2 and f5 of the model.

Appendix B Figure 1. Steady-state open-system box model B modified from Johnston et al., (2005b), developed for Chapter 7.

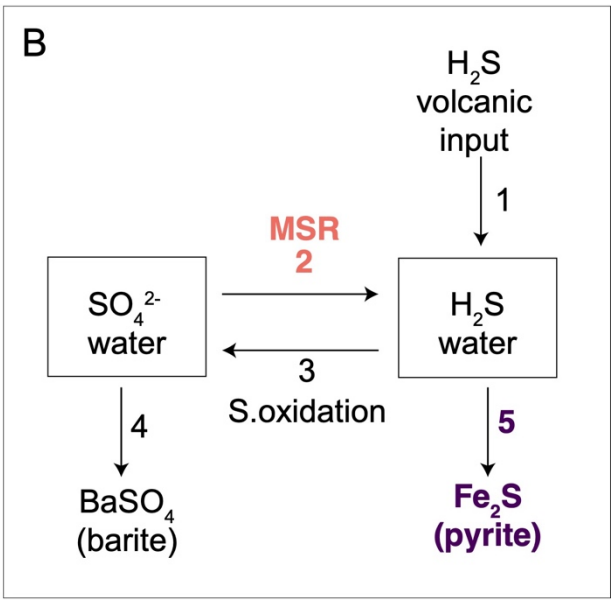

Derivation of equations that apply to model B

The algebraic solutions were derived here for a volcanic environment following the methods of Farquhar et al. (2007) and Zerke et al., (2009). The derivation of the equations are simplified here. Since this is a steady-state model, any flux entering the pool will equal the flux of sulfur leaving the pool. Each flux is defined as gamma (γ) here.

For it, γin = γout. Based on model B, γin are volcanic H_2S and MSR. Where γout are pyrite burial, sulfate mineral formation and S oxidation. Defining the different equations for γin and γout the system there are:

$\gamma 1 = \gamma 4 + \gamma 5$ (global equation) (1)

$\gamma 3 = \gamma 2 + \gamma 4$ (SO_4^{2-} box) (2)

$\gamma 1 + \gamma 2 = \gamma 3 + \gamma 5$ (H_2S box) (3)

The isotopic fractionations associated with the transfer (α) of a specific pathway can be described: $\gamma z = {}^{3X}RH_2S \cdot \alpha z$ or $\gamma z = {}^{3X}RSO_4 \cdot \alpha z$, depending on the box. ${}^{3X}R$ for the isotopic ratio, and z for the number of the pathway given on the box model B. Every pathway has also an associated flow of material leaving a pool (f), relative to the other flows leaving a pool along all possible ways. For example: $f2 = (1 - f4)$. For the ecosystem scale isotope mass balance model B, two sulfur reservoirs were considered, water column sulfate (WC SO_4^{2-}) and water column sulfide (WC H_2S).

Solving for Equation 2, $\gamma 3 = \gamma 2 + \gamma 4$ (SO_4^{2-} box):

$RH_2S \cdot \alpha 3 = RSO_4 \cdot \alpha 2 + RSO_4 \cdot \alpha 4$ (4)

$RH_2S \cdot \alpha 3 = RSO_4 \cdot (1 - f4) + RSO_4 \cdot (f4) \cdot \alpha 4$ (5)

$$\mathbf{RH_2S / RSO_4 = [(1 - f4) + (f4)\,\alpha 4)] / \alpha 3} \quad \mathbf{(6)}$$

Solving equation 1, $\gamma 1 = \gamma 4 + \gamma 5$ (global equation):

$RH_2Sin \cdot \alpha 1 = RSO_4 \cdot \alpha 4 + RH_2S \cdot \alpha 5$ (7)

$RH_2Sin \cdot \alpha 1 = RSO_4 \cdot f4 \cdot \alpha 4 + RH_2S \cdot (1 - f4) \cdot \alpha 5$ (8)

$$\mathbf{RH_2Sin / RH_2S = [(RSO_4 / RH_2S) \cdot (f4 \cdot \alpha 4) + (1 - f4) \cdot \alpha 5] / \cdot \alpha 1} \quad \mathbf{(9)}$$

Solving equation 3, $\gamma 1 + \gamma 2 = \gamma 3 + \gamma 5$ (H_2S box):

$RH_2Sin \cdot \alpha 1 + RSO_4 \cdot \alpha 2 = RH_2S \cdot \alpha 3 + RH_2S \cdot \alpha 5$ (10)

$RH_2Sin \cdot \alpha 1 + RSO_4 \cdot f2 \cdot \alpha 2 = RH_2S \cdot f3 \cdot \alpha 3 + RH_2S \cdot f5 \cdot \alpha 5$ (11)

$$\mathbf{RH_2Sin / RH_2S = [f3 \cdot \alpha 3 + (1 - f4) \cdot \alpha 5 - (RSO_4 / RH_2S) \cdot (1 - f4) \cdot \alpha 2] / \alpha 1} \quad \mathbf{(12)}$$

The equations used for the model are equation 6 and 9.

Appendix B Table 1 are the input parameters for the model for $^{34}RH_2Sin$ and $^{33}RH_2Sin$, calculated from $\delta^{34}S$ and $\delta^{33}S$ from average of literature Icelandic values (Gurnardson et al., 2017).

$^{34}RH_2Sin$	1.004
$^{33}RH_2Sin$	1.002
$\delta^{34}S$	3.63
$\delta^{33}S$	1.85

Appendix B Table 2 are the different fractionation factors for sulfate reduction and sulfur compound disproportionation based on literature experimental work from Johnston *et al.*, (2005), and Johnston, Farquhar and Canfield, (2007).

	Size	**Tested**			
		$^{34}\alpha$	$^{33}\alpha$	^{33}l	
1	medium	0.9773	0.9883	0.51255	Johnston et al., (2007)
2	small	0.9863	0.993	0.509225	Johnston et al., (2007)
3	large	0.954	0.9761	0.513685	Johnston et al., (2007)
4	**max**	**0.94088**	**0.9692**	**0.513365**	**Sim et al. (2011)**

Appendix B Table 3 presents the different input parameters used for the model. It can be seen how all the fractionation factors related to processes are kept constant, a part from MSR. MSR fractionation factor used for the model plotted on Figure 7-5 Chapter 7 are number 4, maximum fractionation factor known from Sim et al., (2011).

	For ^{34}R	**For ^{33}R**	**^{33}ln**
α1 (H_2S input)	1	1	
α2 MSR	0.94088	0.9692	0.513364928
α3 (Sox)	1	1	
α4 (barite)	1	1	
α5 (pyrite)	1	1	

The model was produced by varying fluxes for $f2$ (MSR flux) and $f5$ (pyrite burial flux) for a large fractionation factor (number 4 in table 2). Following are the results from the model, which produced resulting field for figure 7-5 at Chapter 7.

f2	f5	$\delta^{34}SH_2S$	$\Delta^{33}SH_2S$
1	0	-55.707271	0.07877498
1	0.1	-50.091412	0.10924543
1	0.2	-44.408356	0.13143426
1	0.3	-38.65689	0.14510865
1	0.4	-32.835772	0.15002931
1	0.5	-26.943728	0.14595027
1	0.6	-20.979455	0.13261869
1	0.7	-14.941615	0.10977461
1	0.8	-8.8288403	0.07715077
1	0.9	-2.639726	0.03447232
1	1	3.62716667	-0.0185434

f2	f5	$\delta^{34}SH_2S$	$\Delta^{33}SH_2S$
0.9	0	-49.773828	0.02737509
0.9	0.1	-44.690819	0.0551136
0.9	0.2	-39.553136	0.07614024
0.9	0.3	-34.359894	0.09028543
0.9	0.4	-29.110186	0.09737534
0.9	0.5	-23.803085	0.09723183
0.9	0.6	-18.437646	0.08967226
0.9	0.7	-13.012901	0.07450937
0.9	0.8	-7.5278616	0.0515512
0.9	0.9	-1.9815169	0.02060089
0.9	1	3.62716667	-0.0185434

f2	f5	$\delta^{34}SH_2S$	$\Delta^{33}SH_2S$
0.8	0	-43.840384	-0.0145385
0.8	0.1	-39.296641	0.01042278
0.8	0.2	-34.709508	0.03007814
0.8	0.3	-30.07836	0.04430854
0.8	0.4	-25.40256	0.05299236
0.8	0.5	-20.681459	0.05600525
0.8	0.6	-15.914396	0.05322012
0.8	0.7	-11.100697	0.04450704
0.8	0.8	-6.2396731	0.02973316
0.8	0.9	-1.3306237	0.00876264
0.8	1	3.62716667	-0.0185434

f2	f5	$\delta^{34}SH_2S$	$\Delta^{33}SH_2S$
0.7	0	-37.90694	-0.0470532
0.7	0.1	-33.908868	-0.0249238
0.7	0.2	-29.87743	-0.0068588
0.7	0.3	-25.812204	0.00706231
0.7	0.4	-21.712764	0.01675825
0.7	0.5	-17.578678	0.02214627
0.7	0.6	-13.409503	0.02314202
0.7	0.7	-9.2047918	0.01965947
0.7	0.8	-4.964087	0.01161095
0.7	0.9	-0.6869249	-0.001093
0.7	1	3.62716667	-0.0185434

f2	f5	$\delta^{34}SH_2S$	$\Delta^{33}SH_2S$
0.6	0	-31.973496	-0.0702549
0.6	0.1	-28.527489	-0.0510216
0.6	0.2	-25.05686	-0.0347756
0.6	0.3	-21.561343	-0.0215671
0.6	0.4	-18.040672	-0.011447
0.6	0.5	-14.494572	-0.0044671
0.6	0.6	-10.922768	-0.0006799
0.6	0.7	-7.3249783	-0.0001391
0.6	0.8	-3.7009194	-0.0028991
0.6	0.9	-0.0503021	-0.0090151
0.6	1	3.62716667	-0.0185434

f2	f5	$\delta^{34}SH_2S$	$\Delta^{33}SH_2S$
0.5	0	-26.040052	-0.0842281
0.5	0.1	-23.152491	-0.0679643
0.5	0.2	-20.247757	-0.0537759
0.5	0.3	-17.325697	-0.0416918
0.5	0.4	-14.386154	-0.0317414
0.5	0.5	-11.428973	-0.0239545
0.5	0.6	-8.4539924	-0.0183612
0.5	0.7	-5.4610525	-0.0149923
0.5	0.8	-2.4499897	-0.0138786
0.5	0.9	0.57936094	-0.0150517
0.5	1	3.62716667	-0.0185434

f2	f5	$\delta^{34}SH_2S$	$\Delta^{33}SH_2S$

0.4	0	-20.106609	-0.0890564
0.4	0.1	-17.783864	-0.0758446
0.4	0.2	-15.450081	-0.0639615
0.4	0.3	-13.105182	-0.0534219
0.4	0.4	-10.749086	-0.0442409
0.4	0.5	-8.381714	-0.0364335
0.4	0.6	-6.0029837	-0.0300151
0.4	0.7	-3.6128136	-0.0250011
0.4	0.8	-1.211121	-0.0214073
0.4	0.9	1.20217762	-0.0192494
0.4	1	3.62716667	-0.0185434

f2	f5	$\delta^{34}SH_2S$	$\Delta^{33}SH_2S$
0.3	0	-14.173165	-0.0848218
0.3	0.1	-12.421596	-0.0747535
0.3	0.2	-10.663791	-0.0654329
0.3	0.3	-8.8997184	-0.0568662
0.3	0.4	-7.1293432	-0.0490596
0.3	0.5	-5.3526319	-0.0420196
0.3	0.6	-3.5695505	-0.0357525
0.3	0.7	-1.7800646	-0.0302648
0.3	0.8	0.01586028	-0.025563
0.3	0.9	1.81825902	-0.0216537
0.3	1	3.62716667	-0.0185434

f2	f5	$\delta^{34}SH_2S$	$\Delta^{33}SH_2S$
0.2	0	-8.239721	-0.0716051
0.2	0.1	-7.0656754	-0.0647809
0.2	0.2	-5.8888469	-0.058289
0.2	0.3	-4.7092255	-0.0521313
0.2	0.4	-3.5268013	-0.0463097
0.2	0.5	-2.3415643	-0.0408261
0.2	0.6	-1.1535044	-0.0356823
0.2	0.7	0.03738851	-0.0308802
0.2	0.8	1.2311245	-0.0264218
0.2	0.9	2.42771381	-0.0223089
0.2	1	3.62716667	-0.0185434

f2	f5	$\delta^{34}SH_2S$	$\Delta^{33}SH_2S$
0.1	0	-2.3062771	-0.0494862

0.1	0.1	-1.7160917	-0.0460151
0.1	0.2	-1.1252076	-0.0426271
0.1	0.3	-0.5336236	-0.0393225
0.1	0.4	0.05866158	-0.0361015
0.1	0.5	0.65164913	-0.0329642
0.1	0.6	1.24534033	-0.029911
0.1	0.7	1.83973642	-0.0269421
0.1	0.8	2.43483867	-0.0240577
0.1	0.9	3.03064833	-0.0212581
0.1	1	3.62716667	-0.0185434

f2	f5	$\delta^{34}SH_2S$	$\Delta^{33}SH_2S$
0	0	3.62716667	-0.0185434
0	0.1	3.62716667	-0.0185434
0	0.2	3.62716667	-0.0185434
0	0.3	3.62716667	-0.0185434
0	0.4	3.62716667	-0.0185434
0	0.5	3.62716667	-0.0185434
0	0.6	3.62716667	-0.0185434
0	0.7	3.62716667	-0.0185434
0	0.8	3.62716667	-0.0185434
0	0.9	3.62716667	-0.0185434
0	1	3.62716667	-0.0185434

References

Abby, S. S., Melcher, M., Kerou, M., Krupovic, M., Stieglmeier, M., Rossel, C., et al. (2018). Candidatus Nitrosocaldus cavascurensis, an ammonia oxidizing, extremely thermophilic archaeon with a highly mobile genome. *Frontiers in Microbiology*, *9*, 28.

Abramov, O., & Kring, D.A. (2005), Impact-induced hydrothermal activity on early Mars. Journal of Geophysical Research: Planets. 1110 (E12).

Ackiss, S., Horgan, B., Seelos, F., Farrand, W., & Wray, J. (2018.) Mineralogic evidence for subglacial volcanism in the Sisyphi Montes region of Mars. *Icarus*, 311, 357–370. https://doi.org/10.1016/j.icarus.2018.03.026

Allender, E. J., Cousins, C. R., Gunn, M. D., & Caudill, C. M. (2020). Multiscale and multispectral characterization of mineralogy with the ExoMars 2020 rover remote sensing payload. *Earth and Space Science*. doi: 10.1029/2019EA000692

Amils, R., Gonzalez-Torila, E., Fernandez-Remolar, D., Gomeza, F., Aguilera, A., Rodriguez, N.,et al. (2007). Extreme environments as Mars terrestrial analogs: The Rio Tinto case. *Planetary and Space Science*, 55(3), 370–381. https://doi.org/10.1016/j.pss.2006.02.006

Anderson, I., Rodriguez, J., Susanti, D., Porat, I., Reich, C., Ulrich, L. E., .et al. (2008). Genome sequence of Thermofilum pendens reveals an exceptional loss of biosynthetic pathways without genome reduction. *Journal of Bacteriology*, *190*(8), 2957-2965.

Anderson, R. C., Dohm, J. M., Golombek, M. P., Haldemann, A. F., Franklin, B. J., Tanaka, K. L., et al. (2001). Primary centers and secondary concentrations of tectonic activity through time in the western hemisphere of Mars. *Journal of Geophysical Research: Planets*, *106*(E9), 20563-20585. https://doi.org/10.1029/2000JE001278

Andrews-Hanna, J.C., & Philips, R.J. (2007a). Hydrological modelling of outflow channels and chaos regions on Mars'. *Journal of Geophysical Research: Planets*. John Wiley & Sons, LTd, 112 (E8). doi: 10.1029/2006JE002881.

Andrews-Hanna, J. C., Phillips, R. J., & Zuber, M. T. (2007b). Meridiani Planum and the global hydrology of Mars. *Nature*. 446(7132), 163–166. doi: 10.1038/nature05594.

Anguita, F., Farelo, A. F., López, V., Mas, C., Muñoz-Espadas, M. J., Márquez, Á., & Ruiz, J. (2001). Tharsis dome, Mars: New evidence for Noachian-Hesperian thick-skin and Amazonian thin-skin tectonics. *Journal of Geophysical Research: Planets*, *106*(E4), 7577-7589.doi: 10.1029/2000JE001246.

Ármannsson, H. (2016). The fluid geochemistry of Icelandic high temperature geothermal areas. *Applied Geochemistry*, 66, 14-64. https://doi.org/10.1016/j.apgeochem.2015.10.008

Arnold, G. L., Brunner, B., Müller, I. A., & Røy, H. (2014). Modern applications for a total sulfur reduction distillation method-what's old is new again. *Geochemical transactions*, *15*(1), 4.

Arnórsson, S., & Andresdottir, A. (1995). Processes Controlling the Distribution of Boron and Chlorine in Natural-Waters in Iceland. *Geochimica Et Cosmochimica Acta*, 59(20), 4125–4146. https://doi.org/10.1016/0016-7037(95)00278-8

Arnórsson, S., Stefánsson, A., & Bjarnason, J.Ö. (2007). Fluid-Fluid Interactions in Geothermal Systems. *Reviews in Mineralogy and Geochemistry*, 65(1), 259-312. https://doi.org/10.2138/rmg.2007.65.9

Atreya, S. K., Mahaffy, P. R. & Wong, A. S. (2007). Methane and related trace species on Mars: Origin, loss, implications for life, and habitability. *Planetary and Space Science*. Pergamon, 55(3), 358–369. doi: 10.1016/j.pss.2006.02.005.

Aubrey, A., Cleaves, H. J., Chalmers, J. H., Skelley, A. M., Mathies, R. A., Grunthaner, F. J., et al. (2006). Sulfate minerals and organic compounds on Mars. *Geology*, *34*(5), 357-360.

Bhatnagar, S., Badger, J. H., Madupu, R., Khouri, H. M., O'Connor, E. M., Robb, F. T., et al. (2015). Genome sequence of a sulfate-reducing thermophilic bacterium, Thermodesulfobacterium commune DSM 2178T (phylum Thermodesulfobacteria). *Genome announcements*, *3*(1).

Baird, A. K., Toulmin, P., Clark, B. C., Rose, H. J., Keil, K., Christian, R. P., & Gooding, J. L. (1976). Mineralogic and petrologic implications of Viking geochemical results from Mars: Interim report. *Science*, 194 (4271), 1288-1293. doi: 10.1126/science.194.4271.1288.

Bak, F., & Pfenning, N. (1987). Chemolithotrophic growth of Desulfovibrio sulfodismutans sp. Nov. by disproportionation of inorganic sulfur compounds. *Arch. Microbiol.,* 147, 184-189.

Balta, J. B., & McSween, H. Y. (2013) Water and the composition of martian magmas. *Geology*, 41(10), 1115–1118. doi: 10.1130/G34714.1.

Bandfield, J. L. (2002). Global mineral distributions on Mars. *Journal of Geophysical Research E: Planets*. John Wiley & Sons, Ltd, 107(6), 9–1. doi: 10.1029/2001je001510.

Banfield, J. F., Moreau, J. W., Chan, C. S., Welch, S. A., & Little, B. (2001). Mineralogical biosignatures and the search for life on Mars. *Astrobiology*, *1*(4), 447-465.

Barns, S. M., Delwiche, C. F., Palmer, J. D., & Pace, N. R. (1996). Perspectives on archaeal diversity, thermophily and monophyly from environmental rRNA sequences. *Proceedings of the National Academy of Sciences*, 93(17), 9188-9193. doi: 10.1073/pnas.93.17.9188.

Battistuzzi, F. U., Feijao, A., & Hedges, S. B. (2004). A genomic timescale of prokaryote evolution: Insights into the origin of methanogenesis, phototrophy, and the colonization of land. *BMC Evolutionary Biology*. BioMed Central, 4(1), 1–14. doi: 10.1186/1471-2148-4-44.

Battler, M. M., Osinski, G. R., & Banerjee, N. R. (2013). Mineralogy of saline perennial cold springs on Axel Heiberg Island, Nunavut, Canada and implications for spring deposits on Mars. *Icarus*, 224(2), 364–381. doi: 10.1016/j.icarus.2012.08.031.

Benison, K.C., & Bowen, B.B. (2006). Acid saline lake systems give clues about past environments and the search for life on Mars. *Icarus*, 183(1), 225–229. https://doi.org/10.1016/j.icarus.2006.02.018

Berger, S., Welte, C., & Deppenmeier, U. (2012). Acetate activation in Methanosaeta thermophila: characterization of the key enzymes pyrophosphatase and acetyl-CoA synthetase. *Archaea*, *2012*.

Berner, R. A. (1984). Sedimentary pyrite formation: an update. *Geochimica et cosmochimica Acta*, *48*(4), 605-615.

Bibring, J. P., Langevin, Y., Gendrin, A., Gondet, B., Poulet, F., Berthé, M., ... & Drossart, P. (2005). Mars surface diversity as revealed by the OMEGA/Mars Express observations. *Science*, *307*(5715), 1576-1581.

Bibring, J. P., Langevin, Y., Mustard, J. F., Poulet, F., Arvidson, R., Gendrin, A., ... & Berthe, M. (2006). Global mineralogical and aqueous Mars history derived from OMEGA/Mars Express data. *science*, *312*(5772), 400-404.

Bigham, J.M., Schwertmann, U., Traina, S.J., Winland, R.L., & Wolff, M. (1996). Schwertmannite and the chemical modeling of iron in acid sulfate waters. *Geochimica et Cosmochimica Acta*, 60(12), 2111-2121. https://doi.org/10.1016/0016-7037(96)00091-9

Bishop, J. L., Loizeau, D., McKeown, N. K., Saper, L., Dyar, M. D., Des Marais, D. J.,et al. (2013). What the ancient phyllosilicates at Mawrth Vallis can tell us about possible habitability on early Mars. *Planetary and Space Science,* 86, 130-149.

Bishop, J.L. Fairen, A.G., Michalski, J.R., Gago-Duport, L., Baker, L.L., Velbel, M.A., et al. (2018). Surface clay formation during short-term warmer and wetter conditions on a largely cold ancient Mars. *Nature Astronomy*, 2(3), 206–213. http://dx.doi.org/10.1038/s41550-017-0377-9.

Björke, J.K. (2010). Fluid-rhyolite interaction in geothermal systems, Torfajökull Iceland - secondary surface mineralogy and fluid chemistry upon phase segregation and fluid mixing, MSc Thesis, Faculty of Earth Sciences, University of Iceland, Iceland.

Björke, J.K., Stefánsson, A., & Arnórsson, S. (2015). Surface water chemistry at Torfajökull, Iceland-Quantification of boiling, mixing, oxidation and water-rock interaction and reconstruction of reservoir fluid composition. *Geothermics*, 58,75–86. https://doi.org/10.1016/j.geothermics.2015.09.007

Björnsson, H. (2003). Subglacial lakes and jökulhlaups in Iceland. *Global and Planetary Change*, 35(3–4), 255–271. doi: 10.1016/S0921-8181(02)00130-3.

Björnsson, H., & Pálsson, F. (2008). Icelandic glaciers. *Jökull*, 58, 365–386.

Black, S. R. (2018). Identification and characterization of Martian acid-sulfate hydrothermal alteration : An investigation of instrumentation techniques and geochemical processes through laboratory experiments and terrestrial analog studies. PhD Thesis University of Colorado, Boulder, US.

Black, S.R., & Hynek, B.M. (2018). Characterization of terrestrial hydrothermal alteration products with Mars analog instrumentation: Implications for current and future rover investigations. *Icarus*, 307, 235–259. https://doi.org/10.1016/j.icarus.2017.10.032

Van Bodegom, P. M., Scholten, J. C., & Stams, A. J. (2004). Direct inhibition of methanogenesis by ferric iron. *FEMS Microbiology Ecology*, *49*(2), 261-268.

Borg, L. E., Nyquist, L. E., Wiesmann, H., Shih, C. Y., & Reese, Y. (2003). The age of Dar al Gani 476 and the differentiation history of the martian meteorites inferred from their radiogenic isotopic systematics. *Geochimica et Cosmochimica Acta*, 67(18), 3519-3536.

Boston, P. J., Ivanov, M. V. and P. McKay, C. (1992). On the possibility of chemosynthetic ecosystems in subsurface habitats on Mars. *Icarus*, 95(2), 300–308. doi: 10.1016/0019-1035(92)90045-9.

Böttcher, M. E., Thamdrup, B., & Vennemann, T. W. (2001). Oxygen and sulfur isotope fractionation during anaerobic bacterial disproportionation of elemental sulfur. *Geochimica et Cosmochimica Acta*, *65*(10), 1601-1609.

Bowen, B. B., Benison, K. C., Oboh-Ikuenobe, F. E., Story, S., & Mormile, M. R. (2008). Active hematite concretion formation in modern acid saline lake sediments, Lake Brown, Western Australia. *Earth and Planetary Science Letters*, 268(1-2), 52-63.

Bowles, M. W., Mogollón, J. M., Kasten, S., Zabel, M., & Hinrichs, K. U. (2014). Global rates of marine sulfate reduction and implications for sub–sea-floor metabolic activities. *Science*, *344*(6186), 889-891.

Bradley, A. S. (2008). Organic Geochemical Biosignatures in Alkaline Hydrothermal Ecosystems. PhD Thesis, Massachussetts Institute of Technology, US.

Bradley, A. S., Hayes, J. M., & Summons, R. E. (2009). Extraordinary $\delta^{13}C$ enrichment of diether lipids at the Lost City Hydrothermal Field indicates a carbon-limited ecosystem. *Geochimica et Cosmochimica Acta*, 73(1), 102–118. doi: 10.1016/j.gca.2008.10.005.

Bradley, A. S., Leavitt, W. D., Schmidt, M., Knoll, A. H., Girguis, P. R., & Johnston, D. T. (2016). Patterns of sulfur isotope fractionation during microbial sulfate reduction. *Geobiology*, *14*(1), 91-101.

Brain, D. A., & Jakosky, B. M. (1998). Atmospheric loss since the onset of the Martian geologic record: Combined role of impact erosion and sputtering. *Journal of Geophysical Research: Planets*, 103(E10), 22689–22694. doi: 10.1029/98JE02074.

Brandt, K. K., Vester, F., Jensen, A. N., & Ingvorsen, K. (2001). Sulfate reduction dynamics and enumeration of sulfate-reducing bacteria in hypersaline sediments of the Great Salt Lake (Utah, USA). *Microbial Ecology*, *41*(1), 1-11.

Bridges, J. C., Catling, D. C., Saxton, J. M., Swindle, T. D., Lyon, I. C., & Grady, M. M. (2001). Alteration assemblages in Martian meteorites: Implications for near-surface processes. *Space Science Reviews*, 96(1-4), 365-392.

Bristow, T.F., Rampe, E.B., Achilles, C.N., Blake, D.F., Chipera, S.J., Craig, P., et al. (2018). Clay mineral diversity and abundance in sedimentary rocks of Gale crater, Mars. *Science Advances*, 4(6), eaar3330. http://doi.org/10.1126/sciadv.aar3330

Brocks, J. J., Love, G. D., Summons, R. E., Knoll, A. H., Logan, G. A., & Bowden, S. A. (2005). Biomarker evidence for green and purple sulphur bacteria in a stratified Palaeoproterozoic sea. *Nature*, 437(7060), 866-870.

Brunner, B., & Bernasconi, S. M. (2005). A revised isotope fractionation model for dissimilatory sulfate reduction in sulfate reducing bacteria. *Geochimica et Cosmochimica Acta*, *69*(20), 4759-4771.

Burns, R. G., & Fisher, D. S. (1990). Evolution of sulfide mineralization on Mars. *Journal of Geophysical Research: Solid Earth*, *95*(B9), 14169-14173.

Cady, S. L., Farmer, J. D., Grotzinger, J. P., Schopf, J. W., & Steele, A. (2003). Morphological biosignatures and the search for life on Mars. *Astrobiology*, *3*(2), 351-368.

Canfield, D. E. (2001a). Biogeochemistry of Sulfur Isotopes. *Reviews in Mineralogy and Geochemistry*, 43(1), 607–636. doi: 10.2138/gsrmg.43.1.607.

Canfield, D. E. (2001b). Isotope fractionation by natural populations of sulfate-reducing bacteria. *Geochimica et Cosmochimica Acta*, *65*(7), 1117-1124.

Canfield, D. E., & Des Marais, D. J. (1991). Aerobic sulfate reduction in microbial mats. *Science*, *251*(5000), 1471-1473.

Canfield, D. E., Farquhar, J., & Zerkle, A. L. (2010). High isotope fractionations during sulfate reduction in a low-sulfate euxinic ocean analog. *Geology*, *38*(5), 415-418.

Canfield, D. E., Olesen, C. A., & Cox, R. P. (2006). Temperature and its control of isotope fractionation by a sulfate-reducing bacterium. *Geochimica et Cosmochimica Acta*, *70*(3), 548-561.

Canfield, D. E., Raiswell, R., Westrich, J. T., Reaves, C. M., & Berner, R. A. (1986). The use of chromium reduction in the analysis of reduced inorganic sulfur in sediments and shales. *Chemical Geology*, *54*(1-2), 149-155.

Canfield, D. E., & Teske, A. (1996). Late Proterozoic rise in atmospheric oxygen concentration inferred from phylogenetic and sulphur-isotope studies. *Nature*, *382*(6587), 127-132.

Canfield, D. E., & Thamdrup, B. (1994). The production of 34S-depleted sulfide during bacterial disproportionation of elemental sulfur. *Science,* 266(5193), 1973-1975.

Cassanelli, J. P. and Head, J. W. (2019). Glaciovolcanism in the Tharsis volcanic province of Mars: Implications for regional geology and hydrology. *Planetary and Space Science*, 169, 45–69. doi: 10.1016/j.pss.2019.02.006.

Carr, M. H. (2007). *The surface of Mars* (Vol. 6). Cambridge University Press.

Carr, M.H., & Head, J.W. (2010). Geologic history of Mars. *Earth and Planetary Science Letters*, 294(3–4), 185–203. https://doi.org/10.1016/j.epsl.2009.06.042

Chan, M. A., Beitler, B., Parry, W. T., Ormö, J., & Komatsu, G. (2004). A possible terrestrial analogue for haematite concretions on Mars. *Nature*, 429(6993), 731-734.

Chambers, L. A., Trudinger, P. A., Smith, J. W., & Burns, M. S. (1975). Fractionation of sulfur isotopes by continuous cultures of Desulfovibrio desulfuricans. *Canadian Journal of Microbiology*, *21*(10), 1602-1607.

Chemtob, S.M., Nickerson, R.D., Morris, R.V., Agresti, D.G., & Catalano, J.G. (2017). Oxidative Alteration of Ferrous Smectites and Implications for the Redox Evolution of Early Mars. *Journal of Geophysical Research: Planets*, 122(12), 2469–2488. https://doi.org/10.1002/2017JE005331

Cheng, D., & He, J. (2009). Isolation and characterization of "Dehalococcoides" sp. strain MB, which dechlorinates tetrachloroethene to trans-1, 2-dichloroethene. *Appl. Environ. Microbiol.*, *75*(18), 5910-5918.

Claypool, G. E., Holser, W. T., Kaplan, I. R., Sakai, H., & Zak, I. (1980). The age curves of sulfur and oxygen isotopes in marine sulfate and their mutual interpretation. *Chemical geology*, *28*, 199-260.

Cline, J. D. (1969). Spectrophotometric determination of hydrogen sulfide in natural waters 1. *Limnology and Oceanography*, *14*(3), 454-458.

Cockell, C. S., Bush, T., Bryce, C., Direito, S., Fox-Powell, M., Harrison, J. P., et al. (2016). Habitability: a review. *Astrobiology*, 16(1), 89-117.

Cockell, C.S., & Lee, P. (2002). The biology of impact craters - A review. *Biological Reviews of the Cambridge Philosophical Society*, 77(3), 279–310. https://doi.org/10.1017/S146479310100584X

Cochran, J. K., Kallenberg, K., Landman, N. H., Harries, P. J., Weinreb, D., Turekian, K. K., ... & Cobban, W. A. (2010). Effect of diagenesis on the Sr, O, and C isotope composition of late Cretaceous mollusks from the Western Interior Seaway of North America. *American Journal of Science*, *310*(2), 69-88.

Colangelo, J., Pelikan, C., Herbold, C., Altschuler, I., Loy, A., Whyte, L., & Wing, B. (2019). Diversity decoupled from sulfur isotope fractionation in a sulfate reducing microbial community. *bioRxiv*, 518837.

Colaprete, A. and Toon, O. B. (2003). Carbon dioxide clouds in an early dense Martian atmosphere. *Journal of Geophysical Research E: Planets*, 108(4), 6–1. doi: 10.1029/2002je001967.

Colman, D. R., Feyhl-Buska, J., Robinson, K. J., Fecteau, K. M., Xu, H., Shock, E. L., & Boyd, E. S. (2016). Ecological differentiation in planktonic and sediment-associated chemotrophic microbial populations in Yellowstone hot springs. *FEMS microbiology ecology*, 92(9).

Colman, D. R., Lindsay, M. R., Amenabar, M. J., & Boyd, E. S. (2019). The intersection of geology, geochemistry, and microbiology in continental hydrothermal systems. *Astrobiology*, 19(12), 1505-1522.

Conner, A.J., & Benison, K.C. (2013). Acidophilic halophilic microorganisms in fluid inclusions in halite from Lake Magic, Western Australia. *Astrobiology,* 13(9), 850–60. https://doi.org/10.1089/ast.2012.0956

Connerney, J. E. P., Acuña, M. H., Ness, N. F., Kletetschka, G., Mitchell, D. L., Lin, R. P., & Reme, H. (2005). Tectonic implications of Mars crustal magnetism. *Proceedings of the National Academy of Sciences*, 102(42), 14970-14975.

Coram, N. J., & Rawlings, D. E. (2002). Molecular relationship between two groups of the genus Leptospirillum and the finding that Leptospirillum ferriphilum sp. nov.

dominates South African commercial biooxidation tanks that operate at 40 C. *Applied Environmental Microbiology, 68*(2), 838-845.

Coupland, K., & Johnson, D. B. (2008). Evidence that the potential for dissimilatory ferric iron reduction is widespread among acidophilic heterotrophic bacteria. *FEMS microbiology letters*, *279*(1), 30-35.

Cousins, C.R. (2015). Volcanogenic Fluvial-Lacustrine Environments in Iceland and Their Utility for Identifying Past Habitability on Mars. *Life*, 5, 568–586. https://doi.org/10.3390/life5010568

Cousins, C.R. & Crawford, I.A. (2011). Volcano-Ice Interaction as a Microbial Habitat on Earth and Mars. *Astrobiology*, 11(7), 695–710. https://doi.org/10.1089/ast.2010.0550

Cousins, C.R., Crawford, I.A., Carrivick, J.L., Gunn, M., Harris, J., Kee, T.P., Karlsson, M., et al. (2013). Glaciovolcanic hydrothermal environments in Iceland and implications for their detection on Mars. *Journal of Volcanology and Geothermal Research*, 256, 61–77. https://doi.org/10.1016/j.jvolgeores.2013.02.009

Cousins, C.R., Fogel, M., Bowden, R., Crawford, I., Boyce, A., Cockell, C., & Gunn. M. (2018). Biogeochemical probing of microbial communities in a basalt-hosted hot spring at Kverkfjöll volcano, Iceland. *Geobiology*, 16(5), 507–521. https://doi.org/10.1016/j.icarus.2018.03.026

Cousins, C. R., Mikhail, S., Foucher, F., Stelle, A., & Westall, F. (2020). Metamorphic evolution of carbonate-hosted microbial biosignatures. *Geochemical Perspectives Letters*., 12, 40–45.

Cousins, C. R., Smellie, J. L., Jones, A. P., & Crawford, I. A. (2009). A comparative study of endolithic microborings in basaltic lavas from a transitional subglacial–marine environment. *International Journal of Astrobiology*, *8*(1), 37-49.

Craddock, R. A., & Howard, A. D. (2002). The case for rainfall on a warm, wet early Mars. *Journal of Geophysical Research: Planets*, 107(E11), 21-1-21–36. doi: 10.1029/2001JE001505.

Crowley, J.K., Williams, D.E., Hammarstrom, J.M., Piatak, N., Chou, I-ming, C., & Mars, J.C. (2003). Fe-hydroxide , and Fe-sulphate-hydrate minerals associated with sulphide-bearing mine wastes. *Geological Society of London*, 3, 219–228. https://doi.org/10.1144/1467-7873/03-001

Cypionka, H. (1995). Solute transport and cell energetics. In *Sulfate-reducing bacteria* (pp. 151-184). Springer, Boston, MA.

Dahl, C., & Trüper, H. G. (1994). Enzymes of dissimilatory sulfide oxidation in phototrophic sulfur bacteria. *Methods in Enzymology*. Academic Press, 243(C), 400–421. doi: 10.1016/0076-6879(94)43030-6.

Defouilloy, C., Cartigny, P., Assayag, N., Moynier, F., & Barrat, J. A. (2016). High-precision sulfur isotope composition of enstatite meteorites and implications of the formation and evolution of their parent bodies. *Geochimica et Cosmochimica Acta*, *172*, 393-409.

Dehouck, E., Gaudin, A., Chevrier, V., & Mangold, N. (2016). Mineralogical record of the redox conditions on early Mars. *Icarus*, 271, 67–75. https://doi.org/10.1016/j.icarus.2016.01.030

Detmers, J. (2001). Diversity of Sulfur Isotope Fractionations by Sulfate-Reducing Prokaryotes. *Applied and Environmental Microbiology*, 67(2), 888–894. doi: 10.1128/AEM.67.2.888.

DeLong, E. F. (1992). Archaea in coastal marine environments. *Proceedings of the National Academy of Sciences*, *89*(12), 5685-5689.

Djokic, T., Van Kranendonk, M. J., Campbell, K. A., Walter, M. R., & Ward, C. R. (2017). Earliest signs of life on land preserved in ca. 3.5 Ga hot spring deposits. *Nature communications*, *8*(1), 1-9.

Direito, S. O., Marees, A., & Röling, W. F. (2012). Sensitive life detection strategies for low-biomass environments: optimizing extraction of nucleic acids adsorbing to terrestrial and Mars analogue minerals. *FEMS microbiology ecology*, *81*(1), 111-123.

Dong, Y., Sanford, R. A., Inskeep, W. P., Srivastava, V., Bulone, V., Fields, C. J., et al. (2019). Physiology, Metabolism, and Fossilization of Hot-Spring Filamentous Microbial Mats. *Astrobiology*, *19*(12), 1442-1458.

Dridi, B., Fardeau, M. L., Ollivier, B., Raoult, D., & Drancourt, M. (2012). Methanomassiliicoccus luminyensis gen. nov., sp. nov., a methanogenic archaeon isolated from human faeces. *International journal of systematic and evolutionary microbiology*, *62*(8), 1902-1907.

Edwards, C. S., & Ehlmann, B. L. (2015). Carbon sequestration on Mars, *Geology*, 43(10), 863–866. doi: 10.1130/G36983.1.

Dodd, M. S., Papineau, D., Grenne, T., Slack, J. F., Rittner, M., Pirajno, F., et al. (2017). Evidence for early life in Earth's oldest hydrothermal vent precipitates. *Nature*, *543*(7643), 60-64.

Dominova, I. N., Kublanov, I. V., Podosokorskaya, O. A., Derbikova, K. S., Patrushev, M. V., & Toshchakov, S. V. (2013). Complete genomic sequence of "Thermofilum adornatus" strain 1910bT, a hyperthermophilic anaerobic organotrophic crenarchaeon. *Genome Announc.*, *1*(5), e00726-13.

Druschel, G. K., Baker, B. J., Gihring, T. M., & Banfield, J. F. (2004). Acid mine drainage biogeochemistry at Iron Mountain, California. *Geochemical Transactions*, *5*(2), 13.

Ehlmann, B.L., Bish, D.L., Ruff, S.W., & Mustard, J.F. (2012). Mineralogy and chemistry of altered Icelandic basalts: Application to clay mineral detection and understanding aqueous environments on Mars. *Journal of Geophysical Research E: Planets,* 117(10), 1-27. https://doi.org/10.1029/2012JE004156

Ehlmann, B.L., & Edwards, C.S. (2014). Mineralogy of the Martian Surface. *The Annual Review of Earth and Planetary Sciences*, 42, 291–315. https://doi.org/10.1146/annurev-earth-060313-055024

Ehlmann, B. L., Mustard, J. F., Fassett, C. I., Schon, S. C., Head III, J. W., Des Marais, D. J., et al. (2008a). Clay minerals in delta deposits and organic preservation potential on Mars. *Nature Geoscience*, *1*(6), 355-358.

Ehlmann, B.L., Mustard, J.F., & Murchie, S.L. (2010). Geologic setting of serpentine deposits on Mars. *Geophysical Research Letters*, 37(6), 1–5. https://doi.org/10.1029/2010GL042596

Ehlmann, B.L., Mustard, J.F., Murchie, S.L, Bribing, J.P, Meunier A., Fraeman, A., & Langevin, Y. (2011). Subsurface water and clay mineral formation during the early history of Mars. *Nature*, 479, 53- 60. https://doi.org/10.1038/nature10582

Ehlmann, B. L., Mustard, J. F., Murchie, S. L., Poulet, F., Bishop, J. L., Brown, A. J. et al., (2008b). Orbital identification of carbonate-bearing rocks on Mars. *Science*, 322(5909), 1828-1832.

Ehlmann, B.L., Mustard, J.F., Swayze, G.A., Clark, R,N., Bishop, J.L., Poulet, F., & Des Marais, D. (2009). Identification of hydrated silicate minerals on Mars using MRO-CRISM: Geologic context near Nili Fossae and implications for aqueous alteration. *Journal of Geophysical Research E: Planets*, 114(10), 1–33. https://doi.org/10.1029/2009JE003339

Ehlmann, B. L., Swayze, G. A., Milliken, R. E., Mustard, J. F., Clark, R. N., Murchie, S. L., et al. (2016). Discovery of alunite in Cross crater, Terra Sirenum, Mars: Evidence for acidic, sulfurous waters. *American Mineralogist*, *101*(7), 1527-1542.

Eichorst, S. A., Trojan, D., Roux, S., Herbold, C., Rattei, T., & Woebken, D. (2018). Genomic insights into the Acidobacteria reveal strategies for their success in terrestrial environments. *Environmental microbiology*, *20*(3), 1041-1063.

Eigenbrode, J.L., Summons, R.E., Steele, A., Freissinet, C., Millan, M., Navarro-Gonzalez, R., et al. (2018). Organic matter preserved in 3-billion-year-old mudstones at Gale crater, Mars. *Science*, 360(6393), 1096–1101. https://doi.org/10.1126/science.aas9185

Etiope, G., Oehler, D. Z. & Allen, C. C. (2011). Methane emissions from Earths degassing: Implications for Mars. *Planetary and Space Science*, 59(2–3), 182–195. doi: 10.1016/j.pss.2010.06.003.

Fagents, S. A., & Thordarson, T. (2007). Rootless volcanic cones in Iceland and on Mars. *The geology of Mars: evidence from earth-based analogs. Cambridge University Press, Cambridge*, 151-177.

Fairén, A.G. (2010). A cold and wet Mars. *Icarus*, 208(1), 165–175. https://doi.org/10.1016/j.icarus.2010.01.006

Farmer, J. D. (1996, January). Hydrothermal systems on Mars: an assessment of present evidence. In *Ciba Foundation Symposium* (pp. 273-294). JOHN WILEY & SONS LTD.

Farmer, J. D., & Des Marais, D. J. (1999). Exploring for a record of ancient Martian life. *Journal of Geophysical Research: Planets*, *104*(E11), 26977-26995.

Farquhar, J., Bao, H., & Thiemens, M. (2000a). Atmospheric influence of Earth's earliest sulfur cycle. *Science*, 289(5480), 756-758.

Farquhar, J., Canfield, D. E., Masterson, A., Bao, H., & Johnston, D. (2008). Sulfur and oxygen isotope study of sulfate reduction in experiments with natural populations from Faellestrand, Denmark. *Geochimica et Cosmochimica Acta*, *72*(12), 2805-2821.

Farquhar, J., Johnston, D. T. and Wing, B. A. (2007). Implications of conservation of mass effects on mass-dependent isotope fractionations: Influence of network structure on sulfur isotope phase space of dissimilatory sulfate reduction. *Geochimica et Cosmochimica Acta*, 71(24), 5862–5875. doi: 10.1016/j.gca.2007.08.028.

Farquhar, J., Johnston, D. T., Wing, B. A., Habicht, K. S., Canfield, D. E., Airieau, S., & Thiemens, M. H. (2003). Multiple sulphur isotopic interpretations of biosynthetic pathways: implications for biological signatures in the sulphur isotope record. *Geobiology*, *1*(1), 27-36.

Farquhar, J., Savarino, J., Jackson, T. L., & Thiemens, M. H. (2000b). Evidence of atmospheric sulphur in the martian regolith from sulphur isotopes in meteorites. *Nature*, 404(6773), 50-52.

Farquhar, J. & Wing, B. A. (2003). Multiple sulfur isotopes and the evolution of the atmosphere. *Earth and Planetary Science Letters*. Elsevier B.V., 213(1–2), 1–13. doi: 10.1016/S0012-821X(03)00296-6.

Fassett, C. I., Dickson, J. L., Head, J. W., Levy, J. S., & Marchant, D. R. (2010). Supraglacial and proglacial valleys on Amazonian Mars. *Icarus*, 208(1), 86-100.

Fassett, C. I., & Head III, J. W. (2005). Fluvial sedimentary deposits on Mars: Ancient deltas in a crater lake in the Nili Fossae region. *Geophysical Research Letters,* 32(14).

Fassett, C. I., & Head, J. W. (2008). Valley network-fed, open-basin lakes on Mars: Distribution and implications for Noachian surface and subsurface hydrology. *Icarus*, 198(1), 37–56. doi: 10.1016/j.icarus.2008.06.016.

Fernández-Remolar, D., Gomez-Elvira, J., Gomez, F., Sebastian, E., Martiin, J., Manfredi, J.A., et al. (2005). The Río Tinto Basin, Spain: Mineralogy, sedimentary geobiology, and implications for interpretation of outcrop rocks at Meridiani Planum, Mars. *Earth and Planetary Science Letters*, 240(1), 149–167. https://doi.org/10.1016/j.epsl.2005.09.043

Fike, D. A., Finke, N., Zha, J., Blake, G., Hoehler, T. M., & Orphan, V. J. (2009). The effect of sulfate concentration on (sub) millimeter-scale sulfide δ34S in hypersaline cyanobacterial mats over the diurnal cycle. *Geochimica et Cosmochimica Acta*, *73*(20), 6187-6204.

Fike, D. A. & Grotzinger, J. P. (2008). A paired sulfate – pyrite d 34 S approach to understanding the evolution of the Ediacaran – Cambrian sulfur cycle. 72, 2636–2648. doi: 10.1016/j.gca.2008.03.021.

Finster, K. W., Kjeldsen, K. U., Kube, M., Reinhardt, R., Mussmann, M., Amann, R., & Schreiber, L. (2013). Complete genome sequence of Desulfocapsa sulfexigens, a marine deltaproteobacterium specialized in disproportionating inorganic sulfur compounds. *Standards in genomic sciences*, *8*(1), 58.

Fischer, W. W., Fike, D. A., Johnson, J. E., Raub, T. D., Guan, Y., Kirschvink, J. L., & Eiler, J. M. (2014). SQUID–SIMS is a useful approach to uncover primary signals in the Archean sulfur cycle. *Proceedings of the National Academy of Sciences*, *111*(15), 5468-5473.

Fisk, M. R., & Giovannoni, S. J. (1999). Sources of nutrients and energy for a deep biosphere on Mars. *Journal of Geophysical Research,* 104(E5), 11805–11815. doi: 10.1029/1999JE900010.

Flores, G. E., Liu, Y., Ferrera, I., Beveridge, T. J., & Reysenbach, A. L. (2008). Sulfurihydrogenibium kristjanssonii sp. nov., a hydrogen-and sulfur-oxidizing thermophile isolated from a terrestrial Icelandic hot spring. *International journal of systematic and evolutionary microbiology*, *58*(5), 1153-1158.

Flude, S., McGarvie D.W., Burgess, R., & Tindle, A.G. (2010). Rhyolites at Kerlingarfjöll , Iceland : the evolution and lifespan of silicic central volcanoes. *Bulleting of Volcanology*, 72 (5), 523–538. https://doi.org/10.1007/s00445-010-0344-0

Forget, F.& Pierrehumbert, R. T. (1997). Warming early Mars with carbon dioxide clouds that scatter infrared radiation. *Science*, 278(5341), 1273–1276. doi: 10.1126/science.278.5341.1273.

Forget, F., Wordsworth, R., Millour, E., Madeleine, J. B., Kerber, L., Leconte, J., et al. (2013). 3D modelling of the early martian climate under a denser CO_2 atmosphere: Temperatures and CO_2 ice clouds. *Icarus*, 222(1), 81-99.

Forrest, J., & Newman, L. (1977). Silver-110 microgram sulfate analysis for the short time resolution of ambient levels of sulfur aerosol. *Analytical Chemistry*, *49*(11), 1579-1584.

Foster, I. S., King, P. L., Hyde, B. C., & Southam, G. (2010). Characterization of halophiles in natural MgSO4 salts and laboratory enrichment samples: astrobiological implications for Mars. *Planetary and Space Science*, *58*(4), 599-615.

Fox-Powell, M. G., Osinski, G. R., Applin, D., Stromberg, J. M., Gázquez, F., Cloutis, E., et al. (2019). Natural analogue constraints on Europa's non-ice surface material. *Geophysical Research Letters*, 46(11), 5759-5767.

Franz, H. B., Kim, S. T., Farquhar, J., Day, J. M., Economos, R. C., McKeegan, K. D., et al. (2014). Isotopic links between atmospheric chemistry and the deep sulphur cycle on Mars. *Nature*, *508*(7496), 364-368.

Franz, H. B., King, P. L., & Gaillard, F. (2019a). Sulfur on Mars from the atmosphere to the core. In *Volatiles in the Martian crust* (pp. 119-183). Elsevier.

Franz, H.B., Mc Adam, A.C., Ming, D.W., Freissinet, C., Mahaffy, P.R., Eldridge, D.L., et al. (2017). Large sulfur isotope fractionations in Martian sediments at Gale crater. *Nature Geoscience*, 10(9), 658–662. https://doi.org/10.1038/ngeo3002

Franz, H. B., Wu, N., Farquhar, J., & Irving, A. J. (2019b). A new type of isotopic anomaly in shergottite sulfides. *Meteoritics & Planetary Science*, *54*(12), 3036-3051.

Frederiksen, T. M. & Finster, K. (2003). Sulfite-oxido-reductase is involved in the oxidation of sulfite in Desulfocapsa sulfoexigens during disproportionation of thiosulfate and elemental sulfur. *Biodegradation*, 189–198. doi: 10.1023/A:1024255830925.

Freissinet, C., Glavin, D. P., Mahaffy, P. R., Miller, K. E., Eigenbrode, J. L., Summons, R. E., et al. (2015). Organic molecules in the sheepbed mudstone, gale crater, mars. *Journal of Geophysical Research: Planets*, *120*(3), 495-514.

Friedrich, C. G., Rother, D., Bardischewsky, F., Quentmeier, A., & Fischer, J. (2001). Oxidation of reduced inorganic sulfur compounds by bacteria: emergence of a common mechanism?. *Appl. Environ. Microbiol.*, 67(7), 2873-2882.

Friedrich, C. G., Bardischewsky, F., Rother, D., Quentmeier, A., & Fischer, J. (2005). Prokaryotic sulfur oxidation. *Current opinion in microbiology*, *8*(3), 253-259.

Friedrich, M. W. (2002). Phylogenetic analysis reveals multiple lateral transfers of adenosine-5′-phosphosulfate reductase genes among sulfate-reducing microorganisms. *Journal of bacteriology*, *184*(1), 278-289.

Fry, B., Gest, H., & Hayes, J. M. (1984). Isotope effects associated with the anaerobic oxidation of sulfite and thiosulfate by the photosynthetic bacterium, Chromatium vinosum. *FEMS microbiology letters*, *27*(2), 227-232.

Fry, B., Ruf, W., Gest, H., & Hayes, J. M. (1988). Sulfur isotope effects associated with oxidation of sulfide by O2 in aqueous solution. *Chemical Geology: Isotope Geoscience section*, *73*(3), 205-210.

Gaidos, E., Marteinsson, V., Thorsteinsson, T., Johannesson, T., Rúnarsson, Á. R., Stefansson, A., et al. (2009). An oligarchic microbial assemblage in the anoxic bottom waters of a volcanic subglacial lake. *The ISME journal*, *3*(4), 486-497.

Gaillard, F., Michalski, J., Berger, G., McLennan, S. M., & Scaillet, B. (2013). Geochemical reservoirs and timing of sulfur cycling on Mars. *Space Science Reviews*, *174*(1-4), 251-300.

Gendrin, A., Mangold, N., Bibring, J. P., Langevin, Y., Gondet, B., Poulet, F., et al. (2005). Sulfates in Martian layered terrains: the OMEGA/Mars Express view. *Science*, *307*(5715), 1587-1591.

Ghosh, W. & Dam, B. (2009).Biochemistry and molecular biology of lithotrophic sulfur oxidation by taxonomically and ecologically diverse bacteria and archaea. *FEMS Microbiology Reviews*, 999–1043. doi: 10.1111/j.1574-6976.2009.00187.x.

Giggenbach, W.F., & Stewart, M.K. (1982). Processes controlling the isotopic composition of steam and water discharges from steam vents and steam-heated pools in geothermal areas. *Geothermics*, 11(2),71–80. https://doi.org/10.1016/0375-6505(82)90009-8

Golden, D. C., Ming, D. W., Morris, R. V., & Graff, T. G. (2008). Hydrothermal synthesis of hematite spherules and jarosite: Implications for diagenesis and hematite spherule formation in sulfate outcrops at Meridiani Planum, Mars. *American Mineralogist*, *93*(8-9), 1201-1214.

Goudge, T. A., Milliken, R. E., Head, J. W., Mustard, J. F., & Fassett, C. I. (2017). Sedimentological evidence for a deltaic origin of the western fan deposit in Jezero crater, Mars and implications for future exploration. *Earth and Planetary Science Letters*, *458*, 357-365.

Goudge, T. A., Mustard, J. F., Head, J. W., Fassett, C. I., & Wiseman, S. M. (2015). Assessing the mineralogy of the watershed and fan deposits of the Jezero crater paleolake system, Mars. *Journal of Geophysical Research: Planets*, *120*(4), 775-808.

Grady, M. M., Verchovsky, A. B., & Wright, I. P. (2004). Magmatic carbon in Martian meteorites: attempts to constrain the carbon cycle on Mars. *International Journal of Astrobiology*, *3*(2), 117-124.

Grady, M. M., & Wright, I. (2006). The carbon cycle on early Earth—and on Mars?. *Philosophical Transactions of the Royal Society B: Biological Sciences*, *361*(1474), 1703-1713.

Grönvold, K. (1972). Structural and petrochemical studies in the Kerlingarfjöll region, central Iceland. Ph.D. Thesis, University of Oxford, UK.

Grotzinger, J. P., Crisp, J., Vasavada, A. R., Anderson, R. C., Baker, C. J., Barry, R., et al. (2012a). Mars Science Laboratory mission and science investigation. *Space science reviews*, *170*(1-4), 5-56.

Grotzinger, J. P., & Milliken, R. E. (2012b). The sedimentary rock record of Mars: Distribution, origins, and global stratigraphy. *Sedimentary Geology of Mars*, *102*, 1-48.

Grotzinger, J.P., Sumner, D.Y., Kah, L.C., Stack, K., Gupta, S., Edgar, L., et al. (2014). A Habitable Fluvio-Lacustrine Environment at Yellowknife Bay, Gale Crater, Mars. *Science*, 343(6169), 1242777-1- 1242777-7. https://doi.org/10.1126/science.1242777

Gudmundsson, A. (2000). Dynamics of Volcanic Systems in Iceland: Example of Tectonism and Volcanism at Juxtaposed Hot Spot and Mid-Ocean Ridge Systems. *Annual Review of Earth and Planetary Sciences*, 107–140. doi: 10.1146/annurev.earth.28.1.107.

Gudmundsson, M.T. Sigmundsson, F., Björnsson, H., & Högnadóttir, T. (2004). The 1996 eruption ay Gjálp, Vatnajökull ice cap, Iceland: Efficiency of heat transfer, ice deformation and subglacial water pressure. *Bulletin of Volcanology*, 66, 46-65. https://doi.org/10.1007/s00445-003-0295-9

Gulick, V. C. (1998). Magmatic intrusions and a hydrothermal origin for fluvial valleys on Mars. *Journal of Geophysical Research: Planets*, 103(E8), 19365–19387. doi: 10.1029/98JE01321.

Gunnarsson-Robin, J., Stefánsson, A., Ono, S., & Torssander, P. (2017). Sulfur isotopes in Icelandic thermal fluids. *Journal of Volcanology and Geothermal Research*, *346*, 161-179.

Gupta, S., & Horgan, B. (2018). Mars 2020 Science Team Assessment of Jezero crater. Presented in Mars 2020 4th Landing Site Workshop.

Gysi, A.P., & Stefánsson, A. (2012). CO2-water-basalt interaction. Low temperature experiments and implications for CO2sequestration into basalts. *Geochimica et Cosmochimica Acta*, 81, 129–152. https://doi.org/10.1016/j.gca.2011.12.012

Gyure, R. A., Konopka, A., Brooks, A., & Doemel, W. (1990). Microbial sulfate reduction in acidic (pH 3) strip-mine lakes. *FEMS Microbiology Ecology*, *6*(3), 193-201.

Habicht, K. S., & Canfield, D. E. (1997). Sulfur isotope fractionation during bacterial sulfate reduction in organic-rich sediments. *Geochimica et Cosmochimica Acta*, *61*(24), 5351-5361.

Habicht, K. S., Canfield, D. E.& Rethmeier, J. (1998). Sulfur isotope fractionation during bacterial reduction and disproportionation of thiosulfate and sulfite. *Geochimica et Cosmochimica Acta*. Pergamon, 62(15), 2585–2595. doi: 10.1016/S0016-7037(98)00167-7.

Habicht, K. S., Gade, M., Thamdrup, B., Berg, P., & Canfield, D. E. (2002). Calibration of sulfate levels in the Archean ocean. *Science*, *298*(5602), 2372-2374.

Hallberg, K. B., Hedrich, S., & Johnson, D. B. (2011). Acidiferrobacter thiooxydans, gen. nov. sp. nov.; an acidophilic, thermo-tolerant, facultatively anaerobic iron-and sulfur-oxidizer of the family Ectothiorhodospiraceae. *Extremophiles*, *15*(2), 271-279.

Harrison, J. C., & Jackson, M. P. A. (2014). Exposed evaporite diapirs and minibasins above a canopy in central Sverdrup Basin, Axel Heiberg Island, Arctic Canada. *Basin Research*, *26*(4), 567-596.

Havig, J. R., Hamilton, T. L., Bachan, A., & Kump, L. R. (2017). Sulfur and carbon isotopic evidence for metabolic pathway evolution and a four-stepped Earth system progression across the Archean and Paleoproterozoic. *Earth-Science Reviews*, *174*, 1-21.

Havig, J.R., Mccormick, M.L., Hamilton, T.L., & Kump, L.R. (2015). The behavior of biologically important trace elements across the oxic/euxinic transition of meromictic Fayetteville Green Lake, New York, USA. *Geochimica et Cosmochimica Acta*, 165, 389–406. https://doi.org/10.1016/j.gca.2015.06.024

Havig, J. R., Raymond, J., Meyer-Dombard, D. A. R., Zolotova, N., & Shock, E. L. (2011). Merging isotopes and community genomics in a siliceous sinter-depositing hot spring. *Journal of Geophysical Research: Biogeosciences*, *116*(G1).

Hayes, J. M. (2001). Fractionation of carbon and hydrogen isotopes in biosynthetic processes.*Stable Isotope Geochemistry*, 225–277. doi: 10.2138/gsrmg.43.1.225.

Hays, L.E., Graham, H.V., Des Marais, D.J., Hausrath, E.M., Horgan, B., McCollom,et al. (2017). Biosignature Preservation and Detection in Mars Analog Environments. *Astrobiology*, 17(4), 1-38. https://doi.org/10.1089/ast.2016.1627

Hebting, Y., Schaeffer, P., Behrens, A., Adam, P., Schmitt, G., Schneckenburger, P., et al. (2006). Biomarker evidence for a major preservation pathway of sedimentary organic carbon. *Science*, *312*(5780), 1627-1631.

Herkenhoff, K. E., Grotzinger, J., Knoll, A. H., McLennan, S. M., Weitz, C., Yingst, A et al. (2008). Surface processes recorded by rocks and soils on Meridiani Planum, Mars: Microscopic Imager observations during Opportunity's first three extended missions. *Journal of Geophysical Research: Planets*, *113*(E12).

Hiesinger, H., & Head III, J. W. (2004). The Syrtis Major volcanic province, Mars: Synthesis from Mars global surveyor data. *Journal of Geophysical Research: Planets*, *109*(E1).

Hirayama, H., Takai, K., Inagaki, F., Yamato, Y., Suzuki, M., Nealson, K. H., & Horikoshi, K. (2005). Bacterial community shift along a subsurface geothermal water stream in a Japanese gold mine. *Extremophiles*, *9*(2), 169-184.

Hoehler, T. M., & Jørgensen, B. B. (2013). Microbial life under extreme energy limitation. *Nature Reviews Microbiology*, *11*(2), 83-94.

Hoek, J., Reysenbach, A. L., Habicht, K. S., & Canfield, D. E. (2006). Effect of hydrogen limitation and temperature on the fractionation of sulfur isotopes by a deep-sea hydrothermal vent sulfate-reducing bacterium. *Geochimica et Cosmochimica Acta*, *70*(23), 5831-5841.

Hoffmann, H., Belluci, G., Jaumann, R., McCord, T. B., Poulet, F., Neukum, G., et al. (2004). Dark areas on Mars as seen by the HRSC and OMEGA experiments on Mars Express. In *35th COSPAR Scientific Assembly* (Vol. 35, p. 3841).

Holt J.G. (1984). *Bergey's Manual of Systematic Bacteriology*, Vol. 1. Baltimore, MD: Williams and Wilkins.

Horita, J. (2005). Some perspectives on isotope biosignatures for early life. *Chemical Geology*, *218*(1-2), 171-186.

Hou, X., & Jones, B. T. (2000). Field instrumentation in atomic spectroscopy. *Microchemical Journal*, *66*(1-3), 115-145.

House, C. H., Schopf, J. W., & Stetter, K. O. (2003). Carbon isotopic fractionation by Archaeans and other thermophilic prokaryotes. *Organic Geochemistry*, *34*(3), 345-356.

Howard, A. D., Moore, J. M., & Irwin III, R. P. (2005). An intense terminal epoch of widespread fluvial activity on early Mars: 1. Valley network incision and associated deposits. *Journal of Geophysical Research: Planets*, *110*(E12).

Howarth, R. W., & Teal, J. M. (1979). Sulfate reduction in a New England salt marsh 1. *Limnology and Oceanography*, *24*(6), 999-1013.

Humlum, J. (1936). Hveradalir in Kerlingarfjöll , Iceland. Tidsskrift

Hunt, G. R. (1977). Spectral signatures of particulate minerals in the visible and near infrared. *Geophysics*, *42*(3), 501-513.

Hurowitz, J.A., Grotzinger, J.P., Fischer, W.W., McLennan, S.M., Milliken, R.E., Stein, N., et al. (2017). Redox stratification of an ancient lake in Gale crater, Mars. *Science*, 356(6341) ,eaah6849. https://10.1126/science.aah6849

Hurowitz, J.A., McLennan, S.M., Tosca, N.J., Arvidson, R.E., Michalski, J.R., Ming, D.W., Shroder, C., et al. (2006). In situ and experimental evidence for acidic weathering of rocks and soils on Mars. J.Geophys. Res., 111, E02S19. https://doi.org/10.1029/2005JE002515

Hurtgen, M. T., Arthur, M. A., & Halverson, G. P. (2005). Neoproterozoic sulfur isotopes, the evolution of microbial sulfur species, and the burial efficiency of sulfide as sedimentary pyrite. *Geology*, *33*(1), 41-44.

Hynek, B. M., Rogers, K. L., Antunovich, M., Avard, G., & Alvarado, G. E. (2018). Lack of microbial diversity in an extreme Mars analog setting: Poás Volcano, Costa Rica. *Astrobiology*, *18*(7), 923-933.

Icopini, G. A., Anbar, A. D., Ruebush, S. S., Tien, M., & Brantley, S. L. (2004). Iron isotope fractionation during microbial reduction of iron: the importance of adsorption. *Geology*, *32*(3), 205-208.

Ise, K., Suto, K., & Inoue, C. (2011). Microbial diversity and changes in the distribution of dehalogenase genes during dechlorination with different concentrations of cis-DCE. *Environmental science & technology*, *45*(12), 5339-5345.

Itoh, T., Yamanoi, K., Kudo, T., Ohkuma, M., & Takashina, T. (2011). Aciditerrimonas ferrireducens gen. nov., sp. nov., an iron-reducing thermoacidophilic actinobacterium isolated from a solfataric field. *International journal of systematic and evolutionary microbiology*, *61*(6), 1281-1285.

Jakobsson, S.P., Jónasson, K., & Sigurdsson, I.A. (2008). The three igneous rock series of Iceland. *Jökull*, 58, 117–138.

Jackson, B. E., Bhupathiraju, V. K., Tanner, R. S., Woese, C. R., & McInerney, M. J. (1999). Syntrophus aciditrophicus sp. nov., a new anaerobic bacterium that degrades fatty acids and benzoate in syntrophic association with hydrogen-using microorganisms. *Archives of microbiology*, *171*(2), 107-114.

Jóhannesson, T., Thorsteinsson, T., Stefánsson, A., Gaidos, E. J., & Einarsson, B. (2007). Circulation and thermodynamics in a subglacial geothermal lake under the Western Skaftá cauldron of the Vatnajökull ice cap, Iceland. *Geophysical research letters*, *34*(19).

Johnson, D. B., Bacelar-Nicolau, P., Okibe, N., Thomas, A., & Hallberg, K. B. (2009). Ferrimicrobium acidiphilum gen. nov., sp. nov. and Ferrithrix thermotolerans gen. nov., sp. nov.: heterotrophic, iron-oxidizing, extremely acidophilic actinobacteria. *International journal of systematic and evolutionary microbiology*, *59*(5), 1082-1089.

Johnson, D. B., Joulian, C., d'Hugues, P., & Hallberg, K. B. (2008). Sulfobacillus benefaciens sp. nov., an acidophilic facultative anaerobic Firmicute isolated from mineral bioleaching operations. *Extremophiles*, *12*(6), 789.

Johnson, S. S., Mischna, M. A., Grove, T. L., & Zuber, M. T. (2008). Sulfur-induced greenhouse warming on early Mars. *Journal of Geophysical Research: Planets*, *113*(E8).

Johnston, D.T., Farquhar, J., & Canfield, D.E. (2007). Sulfur isotope insights into microbial sulfate reduction: When microbes meet models. *Geochimica et Cosmochimica Acta*, 71(16), 3929–3947. https://doi.org/10.1016/j.gca.2007.05.008

Johnston, D. T., Farquhar, J., Habicht, K. S., & Canfield, D. E. (2008a). Sulphur isotopes and the search for life: strategies for identifying sulphur metabolisms in the rock record and beyond. *Geobiology*, *6*(5), 425-435.

Johnston, D. T., Farquhar, J., Summons, R. E., Shen, Y., Kaufman, A. J., Masterson, A. L., & Canfield, D. E. (2008b). Sulfur isotope biogeochemistry of the Proterozoic McArthur Basin. *Geochimica et Cosmochimica Acta*, *72*(17), 4278-4290.

Johnston, D. T., Farquhar, J., Wing, B. A., Kaufman, A. J., Canfield, D. E., & Habicht, K. S. (2005a). Multiple sulfur isotope fractionations in biological systems: a case study with

sulfate reducers and sulfur disproportionators. *American Journal of Science*, *305*(6-8), 645-660.

Johnston, D. T., Poulton, S. W., Fralick, P. W., Wing, B. A., Canfield, D. E., & Farquhar, J. (2006). Evolution of the oceanic sulfur cycle at the end of the Paleoproterozoic. *Geochimica et Cosmochimica Acta*, *70*(23), 5723-5739.

Johnston, D. T., Wing, B. A., Farquhar, J., Kaufman, A. J., Strauss, H., Lyons, T. W., et al. (2005b). Active microbial sulfur disproportionation in the Mesoproterozoic. *Science*, *310*(5753), 1477-1479.

Jørgensen, B. B., & Marshall, I. P. (2016). Slow microbial life in the seabed. *Annual Reviews*, 8, 311-322

Jung, M. Y., Park, S. J., Kim, S. J., Kim, J. G., Damsté, J. S. S., Jeon, C. O., & Rhee, S. K. (2014). A mesophilic, autotrophic, ammonia-oxidizing archaeon of thaumarchaeal group I. 1a cultivated from a deep oligotrophic soil horizon. *Appl. Environ. Microbiol.*, *80*(12), 3645-3655.

Kaasalainen, H., & Stefánsson, A. (2012). The chemistry of trace elements in surface geothermal waters and steam, Iceland. *Chemical Geology*, 330–331, 60–85. https://doi.org/10.1016/j.chemgeo.2012.08.019

Kaasalainen, H., Stefánsson, A., & Druschel, G.K. (2017). Geochemistry and speciation of Fe(II) and Fe(III) in natural geothermal water, Iceland. *Applied Geochemistry*, 87(October), 146–157. https://doi.org/10.1016/j.apgeochem.2017.10.021

Kamagata, Y., Kawasaki, H., Oyaizu, H., Nakamura, K., Mikami, E., Endo, G., et al. (1992). Characterization of three thermophilic strains of Methanothrix (“Methanosaeta”) thermophila sp. nov. and rejection of Methanothrix (“Methanosaeta”) thermoacetophila. *International Journal of Systematic and Evolutionary Microbiology*, *42*(3), 463-468.

Kamp, A., Stief, P. and Schulz-Vogt, H. N. (2006). Anaerobic sulfide oxidation with nitrate by a freshwater Beggiatoa enrichment culture. *Applied and Environmental Microbiology*, 72(7), 4755–4760. doi: 10.1128/AEM.00163-06.

Kaplan, H. H., Milliken, R., Fernandez-Remolar, D. C., Amils, R., Robertson, K., & Knoll, A. H. (2015). Orbital Evidence for Clay and Acidic Sulfate Assemblages on Mars and Mineralogical Analogs from Rio Tinto, Spain. *AGUFM*, *2015*, P23C-04.

Kaplan, I. R., & Rittenberg, S. C. (1964a). Microbiological fractionation of sulphur isotopes. *Microbiology*, *34*(2), 195-212.

Kaplan, I. R., & Rittenberg, S. C. (1964b). Carbon isotope fractionation during metabolism of lactate by Desulfovibrio desulfuricans. *Microbiology*, *34*(2), 213-217.

Karhadkar, P. P., Audic, J. M., Faup, G. M., & Khanna, P. (1987). Sulfide and sulfate inhibition of methanogenesis. *Water Research*, *21*(9), 1061-1066.

Ten Kate, I. L. (2018). Organic molecules on Mars. *Science*, *360*(6393), 1068-1069.

Kee, T., Bryant, D., Herschy, B., Marriott, K., Cosgrove, N., Pasek, et al. (2013). Phosphate Activation via Reduced Oxidation State Phosphorus (P). Mild Routes to Condensed-P Energy Currency Molecules. *Life*, 3(3), 386–402. https://doi.org/10.3390/life3030386

Kellermann, C., & Griebler, C. (2009). Thiobacillus thiophilus sp. nov., a chemolithoautotrophic, thiosulfate-oxidizing bacterium isolated from contaminated aquifer sediments. *International Journal of Systematic and Evolutionary Microbiology*, *59*(3), 583-588.

Kelly, D. P., & Wood, A. P. (2000). Reclassification of some species of Thiobacillus to the newly designated genera Acidithiobacillus gen. nov., Halothiobacillus gen. nov. and Thermithiobacillus gen. nov. *International Journal of Systematic and Evolutionary Microbiology*, *50*(2), 511-516.

Kendall, M. M., Liu, Y., Sieprawska-Lupa, M., Stetter, K. O., Whitman, W. B., & Boone, D. R. (2006). Methanococcus aeolicus sp. nov., a mesophilic, methanogenic archaeon from shallow and deep marine sediments. *International journal of systematic and evolutionary microbiology*, *56*(7), 1525-1529.

Keppler, F., Vigano, I., McLeod, A., Ott, U., Früchtl, M., & Röckmann, T. (2012). Ultraviolet-radiation-induced methane emissions from meteorites and the Martian atmosphere. *Nature*, *486*(7401), 93-96.

King, P. L., & McSween, H. Y. (2005). Effects of H2O, pH, and oxidation state on the stability of Fe minerals on Mars. *Journal of Geophysical Research: Planets*, *110*(E12).

King, P. L., & McLennan, S. M. (2010). Sulfur on mars. *Elements*, *6*(2), 107-112.

Kirk Nordstrom, D., Blaine McCleskey, R., & Ball, J.W. (2009). Sulfur geochemistry of hydrothermal waters in Yellowstone National Park: IV Acid–sulfate waters. *Applied Geochemistry*, 24(2), 191–207. https://doi.org/10.1016/j.apgeochem.2008.11.019

Kishimoto, N., Kosako, Y., & Tano, T. (1991). Acidobacterium capsulatum gen. nov., sp. nov.: an acidophilic chemoorganotrophic bacterium containing menaquinone from acidic mineral environment. *Current Microbiology*, *22*(1), 1-7.

Kite, E. S., Gao, P., Goldblatt, C., Mischna, M. A., Mayer, D. P., & Yung, Y. L. (2017). Methane bursts as a trigger for intermittent lake-forming climates on post-Noachian Mars. *Nature Geoscience*, *10*(10), 737-740.

Klemps, R., Cypionka, H., Widdel, F., & Pfennig, N. (1985). Growth with hydrogen, and further physiological characteristics of Desulfotomaculum species. *Archives of Microbiology*, *143*(2), 203-208.

Klingelhöfer, G., Morris, R.V., Bernhardt, B., Schroder, C., Rodionov, D.S., De Souza, P.A., et al. (2004). Jarosite and hematite at Meridiani Planum from Opportunity's Mossbauer Spectrometer. *Science*, 306(5702), 1740–5. https://doi.org/10.1126/science.1104653

Kobayashi, K., Makabe, A., Yano, M., Oshiki, M., Kindaichi, T., Casciotti, K. L., & Okabe, S. (2019). Dual nitrogen and oxygen isotope fractionation during anaerobic ammonium oxidation by anammox bacteria. *The ISME journal*, *13*(10), 2426-2436.

Kraal, E. R., Van Dijk, M., Postma, G., & Kleinhans, M. G. (2008). Martian stepped-delta formation by rapid water release. *Nature*, *451*(7181), 973-976.

Van Kranendonk, M., Baumgartner, R., Boyd, E., Cady, S., Campbell, K., Czaja, A., et al. (2018). Terrestrial Hot Springs and the Origin of Life: Implications for the Search for Life Beyond Earth. Paper presented at the 49th Lunar and Planetary Science Conference 2018, Houston, Texas, US.

Kröninger, L., Gottschling, J., & Deppenmeier, U. (2017). Growth characteristics of Methanomassiliicoccus luminyensis and expression of methyltransferase encoding genes. *Archaea*, *2017*.

Kvist, T., Ahring, B. K., & Westermann, P. (2007). Archaeal diversity in Icelandic hot springs. *FEMS microbiology ecology*, *59*(1), 71-80.

Lanz, J. K., & Saric, M. B. (2009). Cone fields in SW Elysium Planitia: hydrothermal venting on Mars?. *Journal of Geophysical Research: Planets*, *114*(E2).

Lee, D. C., & Halliday, A. N. (1997). Core formation on Mars and differentiated asteroids. *Nature*, *388*(6645), 854-857.

Letunic, I., & Bork, P. (2019). Interactive Tree Of Life (iTOL) v4: recent updates and new developments. *Nucleic acids research*, *47*(W1), W256-W259.

Levine, J. S., & Summers, M. E. (2011). Sulfur Chemistry in the Early and Present Atmosphere of Mars. Nasa Scientific Report.

Lillis, R. J., Frey, H. V., & Manga, M. (2008). Rapid decrease in Martian crustal magnetization in the Noachian era: Implications for the dynamo and climate of early Mars. *Geophysical Research Letters*, *35*(14).

Louca, S., Parfrey, L. W., & Doebeli, M. (2016). Decoupling function and taxonomy in the global ocean microbiome. *Science*, *353*(6305), 1272-1277.

Lovley, D. R., Dwyer, D. F., & Klug, M. J. (1982). Kinetic analysis of competition between sulfate reducers and methanogens for hydrogen in sediments. *Appl. Environ. Microbiol.*, *43*(6), 1373-1379.

Lovley, D. R., & Klug, M. J. (1983). Sulfate reducers can outcompete methanogens at freshwater sulfate concentrations. *Appl. Environ. Microbiol.*, *45*(1), 187-192.

Lozano, R., & Bernal, J. P. (2005). Characterization of a new set of eight geochemical reference materials for XRF major and trace element analysis. *Revista Mexicana de Ciencias Geológicas*, *22*(3), 329-344.

Lü, Z., & Lu, Y. (2012). Methanocella conradii sp. nov., a thermophilic, obligate hydrogenotrophic methanogen, isolated from Chinese rice field soil. *PloS one*, *7*(4).

Luo, W., Cang, X., & Howard, A.D. (2017). New Martian valley network volume estimate consistent with ancient ocean and warm and wet climate. *Nature Communications*, 8, 15766. https://doi.org/10.1038/ncomms15766

Luo, G., Ono, S., Beukes, N. J., Wang, D. T., Xie, S., & Summons, R. E. (2016). Rapid oxygenation of Earth's atmosphere 2.33 billion years ago. *Science Advances*, *2*(5), e1600134.

Madeleine, J. B., Forget, F., Head, J. W., Levrard, B., Montmessin, F., & Millour, E. (2009). Amazonian northern mid-latitude glaciation on Mars: A proposed climate scenario. *Icarus*, *203*(2), 390-405.

Magnuson, E., Mykytczuk, N. C., Pellerin, A., Goordial, J., Twine, S. M., Wing, B., ... & Whyte, L. G. (2020). Thiomicrorhabdus streamers and sulfur cycling in perennial hypersaline cold springs in the Canadian high Arctic. *Environmental Microbiology*, 0, 0-16

Malin, M. C., & Edgett, K. S. (2003). Evidence for persistent flow and aqueous sedimentation on early Mars. *Science*, *302*(5652), 1931-1934.

Mangold, N., Dehouk, E., Forni, O., Achilles, C., Bristow, T., Downs, R.T., Frydenvang, J., et al. (2019). Chemical alteration of fine-grained sedimentary rocks at Gale crater. *Icarus*, 321, 619-631.

Mangold, N., Poulet, F., Mustard, J. F., Bibring, J. P., Gondet, B., Langevin, Y., et al. (2007). Mineralogy of the Nili Fossae region with OMEGA/Mars Express data: 2. Aqueous alteration of the crust. *Journal of Geophysical Research: Planets*, *112*(E8).

Mangold, N., Roach, L., Milliken, R., Le Mouélic, S., Ansan, V., Bibring, J. P., et al. (2010). A Late Amazonian alteration layer related to local volcanism on Mars. *Icarus*, *207*(1), 265-276.

Mandon, L., Parkes, A. B., Quantin-Nataf, C., Bridges, J. C., Carter, J., & Pan, L. (2019, July). Spectral diversity and stratigraphy of the clay-bearing unit at the ExoMars 2020 landing site Oxia Planum. 9th International Conference on Mars, Lunar and Planetary Institute, Jul 2019, Pasadena, United States,.6173.

MacDonald, A.M., Black, A.R., O Dochartaigh, B.E., Everest, J., Darling, W.G., Flett, V., & Peach, D.W. (2016). Using stable isotopes and continuous meltwater river monitoring to investigate the hydrology of a rapidly retreating Icelandic outlet glacier. *Annals of Glaciology*, 57(72), 151–158. https://doi.org/10.1017/aog.2016.22

Des Marais, D. J. (1997). Isotopic evolution of the biogeochemical carbon cycle during the Proterozoic Eon. *Organic Geochemistry*, *27*(5-6), 185-193.

Des Marais, D. J., Harwit, M. O., Jucks, K. W., Kasting, J. F., Lin, D. N., Lunine, J. I., et al. (2002). Remote sensing of planetary properties and biosignatures on extrasolar terrestrial planets. *Astrobiology*, *2*(2), 153-181.

Des Marais, D. J., & Jahnke, L. L. (2019a). Biosignatures of cellular components and metabolic activity. In *Biosignatures for astrobiology* (pp. 51-85). Springer, Cham.

Des Marais, D. J., & Walter, M. R. (2019). Terrestrial hot spring systems: introduction. *Astrobiology*, *19*(12), 1419-1432.

Markússon, S.H., & Stefánsson, A. (2011). Geothermal surface alteration of basalts, Krýsuvík Iceland-Alteration mineralogy, water chemistry and the effects of acid supply on the alteration process. *Journal of Volcanology and Geothermal Research*, 206(1–2), 46–59. https://doi.org/10.1016/j.jvolgeores.2011.05.007

Marteinsson, V. T., Runarsson, A., Stefánsson, A., Thorsteinsson, T., Johannesson, T., Magnusson, S. H., et al. (2013). Microbial communities in the subglacial waters of the Vatnajökull ice cap, Iceland. *The ISME journal*, *7*(2), 427-437.

Marzo, G. A., Davila, A. F., Tornabene, L. L., Dohm, J. M., Fairén, A. G., Gross, C., et al. (2010). Evidence for Hesperian impact-induced hydrothermalism on Mars. *Icarus*, *208*(2), 667-683.

McCollom, T. M., & Seewald, J. S. (2006). Carbon isotope composition of organic compounds produced by abiotic synthesis under hydrothermal conditions. *Earth and Planetary Science Letters*, *243*(1-2), 74-84.

McGill, G. E., & Squyres, S. W. (1991). Origin of the Martian crustal dichotomy: Evaluating hypotheses. *Icarus*, *93*(2), 386-393.

McInerney, M. J., Rohlin, L., Mouttaki, H., Kim, U., Krupp, R. S., Rios-Hernandez, L., et al. (2007). The genome of Syntrophus aciditrophicus: life at the thermodynamic limit of microbial growth. *Proceedings of the National Academy of Sciences*, *104*(18), 7600-7605.

McLennan, S. M. (2003). Sedimentary silica on Mars. *Geology*, *31*(4), 315-318.

McLennan, S. M., Bell Iii, J. F., Calvin, W. M., Christensen, P. R., Clark, B. D., De Souza, P. A., et al. (2005). Provenance and diagenesis of the evaporite-bearing Burns formation, Meridiani Planum, Mars. *Earth and Planetary Science Letters*, *240*(1), 95-121.

McLennan, S. M., Boynton, W. V., Karunatillake, S., Hahn, B. C., Taylor, G. J., & Mars Odyssey, G. R. S. (2010). Distribution of sulfur on the surface of Mars determined by the 2001 Mars Odyssey Gamma Ray Spectrometer. In *Lunar and Planetary Science Conference*, 41, 2174.

McLennan, S.M, Grotzinger, J.P., Hurowitz, J.A., & Tosca, N.J. (2018). The Sedimentary Cycle on Early Mars. *Annual Review of Earth and Planetary Sciences*, 47(1), 91-118. https://doi.org/10.1146/annurev-earth-053018-

McLoughlin, N., Furnes, H., Banerjee, N. R., Muehlenbachs, K., & Staudigel, H. (2009). Ichnotaxonomy of microbial trace fossils in volcanic glass. *Journal of the Geological Society*, *166*(1), 159-169.

McSween, H. Y., Taylor, G. J., & Wyatt, M. B. (2009). Elemental composition of the Martian crust. *Science*, *324*(5928), 736-739.

McSween, H. Y., Wyatt, M. B., Gellert, R., Bell, J. F., Morris, R. V., Herkenhoff, K. E., et al. (2006). Characterization and petrologic interpretation of olivine-rich basalts at Gusev Crater, Mars. *Journal of Geophysical Research: Planets*, *111*(E2).

Meyer-Dombard, D. R., Shock, E. L., & Amend, J. P. (2005). Archaeal and bacterial communities in geochemically diverse hot springs of Yellowstone National Park, USA. *Geobiology*, *3*(3), 211-227.

Meyer, C. (2012). The Martian meteorite compendium. *NASA JSC Astromaterials Research & Exploration Science (ARES)*.

Michalski, J. R., Cuadros, J., Niles, P. B., Parnell, J., Rogers, A. D., & Wright, S. P. (2013). Groundwater activity on Mars and implications for a deep biosphere. *Nature Geoscience*, *6*(2), 133-138.

Michalski, J. R., & Niles, P. B. (2010). Deep crustal carbonate rocks exposed by meteor impact on Mars. *Nature Geoscience*, *3*(11), 751-755.

Michalski, J.R., Noe Fobrea, E.Z., Niles, P.B., Cuadros, J. (2017) Ancient hydrothermal seafloor deposits in Eridania basin on Mars. *Nature Communications,* 8, 15978.

Michalski, J. R., Onstott, T. C., Mojzsis, S. J., Mustard, J., Chan, Q. H., Niles, P. B., & Johnson, S. S. (2018). The Martian subsurface as a potential window into the origin of life. *Nature Geoscience*, *11*(1), 21-26.

Milton, D. J. (1973). Water and processes of degradation in the Martian landscape. *Journal of Geophysical Research*, *78*(20), 4037-4047.

Ming, D. W., Gellert, R., Morris, R. V., Arvidson, R. E., Brueckner, J., Clark, B. C., et al. (2008). Geochemical properties of rocks and soils in Gusev crater, Mars: Results of the

Alpha Particle X-ray Spectrometer from Cumberland Ridge to Home Plate. *Journal of Geophysical Research: Planets*, *113*(E12).

Mischna, M. A., Kasting, J. F., Pavlov, A., & Freedman, R. (2000). Influence of carbon dioxide clouds on early Martian climate. *Icarus*, *145*(2), 546-554.

Russell, M. J. (2003). The importance of being alkaline. *Science*, *302*(5645), 580-581.

Moore, E. K., Jelen, B. I., Giovannelli, D., Raanan, H., & Falkowski, P. G. (2017). Metal availability and the expanding network of microbial metabolisms in the Archaean eon. *Nature Geoscience*, *10*(9), 629-636.

Moore, J. M., Howard, A. D., Dietrich, W. E., & Schenk, P. M. (2003). Martian layered fluvial deposits: Implications for Noachian climate scenarios. *Geophysical Research Letters*, *30*(24).

Mori, K., Yamaguchi, K., Sakiyama, Y., Urabe, T., & Suzuki, K. I. (2009). Caldisericum exile gen. nov., sp. nov., an anaerobic, thermophilic, filamentous bacterium of a novel bacterial phylum, Caldiserica phyl. nov., originally called the candidate phylum OP5, and description of Caldisericaceae fam. nov., Caldisericales ord. nov. and Caldisericia classis nov. *International journal of systematic and evolutionary microbiology*, *59*(11), 2894-2898.

Morowitz, H. J. (1993). *Beginnings of cellular life: metabolism recapitulates biogenesis*. Yale University Press.

Morris, R. V., Ruff, S. W., Gellert, R., Ming, D. W., Arvidson, R. E., Clark, B. C., ... & Fleischer, I. (2010). Identification of carbonate-rich outcrops on Mars by the Spirit rover. *Science*, *329*(5990), 421-424.

Mountfort, D. O., Brulla, W. J., Krumholz, L. R., & Bryant, M. P. (1984). Syntrophus buswellii gen. nov., sp. nov.: a benzoate catabolizer from methanogenic ecosystems. *International Journal of Systematic and Evolutionary Microbiology*, *34*(2), 216-217.

Mumma, M. J., Villanueva, G. L., Novak, R. E., Hewagama, T., Bonev, B. P., DiSanti, M. A., et al. (2009). Strong release of methane on Mars in northern summer 2003. *Science*, *323*(5917), 1041-1045.

Murchie, S., Arvidson, R., Bedini, P., Beisser, K., Bibring, J. P., Bishop, J., et al. (2007). Compact reconnaissance imaging spectrometer for Mars (CRISM) on Mars reconnaissance orbiter (MRO). *Journal of Geophysical Research: Planets*, *112*(E5).

Mustard, J. F., Poulet, F., Head, J. W., Mangold, N., Bibring, J. P., Pelkey, S. M., et al. (2007). Mineralogy of the Nili Fossae region with OMEGA/Mars Express data: 1. Ancient impact melt in the Isidis Basin and implications for the transition from the Noachian to Hesperian. *Journal of Geophysical Research: Planets*, *112*(E8).

Navarrete, J. U., Borrok, D. M., Viveros, M., & Ellzey, J. T. (2011). Copper isotope fractionation during surface adsorption and intracellular incorporation by bacteria. *Geochimica et cosmochimica acta*, *75*(3), 784-799.

Nesbitt, H. W., & Young, G. M. (1982). Early Proterozoic climates and plate motions inferred from major element chemistry of lutites. *Nature*, 299, 715–717.

Nesbitt, H. W., & Young, G. M. (1984). Prediction of some weathering trends of plutonic and volcanic rocks based on thermodynamic and kinetic considerations. *Cosmochim. Acta*, 48, 1523–1534.

Newsom, H. E. (1980). Hydrothermal alteration of impact melt sheets with implications for Mars. *Icarus*, *44*(1), 207-216.

Newsom, H.E. (2005). Clays in the history of Mars. *Nature*, *438*(7068), 570-571.

Nicholson, H. & Latin, D. (1992). Olivine Tholeiites from Krafla, Iceland: Evidence for Variations in Melt Fraction within a Plume. *Journal of Petrology*, 33(5), 1105–1124. doi: 10.1093/petrology/33.5.1105.

Niederberger, T. D., Götz, D. K., McDonald, I. R., Ronimus, R. S., & Morgan, H. W. (2006). Ignisphaera aggregans gen. nov., sp. nov., a novel hyperthermophilic crenarchaeote

isolated from hot springs in Rotorua and Tokaanu, New Zealand. *International journal of systematic and evolutionary microbiology*, *56*(5), 965-971.

Nimmo, F., & Tanaka, K. (2005). Early crustal evolution of Mars. *Annu. Rev. Earth Planet. Sci.*, *33*, 133-161.

Nixon, S., Cousins, C. R., & Cockell, C. (2013). Plausible microbial metabolisms on Mars. *Astronomy & Geophysics*.

Norris, P. R., Clark, D. A., Owen, J. P., & Waterhouse, S. (1996). Characteristics of Sulfobacillus acidophilus sp. nov. and other moderately thermophilic mineral-sulphide-oxidizing bacteria. *Microbiology*, *142*(4), 775-783.

Nunoura, T., Takaki, Y., Kakuta, J., Nishi, S., Sugahara, J., Kazama, H., et al. (2011). Insights into the evolution of Archaea and eukaryotic protein modifier systems revealed by the genome of a novel archaeal group. *Nucleic acids research*, *39*(8), 3204-3223.

Óladóttir, B.A., Larsen, G., & Sigmarsson, O. (2011a). Holocene volcanic activity at Grímsvötn, Bárdarbunga and Kverkfjöll subglacial centres beneath Vatnajökull, Iceland. *Bulletin of Volcanology*, 73(9), 1187–1208.https:// doi.org/10.1007/s00445-011-0461-4

Óladóttir, B.A., Larsen, G., & Sigmarsson, O. (2011b). Provenance of basaltic tephra from Vatnajökull subglacial volcanoes, Iceland, as determined by major- and trace-element analyses. *Holocene*, 21(7), 1037–1048. https://doi.org/10.1177%2F0959683611400456

Olafsson, M., Torfason, H., & Gronvold, K. (2000). Surface exploration and monitoring of geothermal activity in the Kverkfjöll geothermal area, central Iceland. Presented at the World Geothermal Congres 2000, Kyushu-Tohoku, Japan.

Ono, S., Eigenbrode, J. L., Pavlov, A. A., Kharecha, P., Rumble III, D., Kasting, J. F., & Freeman, K. H. (2003). New insights into Archean sulfur cycle from mass-independent sulfur isotope records from the Hamersley Basin, Australia. *Earth and Planetary Science Letters*, *213*(1-2), 15-30.

Ono, S., Shanks III, W. C., Rouxel, O. J., & Rumble, D. (2007). S-33 constraints on the seawater sulfate contribution in modern seafloor hydrothermal vent sulfides. *Geochimica et Cosmochimica Acta*, *71*(5), 1170-1182.

Ono, S., Wing, B., Rumble, D., & Farquhar, J. (2006). High precision analysis of all four stable isotopes of sulfur (32S, 33S, 34S and 36S) at nanomole levels using a laser fluorination isotope-ratio-monitoring gas chromatography–mass spectrometry. *Chemical Geology*, *225*(1-2), 30-39.

Osinski, G.R., Tornavene, L.L., Banerjee, N.R., Cockell, C.S., & Roberta, F. (2013). Impact-generated hydrothermal systems on Earth and Mars. *Icarus*, 224(2), 347–363. https://doi.org/10.1016/j.icarus.2012.08.030

Oze, C., & Sharma, M. (2005). Have olivine, will gas: serpentinization and the abiogenic production of methane on Mars. *Geophysical research letters*, *32*(10).

Pellerin, A., Antler, G., Holm, S. A., Findlay, A. J., Crockford, P. W., Turchyn, A. V., et al. (2019). Large sulfur isotope fractionation by bacterial sulfide oxidation. *Science advances*, *5*(7), eaaw1480.

Pellerin, A., Bui, T. H., Rough, M., Mucci, A., Canfield, D. E., & Wing, B. A. (2015). Mass-dependent sulfur isotope fractionation during reoxidative sulfur cycling: a case study from Mangrove Lake, Bermuda. *Geochimica et Cosmochimica Acta*, *149*, 152-164.

Pereira, I. A., Ramos, A. R., Grein, F., Marques, M. C., Da Silva, S. M., & Venceslau, S. S. (2011). A comparative genomic analysis of energy metabolism in sulfate reducing bacteria and archaea. *Frontiers in microbiology*, *2*, 69.

Peretyazhko, T., Sutter, B., and Ming, D.W. (2014) Alteration of basaltic glass to Mg/Fe smectite under acidic conditions: A potential smectite formation mechanisms on Mars. 51st Clay Minerals Society Meeting; 17-21 May 2014; College Station, TX; United States

Perry, E. C., Monster, J., & Reimer, T. (1971). Sulfur isotopes in Swaziland System barites and the evolution of the Earth's atmosphere. *Science*, *171*(3975), 1015-1016.

Pfennig, N. (1977). Phototrophic green and purple bacteria: a comparative, systematic survey. *Annual Review of Microbiology*, *31*(1), 275-290.

Phillips, R.J., Zuber, M.T., Solomon, S.C., Golombek, M.P., Jakosky, B.M., Banerdt, W.B. et al. (2001). Ancient geodynamics and global-scale hydrology on Mars. *Science*, 291(5513), 2587–2591. https://doi.org/10.1126/science.1058701

Pirajno, F., & Van Kranedonk, M.J. (2007). Review of hydrothermal processes and systems on Earth and implications for Martian analogues. *Australian Journal of Earth Sciences*, 52:3, 329-351. https://doi.org/10.1080/08120090500134571

Pollard, W., Haltigin, T., Whyte, L., Niederberger, T., Andersen, D., Omelon, C., et al. (2009). Overview of analogue science activities at the McGill Arctic research station, Axel Heiberg Island, Canadian high arctic. *Planetary and Space Science*, *57*(5-6), 646-659.

Pollard, W., Omelon, C., Andersen, D., & McKay, C. (1999). Perennial spring occurrence in the Expedition Fiord area of western Axel Heiberg Island, Canadian high Arctic. *Canadian Journal of Earth Sciences*, *36*(1), 105-120.

Poulet, F., Bibring, J. P., Mustard, J. F., Gendrin, A., Mangold, N., Langevin, Y., et al. (2005). Phyllosilicates on Mars and implications for early Martian climate. *Nature*, *438*(7068), 623-627.

Porter, D., Roychoudhury, A. N., & Cowan, D. (2007). Dissimilatory sulfate reduction in hypersaline coastal pans: activity across a salinity gradient. *Geochimica et Cosmochimica Acta*, *71*(21), 5102-5116.

Poser, A., Lohmayer, R., Vogt, C., Knoeller, K., Planer-Friedrich, B., Sorokin, D., et al.(2013). Disproportionation of elemental sulfur by haloalkaliphilic bacteria from soda lakes. *Extremophiles*, *17*(6), 1003-1012.

Praharaj, T., & Fortin, D. (2004). Indicators of microbial sulfate reduction in acidic sulfide-rich mine tailings. *Geomicrobiology Journal*, *21*(7), 457-467.

Preston, L.J., Benedix, G.K., Genge, M.J., & Sephton, MA. (2008). A multidisciplinary study of silica sinter deposits with applications to silica identification and detection of fossil life on Mars. *Icarus*, 198(2), 331–350. https://doi.org/10.1016/j.icarus.2008.08.006

Preston, L.J., & Dartnell, L.R. (2014). Planetary habitability : lessons learned from terrestrial analogues. *International Journal of Astrobiology*, 13(1), 81–98. https://doi.org/10.1017/S1473550413000396

Preuß, A., Schauder, R., Fuchs, G., & Stichler, W. (1989). Carbon isotope fractionation by autotrophic bacteria with three different C02 fixation pathways. *Zeitschrift für Naturforschung C*, *44*(5-6), 397-402.

Price, A., Pearson, V.K., Schwenser, S.P., Miot, J., & Olsson-Francis, K. (2018). Nitrate-Dependent Iron Oxidation: A Potential Mars Metabolism. *Frontiers in Microbiology*, 9, 513. https://doi.org/10.3389/fmicb.2018.00513

Quantin, C., Carter, J., Thollot, P., Broyer, J., Lozach, L., Davis, J., et al. (2015). Oxia Planum: a suitable landing site for ExoMars 2018 Rover. *EPSC Abstracts*, *10*, EPSC2015-704.

Raab, M., & Spiro, B. (1991). Sulfur isotopic variations during seawater evaporation with fractional crystallization. *Chemical Geology: Isotope Geoscience section*, *86*(4), 323-333.

Rabus, R., Boll, M., Heider, J., Meckenstock, R. U., Buckel, W., Einsle, O., et al. (2016). Anaerobic microbial degradation of hydrocarbons: from enzymatic reactions to the environment. *Journal of molecular microbiology and biotechnology*, *26*(1-3), 5-28.

Rabus, R., Hansen, T., & Widdel, F. (2013). Dissimilatory sulfate-and sulfur-reducing prokaryotes, p 309–404. *The prokaryotes: prokaryotic physiology and biochemistry. Springer, Berlin, Germany. doi*, *10*, 978-3.

Ramirez, R. M., Kopparapu, R., Zugger, M. E., Robinson, T. D., Freedman, R., & Kasting, J. F. (2014). Warming early Mars with CO_2 and H_2. *Nature Geoscience*, *7*(1), 59-63.

Ramirez, R.M., & Craddock, R.A. (2018). The geological and climatological case for a warmer and wetter early Mars. *Nature Geoscience*, 11(4), 230–237. https://doi.org/10.1038/s41561-018-0093-9

Rampe, E.B., Ming, D.W., Blake, D.F., Bristow, T.F., Chipera, S.J., Grotzinger, J.P., et al. (2017). Mineralogy of an ancient lacustrine mudstone succession from the Murray formation, Gale crater, Mars. Earth and Planetary Science Letters, 471, 172-185. https://doi.org/10.1016/j.epsl.2017.04.021

Rao, G. S., & Berger, L. R. (1971). The requirement of low pH for growth of Thiobacillus thiooxidans. *Archiv für Mikrobiologie*, *79*(4), 338-344.

Rathbun, J. A., & Squyres, S. W. (2002). Hydrothermal systems associated with Martian impact craters. *Icarus*, *157*(2), 362-372.

Rees, C. E. (1973). A steady-state model for sulphur isotope fractionation in bacterial reduction processes. *Geochimica et Cosmochimica Acta*, *37*(5), 1141-1162.

Reese, B. K., Finneran, D. W., Mills, H. J., Zhu, M. X., & Morse, J. W. (2011). Examination and refinement of the determination of aqueous hydrogen sulfide by the methylene blue method. *Aquatic geochemistry*, *17*(4-5), 567.

Reigstad, L. J., Jorgensen, S. L., & Schleper, C. (2010). Diversity and abundance of Korarchaeota in terrestrial hot springs of Iceland and Kamchatka. *The ISME journal*, *4*(3), 346-356.

Reysenbach, A. L., Liu, Y., Banta, A. B., Beveridge, T. J., Kirshtein, J. D., Schouten, S., ... et al. (2006). A ubiquitous thermoacidophilic archaeon from deep-sea hydrothermal vents. *Nature*, *442*(7101), 444-447.

Richardson, S. M., & Hansen, K. S. (1991). Stable isotopes in the sulfate evaporites from southeastern Iowa, USA: indications of postdepositional change. *Chemical geology*, *90*(1-2), 79-90.

Richardson, J. A., Newville, M., Lanzirotti, A., Webb, S. M., Rose, C. V., Catalano, J. G., & Fike, D. A. (2019). Depositional and diagenetic constraints on the abundance and spatial variability of carbonate-associated sulfate. *Chemical Geology*, *523*, 59-72.

Righter, K., Pando, K., & Danielson, L. R. (2009). Experimental evidence for sulfur-rich martian magmas: Implications for volcanism and surficial sulfur sources. *Earth and Planetary Science Letters*, *288*(1-2), 235-243.

Rimmer, P.B., Shorttle, O. (2019). Origin of Life's Building Blocks in Carbon-and Nitrogen-Rich Surface Hydrothermal Vents. *Life*, 9, 12.

Roerdink, D. L., Mason, P. R., Farquhar, J., & Reimer, T. (2012). Multiple sulfur isotopes in Paleoarchean barites identify an important role for microbial sulfate reduction in the early marine environment. *Earth and Planetary Science Letters*, *331*, 177-186.

Rose, C. V., Webb, S. M., Newville, M., Lanzirotti, A., Richardson, J. A., Tosca, N. J., ... & Fike, D. A. (2019). Insights into past ocean proxies from micron-scale mapping of sulfur species in carbonates. *Geology*, *47*(9), 833-837.

Rothschild, L. J., & Mancinelli, R. L. (2001). Life in extreme environments. *Nature*, *409* (6823), 1092-1101.

Ruff, S.W., & Farmer, J.D. (2016a). Silica deposits on Mars with features resembling hot spring biosignatures at El Tatio in Chile. *Nature Communications*, 7, 1–10.https://doi.org/10.1038/ncomms13554

Ruff, S. W., Farmer, J. D., Calvin, W. M., Herkenhoff, K. E., Johnson, J. R., Morris, R. V., et al. (2011). Characteristics, distribution, origin, and significance of opaline silica observed by the Spirit rover in Gusev crater, Mars. *Journal of Geophysical Research: Planets*, *116*(E7).

Ruff, S.W., Farmer, J.D., Calvin, W.M., Herkenhoff, K.E., Johnson, J.R., Morris, R.V., et al. (2016b). Characteristics, distribution, origin and significance of opaline silica observed by the Spirit rover in Gusev crater, Mars. Journal of Geophysical Research, 116, E00F23. https://doi:10.1029/2010JE003767

Ruff, S. W., Farmer, J. D., Calvin, W. M., Johnson, J. R., Arvidson, R. E., Squyres, S. W., & Christensen, P. R. (2007). Evidence for a possible siliceous sinter deposit at home plate in Gusev Crater. In *AGU Fall Meeting Abstracts*.

Rugheimer, S., & Kaltenegger, L. (2018). Spectra of Earth-like planets through geological evolution around FGKM stars. *The Astrophysical Journal*, *854*(1), 19.

Rugheimer, S., Kaltenegger, L., Segura, A., Linsky, J., & Mohanty, S. (2015). Effect of UV radiation on the spectral fingerprints of Earth-like planets orbiting M stars. *The Astrophysical Journal*, *809*(1), 57.

Saltzman, M. R., & Thomas, E. (2012). Carbon isotope stratigraphy. *The geologic time scale*, *1*, 207-232.

Sánchez-Andrea, I., Rodríguez, N., Amils, R., & Sanz, J. L. (2011). Microbial diversity in anaerobic sediments at Rio Tinto, a naturally acidic environment with a high heavy metal content. *Appl. Environ. Microbiol.*, *77*(17), 6085-6093.

Sánchez-Andrea, I., Sanz, J. L., Bijmans, M. F., & Stams, A. J. (2014). Sulfate reduction at low pH to remediate acid mine drainage. *Journal of hazardous materials*, *269*, 98-109.

Sánchez-Andrea, I., Stams, A. J., Amils, R., & Sanz, J. L. (2013). Enrichment and isolation of acidophilic sulfate-reducing bacteria from T into R iver sediments. *Environmental Microbiology Reports*, *5*(5), 672-678.

De Sanctis, M. C., Altieri, F., Ammannito, E., Biondi, D., De Angelis, S., Meini, M., et al. (2017). Ma_MISS on ExoMars: mineralogical characterization of the martian subsurface. *Astrobiology*, *17*(6-7), 612-620.

Savant, D. V., Shouche, Y. S., Prakash, S., & Ranade, D. R. (2002). Methanobrevibacter acididurans sp. nov., a novel methanogen from a sour anaerobic digester. *International journal of systematic and evolutionary microbiology*, *52*(4), 1081-1087.

Scanlon, K.E, Head, J.W., Wilson, L., Marchant, D.R. (2014). Volcano-ice interactions in the Arsia Mons tropical mountain glacier deposits. *Icarus*, 237, 315-339.

Schidlowski, M. (2001). Carbon isotopes as biogeochemical recorders of life over 3.8 Ga of Earth history: evolution of a concept. *Precambrian Research*, *106*(1-2), 117-134.

Schippers, A., & Jørgensen, B. B. (2002). Biogeochemistry of pyrite and iron sulfide oxidation in marine sediments. *Geochimica et Cosmochimica Acta*, *66*(1), 85-92.

Schloss, P. D., Westcott, S. L., Ryabin, T., Hall, J. R., Hartmann, M., Hollister, E. B., et al. (2009). Introducing mothur: open-source, platform-independent, community-supported software for describing and comparing microbial communities. *Appl. Environ. Microbiol.*, *75*(23), 7537-7541.

Schon, S. C., Head, J. W., & Fassett, C. I. (2012). An overfilled lacustrine system and progradational delta in Jezero crater, Mars: Implications for Noachian climate. *Planetary and Space Science*, *67*(1), 28-45.

Schouten, S., Baas, M., Hopmans, E. C., Reysenbach, A. L., & Damsté, J. S. S. (2008). Tetraether membrane lipids of Candidatus "Aciduliprofundum boonei", a cultivated obligate thermoacidophilic euryarchaeote from deep-sea hydrothermal vents. *Extremophiles*, *12*(1), 119-124.

Schrenk, M. O., Edwards, K. J., Goodman, R. M., Hamers, R. J., & Banfield, J. F. (1998). Distribution of Thiobacillus ferrooxidans and Leptospirillum ferrooxidans: implications for generation of acid mine drainage. *Science*, *279*(5356), 1519-1522.

Schubert, G., Soloman, S. C., Turcotte, D. L., Drake, M. J., & Sleep, N. H. (1990). Origin and thermal evolution of Mars.

Schuler, C. G., Havig, J. R., & Hamilton, T. L. (2017). Hot spring microbial community composition, morphology, and carbon fixation: implications for interpreting the ancient rock record. *Frontiers in Earth Science*, *5*, 97.

Schulze-Makuch, D., Dohm, J.M., Fan, C., Fairen, A.G., Rodriguez, J.A.P., Baker, V.R., & Fink, W. (2007). Exploration of hydrothermal targets on Mars. *Icarus*, 189(2), 308–324. https://doi.org/10.1016/j.icarus.2007.02.007

Schwieterman, E. W., Kiang, N. Y., Parenteau, M. N., Harman, C. E., DasSarma, S., Fisher, T. M., et al. (2018). Exoplanet biosignatures: a review of remotely detectable signs of life. *Astrobiology*, *18*(6), 663-708.

Scott, E. R. (1999). Origin of carbonate-magnetite-sulfide assemblages in Martian meteorite ALH84001. *Journal of Geophysical Research: Planets*, *104*(E2), 3803-3813.

Scott, C., Lyons, T. W., Bekker, A., Shen, Y. A., Poulton, S. W., Chu, X. L., & Anbar, A. D. (2008). Tracing the stepwise oxygenation of the Proterozoic ocean. *Nature*, *452*(7186), 456-459.

Seager, S., Bains, W., & Hu, R. (2013). Biosignature gases in H2-dominated atmospheres on rocky exoplanets. *The Astrophysical Journal*, *777*(2), 95.

Segura, T.L., Owen, B.T., Anthony, C., & Kevin, Z. (2002). Environmental Effects of Large Impacts on Mars. *Science*, 298(5600), 1977. https://doi.org/10.1126/science.1073586

Settle, M. (1979). Formation and deposition of volcanic sulfate aerosols on Mars. *Journal of Geophysical Research: Solid Earth*, *84*(B14), 8343-8354.

Shock, E. L., & Schulte, M. D. (1998). Organic synthesis during fluid mixing in hydrothermal systems. *Journal of Geophysical Research: Planets*, *103*(E12), 28513-28527.

Sholes, S.F., Smith, M.L., Claire, M.W., Zahnle, K.J., & Catling, D.C. (2017). Anoxic atmospheres on Mars driven by volcanism: Implications for past environments and life. *Icarus*, 290, 46–62. https://doi.org/10.1016/j.icarus.2017.02.022

Schmitt, B., Brönnimann, C., Eikenberry, E. F., Gozzo, F., Hörmann, C., Horisberger, R. & Patterson, B. (2003). *Nuclear Instruments and Methods in Physics Research*, 501, 267-272.

Sigmarsson, O., & Steinthórsson, S. (2007). Origin of Icelandic basalts: A review of their petrology and geochemistry. *Journal of Geodynamics*, *43*(1), 87-100.

Sigmundsson, F., & Sæmundsson, K. (2008). Iceland: a window on North-Atlantic divergent plate tectonics and geologic processes. *Episodes*, *31*(1), 92-97.

Sigvaldason, G. E. (1974). Basalts from the centre of the assumed Icelandic mantle plume. *Journal of Petrology*, *15*(3), 497-524.

Sim, M. S. (2012). *Physiology of multiple sulfur isotope fractionation during microbial sulfate reduction*. PhD Thesis, Massachusetts Institute of Technology, US.

Sim, M. S., Bosak, T., & Ono, S. (2011a). Large sulfur isotope fractionation does not require disproportionation. *Science*, *333*(6038), 74-77.

Sim, M. S., Ono, S., Donovan, K., Templer, S. P., & Bosak, T. (2011b). Effect of electron donors on the fractionation of sulfur isotopes by a marine Desulfovibrio sp. *Geochimica et Cosmochimica Acta*, *75*(15), 4244-4259.

Simoneit, B. R., Summons, R. E., & Jahnke, L. L. (1998). Biomarkers as tracers for life on early Earth and Mars. *Origins of Life and Evolution of the Biosphere*, *28*(4-6), 475-483.

Skok, J.R., Mustard, J.F., Ehlmann, B.L., Milliken, R.E., & Murchie, S.L. (2010). Silica deposits in the Nili Patera caldera on the Syrtis Major volcanic complex on Mars. *Nature Geoscience*, 3(12), 838–841. https://doi.org/10.1038/ngeo990

Solomon, S. C., Aharonson, O., Aurnou, J. M., Banerdt, W. B., Carr, M. H., Dombard, A. J., et al. (2005). New perspectives on ancient Mars. *Science*, *307*(5713), 1214-1220.

Solomon, S. C., & Head, J. W. (2007, March). If the late heavy bombardment of the Moon was a terminal cataclysm, what are some implications for Mars?. In *Lunar and Planetary Science Conference* (Vol. 38, p. 1636).

Sorokin, D. Y., Tourova, T. P., Mußmann, M., & Muyzer, G. (2008). Dethiobacter alkaliphilus gen. nov. sp. nov., and Desulfurivibrio alkaliphilus gen. nov. sp. nov.: two novel representatives of reductive sulfur cycle from soda lakes. *Extremophiles*, *12*(3), 431-439.

Squyres, S. W., Arvidson, R. E., Bell, J. F., Brückner, J., Cabrol, N. A., Calvin, W., et al. (2004). The Opportunity Rover's athena science investigation at Meridiani Planum, Mars. *Science*, *306*(5702), 1698-1703.

Squyres, S. W., Arvidson, R. E., Ruff, S., Gellert, R., Morris, R. V., Ming, D. W., et al. (2008). Detection of silica-rich deposits on Mars. *Science*, *320*(5879), 1063-1067.

Stefánsson, A., Keller, N.S., Robin, J.G., Kaasalainen, H., Björnsdóttir, S., Pétursdóttir, S., Jóhannesson, H., & Hreggvidsson, G.O. (2016). Quantifying mixing, boiling, degassing, oxidation and reactivity of thermal waters at Vonarskard, Iceland. *Journal of Volcanology and Geothermal Research*, 309, 53–62. https://doi.org/10.1016/j.jvolgeores.2015.10.01

Stefánsson, A., Keller, N. S., Robin, J. G., & Ono, S. (2015). Multiple sulfur isotope systematics of Icelandic geothermal fluids and the source and reactions of sulfur in volcanic geothermal systems at divergent plate boundaries. *Geochimica et Cosmochimica Acta*, *165*, 307-323.

Stern, J. C., Sutter, B., Freissinet, C., Navarro-González, R., McKay, C. P., Archer, P. D., et al. (2015). Evidence for indigenous nitrogen in sedimentary and aeolian deposits from the Curiosity rover investigations at Gale crater, Mars. *Proceedings of the National Academy of Sciences*, *112*(14), 4245-4250.

Stevenson, D. J. (2001). Mars' core and magnetism. *Nature*, *412*(6843), 214-219.

Story, S., Bowen, B.B., Benison, K.C., and Schulze, D.G. (2010) Authigenic phyllosilicates in modern acid saline lake sediments and implications for Mars. *Journal of Geophysical Research,* 115:E12012.

Strauss, H. (1992). Abundances and isotopic compositions of carbon and sulfur species in whole rock and kerogen samples. *The proterozoic biosphere*, 709-798.

Stüeken, E. E. (2016). Nitrogen in ancient mud: a biosignature?. *Astrobiology*, *16*(9), 730-735.

Summons, R. E., Albrecht, P., McDonald, G., & Moldowan, J. M. (2008). Molecular biosignatures. In *Strategies of Life Detection* (pp. 133-159). Springer, Boston, MA.

Summons, R. E., Amend, J. P., Bish, D., Buick, R., Cody, G. D., Des Marais, D. J., ... & Sumner, D. Y. (2011). Preservation of martian organic and environmental records: final report of the Mars Biosignature Working Group.

Szynkiewicz, A., Goff, F., Vaniman, D., & Pribil, M. J. (2019a). Sulfur cycle in the Valles Caldera volcanic complex, New Mexico–Letter 1: Sulfate sources in aqueous system, and implications for S isotope record in Gale Crater on Mars. *Earth and Planetary Science Letters*, *506*, 540-551.

Szynkiewicz, A., Goff, F., Faiia, A. M., & Vaniman, D. (2019b). Sulfur cycle in the Valles Caldera volcanic complex, New Mexico–Letter 2: Aqueous sulfate budget and implications for hydrological transport on early Mars. *Earth and Planetary Science Letters*, *506*, 552-562.

Szynkiewicz, A., Johnson, A. P., & Pratt, L. M. (2012). Sulfur species and biosignatures in sulphur springs, Valles Caldera, New Mexico—implications for Mars astrobiology. *Earth and Planetary Science Letters*, *321*, 1-13.

Takai, K., Komatsu, T., & Horikoshi, K. (2001). Hydrogenobacter subterraneus sp. nov., an extremely thermophilic, heterotrophic bacterium unable to grow on hydrogen gas, from deep subsurface geothermal water. *International journal of systematic and evolutionary microbiology*, *51*(4), 1425-1435.

Tanaka, K. L. (1986). The stratigraphy of Mars. *Journal of Geophysical Research: Solid Earth*, *91*(B13), E139-E158.

Tanaka, K. L., Carr, M. H., Skinner, J. A., Gilmore, M. S., & Hare, T. M. (2003). Geology of the MER 2003 "Elysium" candidate landing site in southeastern Utopia Planitia, Mars. *Journal of Geophysical Research: Planets*, *108*(E12).

Tanaka, K. L., & Chapman, M. G. (1990). The relation of catastrophic flooding of Mangala Valles, Mars, to faulting of Memnonia Fossae and Tharsis volcanism. *Journal of Geophysical Research: Solid Earth*, *95*(B9), 14315-14323.

Tanaka, K. L., & Scott, D. H. (1987). *Geologic map of the polar regions of Mars*. The Survey.

Taylor, S. R., & McLennan, S. (2009). *Planetary crusts: their composition, origin and evolution* (Vol. 10). Cambridge University Press.

Thamdrup, B. O., Finster, K., Hansen, J. W., & Bak, F. (1993). Bacterial disproportionation of elemental sulfur coupled to chemical reduction of iron or manganese. *Appl. Environ. Microbiol.*, *59*(1), 101-108.

Thode, H. G., Monster, J., & Dunford, H. B. (1961). Sulphur isotope geochemistry. *Geochimica et Cosmochimica Acta*, *25*(3), 159-174.

Tian, F., Claire, M. W., Haqq-Misra, J. D., Smith, M., Crisp, D. C., Catling, D., et al. (2010). Photochemical and climate consequences of sulfur outgassing on early Mars. *Earth and Planetary Science Letters*, *295*(3-4), 412-418.

Torssander, P. (1989). Sulfur isotope ratios of Icelandic rocks. *Contributions to Mineralogy and Petrology*, *102*(1), 18-23.

Tosca, N.J., Ahmed, I.A.M., Tutolo, B.M., Ashpitel, A., & Hurowitz, J.A. (2018). Magnetite authigenesis and the warming of early Mars. *Nature Geoscience*, 11(9), 635–639. https://doi.org/10.1038/s41561-018-0203-8

Tosca, N. J., McLennan, S. M., Clark, B. C., Grotzinger, J. P., Hurowitz, J. A., Knoll, A. H. et al. (2005). Geochemical modeling of evaporation processes on Mars: Insight from the sedimentary record at Meridiani Planum. *Earth and Planetary Science Letters*, *240*(1), 122-148.

Tosca, N. J., McLennan, S. M., Dyar, M. D., Sklute, E. C., & Michel, F. M. (2008). Fe oxidation processes at Meridiani Planum and implications for secondary Fe mineralogy on Mars. *Journal of Geophysical Research: Planets*, *113*(E5).

Tosca, N. J., McLennan, S. M., Lindsley, D. H., & Schoonen, M. A. (2004). Acid-sulfate weathering of synthetic Martian basalt: The acid fog model revisited. *Journal of Geophysical Research: Planets*, *109*(E5).

Ueno, Y., Aoyama, S., Endo, Y., Matsu'ura, F., & Foriel, J. (2015). Rapid quadruple sulfur isotope analysis at the sub-micromole level by a flash heating with CoF3. *Chemical Geology*, *419*, 29-35.

Ulery, A. L., & Drees, L. R. (2008). *Methods of soil analysis: Mineralogical methods. Part 5* (Vol. 9). ASA-CSSA-SSSA.

Valentine, D. L., Chidthaisong, A., Rice, A., Reeburgh, W. S., & Tyler, S. C. (2004). Carbon and hydrogen isotope fractionation by moderately thermophilic methanogens. *Geochimica et Cosmochimica Acta*, *68*(7), 1571-1590.

Vaniman, D.T., Bish, D.L., Ming, D.W., Bristow, T.F., Morris, R.V., Blake, D.F., et al. (2014). Mineralogy of a Mudstone at Yellowknife Bay, Gale Crater, Mars. *Science*, 343, 6169 (1243480). 10.1126/science.1243480

Viennet, J-C., Bultel, B., Riu, L., & Werner, S.C. (2017). Dioctahedral Phyllosilicates Versus Zeolites and Carbonates Versus Zeolites Competitions as Constraints to Understanding Early Mars Alteration Conditions. *Journal of Geophysical Research: Planets*, 122(11), 2328–2343. https://doi.org/10.1002/2017je005343

Viviano, C. E., Moersch, J. E., & McSween, H. Y. (2013). Implications for early hydrothermal environments on Mars through the spectral evidence for carbonation and chloritization reactions in the Nili Fossae region. *Journal of Geophysical Research: Planets*, *118*(9), 1858-1872.

Viviano-Beck, C. E., Murchie, S. L., Beck, A. W., & Dohm, J. M. (2017). Compositional and structural constraints on the geologic history of eastern Tharsis Rise, Mars. *Icarus*, *284*, 43-58.

Wadhwa, M. (2018). Redox conditions on small bodies, the moon and mars.*Oxygen in the Solar System*, 493–510. doi: 10.2138/rmg.2008.68.17.

Wang, A., Bell III, J. F., Li, R., Johnson, J. R., Farrand, W. H., Cloutis, E. A., ... & Herkenhoff, K. E. (2008). Light-toned salty soils and coexisting Si-rich species discovered by the Mars Exploration Rover Spirit in Columbia Hills. *Journal of Geophysical Research: Planets*, *113*(E12).

Wang, A., Haskin, L. A., Squyres, S. W., Jolliff, B. L., Crumpler, L., Gellert, R., et al. (2006). Sulfate deposition in subsurface regolith in Gusev crater, Mars. *Journal of Geophysical Research: Planets*, *111*(E2).

Wang, C. Y., Manga, M., & Hanna, J. C. (2006). Can freezing cause floods on Mars?. *Geophysical research letters*, *33*(20).

Walker, J.C. (1977). Evolution of the atmosphere. Collier Macmillan, New York: Macmillan and London.

Wallwork, K. S., Kennedy, B. J. & Wang, D. (2007). The High Resolution Powder Diffraction Beamline for the Australian Synchrotron . *AIP Conference Proceedings,* 879, 879-882.

Watanabe, Y., Farquhar, J., & Ohmoto, H. (2009). Anomalous fractionations of sulfur isotopes during thermochemical sulfate reduction. *Science*, *324*(5925), 370-373.

Webster, C. R., Mahaffy, P. R., Atreya, S. K., Flesch, G. J., Mischna, M. A., Meslin, P. Y., et al. (2015). Mars methane detection and variability at Gale crater. *Science*, *347*(6220), 415-417.

Webster, C. R., Mahaffy, P. R., Atreya, S. K., Moores, J. E., Flesch, G. J., Malespin, C., ... & Gomez-Elvira, J. (2018). Background levels of methane in Mars' atmosphere show strong seasonal variations. *Science*, *360*(6393), 1093-1096.

Wenk, C. B., Wing, B. A., & Halevy, I. (2018). Electron carriers in microbial sulfate reduction inferred from experimental and environmental sulfur isotope fractionations. *The ISME journal*, *12*(2), 495-507.

Westall, F. (2008). Morphological biosignatures in early terrestrial and extraterrestrial materials. *Space Science Reviews*, *135*(1-4), 95-114.

Westall, F., Cavalazzi, B., Lemelle, L., Marrocchi, Y., Rouzaud, J. N., Simionovici, A., ... & Toporski, J. (2011). Implications of in situ calcification for photosynthesis in a~ 3.3 Ga-old microbial biofilm from the Barberton greenstone belt, South Africa. *Earth and Planetary Science Letters*, *310*(3-4), 468-479.

Westall, F., Foucher, F., Bost, N., Bertrand, M., Loizeau, D., Vago, J. L, et al. (2015). Biosignatures on Mars: what, where, and how? Implications for the search for martian life. *Astrobiology*, *15*(11), 998-1029.

Westall, F., Hickman-Lewis, K., Hinman, N., Gautret, P., Campbell, K. A., Bréhéret, J. G., et al. (2018). A hydrothermal-sedimentary context for the origin of life. *Astrobiology*, *18*(3), 259-293.

Whiticar, M. J. (1999). Carbon and hydrogen isotope systematics of bacterial formation and oxidation of methane. *Chemical Geology*, *161*(1-3), 291-314.

Widdel, F. (1988). Microbiology and ecology of sulfate-and sulfur-reducing bacteria. *Biology of anaerobic microorganisms.*, 469-585.

Widdel F, Bak F. (1992). Gram-negative mesophilic sulfate-reducing bacteria. In: Balows A, Truper HG, Dworkins M, Harder W, Schleifer KH (eds) The prokaryotes, 2nd edn. Springer, New York, pp 3352–3378

Widdel, F., & Pfennig, N. (1977). A new anaerobic, sporing, acetate-oxidizing, on April 24, 2014-Published by mbio. asm. org sulfate-reducing bacterium, Desulfotomaculum (emend.) acetoxidans. *Arch. Microbiol*, *112*, 119-122.

Wordsworth, R.D. (2016). The Climate of Early Mars. *Annual Review of Earth and Planetary Sciences*, 44, 381-408. https://doi.org/10.1146/annurev-earth-060115-012355

Wordsworth, R., Kalugina, Y., Lokshtanov, S., Vigasin, A., Ehlmann, B., Head, J., et al. (2017). Transient reducing greenhouse warming on early Mars. *Geophysical Research Letters*, *44*(2), 665-671.

Worsfold, P. J. and Zagatto, E. A. G. (2017). Spectrophotometry: Overview. *Reference Module in Chemistry,* doi: 10.1016/b978-0-12-409547-2.14265-9.

Wray, J. J., Murchie, S. L., Bishop, J. L., Ehlmann, B. L., Milliken, R. E., Wilhelm, M. B., et al. (2016). Orbital evidence for more widespread carbonate-bearing rocks on Mars. *Journal of Geophysical Research: Planets*, *121*(4), 652-677.

Wray, J. J., Milliken, R. E., Dundas, C. M., Swayze, G. A., Andrews-Hanna, J. C., Baldridge, A. M., et al. (2011). Columbus crater and other possible groundwater-fed paleolakes of Terra Sirenum, Mars. *Journal of Geophysical Research: Planets*, *116*(E1).

Wray, J. J., Noe Dobrea, E. Z., Arvidson, R. E., Wiseman, S. M., Squyres, S. W., McEwen, A. S., et al. (2009). Phyllosilicates and sulfates at Endeavour Crater, Meridiani Planum, Mars. *Geophysical Research Letters*, *36*(21).

Wright, I. P., Carr, R. H., & Pillinger, C. T. (1986). Carbon abundance and isotopic studies of Shergotty and other shergottite meteorites. *Geochimica et Cosmochimica Acta*, *50*(6), 983-991.

Wright, I. P., Grady, M. M., & Pillinger, C. T. (1992). Chassigny and the nakhlites: Carbon-bearing components and their relationship to martian environmental conditions. *Geochimica et Cosmochimica Acta*, *56*(2), 817-826.

Wu, N., Farquhar, J., Strauss, H., Kim, S. T., & Canfield, D. E. (2010). Evaluating the S-isotope fractionation associated with Phanerozoic pyrite burial. *Geochimica et Cosmochimica Acta*, *74*(7), 2053-2071.

Xiao, S., Schiffbauer, J. D., McFadden, K. A., & Hunter, J. (2010). Petrographic and SIMS pyrite sulfur isotope analyses of Ediacaran chert nodules: Implications for microbial processes in pyrite rim formation, silicification, and exceptional fossil preservation. *Earth and Planetary Science Letters*, *297*(3-4), 481-495.

Yen, A. S., Morris, R. V., Clark, B. C., Gellert, R., Knudson, A. T., Squyres, S., ... & Schmidt, M. (2008). Hydrothermal processes at Gusev Crater: An evaluation of Paso Robles class soils. *Journal of Geophysical Research: Planets*, *113*(E6).

Zachos, J. C., Röhl, U., Schellenberg, S. A., Sluijs, A., Hodell, D. A., Kelly, D. C., ... & McCarren, H. (2005). Rapid acidification of the ocean during the Paleocene-Eocene thermal maximum. *Science*, *308*(5728), 1611-1615.

Zeebe, R. E., & Wolf-Gladrow, D. (2001). *CO_2 in seawater: equilibrium, kinetics, isotopes* (No. 65). Gulf Professional Publishing.

Zehnder, A. J. B., & Zinder, S. H. (1980). The sulfur cycle. In *The natural environment and the biogeochemical cycles* (pp. 105-145). Springer, Berlin, Heidelberg.

Zeikus, J. G., Dawson, M. A., Thompson, T. E., Ingvorsen, K., & Hatchikian, E. C. (1983). Microbial ecology of volcanic sulphidogenesis: isolation and characterization of Thermodesulfobacterium commune gen. nov. and sp. nov. *Microbiology*, *129*(4), 1159-1169.

Zellner, G., & Winter, J. (1987). Analysis of a highly efficient methanogenic consortium producing biogas from whey. *Systematic and applied microbiology*, *9*(3), 284-292.

Zerkle, A. L., Farquhar, J., Johnston, D. T., Cox, R. P., & Canfield, D. E. (2009). Fractionation of multiple sulfur isotopes during phototrophic oxidation of sulfide and elemental sulfur by a green sulfur bacterium. *Geochimica et Cosmochimica Acta*, *73*(2), 291-306.

Zerkle, A.L., House, C.H., & Brantley, S.L. (2005). Biochemical signatures through time as inferred from whole microbial genomes. *American Journal of Science,* 305, 467–502. https://doi.org/10.245/ajs.305.6-8.467

Zerkle, A. L., House, C. H., Cox, R. P., & Canfield, D. E. (2006). Metal limitation of cyanobacterial N2 fixation and implications for the Precambrian nitrogen cycle. *Geobiology*, *4*(4), 285-297.

Zerkle, A.L., Jones, D.S., Farquhar, J., & Macalady, J.L. (2016). Sulfur isotope values in the sulfidic Frasassi cave system , central Italy : A case study of a chemolithotrophic S-based ecosystem. *Geochimica et Cosmochimica Acta*, 173, 373–386. https://doi.org/10.1016/j.gca.2015.10.028

Zhang, C. L., Fouke, B. W., Bonheyo, G. T., Peacock, A. D., White, D. C., Huang, Y., & Romanek, C. S. (2004). Lipid biomarkers and carbon-isotopes of modern travertine deposits (Yellowstone National Park, USA): implications for biogeochemical dynamics in hot-spring systems. *Geochimica et Cosmochimica Acta*, *68*(15), 3157-3169.

Ziegler, S., Waidner, B., Itoh, T., Schumann, P., Spring, S., & Gescher, J. (2013). Metallibacterium scheffleri gen. nov., sp. nov., an alkalinizing gammaproteobacterium

isolated from an acidic biofilm. *International journal of systematic and evolutionary microbiology*, *63*(4), 1499-1504.

Zillig, W., Gierl, A., Schreiber, G., Wunderl, S., Janekovic, D., Stetter, K. O., & Klenk, H. P. (1983). The archaebacterium Thermofilum pendens represents, a novel genus of the thermophilic, anaerobic sulfur respiring Thermoproteales. *Systematic and applied microbiology*, *4*(1), 79-87.